TEMPORAL EVALUATION OF AN *EX VIVO* BIOREACTOR MODEL OF ABDOMINAL AORTIC ANEURYSM

EMILY RUTH CLARK

Submitted in accordance with the requirements for the degree of

Doctor of Philosophy

The University of Leeds

School of Mechanical Engineering

May 2016

The candidate confirms that the work submitted is her own, except where otherwise stated or where work which has formed part of jointly authored publications has been included. The contribution of the candidate and the other authors to this work has been explicitly indicated below. The candidate confirms that appropriate credit has been given within the thesis where reference has been made to work of others.

A portion of the work in Chapter 5 of the thesis has appeared in publication as follows:

Exploring smooth muscle phenotype and function in a bioreactor model of abdominal aortic aneurysm (2013) Kirsten Riches, Timothy G Angelini, Gurprit S Mudhar, Jean Kaye, Emily Clark, Marc A Bailey, Sourosh Sohrabi, Sotirios Korossis, Peter G Walker, D Julian A Scott, Karen E Porter.

I was responsible for conducting the porcine immunohistochemical studies and capturing images for publication. The contribution of the other authors was leading and participating in execution of porcine and human cellular studies and manuscript drafting (Riches), conducting human cell studies (Angelini), conducting porcine cell studies (Mudhar), designing and developing the bioreactor (Korossis and Walker), establishing and running the bioreactor experiments (Kaye and Porter), design and performance of apoptosis studies (Bailey), responsibility for all aspects of porcine surgery (Sohrabi), obtaining funding and providing clinical perspective (Scott) and conceiving and managing the study with overall responsibility for its execution (Porter).

I. ACKNOWLEDGEMENTS

Firstly, my thanks must go to my supervisors Dr. Karen Porter (who took me on and believed in an engineer) and Dr. Louise Jennings (who kindly agreed to take me on at a late stage). Thank you so much to you both for making this project work despite initial difficulties and providing expert guidance along the way. I am very grateful to Karen for helping me to feel at home in biological sciences.

I have learned so much during the course of this thesis and a large majority of this is thanks to Dr. Kirsty Riches. You are a very patient and wise woman and much of my knowledge is directly from you.

This work would not have been possible without the surgical expertise of Marc Bailey, Katy Bridge and Kathryn Griffin. Thank you for putting in those early mornings!

Thank you to everyone in LICAMM for your scientific and non-scientific support, especially Karen, Aliah and Patri. Those endless days in cell culture would have been even more awful without you.

Another thanks must go to those who were subjected to the CDTMBE programme alongside me. You have all become very valuable friends and I hope to carry this on far into the future. Jeni, Steve and Ash you are the best results of this PhD, if only I could publish you too.

Thanks to Chris and to my mum for moral support during the troughs and for your shared happiness in the peaks.

All I can say is…..PHEW!

II. ABSTRACT

Abdominal aortic aneurysm (AAA) is an asymptomatic dilatation of the abdominal aorta which ultimately leads to rupture without intervention. Rupture is typically fatal. Due to the silent nature of the disease, the National Abdominal Aortic Aneurysm Screening Programme (NAAASP) has recently been implemented in the UK. It is an unprecedented opportunity to explore the nature of early AAA development and uncover new targets for therapeutics.

Smooth muscle cells (SMCs) are the principle component of the arterial wall and have the ability to stabilise the pathological remodelling which is characteristic of AAA. In AAA tissue, SMCs have been shown to be dysfunctional. Phenotypic switching of SMCs has been reported as an early event in AAA development.

The aim of this study was therefore to further characterise an *ex vivo* porcine model of AAA and temporally characterise SMC phenotype. The approach was to harvest porcine carotid arteries and subject them to a protease pre-treatment. They were then cultured under flow and pressure in a vascular bioreactor for specified periods of time to model the early and end stage of AAA. The model was then temporally characterised in terms of the structure and function of arterial tissue and SMCs. This study directly followed a previous study in our laboratory which validated SMCs from the end-stage model with human AAA SMCs.

Histology and immunohistochemistry for SMCs and components of the extracellular matrix were used to qualitatively analyse tissue structure in the early and end-stage models. Uniaxial tensile testing was used to biomechanically characterise the function of the tissue. Whole vessel pressure-dilation analysis was also evaluated as a method of biomechanical characterisation for this model.

The structure of the SMCs in the early and end-stage models were characterised using image analysis and fluorescence microscopy of the actin cytoskeleton. SMC circularity was an indication of a change in phenotype. The function of

the SMCs was also assessed using proliferation assays, scratch wound migration assays, senescence associated beta-galactosidase assays and gelatin zymography for matrix metalloproteinase-2 and 9 (MMP-2 and -9).

It was determined that a combination of the protease pre-treatment and bioreactor culture was required to induce the phenotypic switch seen previously in the end-stage model. This study managed to reproduce the results seen in the previous study; in the end-stage model, protease pre-treatment followed by bioreactor culture for twelve days induced an increase in SMC circularity, impaired proliferation, elevated levels of senescence and decreased levels of MMP secretion. These characteristics are also observed in human AAA SMCs. A period of SMC hyperproliferation was also observed in the early-stage model. The SMCs had not yet undergone the phenotypic switch characteristic of the end-stage model. The SMCs were also more active in terms of MMP secretion and had much lower levels of senescence compared to the end-stage model.

In terms of tissue structure, Sirius Red histological staining revealed a peri-luminal deposition of collagen in the end-stage model which was not present in the early-stage model. It was hypothesised that this was an attempt at an ECM stabilisation mechanism. The early-stage model also reached aneurysmal dimensions but inwards remodelling of the artery had occurred by the end stage of the model.

Uniaxial tensile testing revealed that culture in the bioreactor caused arterial remodelling regardless of pre-treatment. Generally, vessels which received protease pre-treatment tended to be thinner, weaker and less compliant then those without pre-treatment.

This study shows that it may not be appropriate to characterise AAA SMCs according to classical SMC phenotype. The early-stage model may be used to illuminate potential targets which is particularly pertinent given the recent advent of AAA screening, providing a window of opportunity for early therapeutic intervention.

III. STATEMENT OF WORK

During the course of this study, people additional to the candidate have contributed to the work.

Animal sacrifice was conducted under the Humane Killing of Animals under Schedule 1 to the Animals (Scientific Procedures) Act 1986 and was carried out by the technicians of Central Biomedical Services.

A Home Office Project License was not required for this project as no regulated procedures were performed as part of the experiments. All experiments were performed on tissue following Schedule 1 procedure.

Tissue harvesting and surgical expertise were carried out variously by Marc Bailey, Katy Bridge and Kathryn Griffin.

Morphology images and proliferation data for one end-stage AAA model experiment were conducted by Gurprit Mudhar, an intercalating BSc Medical Sciences student.

IV. TABLE OF CONTENTS

V. LIST OF FIGURES

VI. LIST OF TABLES

VII. ABBREVIATIONS

AAA	Abdominal aortic aneurysm
AO	Atherosclerotic occlusive
ApoE	Apolipoprotein E
APS	Ammonium persulphate
BIO	Bioreactor culture
$CaCl_2$	Calcium chloride
CCA	Common carotid artery
CCE	Combined collagenase and elastase
CT	Computed tomography
DAB	3,3'-diaminobenzidine
DAPI	4',6-diamidino-2-phenylindole
DMEM	Dulbecco's Modified Eagle Medium
DMSO	Dimethyl sulphoxide
DPX	Distyrene plasticizer xylene
E_C	Collagen region stiffness
ECM	Extracellular matrix
EDP	Elastin derived peptides
EDTA	Ethylenediaminetetraacetic acid
E_E	Elastin region stiffness
EVAR	Endovascular aneurysm repair
FCS	Foetal calf serum
FGM	Full growth medium
HBSS	Hank's Balanced Salt Solution
IJV	Internal jugular vein
IL-1α	Interleukin-1 alpha
ILT	Intraluminal thrombus
IMA	Inferior mesenteric artery
IMV	Inferior mesenteric vein
L-G	L-Glutamine
LMP	Low Melting Point

MCP	Monocyte chemotactic protein
MGM	Minimal growth medium
miR	MicroRNA
mmHg	Millimetres of mercury
MMP	Matrix metalloproteinase
MPa	Megapascal
MSC	Mesenchymal stromal cell
OSR	Open surgical repair
PBS	Phosphate buffered saline
PDGF	Platelet derived growth factor
PFA	Paraformaldehyde
PMN	Polymorphonuclear neutrophils
PSF	Pencillin / Streptomycin / Fungizone
RNA	Ribonucleic acid
ROS	Reactive oxygen species
S	Static culture
SASP	Senescence associated secretory phenotype
SDS	Sodium dodecyl sulphate
SDS-PAGE	Sodium dodecyl sulphate polyacrylamide gel electrophoresis
SFM	Serum free medium
SGM	Sub-maximal growth medium
SMC	Smooth muscle cell
SM-MHC	Smooth muscle-myosin heavy chain
TEMED	N,N,N',N'-Tetramethylethylene diamine
TIMP	Tissue inhibitor of metalloproteinase
TNF-α	Tumour necrosis factor alpha
TPA	12-O-tetradecanoylphorbol-13-acetate
UTS	Ultimate tensile strength
VEH	Vehicle treatment
α-SMA	Alpha-smooth muscle actin
ε_t	Transition strain

VIII. PROJECT SPECIFIC NOMENCLATURE

Throughout this document, several project specific terms are used for ease of readability. These terms are summarised in Table 1.1.

Table 1.1 Project specific nomenclature

Nomenclature	Meaning
S	Static organ culture in a 6-well plate
BIO	Dynamic *ex vivo* organ culture in the bioreactor
FRESH	Harvested tissue with no manipulation
VEH	Pre-treatment with vehicle control gel
CCE	Pre-treatment with gel containing combination of collagenase and elastase
EARLY	Cultured in the bioreactor for three days
END	Cultured in the bioreactor for twelve days

CHAPTER 1

INTRODUCTION

CHAPTER 1 INTRODUCTION

The aims of this project were: to develop an ex vivo model of AAA in a bioreactor and use the model to investigate the structure and function of the smooth muscle cell with respect to time.

Abdominal aortic aneurysm (AAA) is a disease prevalent in developed countries whereby the abdominal aorta gradually dilates via multifactorial biological processes until rupture. Patients are destined for surgery as there are no current pharmacological or therapeutic treatments. This chapter will examine: the epidemiology and risk factors; the current clinical management techniques; the biomechanics and histoarchitecture compared to healthy aortas; factors involved with aneurysm formation and progression with emphasis on the role of the smooth muscle cell; experimental aneurysm models in terms of animal species; the various methods to induce experimental AAA, and the limitations.

1.1. ABDOMINAL AORTIC ANEURYSMS

Abdominal aortic aneurysm (AAA) can be loosely described as an abnormal dilation which typically occurs in the abdominal aorta between the renal arteries and the iliac branches (Lippincott et al., 2009). It is a condition which affects the abdominal aorta whereby it dilates to greater than 3cm in diameter (approximately 150% of normal diameter), and is considered for elective prophylactic repair when it reaches a diameter greater than 5.5cm: the aneurysm must be large enough for the risk of rupture to exceed the perioperative mortality risk (Powell, 1998, BHF, 2008, Nordon et al., 2011). These are generally accepted thresholds, although definitions such as an aneurysm greater than 4cm and an infrarenal to suprarenal diameter ratio of 1.2 to 1.5 can also be observed (Golledge et al., 2006). Figure 1.1 shows the distortion of the aneurysmal artery in comparison to a healthy aorta.

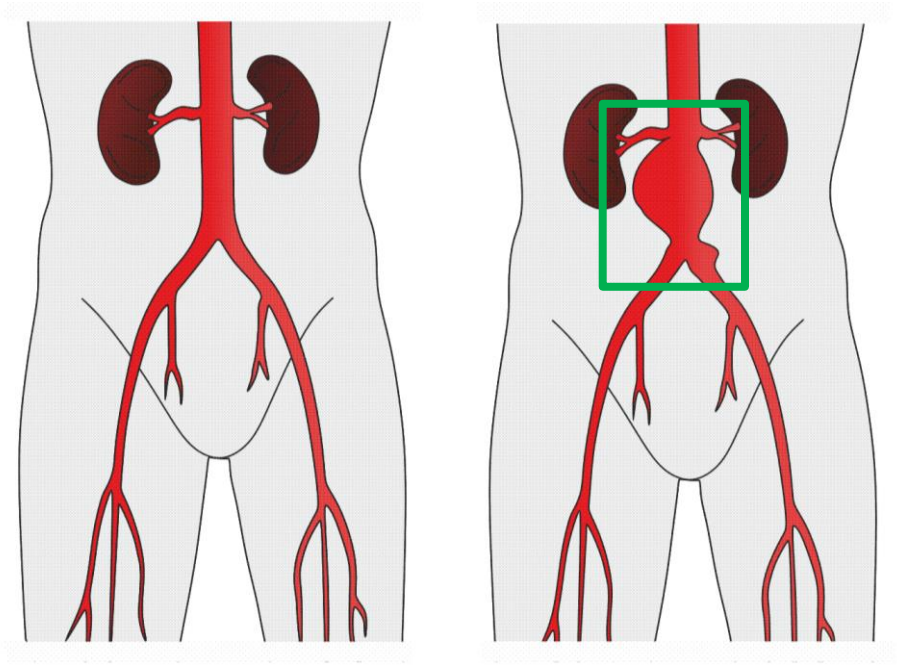

Figure 1.1 Cartoon of the abdominal aorta showing the morphology of left) a healthy aorta, and right) a dilated abdominal aorta indicative of AAA (highlighted in green).

1.2. EPIDEMIOLOGY

Regardless of the formal definition of an AAA, the major consequence if left untreated is aortic rupture resulting in massive internal bleeding due to the inability of the arterial wall to withstand the physiological force exerted by blood. Patients with AAA may experience vague symptoms of back pain or localised abdominal pain, but a vast majority of AAAs are asymptomatic until the point of rupture and diagnosis is often incidental when addressing other medical complaints (Sakalihasan et al., 2005). A ruptured AAA carries an extremely high mortality rate, which has been documented from a 65% mortality rate to as high as 80% for those who reach hospital overall (Sakalihasan et al., 2005, Jagadesham et al., 2008). Even undergoing emergency repair surgery does not bode well for the patient; 50% of those who will undergo emergency surgery for a ruptured aorta will die (Nordon et al., 2009).

The problem of AAA, especially in developed countries, is significant. It has been estimated that aneurysms are prevalent in approximately 5% of men over 65 years of age and an AAA rupture accounts for 1.5% of the total mortality in

males over 55 (Choke et al., 2005, Jagadesham et al., 2008, Michel et al., 2011, Nordon et al., 2011). Another estimate placed AAA as the tenth most common cause of mortality and responsible for approximately 2% of all deaths (Golledge et al., 2006). It has also been argued that the conservative estimates of mortality linked with AAA are hindered by low rates of post-mortems and that it is likely that some sudden deaths attributed to ruptured AAA are certified as cardiac deaths unless a pre-existing AAA was documented (Golledge et al., 2006).

The National Abdominal Aortic Aneurysm Screening Programme (NAAASP) was introduced to the UK in 2010 as an effective way to reduce AAA mortality after a pilot study in 2009 (Thompson et al., 2009). This AAA screening is currently targeted to men over the age of 65 and has been found to reduce the number of deaths related to AAA by half over 10 years (Benson et al., 2016). The screening programme offers the unprecedented opportunity to identify AAAs more often and earlier on in the development of the disease.

AAA disease is more common in men than in women (Anidjar and Kieffer, 1992, Jagadesham et al., 2008, Michel et al., 2011). Incidence rates have been estimated to be between 1.3% and 8.9% for men and 0.5% and 2.2% for women, or approximately six times greater in men than in women (Sakalihasan et al., 2005, Nordon et al., 2011, Svensjo et al., 2013). However, although AAA is rarer in women, they represent a higher mortality rate in comparison to men with increased growth rate, greater likelihood of rupture and rupture at a smaller diameter (Heller et al., 2000, Hultgren et al., 2007, Lo and Schermerhorn, 2016).

Unlike other cardiovascular diseases endemic in industrialised countries, in recent times the incidence of AAA is increasing; this may be due to improved detection as a result of screening regimes and therefore a greater diagnostic efficiency, or even due to improved mortality rates from other cardiovascular diseases (Anidjar and Kieffer, 1992, Golledge et al., 2006). However, the increase in age standardised mortality indicates a genuine increase in the incidence of AAA. For example, a Scottish study found that mortality rates from AAA increased 2.6-fold between 1981 and 2000 (Best et al., 2003). The ageing population of industrialised countries is likely to be a major contributor to this

fact, as the risk of developing AAA increases with age (Sakalihasan et al., 2005).

1.2.1. RISK FACTORS

Cigarette smoking is recognised as the strongest risk factor for AAA; Lederle *et al.* found that the association of ever smoking with aortic aneurysm is 2.5-fold greater than the association of ever smoking with coronary heart disease (Lederle et al., 2003). In another large study, smoking accounted for 75% of the excess prevalence of AAA greater than 4.0 cm (Perlstein and Lee, 2006). This may be due to the fact that cigarette smokers possess increased numbers of circulating markers of inflammation or the ability of cigarette smoke to oxidise α1-antitrypsin, a protease inhibitor (Perlstein and Lee, 2006, Michel et al., 2011). Protease inhibition and inflammatory markers will be examined in more detail later on in this chapter.

Ethnicity may have a role to play in the development of AAA; Afro-Caribbean ethnicity has been associated with decreased aneurysm susceptibility and there is evidence to suggest that AAAs are more commonly found in Caucasians than other races (Lederle et al., 1997, Golledge et al., 2006). AAA has also been linked with familial history of the disorder (Lederle et al., 1997, Sakalihasan et al., 2005, Golledge et al., 2006, Nordon et al., 2011).

The association of both familial history and ethnicity (inherent genetic factors) and smoking (an overtly environmental factor) with AAA indicates that there is likely to be an interplay between genetic predisposition and environmental factors in aneurysm formation. The Swedish Twin Registry has been used to analyse the role of hereditary and environmental factors. Of the 265 pairs of twins affected with AAA, genetic effects accounted for 70% and non-shared environmental effects for 30% of the phenotypic variance (Wahlgren et al., 2010). They found that there was no contribution of shared environmental effects.

1.3. TREATMENT OPTIONS FOR AAA

Although AAA is a major issue in developed countries, at present there are no approved therapeutic or pharmacological treatments for AAA. Prophylactic surgical intervention is the certified route, but only once the aneurysm has a diameter greater than 5.5 cm (Thompson et al., 2009, Benson et al., 2016). Open surgical repair (OSR) involves exposure of the abdominal aorta and replacement of the aneurysmal segment with a prosthetic graft (BHF, 2008). Figure 1.2 is an image of OSR for AAA.

Depending on the morphology of the aneurysm, and the patient's suitability for surgery, it may be possible to undergo endovascular aneurysm repair (EVAR). EVAR as an alternative to OSR was pioneered by Parodi (Parodi et al., 1991). It is a minimally invasive surgery involving insertion of a stent-anchored Dacron graft into the femoral arteries where it is passed through the circulatory system until it sits inside the aneurysm. It is then sutured to the proximal and distal necks of the non-aneurysmal aorta. This excludes the aneurysm from systemic blood pressure and thus prevents enlargement or rupture. Figure 1.3 shows the outcome of EVAR surgery.

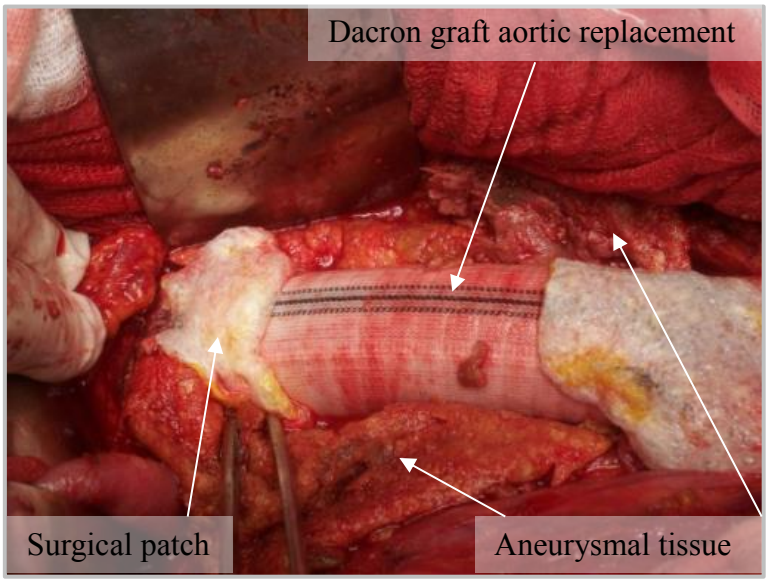

Figure 1.2 Open surgical repair of AAA. The prosthetic graft used to replace the aneurysmal aorta can clearly be seen. Image adapted from Bajardi et al. (2009) *CC BY 2.0*, with addition of labels and arrows.

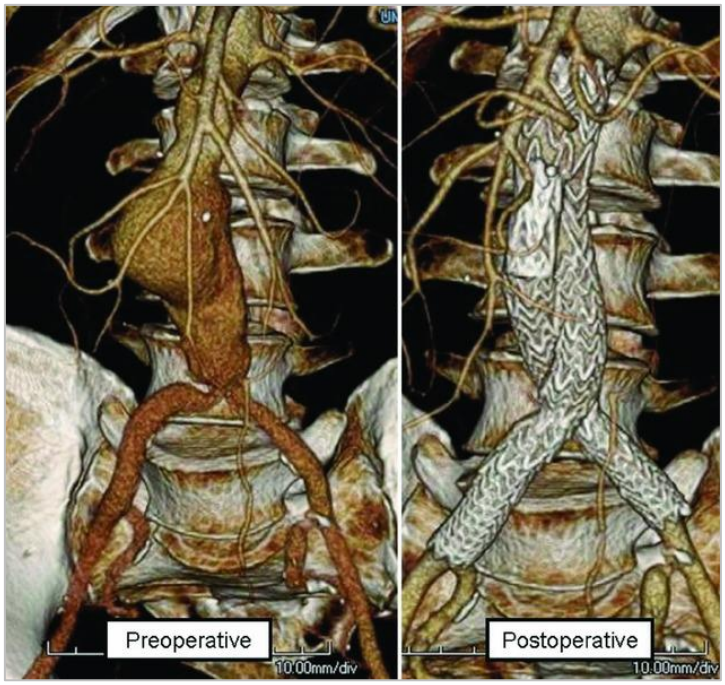

Figure 1.3 Left) Preoperative CT scan of an AAA with 3D reconstruction. Right) Postoperative scan showing endovascular stent within aneurysmal portion of artery. Image taken from Schanzer and Messina (2012), *CC BY 2.5*.

Both OSR and EVAR are major surgical operations, thus the benefits of undergoing prophylactic aneurysm repair surgery must outweigh the risk of surgery; this explains the 'cut-off point' of an arterial diameter greater than 5.5 cm for elective repair. The risk of rupture is less than 1% in patients who have

an AAA diameter of less than 5.5cm, although this markedly increases to a rupture risk as high as 33% once the AAA is above 7cm in diameter (Kent, 2014). Although the procedure is very effective, OSR has a mean 30-day mortality of over 5% in many countries, despite improvements in perioperative care (Nordon et al., 2011). EVAR patients have fewer complications and decreased intensive-care stay compared to patients undergoing OSR, but no difference was found between the treatment options for long term (greater than 2 years) mortality or AAA-related mortality (Nordon et al., 2011). EVAR also carries a risk of re-intervention of 20% at five years, usually as a result of the formation of 'endo-leaks' between the stent and the arterial wall (Golledge et al., 2006). Data from the European Collaborators on Stent/graft Techniques for Aortic aneurysm Repair (EUROSTAR) Registry show that following EVAR there remained a cumulative risk of rupture of 1% per year with a 2.1% risk of late conversion to OSR (Harris et al., 2000). Moreover, EVAR carries morphological contraindications; the most widely accepted is the requirement of a proximal neck either shorter than 15mm or absent (Sakalihasan et al., 2005).

Although AAA is only generally considered for surgical repair once it reaches a diameter greater than 5.5 cm, rupture can also occur in smaller aneurysms (Miller, 2002). A systematic review investigating the effect of small AAA on cardiovascular outcomes found that the death of 37 patients out of a total of 2323 (1.6%) was caused by rupture of small AAA (Bath et al., 2015). Perhaps more worrying was the high risk of cardiovascular death associated with small AAA (335 out of 2323 patients, 14.5%) which increased by 3% each year after diagnosis. There are no generally accepted guidelines for this patient group; only once the AAA has reached greater than 5.5 cm in diameter is preventative surgery considered an option. This maximum diameter criterion has drawn some criticism as it is a blanket 'one size fits all' parameter. There is research into a more reliable rupture risk predictors such as geometry and peak wall stress estimates which are more patient specific parameters (Kontopodis et al., 2016).

Increasing understanding of the cellular and molecular processes involved in the pathogenesis of AAA will enable vulnerability to rupture to be detected through a less crude method, potentially utilising biomarkers in the body as a

predication of oncoming rupture whereupon the patient will undergo prophylactic repair (Hellenthal et al., 2009a), reviewed in (Wanhainen et al., 2016).

Surgery is still the sole option offered to AAA patients; there are no approved alternative pharmacological or therapeutic treatments. Patients – in particular elderly patients – may be deemed unsuitable for surgery due to medical co-morbidity and in these cases there are no forms of effective treatment. For example, out of 251 AAA patients admitted to a specialist vascular unit, 32 (13%) were deemed unsuitable for surgical intervention (Karthikesalingam et al., 2011). Lim *et al.* reported that 59 out of 334 patients (18%) were not able to have intervention within 3 months (Lim et al., 2015). In these cases, it is simply a matter of time until rupture or unrelated death of the patient. However, the advent of a nationwide AAA screening programme offered to at-risk individuals offers the opportunity to detect and diagnose AAAs at an earlier stage. This may reveal stages of the disease where it may be appropriate to intervene with therapeutics or pharmacological treatments which have not previously been identified.

There is also evidence from animal models that anti-inflammatory and immunosuppressive drugs may limit the expansion of AAAs, but as the cellular and molecular targets are unknown, research is still ongoing into non-surgical treatments for AAA (Jagadesham et al., 2008, Davis et al., 2014).

1.4. ARTERIAL ANATOMY

Arteries consist of three well-organised connective tissue layers; the *tunica intima*, the *tunica media* and the *tunica adventitia* as shown in Figure 1.4 and Figure 1.5. The intima lies in proximity to the lumen of the artery. It consists of an endothelium, a single layer of cells lying in direct contact with the blood, and a small amount of subendothelial connective tissue. The media is the middle layer and is the thickest of the layers found within the arterial wall. It is this layer which provides the structural support, vasoreactivity and elasticity of the vessel. The main body of the media comprises of alternating layers of elastic

fibres and smooth muscle cells arranged circumferentially. The outermost layer is the adventitia which is the most robust of all the layers. It consists of longitudinally arranged connective tissue fibres of both elastin and collagen and connective tissue cells such as fibroblasts. (Singh, 2008, D'Souza, 2009).

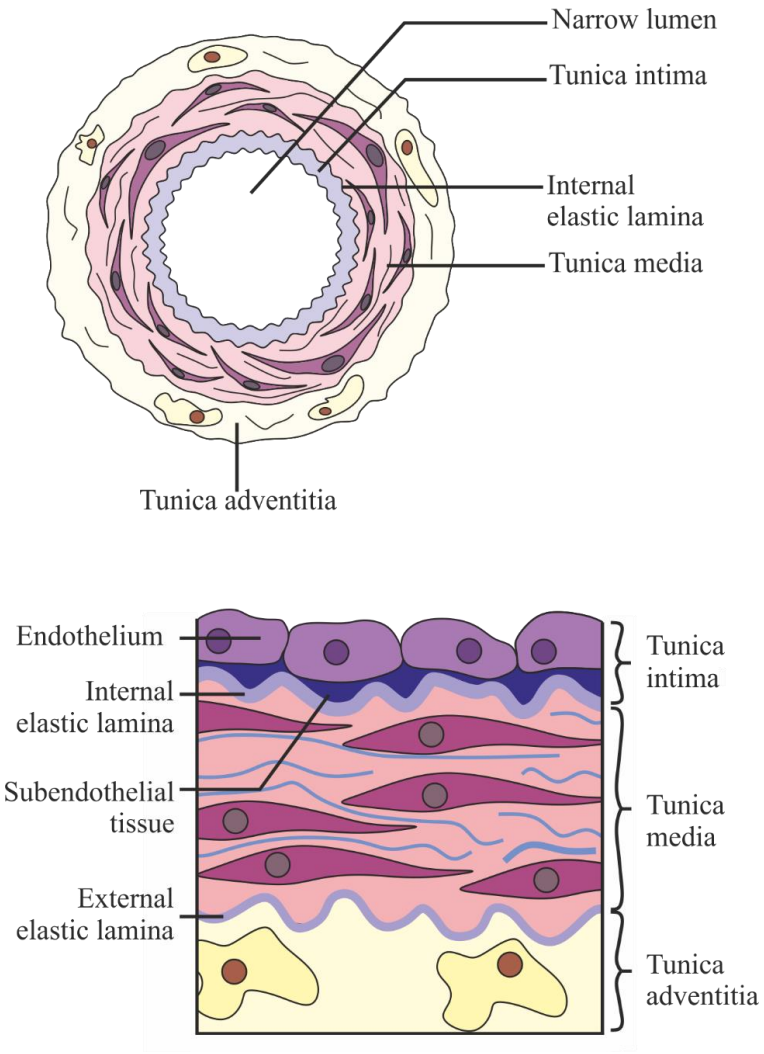

Figure 1.4 Schematic of healthy arterial wall and its components. Top: cross section of arterial wall. Bottom: zoomed in section of arterial wall layers.

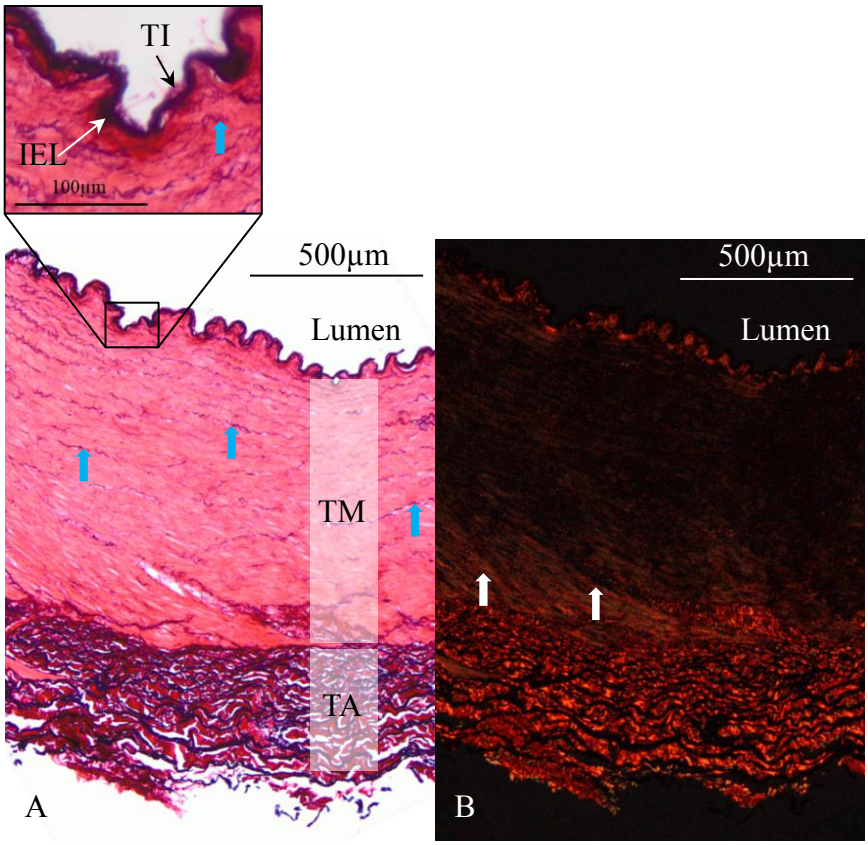

Figure 1.5 Arterial anatomy (porcine carotid artery) - histological staining of healthy arterial wall. IEL = internal elastic lamina (purple stain), TI = tunica intima, TM= tunica media, TA = tunica adventitia. A) Sirius red with Miller's elastin co-stain. Elastin fibres are shown blue-purple and are ordered throughout the wall. B) Sirius red with Miller's elastin co-stain viewed under polarised light. Collagen fibres (white arrows) are birefringent and are red, green or yellow depending on the orientation of the fibres in relation to the polarising filter.

In carotid arteries, used throughout this study and shown in Figure 1.5, there is no real distinction of the intima; it is simply a single cell layer of endothelial cells. The elastic fibres in the tunica media (as seen in purple in Figure 1.5, blue arrows) allow the artery to possess arterial compliance; the artery is able to expand during systole storing elastic energy and then recoil during diastole, releasing the stored energy back into the blood stream, thus transporting the blood through the vasculature. This affects the pressure of the blood throughout the cardiovascular system. In addition to elastin, the majority of the extracellular matrix (ECM) in the aorta is comprised of Type I collagen (as seen in red in

Figure 1.5, white arrows). Smooth muscle cells (SMCs) form the majority of the cellular components and perform both mechanical (e.g. contractile) and synthetic (e.g. ECM) functions. The elastin fibres of the ECM allow passive arterial regulation, whilst the contraction of SMCs is an active component. By periodically relaxing and contracting, the luminal diameter can be controlled thus enabling arteries to maintain appropriate pressure levels throughout the vasculature (Rensen et al., 2007). SMC contraction is initiated by a calcium (Ca^{2+}) dependent phosphorylation of light chain myosin, often triggered by mechanical stretch due to transmural blood pressure (Webb, 2003). In addition to active vasoregulation, SMCs are responsible for the production of the structural proteins in the ECM, and, in addition, are capable of secreting cytokines to recruit other cell types. They also play an important role in vascular remodelling; SMCs are also able to express ECM degrading enzymes (Curci, 2009). This is discussed in detail in Section 1.7.1.

1.5. CHARACTERISTICS OF AAA

1.5.1. HISTOLOGICAL MARKERS

The development of AAA is intrinsically linked to alterations in the connective tissues and cells within the arterial wall. The compliant and viscoelastic properties of the aorta are attributed to the elastin fibres (Figure 1.5), whereas type I and type III collagen provide the tensile strength and maintain the integrity of the aortic wall (Sakalihasan et al., 2005, Shimizu et al., 2006). AAAs are characterised by severe elastin fragmentation and loss of smooth muscle cells (SMCs), as well as chronic inflammation of the adventitia and media (He and Roach, 1994, Henderson et al., 1999, Shimizu et al., 2006). These studies utilised human tissue that had been taken at autopsy or during elective repair of the aorta, and so are only indicative of the state of the tissue at end-stage aneurysm disease. However, perfusion of mouse aortas with elastase will also induce AAAs with these same histological markers within 14 days (Pyo et al., 2000). This characteristic loss of elastin is shown in Figure 1.6.

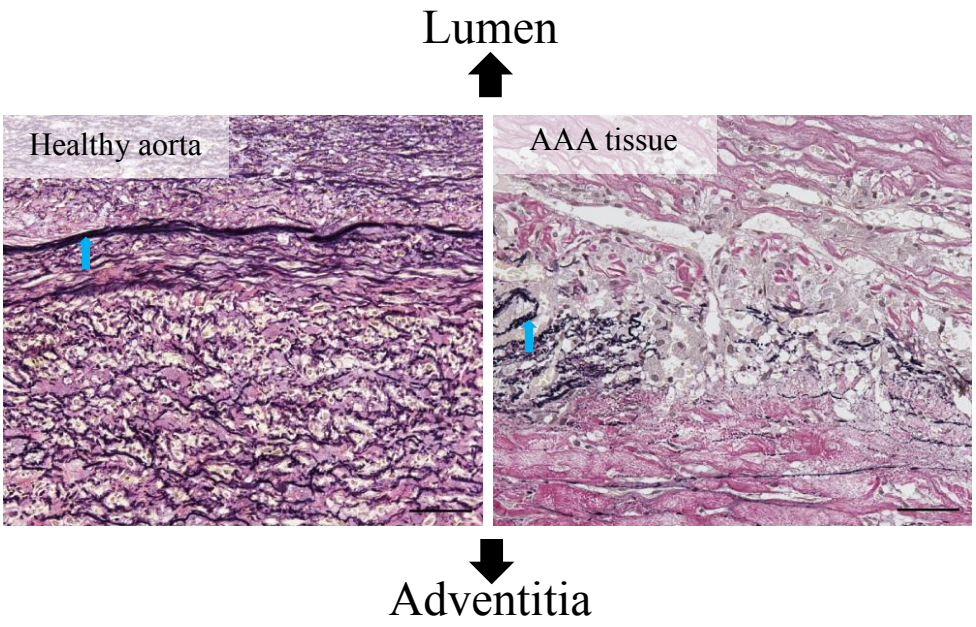

Figure 1.6 Elastin von Gieson staining of intima/media in A) normal aorta and B) AAA wall showing elastin loss in AAA compared to healthy aorta. Elastin fibres are stained purple/black (blue arrows). Scale bar = 50µm. Image adapted from Sano et al. (2014), CC BY 4.0 with additional cropping, rearranging and relabelling.

Healthy aortic media comprises of elastin lamellar units interspersed with SMCs, collagen and ground substance (non-fibre component of the ECM, comprised primarily of water, glycosoaminoglycans and proteoglycans) whereas the structure of the aortic media is disrupted in aneurysmal tissue (Figure 1.6).

This loss of elastin has been quantified in aneurysmal aortas; scarce and disrupted elastic tissue in comparison to healthy controls was observed. The elastin content in the media of tissues taken from AAAs was found to be 8.1% ± 3.2% (n=11) of the dry, defatted weight; a sharp contrast to that of healthy aortic media: 35.0% ± 3.2% (Campa et al., 1987). Studies consistently agree on severe elastin deficiency in AAAs, but there are inconsistencies in reports of collagen content in aneurysmal tissue. One of the seminal early studies found AAA tissue to be deficient in collagen (Sumner et al., 1970). A subsequent study found collagen concentration between normal, AAA and atherosclerotic occlusive aortas to be indistinguishable and another comparison of the

connective tissue matrix in control vs. AAA aortas found that the collagen content was unaltered between the two (Dubick et al., 1988, Gandhi et al., 1994). On the other hand, an early study found that collagen content was significantly increased from 24% ± 5% in healthy aortas to 37% ± 16% in AAA tissue and this has since become the accepted view (Rizzo et al., 1989). A more recent study aiming to link clinical characteristics with histological features, including levels of extracellular matrix proteins found that there was increased collagen content in both electively repaired and ruptured AAAs (Hellenthal et al., 2009c). The structure of the collagen in AAA has been reported to be disordered with a marked decrease in the 'waviness' associated with physiological collagen fibre crimping leading to conclusions that in AAA the collagen fibres did not act as a coherent network (Gandhi et al., 1994). It is also reported that the collagen network in AAA had 350% of the levels of cross-linking of non-aneurysmal aorta, leading to suggestions that collagen accumulates in aneurysmal walls via cross-linking whilst new collagen synthesis is defective (Carmo et al., 2002).

It is not only the extracellular connective tissues of the aortic wall which were found to be abnormal in AAAs; a marked decrease in the number of SMCs in the media has also been widely observed. One study discovered that AAAs lacked the orderly structure of elastic laminae seen in healthy aortic media and demonstrated disorganisation of remaining SMCs. A cell count also revealed an average 44% (range 25% to 60%) reduction in SMC density in AAA tissue (n=29) compared to healthy controls (n=5) (Henderson et al., 1999).

Inflammatory cell infiltrations are also observed in abundant quantities in all layers of the aneurysmal arterial wall (Shimizu et al., 2006, Hellenthal et al., 2009b). This will be discussed in detail in Section 1.7.4.

1.5.2. BIOMECHANICAL BEHAVIOUR

Aortic rupture is the ultimate catastrophic outcome without surgical intervention and this is a biomechanical failure of the aortic wall which occurs when haemodynamic stresses overcome the tissue strength. The SMCs, found

in abundance in the aortic media, define the active mechanical properties of the aorta by their contraction mechanism used to pump blood. The ECM acts as the passive component. The ECM is comprised of two major proteins: elastin, characterised as compliant and eponymously elastic, and collagen, generally stiffer and more robust (Raghavan et al., 1996).

1.5.2.1. ARTERIAL BIOMECHANICS

Elastin enables the large arteries of the body to not only expand during ventricular contraction in order to accommodate the surge of blood from the heart, but also to impart recoil to the arterial wall. It is comprised of soluble tropoelastin monomers cross-linked by lysine residues, rendering the protein as a whole insoluble with a half-life of approximately 40 to 70 years (Rucker and Tinker, 1977, Shah, 1997). Elastin fibres possess an elastic modulus of approximately 0.6 MPa and the ability to stretch as much as 70% of the original length (Lasheras, 2007).

Collagen, in its various forms, is ubiquitous in the connective tissue of the body. In the aorta, Type I collagen is the most abundant with Type III collagen following this, with a ratio of about 70:30 (Rizzo et al., 1989). Polypeptide chains of collagen form into a stable triple helix structure which is only able to stretch 2 – 4% of its original, uncoiled length (Goodall et al., 2002a). Collagen fibres uncoil during loading, and only begin to bear such loads once the fibres have straightened and have been recruited for load-bearing (Sumner et al., 1970, Thubrikar et al., 2001).

The degradation of elastin fibres has been linked with the initiation and expansion of AAAs whereas the ultimate failure of the arterial wall, resulting in arterial rupture, is associated with collagen (Dobrin and Mrkvicka, 1994, Petersen et al., 2002).

Early studies linked these two proteins of the extracellular matrix with the characteristic J-shape stress-strain curves seen in healthy arterial tissue (Roach and Burton, 1957, Sumner et al., 1970, Vaishnav et al., 1972). A schematic of

such a curve can be seen in Figure 1.7. The vessel is compliant at low strains and gradually becomes stiffer as strain increases.

A modified Maxwell model can be used to demonstrate the physiological contributions of the ECM components and the SMCs to the arterial biomechanics which explains this characteristic biphasic behaviour (Bank et al., 1996). A schematic of the model is shown in Figure 1.8. This model highlights the strain-dependent elasticity initiated either by external strain (such as blood pressure) or by contraction of SMCs. The elastin and the parallel collagen component represent the elastic behaviour of the arterial wall when the SMCs are completely relaxed. At low strains, elastin governs the biomechanical behaviour. At increased strains, the collagen is gradually recruited into load-bearing hence increasing the stiffness of the tissue (illustrated in Figure 1.8 with a hook mechanism). The series collagen component also represents the increasing stiffness of the tissue with regards to SMC contraction (Bank et al., 1996).

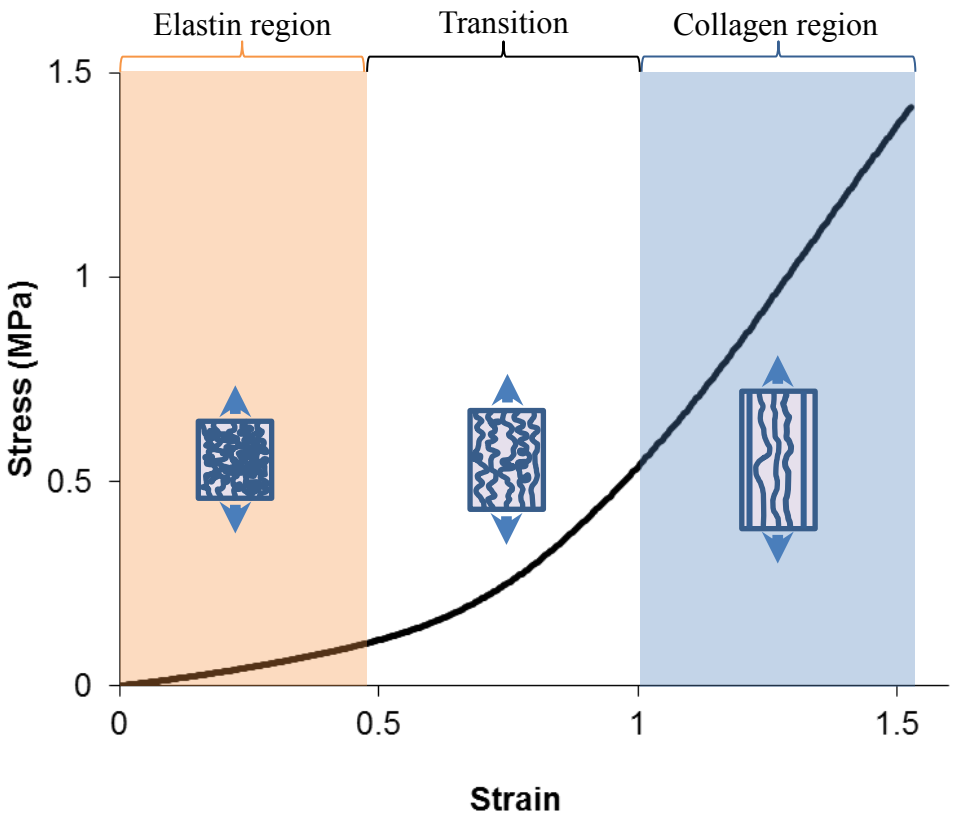

Figure 1.7 Schematic of a J-curve stress-strain graph of a healthy aorta. Collagen fibres are recruited into load bearing via uncoiling due to stretch.

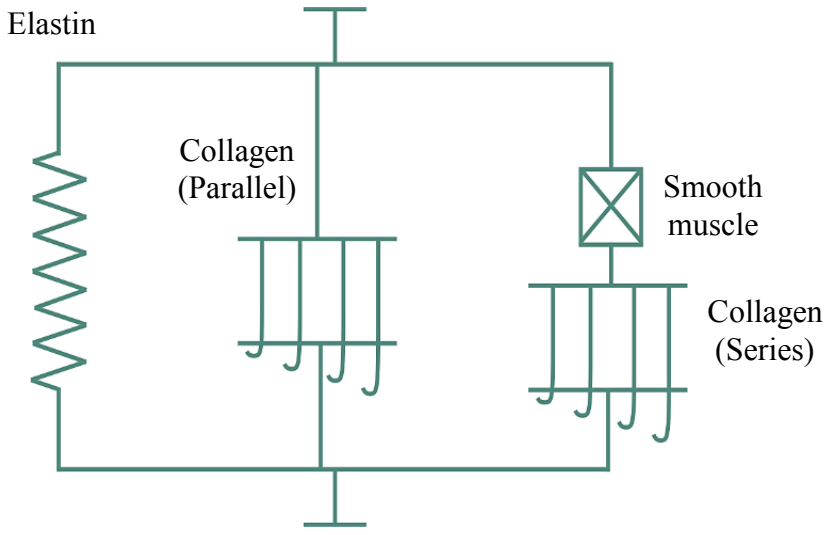

Figure 1.8 Modified Maxwell model of smooth muscle and ECM components. Maxwell and Voigt models have been combined to represent the series and parallel components (Bank et al., 1996).

Arterial tissue, much like many soft tissues in the body, shows anisotropic behaviour as the fibres which constitute the ECM are organised in preferred directions. The collagen fibres that are recruited under higher strains are anisotropically arranged (Roach and Burton, 1957, Holzapfel, 2001, Gasser et al., 2006).

Selective enzymatic digestion of arterial ECM components revealed more about their role in arterial biomechanics. One study involved selective digestion of both elastin and collagen in canine carotid and human iliac arteries and then subjected them to *ex vivo* pressure-dilation studies (Dobrin et al., 1984). Elastase treated arteries showed an increase in vessel dilation and reduction in arterial compliance. Conversely, collagenase treated arteries showed increased arterial compliance but were weaker: all collagenase treated arteries ruptured within the 150 mmHg pressure range. The authors concluded that arterial integrity was dependent on collagen only, with elastin governing the characteristic compliant behaviour. Collagenolytic studies in arteries have determined that arterial strength is inversely correlated to degree of collagen degradation (Dadgar et al., 1997). It has also been shown that arteries with elastin degradation had increased stiffness due to the earlier recruitment of collagen fibres in load bearing regimes and an increase in arterial diameter at zero-load indicating the existence of compressive pre-stresses within the arterial wall (Fonck et al., 2007).

1.5.2.2. BIOMECHANICS OF AAA TISSUE

Uniaxial tensile testing has been widely used to characterise the biomechanical behaviour of AAA tissue as it is a disease characterised by changes to the ECM (and therefore the biomechanics). It carries an inevitable endpoint of aortic rupture: mechanical failure of the arterial wall due to its inability to withstand physiological forces.

One of the earliest papers to characterise AAA tissue biomechanics using uniaxial tensile testing at 8.5%/min strain rate found that the yield strength (σ_y) and ultimate strength (σ_u) were significantly decreased in aneurysmal tissue: σ_y

= 121.0±32.8 N/cm^2 vs. σ_y = 65.2±9.5 N/cm^2, σ_u = 201.4±39.4 N/cm^2 vs. σ_u = 86.4±10.2 N/cm^2 ($p<0.0005$) for healthy and aneurysmal abdominal aortae, respectively (He and Roach, 1994). Aneurysmal aortas were found to be stiffer and less compliant in the longitudinal orientation in comparison to healthy aortas; this was attributed to the characteristic loss of elastin in the AAA tissue.

It is difficult to define a consistent uniaxial tensile testing method applied across the literature. Documented strain rates have been defined variously as 0.2 mm/min (He and Roach, 1994), 10 mm/min (Duprey et al., 2010), 2 mm/min (Kobielarz and Jankowski, 2013), 30%/min (Raghavan et al., 2006), 8.5%/min (Di Martino et al., 2006). Strain rate has been shown to have an effect on the measured mechanical properties of arterial tissue. It has been shown using uniaxial tensile testing on human thoracic aortae that the ultimate tensile stress increased 2-fold in dynamic (80 – 100 s^{-1}) tests compared to quasi-static tests (0.01 – 0.07 s^{-1}) (Mohan and Melvin, 1982). This study also demonstrated that the tissue behaved in a more anisotropic manner at high strain rates – the tissue was virtually anisotropic at low strain rates. Another study also showed that ultimate tensile stress increased with increasing loading rate, demonstrating the inherent viscoelasticity of arterial tissue (Stemper et al., 2007a). However, a study in fresh human cerebral blood vessels found no such strain rate dependence over a strain rate range of four orders of magnitude (Monson et al., 2003). An absence of strain rate dependence in both the stiffness and failure stress of porcine thoracic aortae has also been documented (Miroslav et al., 2009). The mechanical properties measured using uniaxial tensile testing must therefore be considered in the context of the test method as a consensus on strain rate dependence for arterial tissue has not yet been reached.

Uniaxial testing on AAA tissue in varying orientations concluded that aneurysms possessed greater stiffness in the circumferential direction than longitudinally, and so should not be considered to demonstrate isotropic behaviour (Thubrikar et al., 2001). This was expanded upon when a more complex biaxial mechanical evaluation of AAA tissue was performed (Geest et al., 2006). The circumferential stiffness was found to be significantly increased in AAA tissue in comparison to age-matched healthy aortic tissue, which

indicated a higher degree of anisotropic behaviour. The authors concluded that aneurysmal degradation is associated with an increase in mechanical anisotropy, with preferential circumferential stiffening due to loss of elastin in AAA tissue. Biomechanical differences have been documented between electively repaired and ruptured AAA tissue: it was found that ruptured AAAs were significantly weaker in spite of being thicker (Di Martino et al., 2006).

Advances in biomedical imaging techniques have enabled *in vivo* measurement of AAA biomechanics. An ultrasound phase-locked echo-tracking system was used to measure the diameter of healthy abdominal aortas during systole and diastole, hence deriving the arterial compliance in the aneurysm (Lanne et al., 1992). The age range of the subjects was 5 to 71 years old and they concluded that the stiffness of the artery increased exponentially with age. Using an alternative method, computed tomography (CT) scanning was used to determine the aortic distensibility of 67 patients with AAAs (Ganten et al., 2008). Distensibility is a measure of the arterial ability to expand and contract and is therefore related to stiffness measured during uniaxial tensile testing. Mirroring the reports of increased stiffness in AAAs arising from uniaxial tensile testing studies, they reported that the distensibility of AAAs were significantly lower than in the proximal non-aneurysmal aorta and that there was no correlation with AAA size. The authors suggested that the fact that the distensibility of both small and large AAAs were indistinguishable may indicate that this reduced distensibility (and hence increased stiffness) is an early event in AAA development. These findings are comparable to a study which also reported reduced distensibility in AAA tissue and no correlation between distensibility and diameter (Molacek et al., 2011). A follow-up study of 61 AAA patients from a previous study in 1998 reported that the AAA elasticity (as measured by ultrasound) showed positive correlation with the annual AAA expansion rate (Hoegh and Lindholt, 2009).

1.6. ATHEROSCLEROSIS AND AAA

Historically, atherosclerosis was considered to be a cause of AAA. However, in more recent years, there is considerable debate as to whether the relationship between atherosclerosis and aortic aneurysm is causal or whether the two forms of vascular remodelling simply share common risk factors. Golledge and Norman outlined the three philosophies regarding this relationship. Firstly, patients who are afflicted with an AAA are likely to also have atherosclerosis so it is postulated that atherosclerosis plays a causative role. Secondly, various shared genetic and environmental risk factors are causal in the development of both atherosclerosis and AAA but the two mechanisms are distinct and independent. The third theory is a combination of the previous two; either AAA or atherosclerosis can develop first and then promote the development of the other (Golledge and Norman, 2010).

Although patients with AAA are likely to also suffer from atherosclerosis, not all patients with atherosclerosis go on to develop an aneurysm; in fact only 9% to 16%, of patients with atherosclerotic abdominal aortas develop an AAA (Shimizu et al., 2006). At present, there is fervent discussion as to whether some sort of defining mechanism between AAA and atherosclerosis exists. The Tromsø study, with a large sample size (n=6446) recently found that atherosclerosis was more common in patients with AAA and that it was an independent risk marker for AAA, but could not conclude as to whether atherosclerosis played a causative role (Johnsen et al., 2010).

A paradox that has recently emerged is the relationship of AAA and atherosclerosis with diabetes. Diabetes is a risk factor for cardiovascular disease but there has been an increasingly large amount of evidence that there is, in fact, a negative association with AAA whilst it delivers the opposite effect with atherosclerosis (Shantikumar et al., 2010, Lederle, 2012, Pafili et al., 2015). Although more investigation is required with regards to the exact biological mechanism, this paradox provides strong evidence that aneurysmal and atherosclerotic disease are separate diseases with separate aetiologies, though they may exacerbate each other. The ineffectiveness of pharmacological agents commonly used to treat atherosclerosis in treating AAA also suggests that

differing biological mechanisms are involved (Ferguson et al., 2010, Golledge and Norman, 2010).

1.7. AAA PATHOPHYSIOLOGY

As previously discussed in section 1.4.1, one of the defining markers of AAA is severe elastin degradation in the aortic media. Elastin possesses an extremely long half-life of anywhere from 40 to 70 years and so is a highly stable ECM protein. The loss of elastin in AAA tissue is therefore almost certainly due to active elastolytic processes rather than insufficient synthesis or natural passive degradation (Thompson et al., 1995, Shah, 1997, Shimizu et al., 2006). In basic terms, AAA pathophysiology can be divided into several separate, yet inextricably linked, processes. Characteristics and physiology of aneurysmal arterial wall are shown in Figure 1.9. The subsequent sections of this chapter will examine the biological and mechanical mechanisms underlying AAA disease.

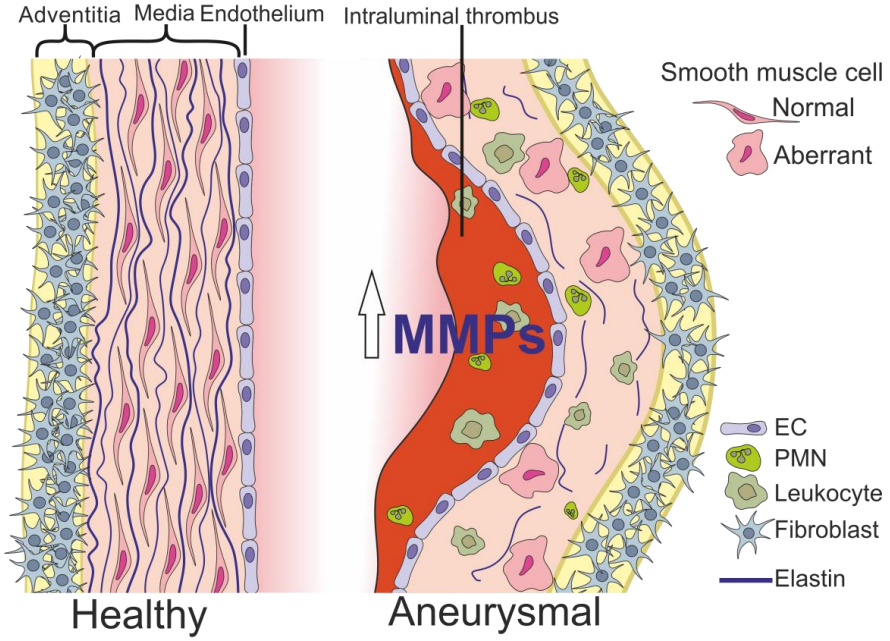

Figure 1.9 Diagram of changes in AAA wall compared to healthy artery. MMPs = matrix metalloproteinases, SMC = smooth muscle cell, PMN = polymorphonuclear neutrophils. The media thickens in AAA compared to healthy arterial wall and AAA are often found with intra-luminal thrombus (red) present.

1.7.1. EXTRACELLULAR MATRIX DEGRADATION

The number one culprit responsible for the ECM degradation in AAA tissue is a family of endopeptidases known as matrix metallo-proteinases (MMPs). MMPs are vital in normal body function for organ development, wound healing and necessary protein remodelling, but can also contribute to various pathological remodelling mechanisms (Galis and Khatri, 2002).

Various members of the MMP family have previously been identified in the aneurysmal aorta, including MMP-2 (gelatinase A), MMP-9 (gelatinase B), MMP-3 (stromelysin), MMP-1, MMP-7, MMP-12 and MMP-13 (Shah, 1997, Lijnen, 2001, Fontaine et al., 2002, Wilson et al., 2008).

A study to determine the role of 92kD gelatinase-B (MMP-9) in the formation of AAA, with atherosclerotic occlusive (AO) and healthy controls found that conditioned medium from AAA tissue in organ culture consistently secreted prominent proteolytic activity in comparison to AO and healthy tissue. AAA tissue produced 10.5-fold and AO tissue produced 5.9-fold the level of MMP-9 versus normal tissue (Thompson et al., 1995). It must be noted that MMP-9 is a prominent elastolytic enzyme, so this finding is supported by the severe elastin degradation observed in AAA tissue.

Furthermore, an *in vivo* study investigated the levels of MMP-9 in the serum levels of AAA patients. Again, it was found AAA patients had increased levels of this enzyme in comparison to AO and normal patients. Severely elevated levels were found in 48% of AAA patients in comparison to 7% of AO patients. These elevated levels decreased by 92.7%±3.2% following surgical AAA repair, indicating a relationship between expanding AAAs and MMP-9 levels (Hovsepian et al., 2000).

Both of these studies used tissue where an aneurysm had already manifested, and so was at end-stage disease. Therefore, the role of MMP-9 in initial causation of human AAA disease cannot be determined from these cases. The role of MMP-9 in AAA formation has been investigated in animals using a genetically modified mouse model with targeted MMP-9 and MMP-12 deficiency. Elastase perfusion in wild-type mice induced AAAs in 91% of

cases, whereas the aortic diameter in MMP-9 only and MMP-9 with MMP-12 deficient animals was markedly reduced at 7 days and 14 days after perfusion. MMP-12 deficient only mice exhibited a similar increase in aortic diameter to wild-type mice (Pyo et al., 2000). The authors concluded that their observations showed evidence that MMP-9 is required for AAA development.

Biopsies of human AAAs revealed that expression of MMP-2 was predominant in smaller, earlier AAAs, and MMP-9 became more prevalent once aortic diameter had further increased (Freestone et al., 1995). A positive correlation has been documented with regards to MMP-9 expression and aortic diameter (McMillan et al., 1997). Elevated serum levels of MMP-1 and MMP-9 in AAA patients was associated with imminent aortic rupture (Wilson et al., 2008). However, a large cohort study of AAA patients (n=987) found that MMP-9 serum levels in AAA patients failed to serve as a potential biomarker for AAA (Eugster et al., 2005).

MMPs are secreted by SMCs as a normal physiological remodelling process. However, other cell types are implicated in MMP expression in AAAs. Firstly, adventitial mast cells (involved in innate and adaptive immunity) have been shown to contribute towards progression of AAAs. Significantly increased number of mast cells have been found in human AAA tissue showing a positive relationship between number and AAA diameter (Tsuruda et al., 2008). Additionally, mast cell deficient rats did not develop AAA using a standard calcium chloride ($CaCl_2$) animal model. Secondly, mesenchymal stromal cells (MSCs) have been implicated in AAA progression through impaired immunomodulatory activity and MMP-9 secretion (Ciavarella et al., 2015). MSCs were isolated from AAA tissue and were shown to have a 400-fold increased expression of MMP-9 compared to MSCs from healthy controls. Finally, MMP-9 is readily secreted by infiltrating macrophages in AAA tissue which exhibited a 10-fold increased MMP-9 expression compared to normal aorta. This was entirely localised to the numerous macrophages in the tissue (Thompson et al., 1995)

The evidence seems to suggest that elevated levels of ECM-degrading MMPs are responsible for the formation, expansion and rupture of AAAs. In addition

to this, the enzyme inhibitors are compromised. Tissue inhibitors of metalloproteinases (TIMPs) have been found to be reduced in AAA tissue, in both human and genetically modified animal studies (Brophy et al., 1991, Basu et al., 2011). Elevated levels of MMPs are therefore not strictly necessary for AAA formation; simply the lack of MMP inhibitors may be sufficient.

A study of 36 men with small AAAs found that MMP-9 serum levels were significantly associated with AAA size ($p=0.04$) and expansion $p=(0.01)$, but overall MMP levels and an MMP:TIMP ratio did not predict either (Lindholt et al., 2000). In contrast, a later study did not find a correlation between AAA expansion and serum MMP-9 levels in a study of 208 small aneurysm patients (Karlsson et al., 2009). Contrasting clinical evidence indicates that the specific role of MMPs and TIMPs *in vivo* must still be investigated further.

MMPs can also be activated via a biological cascade emanating from plasmin activators. Plasmin, either generated from urokinase-type (u-PA) or tissue-type plasminogen activator (t-PA), is an enzyme that primarily plays a role in fibrinolysis, and has been implicated in the formation of AAAs (Carmeliet et al., 1997). Although plasmin possesses a limited elastolytic capability, and so is not directly implicated in the severe elastin degradation in AAAs, it is the role that it plays in MMP activation which may lead to AAA formation. A study using a genetically modified mouse model demonstrated that u-PA activated MMPs that led to aneurysm formation (Carmeliet et al., 1997). In a rat xenograft model, it was found that aneurysm formation was prevented when a plasminogen activator inhibitor is over-expressed (Allaire et al., 1998).

Collagen degradation occurs simultaneously to this pathological elastolysis. The degradation of collagen is mitigated by an increase in collagen synthesis during early AAA formation suggesting some sort of stabilising repair process (Shimizu et al., 2006). During later stages of AAA development, this collagen synthesis is outstripped by the rate of collagen degradation by proteolysis, instigating rupture; elevated levels of MMP-1, a collagenase, are associated with rupture and mortality (Wilson et al., 2008).

1.7.2. ROLE OF THE INTRA-LUMINAL THROMBUS

In many cases, the blood flow is maintained in AAA formation because a mural thrombus develops. This maintains the lumen at normal diameter, in spite of the fact that the total aortic diameter is greatly increased. Fontaine *et al.* provided evidence that polymorphonuclear neutrophils (PMN) (an immune response cell) were found in greater abundance in the mural thrombus than in the aneurysmal arterial wall. It was shown that PMNs were implemented in 'trapping' and storing MMP-9 in the thrombus and also that plasminogen and u-PA were present (Fontaine et al., 2002). This could possibly cause activation of large amounts of plasmin which, as has previously been discussed in section 1.6.1, may activate ECM degrading MMPs. Samples used in that study were, however, taken from elective AAA repair and so could only give a picture of the disease at end-stage.

This study also demonstrated *in vitro* that spontaneous thrombosis in human blood released pro-matrixmetalloproteinase-9 (pro MMP-9) into the serum, at levels four-fold higher than control plasma. When pro MMP-9 is activated, it becomes a potent gelatinase and so is associated with the ECM degradation that is characteristic of AAA disease.

1.7.3. OXIDATIVE STRESS

Oxidative stress is the process whereby tissue damage occurs due to increased production or decreased destruction of reactive oxygen species (ROS) (McCormick et al., 2007). These species can include hydrogen peroxide (H_2O_2), superoxides (O_2^-) and hydroxyl radicals ($^{\bullet}OH$) (Satoh et al., 2011). The levels of ROS in AAA tissue have been compared with matched healthy aortic specimens; the data suggest that ROS are increased in AAAs (McCormick et al., 2007). This, however, does not determine whether increased ROS levels are solely found in localized AAA or are found globally throughout the vasculature of the AAA patient.

A later study measured ROS levels in AAA tissues and compared these to non-aneurysmal aortic adjacent aortic segments (Miller et al., 2002). It was found that levels of ROS – and therefore also oxidative stress – were 2.5-fold higher in AAA tissue than in the non-aneurysmal adjacent segments. Again, the problem emerges that the tissues used in this experiment were taken from patients at elective repair, and so only represented the state of the tissue at end-stage disease. Therefore no conclusions can be drawn regarding the role of ROS in AAA formation or early development. Figure 1.10 presents some of the mechanisms by which ROS has the potential to augment aneurysm formation.

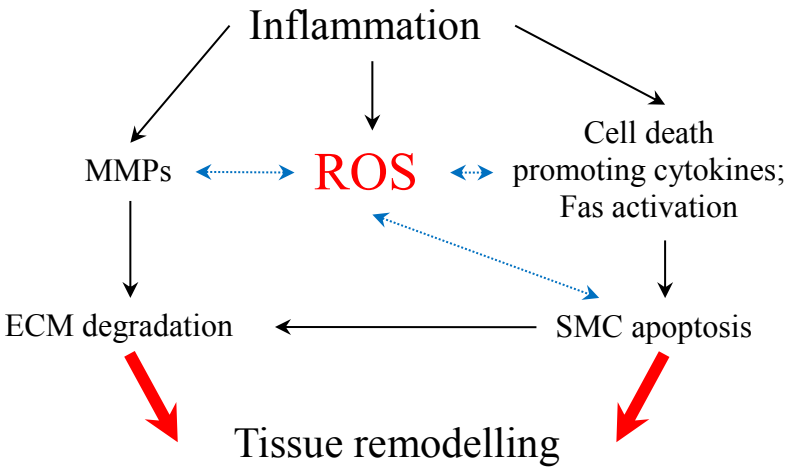

Figure 1.10 Interactive pathways of possible promotion of aneurysm formation. ROS = reactive oxygen species. Blue arrows denote aneurysmal promotion effects of ROS.

1.7.4. INFLAMMATION

Immune response cells involved in the inflammatory process are also found in abundance in AAA tissue (Shimizu et al., 2006, Hellenthal et al., 2009b). Figure 1.11 shows typical AAA histology and highlights the presence of these inflammatory cells.

These dense localisations of inflammatory cells occur more frequently and abundantly in AAA tissue than in normal or stenosed atherosclerotic arteries (Koch et al., 1990). B-cells are only very rarely found in atherosclerotic aortae,

whereas local depositions of immunoglobulin, secreted by B-cells, are frequently observed in AAAs (Shimizu et al., 2006).

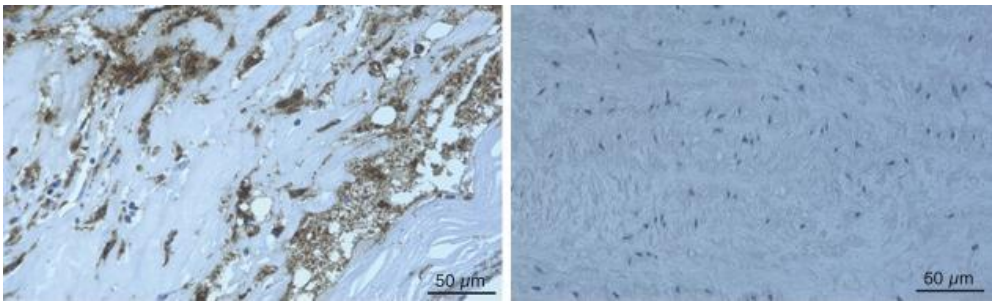

AAA Control aorta

Figure 1.11 Inflammatory infiltrate in AAA (left) compared to healthy control aortae (right). Immunostaining for CD68+ cells (brown) shows distribution of monocytes and macrophages, common inflammatory cell types. Image taken from Kin et al. (2012), CC BY 2.5.

It was determined that the majority of the inflammatory infiltrate was generally located at the medial-adventitial junction and was composed of immunophenotypic cells: T-cells, B-cells and macrophages (alongside very small numbers of neutrophils) (Satta et al., 1998). The specimens used were taken from patients undergoing elective repair and so this is only an insight into the inflammatory state of the tissue at end-stage disease. Therefore, it is unclear at which stage of arterial wall degeneration this infiltration occurred and its role in aneurysm formation. That study also suggested that the degree of inflammation in each aneurysm positively correlated with the degree to which elastin degradation had occurred, especially with respect to T and B lymphocytes and macrophages.

Adventitial mast cells have also been documented as contributing to AAA progression and development. It was found that there was a significant positive correlation between this type of cell and the maximum aortic diameter, and that the proportion of degranulated mast cells was significantly increased in AAA compared to atherosclerotic controls (Tsuruda et al., 2008). Mast cells are also involved in the recruitment of T lymphocytes and macrophages via pro-

inflammatory mediators. Macrophages contribute to AAA development by directly secreting ECM degrading elastases and collagenases (Shimizu et al., 2006).

It is theorised that the recruitment of inflammatory cells into the media and adventitia of the aneurysm stems from elastin-derived peptide (EDP) induced chemotaxis. Elastolysis produces these EDPs which then recruit inflammatory cells into the media. The inflammatory cells are then able to secrete additional proteolytic enzymes, trapping the artery in a vicious cycle of pathological vascular remodelling, resulting in aneurysm (Satta et al., 1998).

It has been proposed that the inflammatory cell infiltrates that are so pervasive in AAA disease are part of a dysregulated autoimmune system response against the arterial wall (Jagadesham et al., 2008).

A current frame of thinking is that inflammatory cell recruitment following an unknown instigating factor is the first stage of AAA progression. These cells, in addition to SMCs, then produce the proteases required for the observed ECM degradation (Ailawadi et al., 2003).

1.7.5. ROLE OF THE SMOOTH MUSCLE CELL IN AAA

Inflammatory characteristics of AAA have been studied for many years, yet relatively fewer studies have considered the role of SMCs in AAA pathogenesis. One main aim of this project is to characterise the alterations in SMC function over time in an *ex vivo* AAA bioreactor model.

1.7.5.1. SMC PHENOTYPIC MODULATION

It has been well documented that vascular SMCs are able to undergo profound changes in phenotype in response to alterations in the extracellular environment (such as growth factors/inhibitors, mechanical influences, cell-cell and cell-matrix interactions, and various inflammatory mediators) and are also able to exhibit a wide variety of cell phenotypes at different stages of development or

disease pathogenesis (Owens et al., 2004). Indeed, the vascular SMC, even in adult mammals, is not terminally differentiated. SMCs are subject to a variety of mechanical forces in their physiological environment (such as shear stress via endothelial modulation, passive blood flow stretch, wall stress and axial wall tension) and as such are able to react and adapt to these forces via mechanotransduction (Osol, 1995, Lehoux et al., 2006, Lu and Kassab, 2011).

SMC are generally characterised as having two distinct phenotypes: the specialised and differentiated contractile phenotype and the de-differentiated secretory phenotype (Rzucidlo et al., 2007, Porter and Riches, 2013, Shi and Chen, 2016). A schematic of this phenotypic modulation is shown in Figure 1.12.

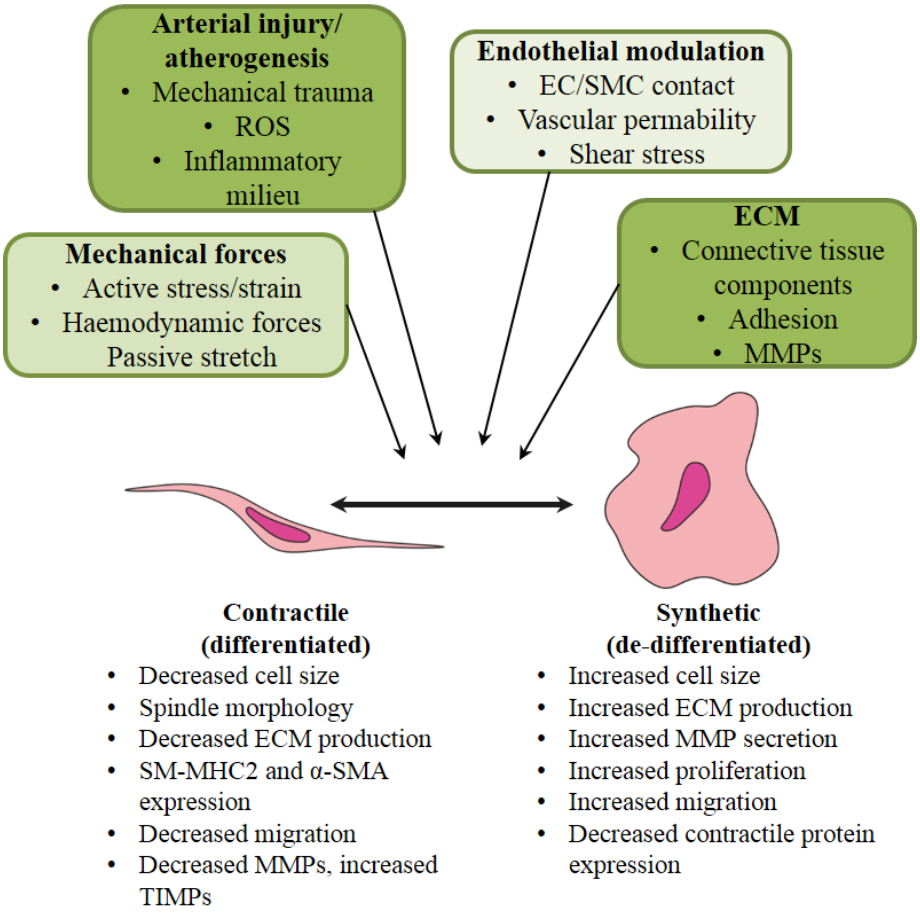

Figure 1.12 SMC phenotype structure and function. Phenotype switch is driven by extracellular and environmental cues.

The main function of the SMC in the heathy artery is to regulate blood flow and pressure via contracting and relaxing to force blood through the artery by altering the vessel diameter (Owens et al., 2004, Shi and Chen, 2016). Under these circumstances, SMCs possess low turnover and synthetic activity (Porter and Riches, 2013). Differentiated SMCs express high levels of smooth muscle specific proteins, including α-smooth muscle actin (α-SMA), smooth muscle myosin heavy chain (SM-MHC), calponin and smoothelin (Hungerford et al., 1996, Shi and Chen, 2016). Differentiated SMCs have a spindle morphology with highly aligned actin fibres which are reorganised during phenotypic modulation (Worth et al., 2001b, Han et al., 2009).

In response to a multitude of external factors (including arterial injury, mechanical forces and atherogenesis) SMCs de-differentiate into a secretory phenotype. In contrast to the low SMC turnover often observed in the differentiated phenotype, de-differentiated SMCs are highly proliferative and migratory and are also able to remodel the ECM with increased secretion of MMPs and matrix proteins (Owens et al., 2004, Rensen et al., 2007, Porter and Riches, 2013). This process of reversible differentiation is relatively poorly understood due to the derivation of SMCs from multiple precursors throughout embryogenesis (Majesky, 2007). Extensive studies into the mechanism behind SMC differentiation have found that it is orchestrated by a precisely co-ordinated molecular network which incorporates different environmental cues, mechanical forces, signalling pathways, transcription factors, reactive oxygen species, extracellular matrix and micro RNAs (most notably miR-145 and miR 143) (Rensen et al., 2007, Cordes et al., 2009, Alexander and Owens, 2012, Qiu et al., 2014, Shi and Chen, 2016) and reviewed in Zhang et al. (2015). MicroRNAs are small, non-coding endogenous RNAs which are able to post-transcriptionally regulate gene expression via RNA silencing and repression in a field of study termed epigenetics, reviewed in Alexander and Owens (2012)

Many studies have detailed the changes that SMCs undergo due to development of cardiovascular diseases, such as atherosclerosis, via gene profiling (as reviewed in Owens et al. (2004)). However, studies such as this are limited in capturing the dynamic nature of SMC phenotypic modulation; for example,

SMC proliferation generally increases following early stages of disease, but is decreased in mature lesions (Owens et al., 2004, Ailawadi et al., 2009).

1.7.5.2. SMOOTH MUSCLE CELL LOSS AND DYSFUNCTION IN AAA

As mentioned in chapter 1.4.1, in addition to degradation of the ECM, SMC apoptosis is a defining characteristic of AAA. The inflammatory cell infiltration of macrophages and T lymphocytes produce significantly increased numbers of cell death promoting proteins, such as perforin, Fas and FasL, in end-stage aneurysm disease tissue (Henderson et al., 1999). The authors of that study suggest that the secretion of mediators of apoptosis may be mainly targeted to the inflammatory cells themselves, rather than the SMCs, as a potential mechanism of self-limitation of the immune response. The medial SMC and the adventitial fibroblasts are principally responsible for the synthesis of collagen and elastin in the aortic wall; hence the depletion of medial SMC has the potential to be a major factor in AAA development.

SMCs contribute to the architecture of the aortic wall in addition to their ECM remodelling capabilities – a decrease in the number of SMCs will therefore have a notable effect on the functional and structural integrity of the aorta. It has been shown that there was no significant difference in medial SMC density measured via immunohistochemistry for α-SMA and direct cell counts between normal (n=5) and atherosclerotic occlusive (AO) aorta (n=6), but a 74% decrease in SMC number in AAA tissue (n=10) (Lopez-Candales et al., 1997). Light and electron microscopy revealed ultrastructural changes consistent with SMC apoptosis and up to 30% of AAA SMC demonstrated fragmented DNA. Apoptotic SMC were found solely in the neointimal plaque in AO disease but were distributed throughout the degenerative media in AAA tissue.

The problem remains that the AAA and AO samples were taken from end-stage diseases, and so again cannot give any information as to the development of the pathology. A decrease in the number of SMCs in the aneurysmal aortic wall implies that the rate of ECM synthesis is decreased hence there exists an imbalance between proteolytic degradation and matrix synthesis in favour of

proteolysis. The potential paracrine effect of SMCs has been demonstrated in two studies which both showed that SMC seeding in a decellularised xenograft aneurysm model was able to stabilise this proteolytic imbalance (Losy et al., 2003, Allaire et al., 2004). These data provided the foundations for therapeutic treatments for AAA disease.

SMCs have a protective role against ECM degradation by proteolysis and inflammation – two key mechanisms involved in AAA progression (Sakalihasan et al., 2005). A guinea pig-to-rat xenograft seeded either with or without syngeneic SMCs found that the recellularised graft prevented AAA formation after 2 weeks following implantation – aortic diameter increase was 198.2%±106.6% in non-seeded grafts versus 35.3%±17.8% ($p<0.01$) (Allaire et al., 2002). Seeding of SMCs also prevented elastin degradation and inflammation in this study. It is therefore conceivable that SMC apoptosis in the early stages of the disease is able to exacerbate the proteolysis imbalance and spur on inflammatory cell recruitment, leading to a vicious cycle of pathological remodelling.

In addition to their paracrine effect, SMCs are primarily responsible for the synthesis of ECM proteins – severe SMC apoptosis would therefore lead to a decrease in ECM synthesis rate, rendering the aorta prone to aneurysm progression (Ailawadi et al., 2003).

Loss of SMCs is thought to occur later in the stages of aneurysm development (Ailawadi et al., 2003). However, in a murine elastase induced aneurysm model study, SMC phenotypic modulation characterised by protease upregulation and SMC marker gene downregulation occurred prior to aneurysm formation at fourteen days (Ailawadi et al., 2009). At seven days postoperatively, elastase-perfused mice showed a 78% and 85% reduction in smooth muscle cell marker genes SM22A and SM α-actin respectively compared to saline-perfused mammals, but an 80% increase in MMP-2 expression. It has not yet been determined as to how this may apply to human AAA, but it offers some promising insight into possible pre-symptomatic events.

The role of the SMC in the formation and development of AAA may not be limited to apoptosis. There is a growing body of evidence which suggests that the SMC phenotype found in aneurysms may be unique in comparison to those found in healthy aorta as per the *in vitro* growth characteristics (Lopez-Candales et al., 1997, Henderson et al., 1999, Curci, 2009). An earlier study demonstrated that SMCs from AAA tissue differ in their response to addition of cytokines in comparison to SMCs taken from normal tissue. The addition of interleukin-1 β caused an 82% rise in messenger RNA levels for TIMP-1 in aneurysmal SMCs, whereas the levels did not change in healthy SMCs (Keen et al., 1994). Furthermore, the migration properties of SMCs from the inferior mesenteric vein (IMV) of AAA patients have been shown to be enhanced compared to SMCs from non-AAA patients (Goodall et al., 2002b). These enhanced migration properties of SMCs are ubiquitous in AAA patients and were not confined to SMCs from aneurysmal tissue.

1.7.5.3. SMOOTH MUSCLE CELL SENESCENCE

It is thought that cell senescence also plays a role in the depletion of SMC in the aneurysmal aorta: aneurysm incidence is linked with advanced age and so suggests that the aging process may be associated with aneurysmal degeneration (Thompson et al., 2002). The paucity of SMC in aneurysmal tissue may be due to the inability of senescent cells to sustain proliferation to the required level. Proliferation of SMCs taken from the aneurysmal aorta of patients undergoing elective AAA repair were compared with SMCs taken from the adjacent non-aneurysmal inferior mesenteric artery (IMA) for use as a control (n=15) (Liao et al., 2000). All 15 IMA explants were able to produce a sustainable SMC culture, whereas this was only possible in 9 out of 15 AAA explants, as well as a prolonged primary explant growth interval in AAA compared to IMA cultures (16.4 ± 2 versus 6.4 ± 1 days). SMC growth showed no discernible relation to original aneurysm size, gender or patient age. The maximal proliferation of the AAA-derived SMC was reduced by 44.2 ± 8% ($p < 0.01$) when compared to IMA-derived SMC. An extremely intriguing outcome was that the morphology of the AAA-derived SMC differed greatly to that of the IMA-derived SMC; the

cells were a rounder, more rhomboid shape in comparison to the spindle morphology typically observed in healthy SMC. IMA-derived SMC continued to proliferate beyond passage 20 in serial culture, whilst all AAA-derived SMC developed replicative senescence by passage 12. These observations demonstrated that AAA-derived SMCs demonstrate a distinctive morphologic appearance in culture, diminished proliferative capacity and a limited life span during *in vitro* culture in comparison to SMCs taken from adjacent, non-aneurysmal artery. The observations reflect intrinsic changes to SMC growth capacity that was independent of patient age. Tissue-specific processes may therefore be implicated in the accelerated SMC senescence which contributes to the ubiquitous depletion of SMC in the aneurysmal media.

1.7.5.4. SUMMARY

The reviewed literature in this Section suggests that alterations in SMC phenotype in the abdominal aorta may contribute to the early development of AAA, but the mechanisms are not well defined. Temporal characterisation of these dynamic changes in the arterial SMC will form the basis of development of cell-based therapeutic techniques due to their ability to synthesise ECM proteins which are lost in end-stage AAA. One aim of this study is to use an *ex vivo* model of AAA in order to characterise the changes in SMC phenotype over time in terms of structure and function.

1.7.6. AAA HAEMODYNAMICS

In this study, an *ex vivo* bioreactor model of AAA will be developed. Producing a model in a bioreactor will allow greater control of the dynamic environment than using an *in vivo* model. From this, the relationship between various haemodynamic factors and the progression of aneurysm or response of SMCs may be quantified.

The arterial wall is subject to three separate fluid-induced forces: internal pressure exerted by hydrostatic forces, internal wall stresses and wall shear

stress exerted by the flow of blood (Miller, 2002). Circumferential stress is calculated approximately as the product of the pressure and the radius of the vessel, divided by the wall thickness, according to the law of Laplace (Equation 1). The assumptions for this equation is that the vessel is a thin walled cylinder, where the thickness does not exceed 10% of the radius. AAA tissue may therefore not meet this assumption, and so it is only a simple way of modelling AAA mechanics. Starting with the law of Laplace, modelling of AAA mechanics has become much more complex, incorporating finite element and computational fluid dynamics components with less stringent mathematical assumptions (Vorp, 2007). Shear stress is proportional to blood viscosity and the flow rate. Pressure is regulated via contraction or relaxation of the SMCs to alter the lumen size in addition to the elastic recoil of the artery.

Equation 1 Law of Laplace

$$\text{Circumferential Stress} \sim \frac{(\text{Pressure}_{\text{mean}})(\text{radius})}{\text{wall thickness}}$$

(Laplace, 1805)

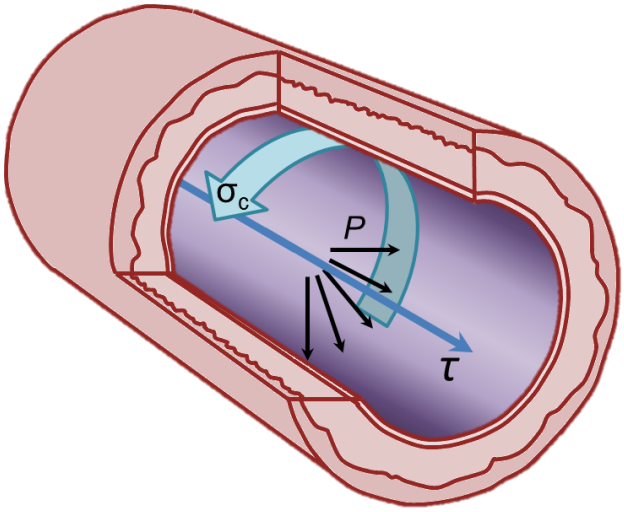

Figure 1.13 Haemodynamic forces involved in blood flow through arteries. P = pressure, τ = shear stress, σ_c = circumferential stress.

Figure 1.13 shows the haemodynamic forces relevant to AAA pathology. It would be reasonable to assume that the increase in aortic diameter would result

in a thinning of the aortic wall. However, Freestone *et al.* have shown that this is untrue, and that it is in fact the larger aneurysms that have a thicker, but weaker, wall (Freestone et al., 1995). This may be described as a reaction of the vascular remodelling system to reduce the circumferential stress (σ_c, Figure 1.13) in the aortic wall – increasing the thickness would theoretically reduce this stress, according to Laplace's law.

This may indicate why the levels of mediators of vascular remodelling, such as MMPs, are found at increased levels in AAA tissue; the remodelling process is attempting to normalise the biomechanical stresses.

Disturbed flow conditions (turbulent flow) contribute to aneurysm development via endothelial injury and acceleration of the degeneration of the arterial wall (Miller, 2002). An aneurysm will change the physiological haemodynamic conditions of the native aorta as the geometry will have been altered. However, the extent to which the haemodynamic environment changes depends on the shape of each individual aneurysm; clinical studies have shown that flow through the aneurysm can either be turbulent or laminar (Bluth et al., 1990).

Some light can be shed onto the role of mechanical forces in the progression of AAA by examining EVAR. EVAR involves insertion of an endovascular stent whereby the arterial wall is excluded from circumferential stress, pressure and shear stress exerted via blood flow. EVAR is a relatively successful surgical technique and is able to prevent further AAA growth: once the mechanical forces are removed from the pathological biological environment AAA progression is attenuated (Nordon et al., 2011). EVAR graft failure and AAA progression even after EVAR is typically caused by endoleaks. These leaks allow blood to flow directly next to the arterial wall and can restart aortic dilatation (Harris et al., 2000, Golledge et al., 2006). This implies that mechanical forces are key to driving the pathological biological processes underpinning AAA progression: removing them stops arterial dilatation. The haemodynamic environment also plays a role in regulating the behaviour and phenotypes of cells, in a process known as mechanotransduction. Vascular cells respond to shear stress, by upregulating or downregulating certain genes

(Miller, 2002). MMP-2 and -9 are also shear dependent; these are implicated in the degradation of the ECM (Grote et al., 2003, Norman and Powell, 2010).

There is evidence that blood flow dynamics can contribute to the levels of ROS in the arterial wall. In a murine aneurysm model study, Nakahashi *et al.* found that ROS levels were reduced in rat aortas with artificially increased flow (flow-loading via creation of a femoral arteriovenous fistula) compared to non flow-loaded rats, following elastase perfusion to induce AAA (Nakahashi et al., 2002). In addition, vascular SMCs cultured *in vitro* produced mediators of oxidative stress (inducible nitric oxide synthase) in proportion to shear stress intensity (Gosgnach et al., 2000). It was also found that expression of heme oxygenase-1 (HO-1), a mediator of oxidative stress and a ROS, is regulated by shear and strain forces in cultured SMCs *in vitro* (Nakahashi et al., 2002). This phenomenon has also been shown to occur *in vivo,* using a rat model (Hansson et al., 1994). The consequent role of ROS in aneurysm development has already been shown to be important (Raaz et al., 2014). A study comparing low (iliac artery ligation) and high-flow (arteriovenous fistula) experimental AAA in a rodent model examined the effect of wall shear stress (WSS) on vascular cells (Hoshina et al., 2003). Low-flow AAA reduced WSS by 60% whilst WSS in high-flow AAA was increased by 300%. The pressure was the same in both groups. Low-flow AAAs were found to be larger, populated with fewer SMCs and endothelial cells had lower growth factor production, impaired cell proliferation and increased apoptosis compared to high-flow AAA. This may indicate that there is some sort of critical point between ceasing shear stress application on the aortic wall via EVAR and high flow AAA where progression is maximally exacerbated.

Decreased flow rates in AAA disease may also exert an indirect effect on AAA progression by promotion of monocyte binding and mural infiltration. In was shown in experimental rat AAAs that WSS inversely correlates with medial macrophage densities in addition to levels of proinflammatory cytokines such as monocyte chemoattractant protein-1 (MCP-1) and granulocyte-macrophage colony-stimulating factor (GM-CSF) (Sho et al., 2004). Computational studies conducted with computational have shown that the distribution of inflammatory

cell infiltration correlated with areas of low wall shear stress (Hardman et al., 2010).

A question also remains as to why the abdominal aorta is such a preferential site for the manifestation of aneurysm. Aneurysms of the thoracic aorta are approximately five times less common than those of the abdominal aorta (Norman and Powell, 2010). A number of reasons may exist for this. Firstly, the abdominal aorta differs in anatomy to the thoracic aorta; it contains fewer elastic lamellar units than its diameter and thickness would imply and it increases in rigidity (reflecting a decrease in elastin and an increase in collagen) from proximal to distal (Anidjar and Kieffer, 1992, Dua and Dalman, 2010). Secondly, the haemodynamics differ greatly between the two sites. The thoracic aorta contains forward blood flow throughout the cardiac rhythm, resulting in continuous forward laminar shear stress (Dua and Dalman, 2010). In contrast to this, the abdominal aorta possesses lower values of shear stress and reverse flow is present during late systole and diastole, and also experiences increased peripheral resistance (Dua and Dalman, 2010, Norman and Powell, 2010). Norman and Powell state that the specific haemodynamic conditions in the abdominal aorta could potentially upregulate inflammatory pathways, predisposing it to aneurysm. (Norman and Powell, 2010). In addition, these kinds of shear stresses can promote oxidative stress, as explored previously.

Gaining a greater understanding into the haemodynamics of aneurysms is therefore a powerful tool in understanding AAA pathogenesis.

1.8. ANIMAL MODELS OF AAA

This section will discuss the necessity of animal models in AAA research. Each model has its own advantages and limitations and so the use of each depends on the nature and direction of the research. An *ex vivo* model of AAA will be developed in a bioreactor during this project and so a review of current animal models contextualises the need for such a model.

Using human aneurysm tissue to analyse the development and progression of the disease seems to be an obvious path for research. However, the nature of AAA is that it is not detected until it has actually progressed to a detectable stage: it is usually asymptomatic until it has ruptured and is detected through screening only when it has begun to increase in diameter (Sakalihasan et al., 2005). There is a recurrent issue with using human aneurysmal tissue for the study of early aneurysm events in that it can only be retrieved from patients when surgery to correct it is performed and so it has progressed to late-stage or end-stage disease (He and Roach, 1994, Hovsepian et al., 2000, Haskett et al., 2011, Trollope et al., 2011).

Animal models have therefore become the focus of early aneurysm development research, as they can be examined and manipulated from the initiation of the aneurysm, validate therapeutic targets and be used to study the stages of AAA pathophysiology. However, naturally forming aneurysms occur very rarely in animals; certain breeds of turkey and very small populations of squirrel monkeys (approximately 1.5%) have been found to develop them, mostly when subjected to certain diets (Gresham and Howard, 1961, Dobrin, 1999). The aneurysm model should therefore be created artificially *in vivo* in order to examine aneurysm pathogenesis and treatment.

The ideal animal model should completely mirror the human pathology in cellular and biomechanical terms, be reproducible and relatively simple to achieve. The model should permit specific investigations into the underlying mechanisms underpinning human aneurysms (Trollope et al., 2011).

1.8.1. SPECIES SELECTION

The species of animal chosen for an experimental AAA model is dependent upon the similarities to humans in anatomy, biochemical factors and cellular processes. There are distinct advantages and disadvantages associated with each species. For example, mice are commonly used for AAA models as the mouse genome has been mapped; genetic manipulation is used to determine genetic factors in AAA development (Andrews et al., 1975, Daugherty and Cassis,

2004). In addition to this, mice have good practical advantages – they are relatively simple to handle in large numbers at modest cost. Consequently, murine models are the most widely used at present (Zaragoza et al., 2011). Rat models are also used, as they are larger and therefore the surgery is less complex (Anidjar et al., 1990). Small mammals are, however, limited due to their miniature size especially when considering arterial biomechanics.

Table 1.1 Summary of small animal species used as models for AAA research.

Species	Advantages	Disadvantages
Mouse	Easy to handle at low cost in large quantities	Miniature vasculature, resulting in complex surgical manipulation
	Low husbandry requirements	Low tissue yield
	Genetic manipulation possible (Daugherty and Cassis, 2004)	Distinct cardiovascular physiology from humans (Argenta and Pereira, 2009)
	Has similar gender susceptibility as in humans (Brophy et al., 1988, Reilly et al., 1990)	
	Shorter life span, so accelerated time course for disease (Haskett et al., 2011)	
Rat	Easy to handle at low cost in large quantities	Distinct cardiovascular physiology
	Low husbandry requirements	Miniature vasculature, resulting in complex surgical manipulation
	Increased tissue yield compared to mouse	Genetic manipulation in rats is more complex than in mice (Twigger et al., 2008)
	Aneurysms can be induced via multiple methods (Anidjar et al., 1990, Allaire et al., 1998)	
	Shorter life span, so accelerated time course for disease (Haskett et al., 2011)	
Rabbit	Relatively easy to handle at modest cost	Small vasculature
	Relatively low husbandry requirements	Difficult genetic manipulation
	More closely resemble human AAA compared to other small mammals (Zaragoza et al., 2011)	
	Aneurysm development can be monitored through femoral artery (Dai et al., 2006)	

Table 1.2 Summary of large animal species used for AAA research

Species	Advantages	Disadvantages
Dog	Lack of spontaneous endothelialisation of prosthetic surfaces, as in humans (Kónya et al., 2008) Sufficiently large peripheral arteries for endovascular graft testing (Chuter et al., 1997) Able to survive prolonged anaesthesia (Trollope et al., 2011) High ease of handling for a large mammal species	Relatively large husbandry requirements Relatively high initial cost and maintenance costs Extremely potent fibrinolytic system (Kónya et al., 2008)
Sheep	Sufficiently large arteries for endovascular graft testing (Gorin et al., 1997) Coagulation pathways are closer to humans than that of dogs or pigs (Kónya et al., 2008)	Large husbandry requirements High maintenance costs Safety issues with human transmissible diseases (Kónya et al., 2008)
Pig	Sufficiently large arteries for endovascular graft testing (Moláček et al., 2009) Large mammal with the most similarities to human arterial morphology (Kónya et al., 2008)	Large husbandry requirements High maintenance costs Difficult to handle (Trollope et al., 2011)
Primate	Closely related to humans Similar fibrinolytic and clotting systems to humans (Trollope et al., 2011)	High maintenance costs Difficult to handle More stringent ethical regulations (Great Britain, 1986)

Pigs have a similar arterial morphology to humans, whereas dogs show a comparable lack of spontaneous endothelialisation. Sheep and humans share similar coagulation pathways (Kónya et al., 2008). Primates have similar anatomy and fibrinolytic systems, but are limited in use due to ethical concerns (Abildgaard et al., 1971, Trollope et al., 2011). In contrast to murine models, large mammal models are constrained by their practical aspects; they are more expensive to house and sustain, they require greater husbandry capacity,

increased doses of anaesthetic and have more stringent ethical considerations (Yazdani and Berry, 2009).

As is demonstrated by Table 1.1 and Table 1.2, it is clear that the choice of animal for *in vivo* models is often a trade-off between arterial geometry and morphology, physiological comparisons with humans, ease of genetic manipulation, availability, and cost. Murine and other small mammal models are extremely useful when investigating the cellular and genetic processes which contribute to aneurysm development. The pre-clinical testing of endovascular stents is, however, virtually impossible in all but large mammals due to the discrepancy in size and arterial haemodynamics compared to humans. This type of pre-clinical testing is essential in the development and assessment of novel devices and technologies, but is heavily limited by the high costs and time-consuming protocols associated with research on larger animals, making temporal studies routinely prohibitive. The result is that a high number of new devices are available for testing, but only a limited number of animals can be obtained (Touroo and Williams, 2012).

Disease models each have a set of advantages and limitations and so the model must be chosen carefully considering the nature of the investigation. *In vivo* models are able to directly inform about the underpinning mechanisms and processes of the disease as it exists physiologically. However, compounding systemic effects are present and, especially where human tissues are used, safety and ethical consideration must be upheld. The premise of *ex vivo* models is that the tissue is removed from an organism to an external environment whilst attempting to minimally alter the natural conditions. *Ex vivo* models allow more stringent experimental control, may remove compounding factors and safety and wellbeing of the organism is less of a concern. These apparent advantages are also inextricably linked with the decreased model similarity to the physiological condition (Denayer et al., 2014).

This study aims to develop and use an *ex vivo* bioreactor model of AAA in porcine arteries which would not be subject to the same costs and logistical complexities associated with *in vivo* large animal models.

1.8.2. METHODS OF EXPERIMENTAL AAA CREATION

A wide variety of techniques have been developed in order to create animal models of AAA encompassing physical, chemical and genetic manipulations each with their own considerations and limitations.

1.8.2.1. SPONTANEOUS MUTATION

The earliest AAA models included certain strains of species that demonstrated a higher level of spontaneous aneurysm formation and rupture than others of their kind, such as the broad-breasted bronze turkey and the Blotchy mouse strain. These animals develop aortic disruptions that often lead to aortic rupture associated with genetic defects in connective tissue structure (Gresham and Howard, 1961, Neumann and Ungar, 1973, Brophy et al., 1988). Both animals also demonstrate a gender bias in aortic rupture similar to that in humans: increased in males in comparison to females (Daugherty and Cassis, 2004, Trollope et al., 2011).

However, the pathologic features of the diseases in these animals bear greater resemblance to aortic dissection as opposed to aneurysm (Thompson et al., 2002). As the animals possess a generalized disorder in their connective tissues, compounding factors such as aneurysms in other parts of the vasculature and emphysema have limited the usefulness of this type of model (Daugherty and Cassis, 2004). Furthermore, the advent of alternative models which are more representative of human AAA disease have led to the decrease in use of the spontaneous formation model.

1.8.2.2. GENETIC MANIPULATION

As with the spontaneous formation model, animals are ‘bred’ to develop aortic aneurysms that are analogous to the human disease. However, advances in genomic understanding and techniques have progressed so that specific genes can be omitted in order to understand their role in the pathogenesis of disease.

Knockout mice have recently become extremely useful models when investigating vascular disease aetiology. This term refers to the targeted disruption of one or more specific alleles for which the role of that gene in AAA disease can be determined. As discussed in the previous section, this type of model is currently only possible with small animals where the genome has been sufficiently mapped for genetic manipulation: mice and, more recently, rats.

Mice lacking the apolipoprotein E (ApoE) gene or low-density lipoprotein receptor (hyperlipidemic mice) form aortic aneurysms when subjected to a cholesterol-rich diet for prolonged periods of time (Tangirala et al., 1995). The purpose of that study was to induce atherosclerotic lesions but aneurysm formation was frequently noted in advanced lesions. The links between atherosclerosis and aneurysm formation in humans have already been previously discussed earlier in section 1.5.

Subcutaneous angiotensin-II (part of the renin-angiotensin system that regulates vasoconstriction) infusion into hyperlipidemic mice has also shown to induce aortic aneurysms in mice. This model has several parallels to human AAA disease; there is preponderance for aneurysm development in males, luminal dilation, medial degeneration, thrombus formation, inflammatory influx, consistent localization and cytokine upregulation similar to that observed in humans (Manning et al., 2002). Although generally reproducible, some hyperlipidemic mice infused with angiotensin-II appeared to be resistant to aneurysm formation and displayed aortic diameters indistinguishable from control mice. In addition, the aneurysms are consistently localized at the suprarenal aorta in mice contrasting with aneurysms commonly found in the infrarenal aorta in humans. It is postulated that this may be due to one or all of the following factors: inherent differences in cell properties at this level, the ratio of collagen to elastin or the density and subtype expression of the angiotensin-II receptor in this region (Manning et al., 2002). Dilation of the lumen and degradation of the ECM analogous to human AAA can be observed.

This model has been used to generate relevant pharmacological and mechanistic data for the human AAA, and so has proved useful for determining genetic factors implicated in AAA formation and progression (Trollope et al., 2011).

The role of MMPs in aneurysm development can also be investigated using genetically modified animal models. One group produced AAAs in mice with a combined apolipoprotein E and TIMP-1 (tissue inhibitor of MMP-1) deficiency (Silence et al., 2002). Aneurysms were more common in mice with combined deficiency than those with apolipoprotein deficiency only (23±5.1 vs. 11±3.0 aneurysms per 100 sections analysed, $p<0.001$). Atherosclerotic lesions were significantly larger in apolipoprotein deficiency only compared to combined deficiency ($p<0.001$). As with human AAAs, a paucity of SMCs was observed and the role of MMPs has been implicated in AAA progression. This strain may therefore be extremely useful when conducting AAA-specific studies.

The roles of MMP-9 and MMP-12 in AAA development have been confirmed by studies in genetically modified animals. Mice deficient in MMP-9, either alone or in combination with MMP-12 deficiency exhibited significant reduction in aortic dilatation (Pyo et al., 2000). MMP-12 deficiency in isolation did not show a significant difference from wild-type mice. The study used a genetically modified animal model to give information about the requirements for aneurysms to form. Genetically modified mouse studies have implicated the COX-2 gene in AAA development. AAA incidence in wild-type mice was 54% (n=24) whereas no aneurysms were detected in COX-2 deficient mice (Gitlin et al., 2007). Inhibition of COX-2 with celecoxib has since been shown to reduce AAA incidence by 61% and AAA severity in mice subjected to angiotensin treatment, in addition to attenuation of late-stage AAA progression (Ghoshal and Loftin, 2012). This shows that COX-2 inhibition may have therapeutic potential in the future.

This type of model is extremely useful in determining molecular events involved in aneurysm formation and can aid focus in developing therapeutic targets, but can only be used in animals where the genome has been mapped: namely mice and rats.

1.8.2.3. PHYSICAL MODELS

Genetic manipulation is not currently feasible in large mammals, but models are needed that are more biomechanically relevant to humans as well as being sufficiently large to test surgical treatment devices.

It is possible to induce AAA by surgically weakening a portion of the aortic wall in large mammals via crushing or blunt force trauma (Zatina et al., 1984, Schmoker et al., 2008). Even lasers have been employed to physically injure the wall of a rat common carotid artery, resulting in development of focal aneurysms at the injured site (Ammirati et al., 1988). These methods are not widely used due to extremely variable size, growth rate and rupture risk as well as a tendency to produce saccular aneurysms or pseudoaneurysms which are not relevant to human AAA (Tsui, 2010).

A widely used method of experimental aneurysm creation is the arterial patch method; this is an especially common aneurysm creation method in large mammals for the testing and development of endovascular stents (Haskett et al., 2011). The premise of the arterial patch method is that an incision in the arterial wall is repaired using a structurally weaker material. A schematic of the surgical construction of the AAA is shown in Figure 1.14.

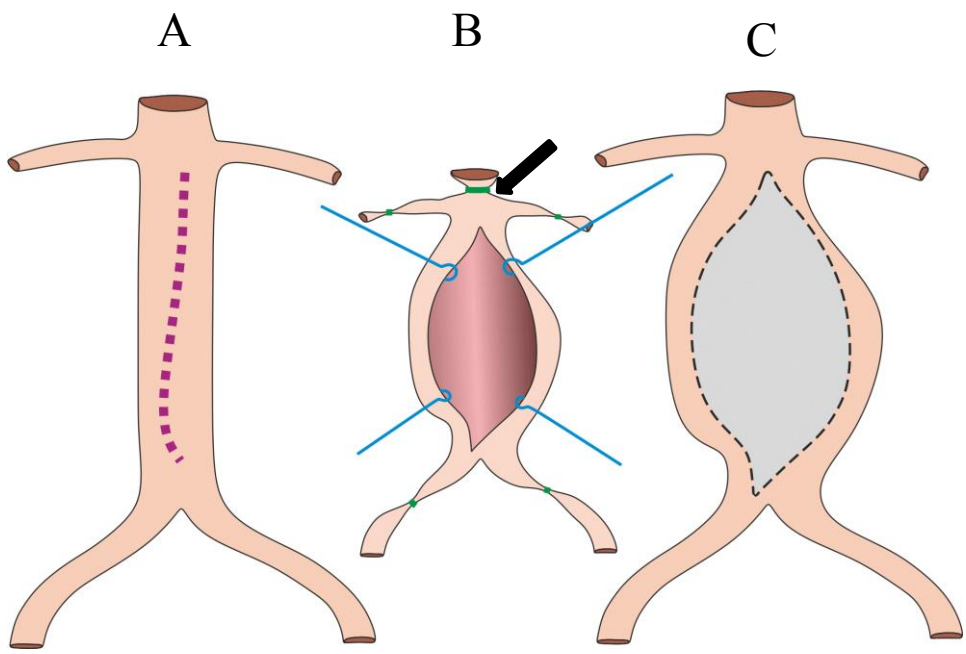

Figure 1.14 Schematic of experimental aneurysm creation via the arterial patch method. A) a longitudinal incision is made. B) the aorta is ligated (green, arrow) and opened up. C) ellipsoid arterial patch is sewn into place.

An aneurysm is created due to the insertion of the arterial patch and the postoperative dilation of the graft until an endovascular stent is deployed to bypass the experimental aneurysm and prevent further dilation. Various materials have been used as arterial patches in the creation of experimental aneurysms, including synthetic Dacron (Laborde et al., 1992, Verbin et al., 1995, Moláček et al., 2009) and ePTFE (Murphy et al., 2007), in addition to venous, peritoneal and fascial tissues (Palmaz et al., 1995, Eton et al., 1996, Maynar et al., 2003, Lerouge et al., 2004). The use of analogous tissue is advantageous in that it allows progressive expansion of the experimental aneurysm and furthermore the tendency to rupture can be controlled based upon the tissue type used (Haskett et al., 2011).

A similar method is the graft aneurysm model whereby a whole section of abdominal aorta is removed and replaced with a graft forming a conduit. As with the arterial patch method, a dearth of graft materials have been used, including crimped pre-formed Dacron, and gluteraldeyde-tanned jugular vein (Parodi et al., 1991, Whitbread et al., 1996, del Moral et al., 2015). The graft

method has been interestingly used by one group to create experimental aneurysms based on the immune rejection of arterial xenografts, which have the gross and histologic features of AAA and have shown that SMC seeding has a therapeutic effect on reducing progression of the AAA (Allaire et al., 2002, Allaire et al., 2004).

Both the arterial patch method and the conventional graft method allow the formation of either saccular or fusiform aneurysms of comparable morphology and geometry to human AAA, and have proved themselves to be extremely useful in stent development and surgical experience (Trollope et al., 2011). The graft model allows a much greater control of the final size and configuration of the experimental aneurysm in comparison to the arterial patch method, but conversely, the arterial patch maintains more native arterial tissue and so can demonstrate some histologic features of AAA (Moláček et al., 2009). Neither method, however, is considered suitable for studying the biological mechanisms or mechanical properties of AAA as they incorporate material not found naturally within the arterial wall; the processes behind their creation are artificial. Histologic features of AAA (such as damaged elastin fibres and inflammatory infiltration) found in the arterial patch method are contradicted by other histological features, such as increase in number of SMC and arterial fibroblasts, suggesting that pathological pathways in this model are different and distinct from human AAA development (Moláček et al., 2009, Trollope et al., 2011). It is perhaps this reason why there has been reported failure to predict late complications in EVAR (Carrell et al., 1999). A large mammal model with the same pathophysiological features of human AAA disease may allow more valid studies on the long-term effects of EVAR.

1.8.2.4. CHEMICAL MODELS

Chemical models have been used in both small and large mammal species and hence are the most transferable method of inducing experimental aneurysms.

Over two decades ago, an experimental aneurysm was first produced in rats using application of elastase via intraluminal perfusion (Anidjar et al., 1990). It

had recently been discovered through clinical trials that elastase may have a role in aneurysm pathogenesis due to the increased elastolytic activity and degradation of elastin in the media of human AAA. All rats (n=10) that underwent elastase perfusion for 2 hours developed macroscopic aneurysms within 14 days, along with microscopic characteristics such as medial elastin disruption, inflammation, thrombus and fibrous aneurysm wall. The elastase perfusion method has since proved to be reproducible and has been used to elucidate the effects of hypertension, gender and cigarette smoke on the formation and development of aneurysms in mice and rats (Gadowski et al., 1993, Bergoeing et al., 2007, Cho et al., 2009). In addition, the elastase method allows evaluation of the effects of pharmacological agents on aneurysm development. Doxycycline (an MMP-inhibiting tetracycline) has been found to reduce incidence of AAA in an elastase-induced aneurysm model in rats from 83% to 8% (Petrinec et al., 1996). Angiotensin-converting enzyme inhibitors have been shown to suppress aneurysm development in an elastase-induced rat model, and disodium cromoglyate, an inhibitor of mast cell degranulation, reduced aortic expansion by 40% in a similar mouse model (Liao et al., 2001, Sun et al., 2007).

Elastase-induced experimental aneurysms in small mammals have been established as a successful, reproducible and, most importantly, useful model for determining aneurysm aetiology and potential pharmacological treatment options. However, there is an inherent issue with small mammal models relating to differences in the vascular system (as described previously) and their miniature size. The elastase induced aneurysm was at first less successful in large mammals, and experienced initial reproducibility issues.

A 1.66-fold increase in arterial diameter was reported when applying the elastase perfusion method to the abdominal aorta in eight dogs, before repairing the aneurysm with an endovascular stent (Boudghene et al., 1993). A later study was unable to reproduce these results and so explored modifications to methodology including longer perfusion times, variations in elastase doses, intraluminal inflation of a balloon catheter and combination with collagenase perfusion (Strindberg et al., 1998). The combined elastase and collagenase

method produced a mean increase in arterial diameter of 65.6 ± 20.8%, with irregular dilation. No significant dilation was attained with the method of Bhoudghène *et al.* with inflation of a balloon catheter immediately after perfusion or 3 weeks later. The modifications made to the method failed to produce an aneurysmal dilation with enough expansion to make it a reliable model, although it did produce histopathological characteristics such as loss of elastin network, inflammation and mural or intraluminal thrombus.

The first elastase-induced porcine model was carried out in miniature swine (Marinov et al., 1997). Destruction of the elastin network, altered SMC phenotype, inflammation and a reduction in the number of medial SMCs were observed, consistent with characteristics of human AAA. However, no significant aneurysmal dilation was observed in any of the treated animals and large numbers of necrotic lesions associated with calcium deposits were present. This is a further demonstration of the reproducibility issues with the elastase perfusion method in large mammals.

In more recent years, there have been two successful reports of elastase induced experimental aneurysm in a porcine model. Firstly, the researchers surgically exposed the abdominal aortas of ten male pigs and introduced an intraluminal angioplasty balloon, which was then dilated to 14mm diameter (Hynecek et al., 2007). Immediately following dilation, the balloon was removed and a solution of elastase and collagenase was perfused through the artery for 20 minutes. All animals that underwent this treatment developed macroscopic aortic dilation of a mean increase in arterial diameter of 62±35% compared to preoperative diameter. After six weeks, histological evaluation of the aortae demonstrated limited SMC repopulation, persistent elastin degradation and continued collagen deposition. The second study used a combination of intraluminal elastase perfusion and a stenosing cuff in order to induce turbulent flow to create the second instance of successful elastase induced aneurysm in a porcine model (Moláček et al., 2009). Elastase was perfused through the surgically exposed abdominal aorta of seven pigs for 30 minutes and then removed. The proximal aorta was then fitted with a plastic cuff to induce stenosis and hence turbulent blood flow. The diameter of the treated aorta was 2.14 times larger, on average,

than the pre-treatment diameter 21 days post-operatively. Similar to the first model, this model resulted in histological changes concordant with human AAA: fragment elastin fibres, inflammatory infiltration and effect on SMC proliferation.

The combination of a stenosing cuff with elastase degradation has emerged as a reliable method of experimental AAA formation within 3 weeks and has been used to study AAA mechanisms (Turnbull et al., 2011, Houdek et al., 2013, Kloster et al., 2015). Experimental AAA have also be induced in a porcine model using an arterial stenosing cuff alone, without the need for elastase, but was reported to take up to 12 weeks to form (Lin et al., 2013).

In addition to elastase perfusion, adventitial application of calcium chloride ($CaCl_2$) has been used to induce experimental AAAs. The rationale for this method is that calcification and the following elastic fragmentation has been identified as a major feature of atherosclerosis, and so $CaCl_2$ application mimics this pathology (Trollope et al., 2011). Almost three decades ago, this method was first described in male rabbit carotid arteries and showed a significant increase in diameter, intimal thickening, disruption of elastin fibres and an inflammatory infiltrate, comparable to features of human AAAs (Gertz et al., 1988). More recently, application of $CaCl_2$ in order to induce experimental aneurysms has been used to investigate the role of anti-inflammatory agents in the attenuation of aneurysm progression in a rat model (Karapolat et al., 2006). However, this method has only been used in murine and rabbit models and not in large mammals (Haskett et al., 2011).

Treatment of arterial walls with elastin has been shown to produce aneurysms in both small and large animal species and induces histological changes in line with AAA without causing physical injury to the arterial wall. In large animal models, collagenase has been used in conjuction with elastase in order to induce an aneurysmal dilatation (Strindberg et al., 1998, Hynecek et al., 2007). Previously in this laboratory, elastase and collagenase alone and in combination were used prior to *ex vivo* culture (Riches et al., 2013). It was discovered that only by using a pre-treatment of combined collagenase and elastase prior to bioreactor culture for 12 days would the SMCs exhibit similar structural and

functional characteristics to end-stage human AAA SMC. Neither elastase nor collagenase alone did not have any observable effect on the SMCs.

1.8.2.5. *IN VITRO* MODELS

The concept of an *in vitro* large mammal aneurysm model was introduced as a potentially valuable tool in endovascular testing; the cost of animal husbandry is all but eliminated and invasive measurement techniques would become possible (Dadgar et al., 1997). It was hypothesised that an aneurysm-like dilatation may be induced in the thoracic aortae of dogs *in vitro* by tensile loading following enzymatic collagen digestion, hence producing a low cost model for endovascular device testing. Collagenase treatment resulted in digestion of the endothelium and elastic lamina and a reduction in arterial wall thickness. Tensile testing revealed a reduction in stiffness and yield strength. Although collagenase treated arteries were weaker and more compliant compared to controls, there was no evidence given of a plastic (permanent) stretch which may lead to an aneurysm-like dilatation. This *in vitro* work has since been built upon to assess the feasibility of inducing a plastic deformation in enzymatically treated porcine thoracic aortae to induce a dilatation analogous to AAA (Kratzberg et al., 2009). The effects of partial elastin, complete elastin, partial collagen and partial combined elastin and collagen degradation on the plastic deformation of tissue were examined. The plastic deformation was not significantly different in any of the experimental groups in comparison to untreated controls. Maximum plastic strain achieved in one artery was 78.6% - far lower than the necessary 150% strain required to induce an aneurysmal-like stretch. The authors then concluded that passive stretching, even with ECM degradation, was unlikely to produce an *in vitro* aneurysm model because dynamic growth and active remodelling of the arterial wall are essential for AAA formation.

The tissue must be kept viable and subject to mechanical forces in order to induce an experimental aneurysm. The induction of an aneurysm *in vitro* has been shown to be unachievable and so research has now gravitated towards to

use of *ex vivo* models in which the artery is maintained in a bioreactor attempting to simulate the physiological environment, as will be used in this project. Bioreactors are further discussed in section 1.9.

1.8.3. BIOMECHANICAL CHARACTERISATION OF AAA MODELS

Experimental animal models of AAA have started to be validated and characterised in biomechanical terms in addition to histological and geometric characterisation. A whole artery pressure-dilation method determined the biaxial mechanical properties of the mouse aorta *ex vivo*, with implications for mouse models of AAA (Collins et al., 2011). The authors stressed the importance of understanding the evolving mechanical properties in AAA models due to the difficulty in obtaining longitudinal AAA patient data. Another study characterised the biomechanical response of the commonly used ApoE knockout mouse model of AAA *ex vivo* using a pressure-dilation method (Haskett et al., 2013). The authors found that the aneurysm had progressive circumferential stiffening and decreasing circumferential strain between 14 and 28 days after AngII perfusion along with temporal microstructural and biomechanical reorganisation which was affected at 14 days but had improved by 28 days. Understanding and promotion of such biomechanical remodelling may enable translation into therapeutics for human AAAs. The AngII ApoE knockout model was compared with the elastase perfusion model in rats and mice in terms of morphology and biomechanics over 28 days (Phillips et al., 2015). *In vivo* ultrasound imaging was used to characterise these parameters and they found that circumferential strain decreased in AAAs, even prior to expansion of the aorta and so may be indicative of underlying disease processes in the early AAA. Uniaxial tensile testing of a decellularised rodent xenograft model has shown that implantation mesenchymal stromal cells (MSCs) is able to increase ECM density, attenuate wall stress variations and restore biomechanical integrity to the tissue, which show compelling evidence for the role of stem cell therapy in AAAs (Zidi and Allaire, 2015). Another study used uniaxial tensile testing to biomechanically characterise an elastase AAA model

in pigs: the aneurysmal aortic wall had increased stiffness and reduced strength compared to controls (Lederman et al., 2014).

Generally the biomechanical properties of experimental AAAs created *in vivo* through well characterised methods exhibit increased stiffness (with preference to the circumferential orientation) which is mirrored in the human disease. This study uses an *ex vivo* porcine bioreactor model of AAA and aims to biomechanically characterise the tissue.

1.9. BIOREACTORS IN VASCULAR RESEARCH

In tissue engineering research, the bioreactor is commonly used to provide an optimum growth environment for cells. The chemical requirements of the cells, such as oxygen level, nutrients, waste removal, growth factors and pH are met and so cells are able to maintain viability and function. However, it is not solely the biological environment that invokes cell response. The dynamic mechanical environment also plays a major role upon cell function and growth; consequently this determines the macrostructure of the tissue. The mechanical forces are transformed into biochemical signals by the cells via mechanotransduction (Vogel and Sheetz, 2006). Increased wall stress due to an increase in blood pressure triggers contraction of vascular SMCs narrowing the arteries and so inducing an increase in resistance. The blood flow is therefore kept constant in downstream capillaries (Hahn and Schwartz, 2009). SMCs may remodel the arterial wall by increasing its thickness if pressure remains elevated in order to resist these forces (Hahn and Schwartz, 2009). As the dynamic as well as the biochemical environment plays a significant role in the behaviour of the vascular cells, bioreactors must mimic these *in vitro*.

The viability of vascular constructs and bioartificial heart valves rely on haemodynamic shear stresses acting on and influencing the endothelial biology (Davies, 1995, Ruel and Lachance, 2009). Transmural pressure, cyclic strain from the pulsatile pumping action of the heart, shear stress and wall stress modulate the behaviour of SMCs (Osol, 1995). Studies have shown that organ culture which mimics the physiological environment enhances mechanical

properties and expression of essential cellular functions (Niklason et al., 1999, Nerem and Seliktar, 2001, Smith et al., 2001, Hynecek et al., 2007)

Bioreactors enable control and manipulation of the *ex vivo* mechanical environment in order to achieve the correct structure for specific tissue types. Therefore bioreactor designs are numerous and varied in order to meet these requirements.

1.9.1. BIOREACTOR MODELS OF AAA

The creation of an experimental aneurysm *ex vivo* would abrogate the time and cost implications of a large animal model whilst allowing more comparable physiology to humans versus a small animal model. Porcine carotid arteries were cultured *ex vivo* in order to assess SMC proliferation in stents used for stenotic arteries (Yazdani and Berry, 2009). Healthy porcine carotid arteries installed with one of three types of stents were cultured in a pulsatile flow environment for seven days in order to compare stent function between the designs. The SMCs remained viable after seven days and the effects of the stent designs and placement on SMC proliferation and histoarchitecture were characterised. This shows that an *ex vivo* vascular model is quite possible.

In the context of AAA, a recent study used a bioreactor to culture human SMCs seeded into a PTFE graft which had been focally dilated with a balloon (Touroo and Williams, 2012). The SMCs proliferated and formed a functional neointima over the scaffold after 14 days. Although this model may prove to be a useful tool in evaluating endovascular stent delivery, its capacity for analysis of interaction between stent devices and the arterial wall is limited in a clinical context. Stents are placed into the vasculature of patients with diseased arteries, and so, optimally, the model must reflect the biological aspects of the disease. There were histoarchitectural differences between the dilated and non-dilated parts of the graft, but the ubiquitous AAA characteristics (such as elastin disruption and SMC dysfunction) were not present in this model.

An *ex vivo* large animal model of AAA cultured in a bioreactor which reflects the biological aspects of the disease will be a useful research tool. This thesis aims to develop such a model in order to temporally characterise alterations in biomechanics, tissue structure and SMC behaviour in order elucidate the mechanisms involved of AAA formation and early disease.

1.10. CONCLUSIONS

AAA disease has myriad aspects of pathogenesis and progression, but is usually only discovered in humans after aortic dilatation has been initiated. Currently, no pharmacological or therapeutic treatments are available for attenuation or inhibition of AAA progression and so patients are destined for surgery. The instigating factor or factors in development of AAA is unknown, and so this has driven researchers to examine the early stages of the disease. However, research is limited by the paucity of human aneurysmal tissue which is at an early stage of AAA progression. In order to combat this, *in vivo* animal models are widely used; murine models offer a low cost, genetically malleable solution. Small mammal models are limited in evaluation of surgical solutions and biomechanics due to their miniature size and are not as similar physiologically to humans as large mammals. Studies with large mammals are limited due to great expense in terms of both time and cost, but *ex vivo* culturing of the arteries of large mammals in a bioreactor may hold the solution to this problem.

Comparatively fewer studies have been conducted to reveal the role of the SMC in AAA pathogenesis versus other aspects of the disease. Given that SMCs are known to have an inherently plastic nature, the temporal mapping of alterations in SMC phenotype over time in the context of early aneurysmal events may lead to the identification of AAA prior to aortic dilatation. Biomechanical analysis will investigate the function of the whole artery, as the ECM is maintained by the SMCs. Identifying changes in SMCs may also uncover targets for therapeutic or pharmacological therapies which have not yet been identified.

1.11. PROJECT RATIONALE

AAA is a progressive dilatation of the abdominal aorta which will lead to rupture without intervention. Rupture of an AAA carries an extremely high mortality rate. The only treatment options currently available for AAA are surgical procedures which leave no treatment options for patients who are unable to undergo surgery. Recently, a national programme has been implemented whereby AAA screening is offered to individuals considered to be at risk of developing the disease. Prior to this, AAAs were often detected incidentally to other medical conditions.

The AAA screening programme offers unprecedented opportunity to study the *in vivo* progression from the early to end-stages of the disease. This may reveal earlier stages of the disease where it would be appropriate to intervene with therapeutic or pharmacological agents. However, understanding the underlying mechanisms behind AAA formation and early development is essential for uncovering early therapeutic targets. It is virtually impossible conduct research on human AAA tissue in the earliest stages of the disease due to its very nature. Therefore, over the past four decades, a wide range of AAA models have been developed to order to understand the longitudinal disease and the underlying mechanisms which are implicated in AAA.

SMCs are vascular cells responsible for maintaining the arterial ECM and are thought to play a role in AAA development. SMCs from human AAA tissue are dysfunctional and SMC seeding has been shown to attenuate AAA progression animal models. Given the inherent plasticity of adult SMCs and their ability to maintain the ECM they have been identified as an appealing target for study.

1.12. AIMS AND OBJECTIVES

It has been shown that using an *ex vivo* bioreactor porcine model of end-stage AAA causes the SMCs to adopt a phenotype which is comparable to SMCs from end-stage human AAA tissue. The main aim of this study was to develop and

use this *ex vivo* model to investigate and characterise the temporal phenotypic modulation in SMCs and relate this to function of the whole artery via biomechanical testing. This may reveal potential early targets for AAA disease which is especially important in the context of the recent implementation of AAA screening.

An early AAA model was developed and the arterial structure and SMC morphology and function were characterised and compared to SMC behaviour in the end-stage model. The biomechanical behaviour of the end-stage AAA model was characterised in order to relate SMC dysfunction to the function of the artery as a whole organ.

Specific objectives:

1 To characterise the structure of the artery in the early- and end-stage model
2 To determine the role of chemical ECM degradation and bioreactor culture on SMC morphology
3 To determine changes in SMC structure and function with respect to time
4 To characterise and calibrate the dynamic environment within the bioreactor
5 To investigate the biomechanical impact of ECM degradation used to induce the experimental AAA model
6 To characterise the biomechanical properties of the end-stage AAA model

CHAPTER 2

MATERIALS AND METHODS

CHAPTER 2 MATERIALS AND METHODS

This chapter describes the materials and methods used to investigate the cellular, histological and biomechanical properties of aneurysm model arteries and their respective explanted SMCs after two different intervals of time in culture. Firstly, details of all reagents and consumables and their suppliers are given, along with the general experimental approach used for this study. The cell culture and primary SMC explant and isolation techniques are also described.

Secondly, the methods used to characterise the structure and function of the tissues and cells are described. Lastly, the methods for biomechanical assessment of the *ex vivo* model are given. The aforementioned biomechanics section is separated into two sections: methods for uniaxial tensile testing and whole artery dilation testing.

2.1. SUPPLIERS OF MATERIALS AND REAGENTS

The supplier details for the materials, reagents and equipment used throughout this study are listed in Appendix A, categorised in Tables A.1 to A.7.

2.2. GENERAL EXPERIMENTAL APPROACH

The workflow for the overall project is shown in Figure 2.1. Carotid arteries were aseptically harvested from a total of 12 pigs by two trained surgeons. Animal sacrifice was conducted by technicians from Central Biomedical Services under the Humane Killing of Animals under Schedule 1 to the Animals (Scientific Procedures) Act 1986. For each animal, a sample of fresh tissue was taken straight after harvest for SMC explant cultures and tissue fixation for histology and immunohistochemistry (FRESH). FRESH tissue was taken in order to analyse the SMC characteristics of each individual animal with no treatment.

Each of the remaining carotid arteries was either pre-treated with an agar gel containing elastase and collagenase (CCE) or a vehicle agar gel (VEH). The vehicle gel-treated artery served to act as a control vessel. Each of the treated vessels (VEH and CCE) was then divided into two: one length was installed in the bioreactor (BIO) and cultured under flow and the other length was cultured under static conditions (S) in a 6-well plate. The full details for the gel treatments and the culture conditions are included within Chapter 3.

The time during which the arteries remained as a whole organ in culture was as follows: the arteries of three animals were cultured for three days (EARLY) and the arteries of two animals were cultured for twelve days (END). It has previously been shown using this *ex vivo* model that SMCs derived from arteries which received CCE pre-treatment prior to culture in the bioreactor for twelve days had a similar phenotype to human end-stage AAA SMCs (Riches et al., 2013). In a mouse model, it was shown that 14 days after treatment, an aneurysmal arterial dilation was observed, but SMC phenotypic switching was present seven days after treatment (Ailawadi et al., 2009). Therefore, the culture period in the bioreactor for the EARLY model was chosen to be three days in order to explore the behaviour of the SMCs prior to the observed phenotypic switch.

Once the culture time had elapsed, a small segment of each these arteries was used for generating explant SMC cultures and the remaining portion was fixed

for histological and immunohistochemical analysis. Arteries from an additional three animals were cultured for 12 days (END) and were used for uniaxial tensile testing for biomechanical analysis once the culture time was complete. All of the aforementioned analysis could not all be conducted on every artery, as the experiments were limited by the tissue yield per animal.

Parallel to this, non-sterile carotid tissue was obtained from the abattoir for biomechanical characterisation of the effects of CCE and VEH treatment. Each carotid artery was bisected and one segment underwent uniaxial tensile testing whilst the other segment was subjected to whole artery dilation testing. The methods were evaluated as appropriate for the testing of END model tissue.

2.2.1. EXPERIMENTAL TISSUE GROUPS

According to specified treatment and culture conditions, the tissue was allocated into five groups, detailed in Table 2.1 below. The abbreviations detailed below are used for reference to these groups throughout this document.

Table 2.1 Experimental tissue groups and the corresponding methods of treatment

Group	Treatment
FRESH	No gel treatment, no culture
SVEH	Treatment with vehicle gel, static culture in a 6 well plate
SCCE	Treatment with CCE gel, static culture in a 6 well plate
BIOVEH	Treatment with vehicle gel, dynamic culture in bioreactor
BIOCCE	Treatment with CCE gel, dynamic culture in bioreactor

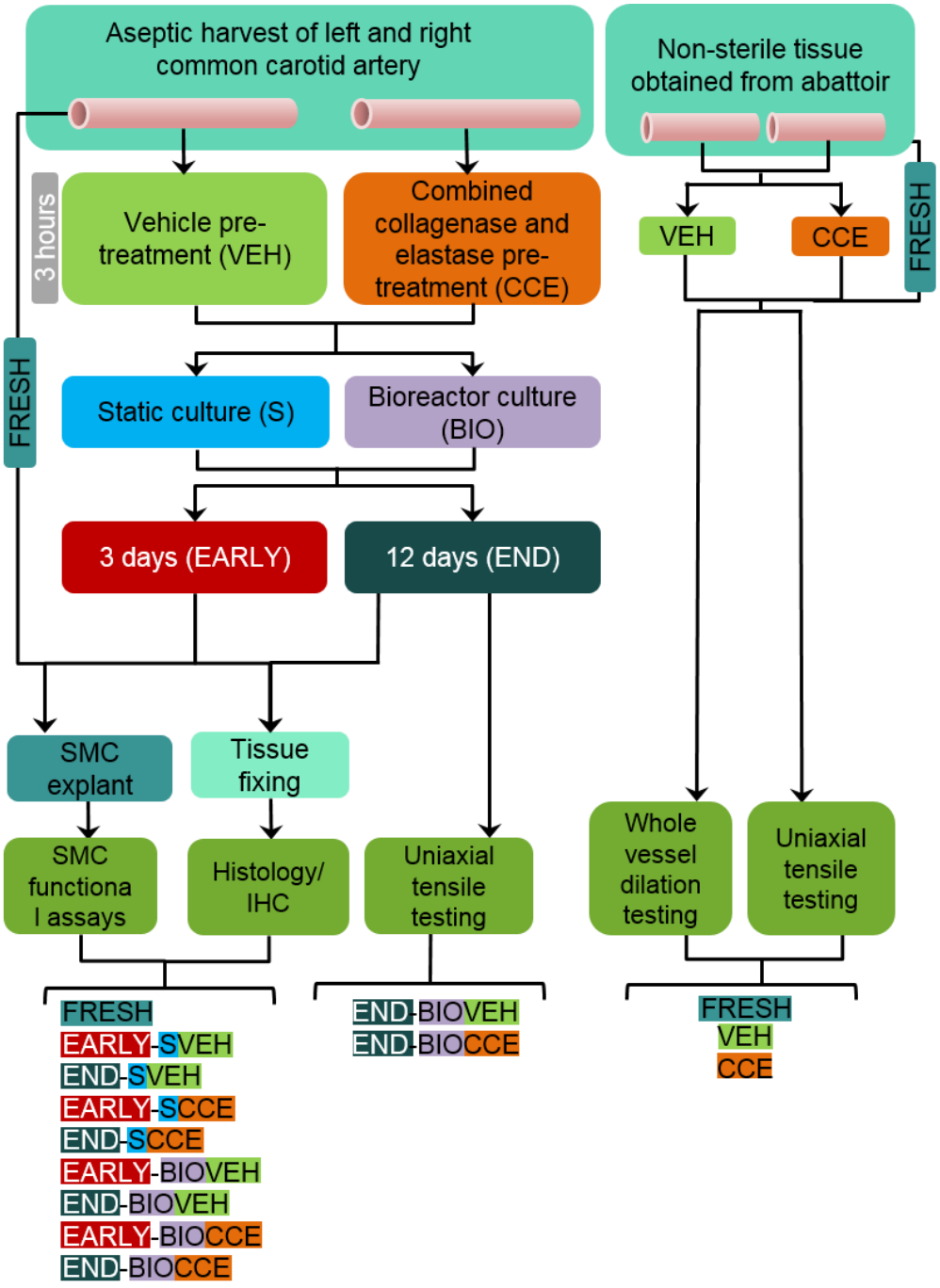

Figure 2.1 Workflow for overall project showing experimental approach and SMC experimental groups. The groups are referred to with these abbreviations throughout this thesis.

2.3. MEDIA AND REAGENT COMPOSITION

The compositions of media used throughout cell culture are detailed in Appendix B. These media were used throughout the project and are referred to throughout this document by abbreviations, as follows.

Table 2.2 Cell culture media compositions

Media	Abbreviation
10% full growth medium	**FGM**
5% sub-maximal growth medium	**SGM**
0.4% minimal growth medium	**MGM**
Serum free medium	**SFM**

2.4. CELL CULTURE TECHNIQUES

All cell culture procedures and techniques were carried out aseptically in a Class II laminar flow hood. All culture media and reagents were warmed to 37°C before use.

2.4.1. CELL PASSAGING

Once the cells had formed a confluent layer, the culture medium was aspirated from the flasks, along with detached cells and cell debris. The cells were then washed in PBS to remove traces of the culture medium. Trypsin/EDTA (2 ml) was then added and the flasks incubated at 37°C for 5 to 10 minutes to facilitate cell detachment. Detachment was aided by gentle physical agitation and monitored via a light microscope. When cell detachment had occurred, medium containing serum (SGM) (10 ml) was then added to inhibit the action of the trypsin/EDTA, and the cell suspension was transferred to a conical bottomed centrifuge tube and centrifuged for 6 minutes at 600g. Following centrifugation, the supernatant was carefully poured off. The cell pellet was re-suspended in FGM (10 ml) and an equal volume was transferred to three new tissue culture flasks. The culture medium was half changed every 3 to 4 days until cell confluence had once again been reached.

2.4.2. CELL COUNTING

Cells were detached from the tissue culture flask and centrifuged to attain a cell pellet (Section 2.4.1). The cell pellet was then re-suspended in FGM (1 ml). A haemocytometer was used to count live cells under a light microscope. Trypan blue dye (0.2%; 50 μl) was added to an equal volume of cell suspension and mixed carefully with the pipette. Trypan blue is excluded from viable cells (which appear white/colourless) but is taken up by non-viable cells (appearing blue). Viable cells were counted in one grid on each side of the haemocytometer and cell density was calculated as follows:

$$\text{Cell density} = \frac{\text{sum of viable cell counts} \times 10^4}{\text{volume in ml}}$$

Volumes of cell suspension were then added to the calculated volume of FGM and seeded at the required cell density for each assay.

2.4.3. CELL CRYOPRESERVATION

Cells were detached from tissue culture flasks and centrifuged to attain a cell pellet (Section 2.4.1). The cell pellet was then re-suspended in cryopreservation medium (1ml), and aliquoted in 0.5 ml volumes into labelled cryovials. These were then immediately placed overnight in a freezing container containing isopropanol at -80ºC to ensure a cooling rate of 1°C/minute (optimal for cell preservation). The cryovials were then transferred to liquid nitrogen for long term storage.

Due to practical constraints intrinsic to the nature of the study, SMCs were not uniformly cryopreserved. The timecycle for this is shown in Figure 2.2.

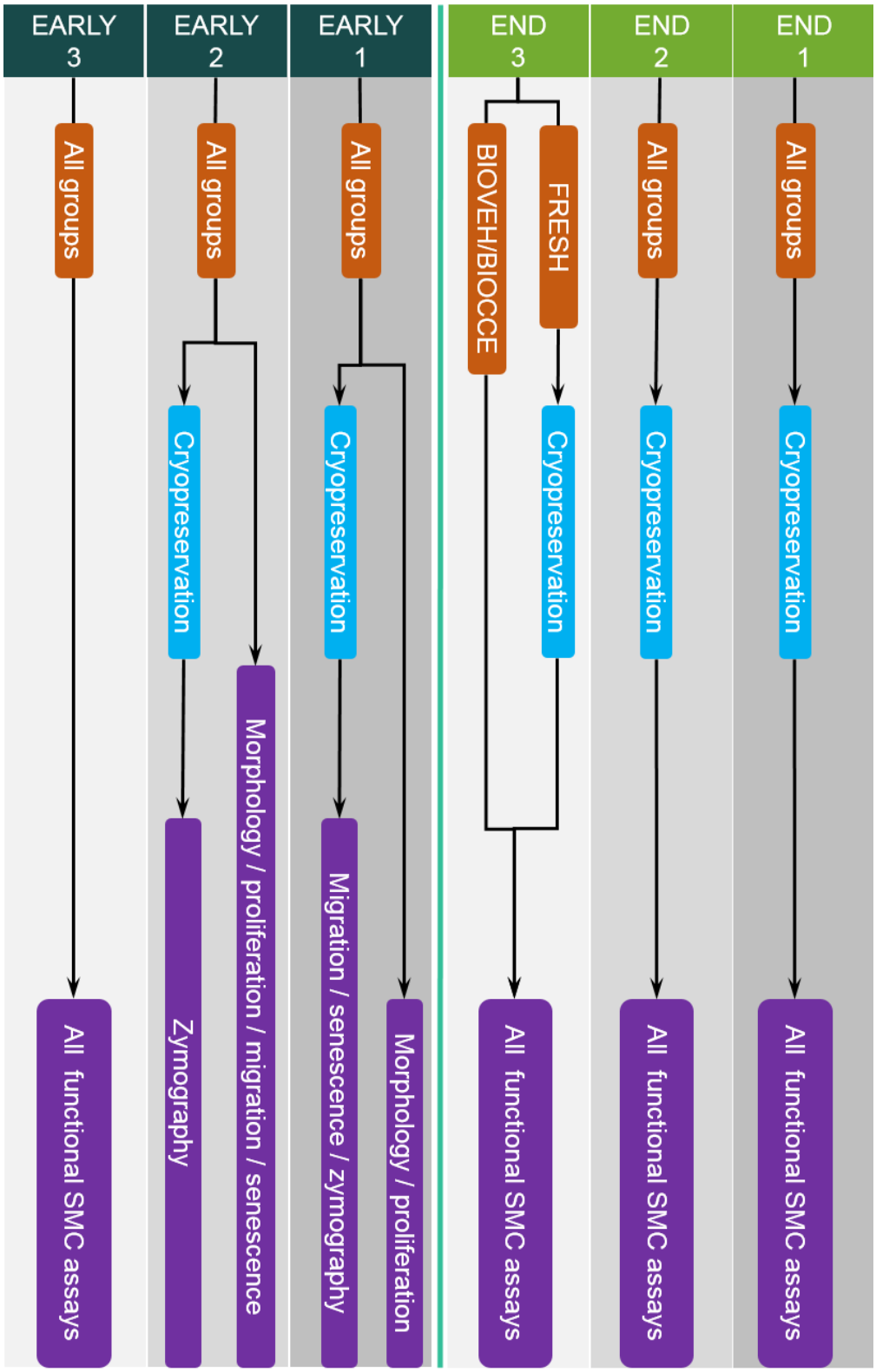

Figure 2.2 Timecycle schematic of SMC cryopreservation. END = End model artery, EARLY = Early model artery, (n=3).

Particularly for the END model SMCs, the FRESH control had normally reached confluency before the BIOVEH and BIOCCE SMCs. This was because the FRESH SMCs were explanted on the day of the tissue harvest, whilst BIOVEH and BIOCCE SMCs were only explanted from tissue fragments once the artery had been cultured in the bioreactor for twelve days. In addition, the effect on the proliferation rate of the SMCs was also a factor in the time lag between treatment groups. For this reason, and in order to maintain the primary cells at a low passage (<p5), some SMC groups were cryopreserved. In addition to this, the SMC explanted from arteries which were carried out earlier on in the project were cryopreserved in order to allow time to master the techniques involved in the functional assay characterisation. This was parallelised in order to complete the study within the required timeframe.

2.5. PRIMARY SMOOTH MUSCLE CELL ISOLATION

Once the tissue had been subjected to necessary specified treatment and culture conditions, a small tissue fragment was taken for SMC explant cultures as follows. The tissue fragments were transferred to a sterile petri dish containing 2 ml FGM and minced using a sterile scalpel blade into approximately 1 mm^3 pieces. The minced tissue and FGM were then transferred together into a 25 cm^2 tissue culture flask, incubated at 37ºC in a humidified incubator gassed with 5% v/v CO_2 in air and monitored until cells explanting outwards from the tissue fragments could be observed (Figure 2.3).

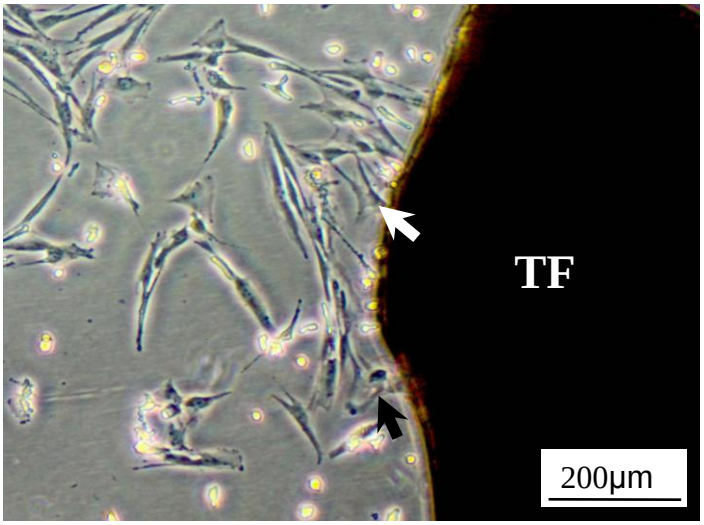

Figure 2.3 Primary SMC explanting from a fragment of porcine carotid artery. TF = tissue fragment. Arrows showing explanting SMC.

Supplementary FGM was added in 0.5 ml volumes until the total volume was 4 ml and then the media was half-changed twice per week until the SMC had reached confluence (Figure 2.4). Cells were used for structural and functional assays at passages between 2 and 5.

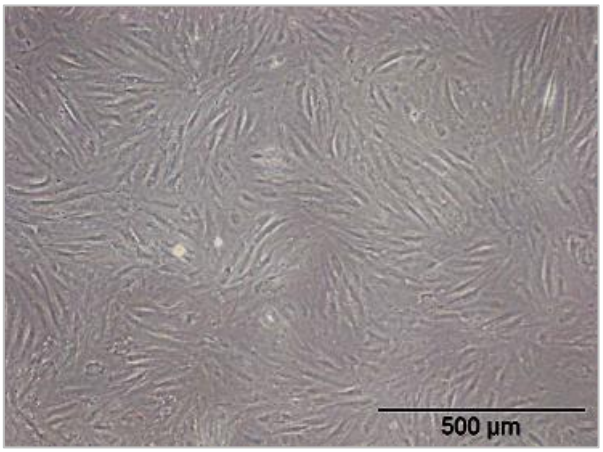

Figure 2.4 Representative image of SMC grown to confluence - cells exhibit characteristic 'hill and valley' growth pattern.

Once grown to confluence, SMC explant cultures were used for assessment of SMC phenotype and functional SMC assays. SMCs were stored in liquid nitrogen as per Section 2.4.3.

2.6. PREPARATION OF ARTERIAL TISSUE

2.6.1. FIXATION OF ARTERIAL SEGMENTS

Vessels removed from the bioreactor were divided into three portions representing the inlet, centre and outlet portions. These arterial portions, along with the portions cultured statically were fixed in neutral buffered 10% Formalin for 3 to 5 days. Fixed tissues were then either subjected to tissue processing, or were held in 70% ethanol until they were able to be processed in order to prevent over-fixation.

2.6.2. TISSUE PROCESSING

Fixed tissues (see section 2.6.1) were placed in plastic histology cassettes and processed using a Leica TP 1020 Tissue Processor (Leica, Wetzlar, Germany) on an overnight programme starting through graded alcohols (70%, 1hr; 90%, 1hr; 95%, 1hr; 100%, 1hr; 100%, 2hrs) then moving to Histo-Clear (3 buckets; 1hr, 1hr, 1.5hrs) then ending in molten paraffin wax (2 buckets; 2hrs, 2hrs).

2.6.3. PARAFFIN WAX EMBEDDING

Tissue embedding was performed on a Medite TES99 embedding system (Medite, Hannover, Germany). Molten wax was poured into moulds and the arterial segments orientated to provide a transverse arterial section on cutting. The top of the processing cassette was then embedded into the molten wax mould to provide grip for the microtome. The wax blocks were then left to harden at room temperature overnight.

2.6.4. SECTIONING OF EMBEDDED TISSUE

Wax blocks containing embedded tissue were placed on ice prior to sectioning in order to increase the quality of the cut. Sections 5 μm thick were cut using a

Leica RM2235 microtome (Leica, Wetzlar, Germany) and then floated onto distilled water at 50°C to smooth creases in the tissue. Glass slides were placed underneath the floating sections so that they adhered to the slide as it was lifted out of the water. Slides were then left to dry vertically and then were placed into a 50°C incubator overnight to ensure complete adherence of the tissue to the glass slide.

2.7. HISTOLOGY AND IMMUNOHISTOCHEMISTRY

2.7.1. ALPHA-SMOOTH MUSCLE ACTIN AND MILLER'S ELASTIN CO-STAIN

Alpha-smooth muscle actin (α-SMA) with Miller's elastin co-stain allows visualisation of α-SMA, which is a marker of SMCs, and of the elastin fibres in the tissue, respectively. Horse-radish peroxidase methods of immunohistochemistry form a brown precipitate in the presence of primary antibody binding (α-SMA). Miller's elastin stains elastin fibres purple.

Sections were deparaffinised by submerging slides in two changes of Histo-Clear for 8 minutes each and then rehydrated by passing through a series of graded alcohols (100%, 5 minutes; 100% 3 minutes; 90%, 3 minutes; 70%, 2 minutes) and then tap water for 2 minutes. Endogenous peroxidase activity was blocked by submerging the slides in 3% v/v hydrogen peroxide in distilled water for 10 minutes. Slides were then briefly washed in still tap water before being transferred to 100 µl coverplate chambers for all subsequent steps unless stated.

Sections were then washed continuously by pipetting 1X Tris buffered saline (TBS) (1M Tris base, 1.5 NaCl in distilled water) into the coverplates for 5 minutes. To block non-specific binding of the primary antibody, 100 µl per slide of normal goat serum diluted 1:20 with 1X TBS was added to the coverplates and then incubated for 10 minutes. Sections were then incubated overnight at 4°C with 100 µl per slide of mouse monoclonal anti-alpha smooth muscle actin clone 1A4 diluted 1:400 with 1X TBS. Sections were then washed for 20 minutes by continuous pipetting of 1X TBS into the coverplates, then incubated

in horse radish peroxidase-conjugated anti-mouse secondary IgG antibody diluted 1:50 with 1X TBS for 30 minutes at room temperature. Slides were once again washed continuously with 1X TBS for 20 minutes. Detection of subsequent peroxidase activity was carried out using a solution containing 0.7 $mg.ml^{-1}$ 3,3'-diaminobenzidine (DAB) and 2.0 $mg.ml^{-1}$ urea hydrogen peroxide (SIGMA*FAST*™) in deionised water. Formation of brown precipitate was monitored closely and 1 – 2 minutes was sufficient for all sections.

Slides were quickly detached from the Shandon coverplate system and washed in still tap water to inactivate DAB action. Slides were then rinsed in 95% methylated spirits (5% v/v methanol in ethanol) followed by a rinse in 95% ethanol. For the elastin co-stain, slides were then submerged in Miller's staining solution for 20 minutes. The slides were then put through a series of 95% ethanol washes in order to remove the surface stain (3 x 3 minute washes). Slides were then fully dehydrated by submerging in 100% ethanol (2 x 2 minutes) and cleared with Histo-Clear for 10 minutes. Slides were then mounted with DPX mountant and glass coverslips and allowed to air dry for at least 24 hours before microscopic visualisation.

2.7.2. PICRO-SIRIUS RED

Fixed tissue segments from one animal were stained with picro-sirius red in the laboratory. All other picro-sirius red staining was completed by Mike Shires of the Leeds Institute of Cancer and Pathology. Picro-sirius red allows visualisation of collagen fibres under polarised light (appearing red, green or yellow depending on fibre orientation).

Sections were deparaffinised by submerging slides in two changes of Histo-Clear for 8 minutes each and then rehydrated by passing through a series of graded alcohols (100%, 5 minutes; 100% 3 minutes; 90%, 3 minutes; 70%, 2 minutes) and then running tap water for 3 minutes. The nuclei of the tissue were then stained by immersing the slides in Weigert's haematoxylin (1:1 ratio solution A to solution B) for 10 minute. The sections were then washed in tap water for 1 minute. The slides were then immersed in picro-sirius red (0.1% w/v

aqueous saturated picric acid solution) for 1 hour. The excess dye was then removed by washing each slide in distilled water and then blotting dry. The slides were then dehydrated by passing them through a series of graded alcohols (70% ethanol v/v in distilled water, 5 seconds; 95% ethanol v/v 5% methanol, 5 seconds; 95% ethanol v/v 5% methanol, 2 minutes; 95% ethanol v/v 5% methanol, 3 minutes). Sections were then cleared in Histo-Clear for 10 minutes before being mounted with glass coverslips with DPX mountant. Slides were allowed to air dry for at least 24 hours before microscopic visualisation.

2.7.2.1. VISUALISATION OF PICRO-SIRIUS RED STAINED SLIDES

The collagen of picro-sirius red stained sections was visualised using brightfield microscopy with a linear polarising filter.

2.7.2.2. LUMINAL PERIMETER

Analysis of luminal circumference was carried out post-tissue fixation on paraffin embedded fixed slides. The luminal circumference of ten 5 μm sections from the centre portion of the fixed artery were measured per artery (n=5). Whole stained sections were visualised using low magnification brightfield microscopy. The 'Find Edges' tool in ImageJ was used to emphasise the edges of the lumen. The 'Find Edges' tool uses a Sobel edge algorithm to complete this task, and is commonly used in image processing. The images were then converted into a binary image (Figure 2.5) using ImageJ and the 'magic wand' tool used to select the luminal region (http://imagej.nih.gov/ij/). The perimeter of the luminal section was then recorded.

Figure 2.5 Measurement of luminal perimeter. Left: unprocessed image. Centre: image converted into a binary image with magic wand selection (green). Right: zoom in of magic wand selection (green).

An idealised arterial diameter was calculated via representing the artery as a perfect circle with a circumference equal to the measured arterial perimeter. This measured perimeter was divided by the ratio π to give the idealised arterial diameter by representing the artery as a circle. Transforming measured luminal perimeter into idealised diameter allowed the arteries to be subject to the clinical definition of AAA, where the arterial diameter is 150% that of the healthy aorta (Nordon et al., 2011). This transformation of the measurements to idealised arterial diameter is shown in Figure 2.6. Luminal area, unlike luminal perimeter, is affected by the shape of the fixed tissue and so could not be used to investigate geometrical changes as the tissue was not perfusion-fixed.

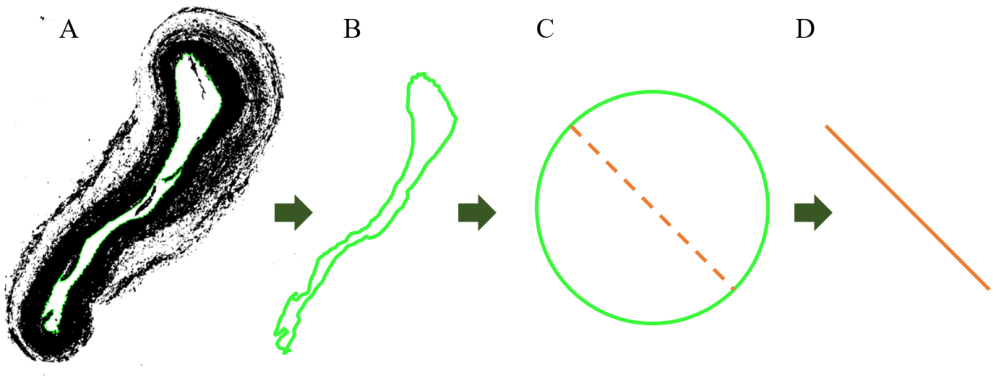

Figure 2.6 Transformation of measured luminal circumference to idealised diameter. A) luminal perimeter was measured according to stated methods. B and C) the artery is represented as a perfect circle with circumference equal to the measured perimeter. D) the circumference is divided by π to give the idealised diameter.

2.7.2.2.1. DATA AND STATISTICAL METHODS

A total of three animals per model stage was used. Vessels which underwent vehicle (VEH) and protease (CCE) treatment were normalised to the mean FRESH idealised diameter, in order to ameliorate the effects of inter-animal variance. Ten sections were measured per treatment condition per animal, giving a total of 30 individual datapoints in each set. A two way ANOVA with post-hoc Tukey test was used to determine the effect of model stage (END/EARLY) and treatment group (FRESH/VEH/CCE) on the idealised luminal diameter in OriginPro 2015 (OriginLab, MA, USA). A p-value of <0.05 was taken to denote statistical significance.

2.8. CELLULAR CHARACTERISATION

The smooth muscle cell is able to dynamically contract or relax in order to maintain blood flow and pressure throughout the vasculature. Vascular smooth muscle cells are not terminally differentiated and are able to undergo profound changes in phenotype according to local environmental cues (Owens et al., 2004, Rzucidlo et al., 2007). SMCs are generally considered to have two major phenotypes – contractile and secretory – which influence SMC morphology and

function (Porter and Riches, 2013). Switching of SMC phenotype is an event which occurs early in the progression of AAA disease, and so one of the aims of this project was to elucidate the temporal mapping of phenotypic switches in the *ex vivo* model (Ailawadi et al., 2009). This section contains the methods used to structurally and functionally characterise the EARLY and END stage SMCs in the bioreactor model.

2.8.1. MORPHOMETRIC ANALYSIS

Cells were seeded at a density of 2 x 10^5 cells per 75 cm^2 cell culture flask and cultured at 37°C in a humidified incubator gassed with 5% CO_2 v/v in air for 72 hours in 4 ml FGM. Brightfield microscopy was then used to capture at least 10 fields of view at 100x magnification in a prescribed pattern for every experiment in order to remove observer bias (Figure 2.7). The boundary of 50 individual cells per condition were traced and the circularity of cells was recorded using ImageJ software (http://imagej.nih.gov/ij/). Circularity is a dimensionless geometric descriptor value built-in to ImageJ software calculated using the formula described in Equation 2.

$$\text{circularity}=4\pi\left(\frac{\text{area}}{\text{perimeter}^2}\right)$$ **Equation 2 Circularity**

Circularity is a scale from 0.0 to 1.0: a value of 1.0 denotes a perfect circle and as the value approaches 0.0 it indicates an increasingly elongated polygon (Cox, 1927, Helmy and Azim, 2012).

2.8.1.1. DATA AND STATISTICAL METHODS

The assay was performed at a passage which was identical for each animal (p3). This gave a total of 150 cell circularity measurements per model stage. A two-way ANOVA with post-hoc Tukey test was used to determine the effects of model stage and treatment group and the interaction between them on mean cell circularity. The ANOVA was carried out using OriginPro 2015 software

(OriginLab, MA, USA). A p-value of <0.05 was taken to denote statistical significance.

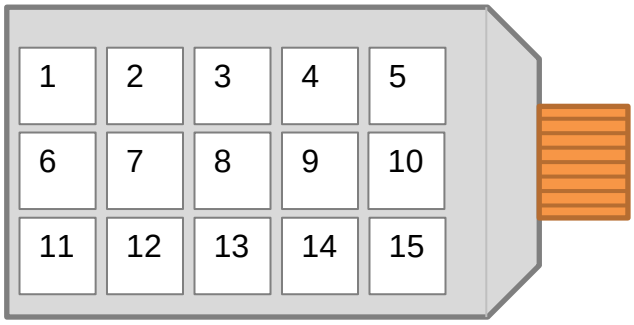

Figure 2.7 Pattern of field of view capture in a 75 cm^2 flask for morphometric cell analysis

2.8.2. F-ACTIN IMMUNOFLUORESCENCE

The cytoskeletal f-actin microfilament was visualised by staining with rhodamine phalloidin fluorescent probe. Cell nuclei were visualised by using a mounting medium containing 4',6-diamidino-2-phenylindole (DAPI), a nuclear dye specific to DNA.

2.8.2.1. CELL SEEDING AND FIXATION

Cells were seeded in a 24-well plate at a density of 1 x 10^4 cells per well on top of sterilised, circular coverslips and cultured in 1 ml FGM at 37°C in a humidified incubator gassed with 5% CO_2 v/v in air for 96 hours. The media was then removed and the cells washed with 1X PBS. Cell fixation was achieved by adding 400 – 500 µl per well of 4% paraformaldehyde (PFA) and then leaving the plate on a rocker for 20 minutes. The PFA was then removed and the cells once again washed with 1X PBS. Wells were then filled with 1X PBS and stored at 4°C until staining.

2.8.2.2. RHODAMINE PHALLOIDIN STAIN

Coverslips were washed twice with 1X PBS. SMCs were permeabilised and blocked for non-specific binding by incubating with 10% goat serum in 0.05% Triton X-100 in PBS for 5 minutes. SMCs were then washed twice again with 1X PBS. The cells were then incubated with rhodamine-phalloidin diluted 1:40 in PBS in the dark for 20 minutes and washed twice again with 1X PBS. The cells were then mounted using ProLong® Gold Antifade Mountant with DAPI to achieve a nucleus stain. Slides were left in the dark overnight to allow the mountant to set. The f-actin cytoskeleton was visualised using a Zeiss LSM700 (Carl Zeiss AG, Oberkochen, Germany) confocal microscope.

2.8.3. CELL PROLIFERATION

Cells were seeded in a 24-well plate at a density of 1 x 10^4 cells per well in 1 ml FGM and incubated at 37°C in a humidified incubator gassed with 5% CO_2 v/v in air for 24 hours. After this period, the media was removed and the cells were washed with 1X PBS and then supplemented with 1 ml SFM for 72 hours in order to drive the cells into a quiescent state. Cells were then placed back into 1 ml FGM for the remainder of the experiment. Cell counts were made at days 0, 2, 4 and 7 with a media change on days 2 and 4. For cell counts, each well was aspirated, washed in PBS and trypsinised. Viable cell counts were quantified using 0.2% Trypan blue in PBS and a haemocytometer (See Section 2.4.2. for method in detail). Quadruplicate counts were taken at each time point. The proliferation assay was repeated at passages 3, 4 and 5 for every animal. A proliferation curve was then plotted using OriginPro 2015 software (OriginLab, MA, US) and the area under the curve calculated to determine the proliferative capacity of the cells.

2.8.3.1. DATA AND STATISTICAL ANALYSIS

A quadruplicate cell count per assay and a repeat of three passages comprised the dataset for each animal, giving a total of twelve individual data points per

day per animal. Each passage of cells from each animal was normalised and represented as a percentage of the respective FRESH day 0 count in order to mitigate inter-animal and passaging effects. A one-way ANOVA with post-hoc Tukey test was used on day 7 count data to determine the effects of the vessel treatment within each model stage (EARLY/END). The area under the curve was calculated to represent the total growth over the seven day period. A t-test was used to determine the effects of model stage within each vessel treatment group. The statistical analysis was performed using OriginPro 2015 (OriginLab, MA, USA). A p-value of <0.05 was taken as the significance threshold.

2.8.4. SCRATCH WOUND MIGRATION

Cellular migration in a monolayer was determined as previously described (Riches et al., 2009). Prior to plating, migration guidelines were etched into the underside of a 12-well plate (Figure 2.8). One vertical line was etched in the centre of each well with five horizontal parallel transecting lines approximately 1 mm apart also drawn.

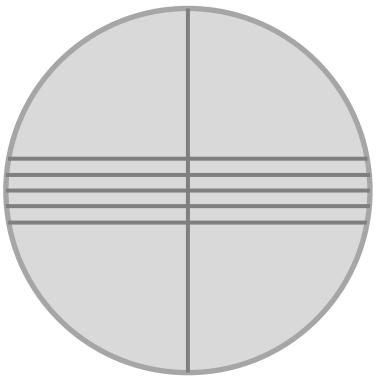

Figure 2.8 Schematic of etching pattern on underside of one well of a migration plate

Cells were then seeded at a density of 1×10^5 cells per well in 1.5 ml FGM and cultured at 37°C until confluent. The media was then removed and the cells washed with PBS and then supplemented with 1.5 ml SFM for 72 hours in order to bring the cells into a quiescent state.

The cell monolayer was then wounded in line with the vertical etched line using a sterile 10 ml Gilson pipette tip (Figure 2.9). Once an adequate uniform scratch wound has been achieved, medium was aspirated and wells were washed in PBS to remove cellular debris and replenished with 1.5 ml SFM.

Images of the four spaces between the transecting horizontal lines were then taken using brightfield microscopy at this 0 hour (0h) time point; four images were taken per well. The cells were then aspirated once more and placed into 1.5 ml SGM and incubated at 37°C for 24 hours. This assay was performed in SGM as it provides a submaximal stimulus compared to FGM (maximal stimulus) and so any subtle changes in migration were not potentially masked by the maximal stimulus. After 24 hours, images of each of the same areas were taken (24h).

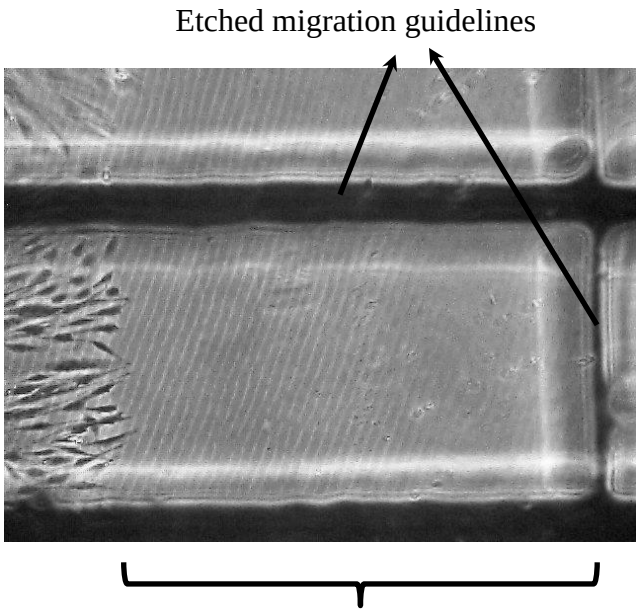

Figure 2.9 Confluent monolayers of SMC wounded to give area clear of cells

2.8.4.1. DATA AND STATISTICAL ANALYSIS

Each 0h image was then imported into Microsoft Office along with its corresponding 24h image and aligned using the guidelines etched onto the underside of the well. The wound edge was traced, duplicated and translated 1.52 cm towards the vertical etched line – previous study in our laboratory using

a microscope and a ruler has shown that 1.52 cm is equivalent to 200 μm. The number of cells migrated past the 200 μm marker was then recorded. The distance (in cm) between the etched horizontal guidelines was measured and converted into actual distance in mm on the plate. Data was displayed as the number of cells migrated past the 200 μm marker per mm of wound width.

Each count was performed in quadruplicate in 4 wells per condition. Three animals were used per model stage and counts from passages 3, 4 and 5 were collected from each animal to give twelve individual data points for each of the three animals. The mean migration data calculated from the quadruplicate count was expressed as a percentage of the corresponding FRESH mean migration data for the same passage in order to mitigate the effects of passaging and variations between animals. A two-way ANOVA was performed using OriginPro 2015 (OriginLab, MA, USA). A p-value of <0.05 was taken to be significant. Effects of SMC orientation were analysed with a one-tailed t-test.

2.8.5. SENESCENCE ASSOCIATED BETA-GALACTOSIDASE STAINING

The Cell Signalling Senescence-associated β-galactosidase (SA-βgal) Staining Kit detects β-galactosidase at pH6, a known characteristic of senescent cells not found in presenescent, quiescent or immortal cells. The manufacturer's instructions were followed. Briefly, cells were seeded in a 6-well plate at a density of 7.5×10^4 cells per well in 2 ml FGM and incubated at 37°C in a humidified incubator gassed with 5% CO_2 v/v in air for 24 hours.

After this period, the culture media was aspirated and the cells were washed with 2 ml 1X PBS per well. The cells were then fixed using the kit Fixative Solution (20% formaldehyde, 2% gluteraldehyde in 10X PBS). Following two washes of 1X PBS, 1 ml per well of β-galactosidase Staining Solution (930 μl 400 mM citric acid/sodium phosphate, 1.5 M NaCl, 20 mM $MgCl_2$ + 10 μl 500 mM potassium ferrocyanide + 10 μl 500 mM potassium ferricyanide + 50 μl 5-bromo-4-chloro-3-indolyl-βD-galactopyranoside (X-gal) in N-N-dimethylformamide (DMF)) ensuring that the final pH of the staining solution was between pH5.9 – 6.1. 1 M hydrochloric acid was used to adjust the pH if

necessary. The plate was then incubated at 37°C overnight in a non-humidified incubator. For long term storage, the staining solution was removed and the cells overlaid with 70% v/v glycerol in distilled water.

2.8.5.1. DATA AND STATISTICAL ANALYSIS

The level of senescence was determined by ten 40x microscope images per well, taken in the exact same pattern for every well in order to remove observer bias (Figure 2.10). This protocol was used to determine the senescence levels of human AAA SMC previously (Riches et al., 2013) The images were then analysed by expressing the number of β-galactosidase positive stained cells as a percentage of the total number of cells in each field of view.

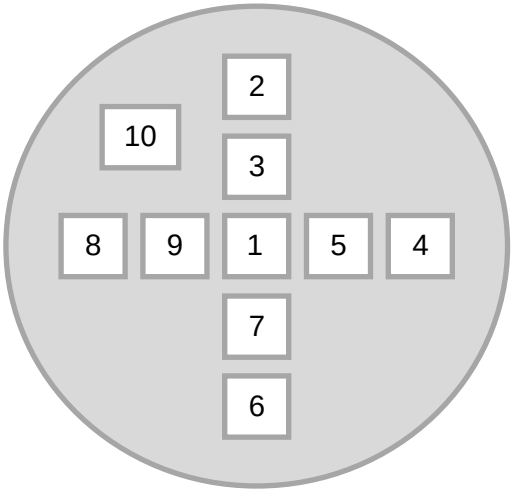

Figure 2.10 Schematic of image order pattern for each well to determine senescence levels.

Each assay was performed in triplicate for three matched passages to give 30 senescence images per animal (p3, p4 and p5 for all treatment conditions). The senescence level of the treatment conditions within each assay and passage was expressed as a percentage of the respective FRESH control in order to mitigate the effects of passage and animal related variance. The mean of these relative senescence indices was then taken to give a mean relative senescence index for each treatment group. The relative senescence level was analysed using a one-

way ANOVA per treatment group with a post-hoc Tukey test. A p-value of <0.05 was taken to denote statistical significance.

2.8.6. GELATIN ZYMOGRAPHY

Gelatin zymography allows analysis of levels of secreted matrix metalloproteinases (MMP) on a gelatin based acrylamide gel. MMP activity is visualised by clear bands of lysis on a stained dark background.

The effect of treatment group and model stage on stimulated, as well as basal level, secretion was also investigated in order to explore their effects on reaction to normal stimuli. A known stimulus of MMP secretion, phorbol ester (12-O-Tetradecanoylphorbol-13-acetate), and a more physiologically relevant combination of pro-inflammatory cytokines – platelet-derived growth factor (PDGF) and interleukin-1α (IL-1α) – were used to investigate changes in secretion in response to these stimuli.

2.8.6.1. COLLECTION OF CONDITIONED MEDIA

SMCs were seeded at a density of 2×10^5 cells per 25 cm^2 flask and cultured in 4 ml FGM in a humidified incubator at 37°C and gassed with 5% CO_2 v/v in air for 24 hours. Per condition, three separate flasks were needed. The media was then removed, the SMCs washed with PBS and then supplemented with SFM for 72 hours to bring them into a quiescent state. Each of the three flasks per experimental condition was then subjected to either a vehicle control, 12-O-Tetradecanoylphorbol-13-acetate (TPA) or a combination of PDGF and IL-1α as shown in Table 2.3.

A volume of 1.4 ml of each treatment was added to each of the flasks and cultured at 37°C in a humidified, gassed (5% CO_2 v/v in air) incubator for 48 hours. Conditioned media was then collected from the cells and centrifuged for 6 minutes at 600 x g and 4°C to remove any remaining cellular debris. The supernatant was then aliquoted into 100 µl volumes – to prevent freeze-thaw cycle of conditioned media once used – and snap frozen in liquid nitrogen. Conditioned media was then stored at -20°C until required.

Table 2.3 Stimuli used on SMC to collect conditioned media for gelatin zymography

Flask #	Stimuli
1	10 µl.ml^{-1} PBS in MGM (Vehicle)
2	100 nM TPA in MGM
3	10 ng.ml^{-1} PDGF + 10 ng.ml^{-1} IL-1α in MGM

2.8.6.2. MAKING AND RUNNING GELS

The polyacrylamide gel constituents for the separating and stacking gels used for gelatin zymography are detailed in Appendix C.

Separating gel (Appendix C) containing a final concentration of 1 mg.ml^{-1} gelatin was cast into 1 mm cassettes and allowed to polymerise at room temperature (approx.. 30 min) under water-saturated butanol. The water-saturated butanol was then removed carefully with filter paper and the separating gel was overlaid with stacking gel (Appendix C). A 10-well gel comb was inserted and the gel allowed to polymerise at room temperature (approx. 15 min) Conditioned media was then mixed with sample loading buffer (40% glycerol, 62.5 mM Tris buffer pH 6.8, 4% SDS and 0.1% bromophenol blue) in a ratio of 25 µl to 12.5 µl respectively, and 30 µl volume per well was added to result in an end loading volume of 20 µl of conditioned media (as determined by calibration curve in Section 5.4.4.1). The loading samples were then added to the gel wells and subjected to sodium dodecyl sulphate-polyacrylamide gel electrophoresis (SDS-PAGE) in running buffer (5 mM Tris base, 50 mM NaCl,

0.02% SDS) for 110 minutes at 120 V. The gels were then removed from the electrophoresis apparatus and washed three times in 2.5% Triton X-100 for 20 minutes on a rocker to remove the SDS and allow the MMPs to renature. The gels were then incubated with incubation buffer to allow MMP digestion of the gelatin substrate (5mM Tris base, 1% $CaCl_2$, 5 mM NaCl, 0.5% Brij-35, pH 7.6) for 26 hours in a non-gassed dry incubator at 37°C.

Visualisation of gelatinolytic activity was achieved by staining the gels with Coomassie Blue (25% methanol, 10% glacial acetic acid, 0.02% w/v Coomassie Brilliant Blue) for 20 minutes. Gelatinolytic activity was seen as clear bands of digested gelatin on a bright blue background of intact substrate.

2.8.6.3. DATA AND STATISTICAL ANALYSIS

Densitometry of the total levels of gelatin digestion was conducted using the Analyze Gels tool in ImageJ (http://imagej.nih.gov/ij/). The total level of gelatin digestion was expressed as a percentage of the respective FRESH control for each of the three animals to give a relative total MMP level for the EARLY and END models. A three-way ANOVA was used to measure significance between model stage (EARLY / END), treatment condition (FRESH /BIOVEH /BIOCCE), stimulus (VEH /TPA /PDGF+IL-1α) and any interaction between the levels. A post-hoc Tukey test was performed for direct means comparison and a p-value of <0.05 was taken to denote statistical significance.

2.8.6.4. HT1080 CELL LINE

Each of the gels were subjected to SDS-PAGE with a well containing a sample of conditioned media from the HT-1080 cell line. This is a human fibrosarcoma line originally derived from biopsy of a 35 year old Caucasian male in 1972 who presented with metastatic tumour and received no chemotherapy or radiotherapy. These highly invasive tumorigenic cells constitutively secrete high levels of MMP-2 and MMP-9 which are involved with basement

membrane degradation (Giambernardi et al., 1998). This cell line serves as a useful reference for MMP-2 and MMP-9 secretion during zymography.

2.9. BIOMECHANICAL CHARACTERISATION

As described in Section 1.4, the arterial wall is composed of three distinct layers: the intima, media and adventitia. Alongside the individual cell types residing within the arterial wall, collagen and elastin fibres form the extracellular matrix and contribute to the bi-phasic strain-dependent material behaviour of the arterial wall (He and Roach, 1994, Bank et al., 1996, Kobielarz and Jankowski, 2013). The artery itself exhibits anisotropic behaviour due to the circumferential arrangement of cells and extracellular matrix fibres in the media hence it is important to evaluate the mechanical behaviour in both directions (Gasser et al., 2006, Geest et al., 2006).

In the human disease the effect of aneurysm is to decrease the strength of the arterial wall whilst inducing stiffening of the aorta, especially in the circumferential direction (He and Roach, 1994, Raghavan et al., 1996, Thubrikar et al., 2001, Geest et al., 2006). With this in mind, the aim of this part of the study was to characterise the mechanical behaviour of the end-stage *ex vivo* model and validate this against human data reported in the literature. Encompassed within this aim was also the characterisation of the protease pre-treatment so that the state of the biomechanical properties of the artery prior to any culture (and therefore any active remodelling role of the SMC) in the bioreactor were known and understood. Uniaxial tensile testing in longitudinal and circumferential orientations was used in order to understand the inherent mechanical properties within the artery. Dilation burst-pressure testing was used alongside this to assess the behaviour of the artery as it exists physiologically, as a whole organ.

2.9.1. CHARACTERISATION OF PROTEASE PRE-TREATMENT

In order to investigate the effects of the CCE pre-treatment prior to bioreactor culture, non-sterile arteries were used. Porcine external carotid arteries used for characterisation of the protease pre-treatment were sourced from an abattoir from 7-8 month old Large White pigs with a carcass weight of 65 – 85kg. Arteries were not considered to be sterile and this method of tissue procurement was used as opposed to harvesting fully sterile arteries because this was not required if no organ or cell culture occurred. Arteries were removed during slaughter and delivered on the day of slaughter. On collection, excess connective tissue surrounding the adventitia was removed by blunt dissection. Arteries were then washed three times for 30 minutes each in 1X PBS containing EDTA (2.7mM; w/v 0.1%) to remove excess blood. After washing, any remaining superfluous tissue was removed by blunt dissection. The left or right carotid artery was isolated from the ascending aorta and was then stored individually at -80°C wrapped in 1X PBS soaked filter paper until required. Studies have shown that freezing at such a temperature for up to 3 months has no impact on vessel mechanics, including ultimate stress and Young's modulus measurements (Stemper et al., 2007b).

Prior to mechanical testing, the specimens were allowed to stabilise to room temperature. Each artery was bisected and treated according to experimental groups as shown in Table 2.4.

Table 2.4 Experimental groups including fresh control and vehicle control for biomechanical testing

Group (n=6)	Treatment
FRESH	No treatment
VEH	Pre-treatment with 1% agar gel containing no enzymes (vehicle)
CCE	Pre-treatment with 1% agar gel containing 1.5 $mg.ml^{-1}$ elastase and 3 $mg.ml^{-1}$ collagenase

Bisection of each artery was carried out to ensure that each specimen was subjected to both dilation burst pressure testing and uniaxial tensile testing in matched experiments; the workflow for this is shown in Figure 2.11.

For CCE and VEH groups, each arterial segment was treated either with vehicle gel pre-treatment or with CCE pre-treatment as required with additional FGM (as fully described in Chapter 3). They were then incubated for 3 hours at 37°C in a humidified gassed incubator (5% CO_2 v/v in air). Specimens within the FRESH group received no pre-treatment but were incubated in parallel in FGM.

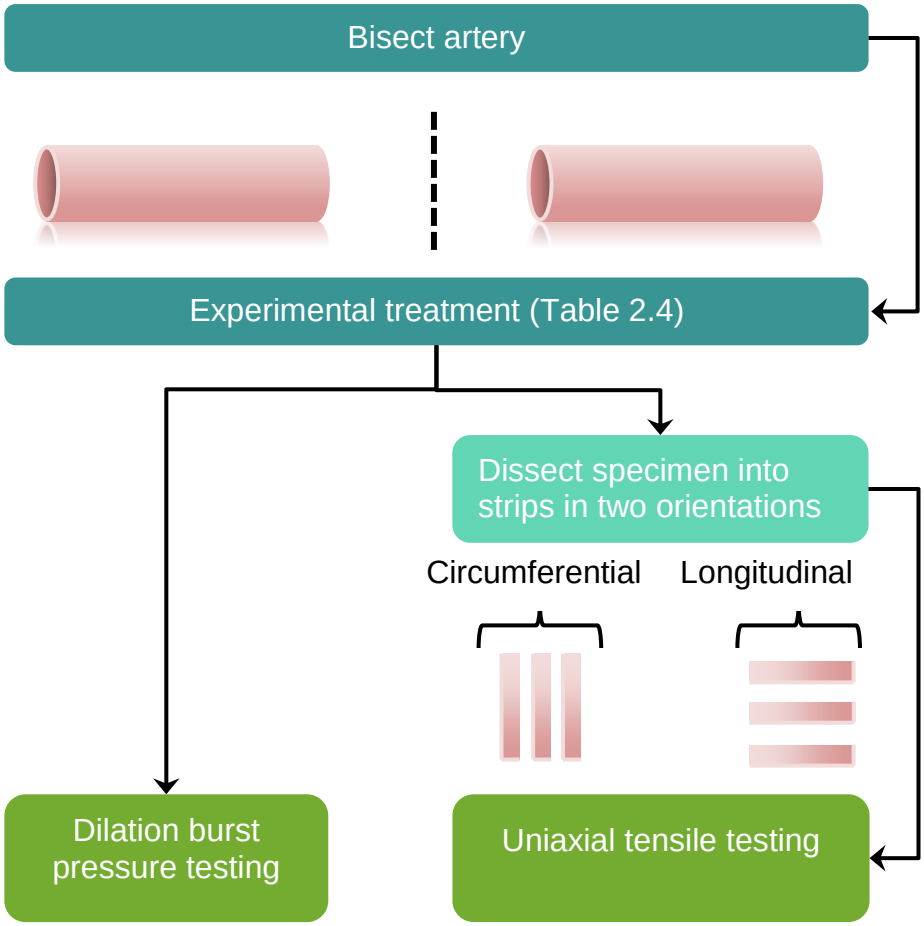

Figure 2.11 Experimental workflow of biomechanical characterisation of CCE pre-treatment with matched specimens for each method.

2.9.2. UNIAXIAL TENSILE TESTING

The specimens destined for uniaxial tensile testing were divided into circumferential (C) and longitudinal (L) test strips of at least three per group as shown in Figure 2.12. The circumferentially orientated tissue strips were always taken from the distal section of the arteries, as this has a slightly larger diameter than the proximal part. Longitudinally orientated tissue strips were always taken from the proximal part of the artery. This was done as it was necessary for the circumference to be at least 6mm with extra for the tissue to be gripped in the tensile testing equipment. A tissue cutter of parallel razor blades mounted in a cutting block was used to cut the test strips to 3 mm in width and 6 mm gauge length (Figure 2.13). Rectangular shaped strips were used as opposed to dumbbell shaped tissue strips in order to maximise the tissue yield per artery. The dimensions of the tissue testing strips were chosen as these were the smallest possible with the existing tissue grips for the tensile testing equipment. The thickness of each strip was measured in three places using a digital micrometer and the mean value was calculated and recorded. The samples were kept moist with PBS during specimen preparation and testing. The tissue strips were not subjected to any preload or preconditioning regime. Preload can mask the inherent properties in the tissue in the elastin phase by starting the data collection at an arbitrary value rather than the true relaxed state of the tissue.

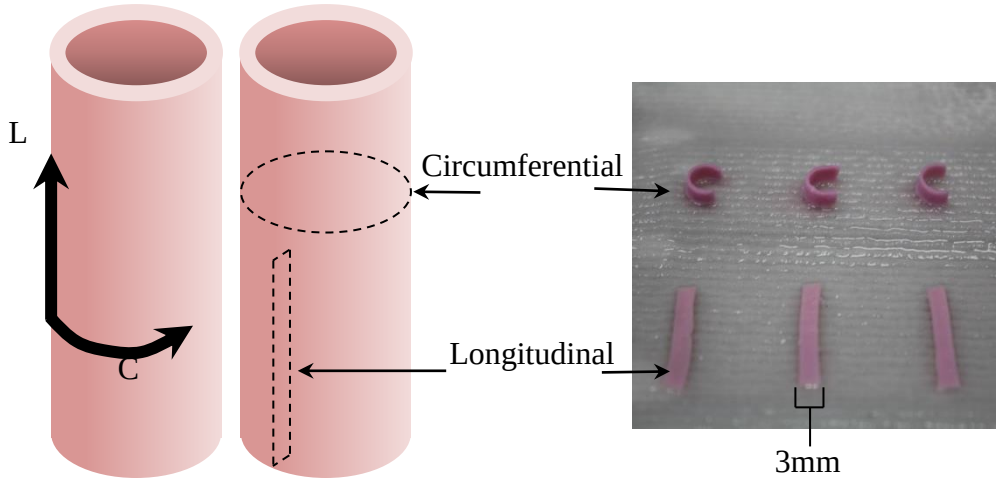

Figure 2.12 Tissue strips for uniaxial tensile testing

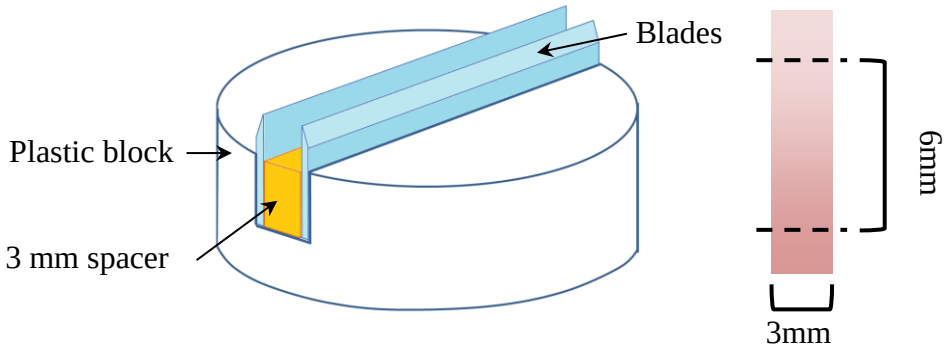

Figure 2.13 Left: tissue cutting block. Right: desired dimensions of tissue strip (3mm width, 6mm gauge length).

2.9.2.1. APPARATUS AND TEST METHOD

Custom-made soft tissue specimen clamps were used together with a small piece of fine grade sandpaper on the endothelial side to minimise tissue slippage. The specimen clamps were fitted onto a removable gauge block with a divider of 6 mm in width which ensured that no loading was imposed onto the tissue prior to the start of the test (Figure 2.14). The 6 mm divider was the smallest available and so dictated the dimensions of the tissue testing strips.

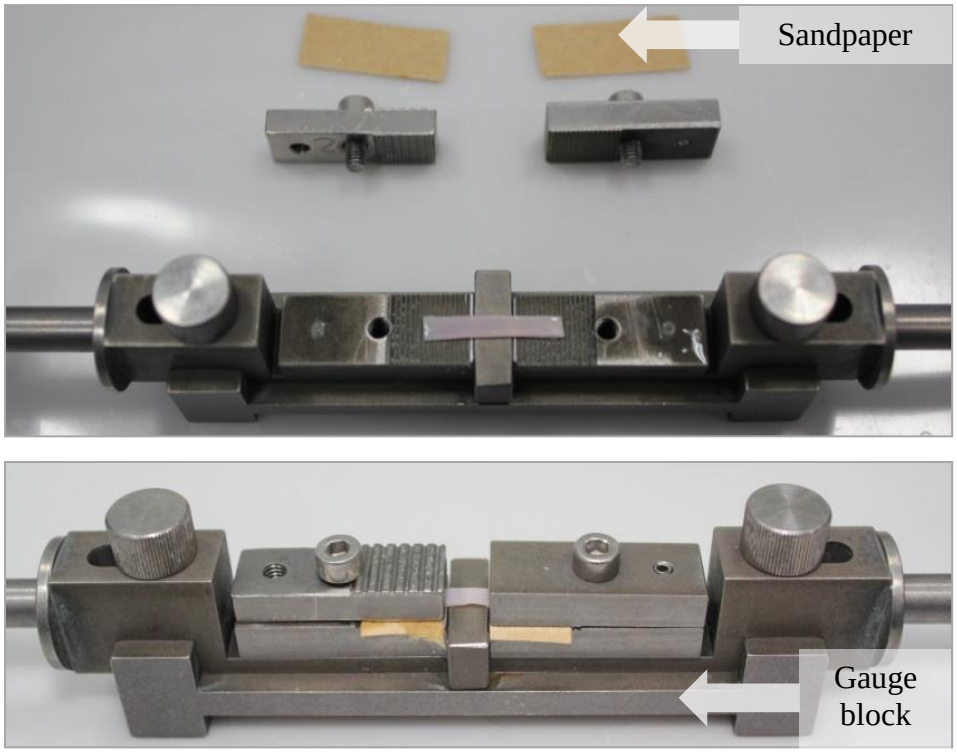

Figure 2.14 Soft tissue grips used in tandem with sandpaper for optimal tissue grip during uniaxial testing.

The inferior part of the specimen clamp was fitted into the base of an Instron® 3365 Machine materials tester equipped with a 50 N load cell which recorded the load and displacement at intervals of 0.1 seconds. The crosshead was then slowly lowered until the superior part of the specimen clamp was able to slot in. The gauge block was then removed prior to testing. All tests were carried out at 37°C in an Instron BioPuls Temperature Controlled Bath filled with 1X PBS to mimic physiological conditions. The tissue was then tested to failure at a constant nominal displacement rate of 10 $mm.min^{-1}$, corresponding to a strain rate of 0.028 s^{-1}. Sandpaper was replaced for each new testing strip. Failure was defined as complete dissection of the specimen due to tensile load. The experimental set up for uniaxial tensile testing is shown in Figure 2.15.

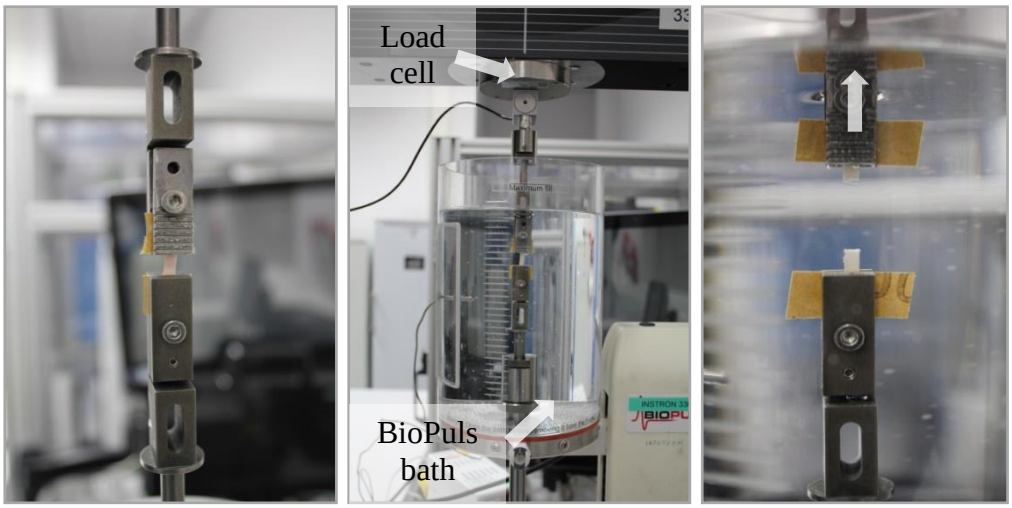

Figure 2.15 Left: tissue strip installed into soft tissue grips in tensile tester with gauge block removed. Centre: Configuration of BioPuls bath. Right: Tissue is tested until failure in centre of strip. Arrow indicates direction of load.

2.9.2.2. DATA ANALYSIS

Data was presented in terms of engineering stress and strain. The data output from the materials testing machine was displacement vs. load. This data was then transformed into engineering stress-strain via Equation 3 and Equation 4.

$$\sigma_e = \frac{F}{A_0}$$ **Equation 3 Engineering stress**

$$\varepsilon_e = \frac{\Delta l}{l_0}$$ **Equation 4 Engineering strain**

Where F is the applied load, A_0 is the initial cross-sectional area (width × thickness) and l_0 is the initial specimen length.

A typical stress-strain curve is shown in Figure 2.16. These curves can be divided into two approximate main phases (as fully described in Section 1.5.2): the elastin region (E_E), where the material behaviour is governed by elastin fibres and where the majority of collagen fibre recruitment and alignment occurs, and the collagen region (E_C), in which the fully recruited collagen fibres are stretched.

The elastin and collagen regions were defined by fitting a linear regression curve with a coefficient of regression value that was at least greater than 0.9 for all specimens. The linear regression curve was fitted to each region using a script built in MATLAB and the gradient used to determine the stiffness in each of these regions (MathWorks, Cambridge, UK). Other outputs from this data include the ultimate tensile strength (σ_{uts}) and the transition strain (ε_t) defined as the maximum stress and the intercept of the linear regression curves of the elastin and collagen regions respectively.

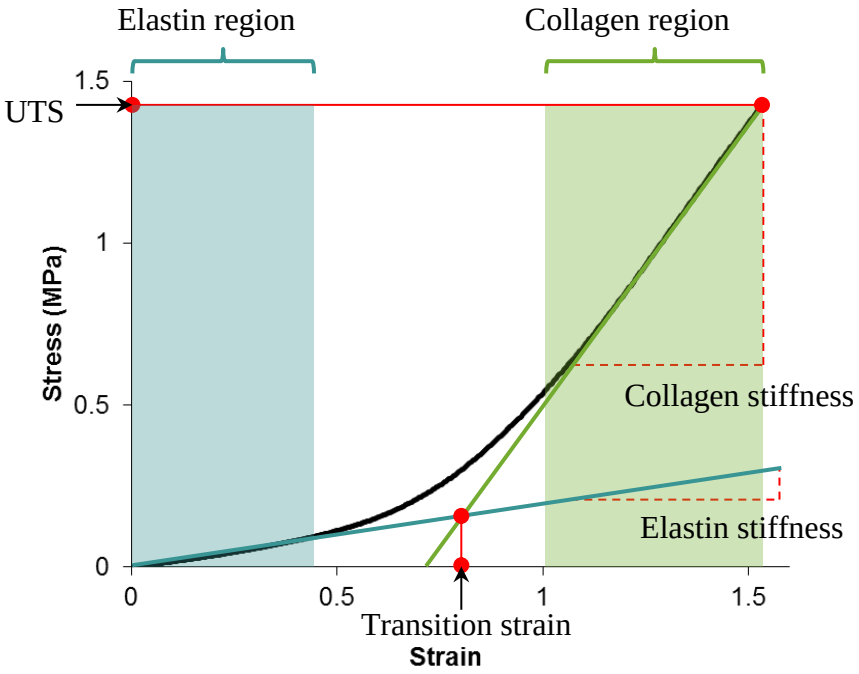

Figure 2.16 Typical stress-strain curve detailing outputs (shown in red).

Load-extension data obtained during testing was exported from the Bluehill® operating software (Instron, Bucks., UK) of the Instron® tester to Microsoft Excel spreadsheets for further processing. The load-extension data was converted to engineering stress-strain data using the formulae described in Equation 3 and Equation 4.

All outputs from this method (E_E, E_C, σ_{uts} and ε_t) were collected using the MATLAB script and are shown in Figure 2.16. The script enables the user to select regions of the data which represent the two separate linear slope regions (E_E and E_C). It then draws a linear regression line for the regions of data selected

and displays the equation of each of the linear regression lines in the format y=mx + c, where m is equal to either E_E or E_C depending on the region being analysed. The coefficient of determination (R^2) was also displayed and in all cases it was ensured that this was greater than or equal to 0.9. The script also displays the maximum stress reached (taken to be σ_{uts}) and the strain at which the linear regression lines E_E and E_C intercept (taken to be ε_t). The script is reproduced fully in Appendix D and a representative image of the script output is displayed below in Figure 2.17.

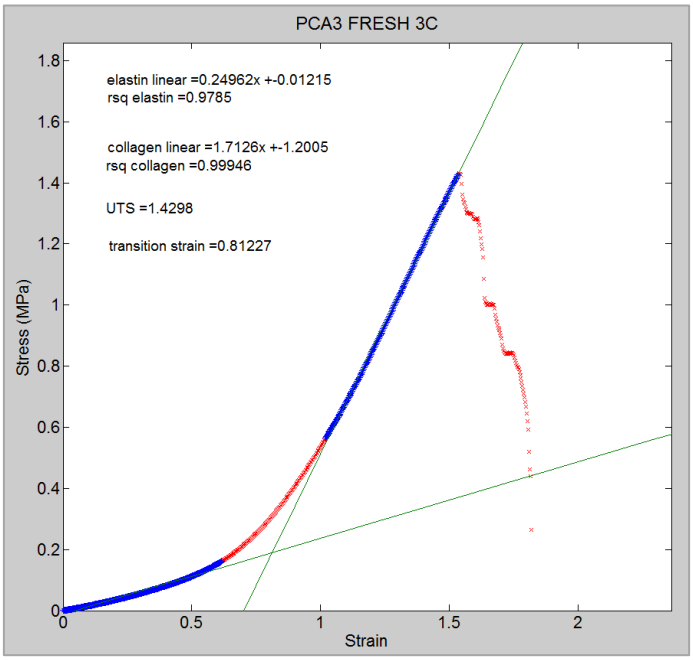

Figure 2.17 Representative MatLab script output, showing selections.

2.9.2.3. STATISTICAL ANALYSIS

Statistical analysis of the results was performed using a one-way ANOVA per tissue orientation with a post-hoc Tukey test for means comparison in OriginPro (OriginLab, MA, USA). A p-value of less than 0.05 was taken to be significant. All data are presented as the mean ± 95% confidence intervals.

2.9.3. DILATION BURST PRESSURE TESTING

One section of each treated artery was tested whole for dilation analysis so as to match all data with that from uniaxial tensile testing analysis (Figure 2.11). The dilation testing rig is shown in Figure 2.18.

The artery was left whole and tested for leakage using a syringe filled with 1X PBS. If no leaks were apparent in the vessel, it was painted with blue tissue dye to ensure high contrast for image analysis. The vessel was then secured to a hose barb using cable ties and catgut. The hose barb was then inserted into a push fit connector so that the vessel sat within a clear Perspex chamber. A 10 g weight was attached to the free end of the vessel to exert a 0.1 N longitudinal pre-load to vessel to ensure that it remained horizontal throughout the experiment. Previous investigation has shown that 10 g is the optimum weight to use (Jake Milton Barker, iMBE SOP). A volume of 120 ml of 1X PBS was syringed into the compliance chamber and the air supply tube connected to the rig. A camera was set up on a tripod so that both the calibration rule and the digital display of the pressure gauge was within the field of view and so the exact pressure at the instant the image was taken was recorded. The pressure meter was then set to 0 mmHg.

The air supply valve was turned on such that the pressure through the vessel slowly increased at a constant rate. Images were taken on the camera at approximate 20 mmHg intervals up to 180 mmHg. Post-180 mmHg, the display on the pressure gauge was changed to record the maximum pressure reached. The pressure was then increased at a constant rate until either rupture of the vessel or the pressure reached 5000 mmHg. The burst pressure was then recorded and the air supply quickly turned off.

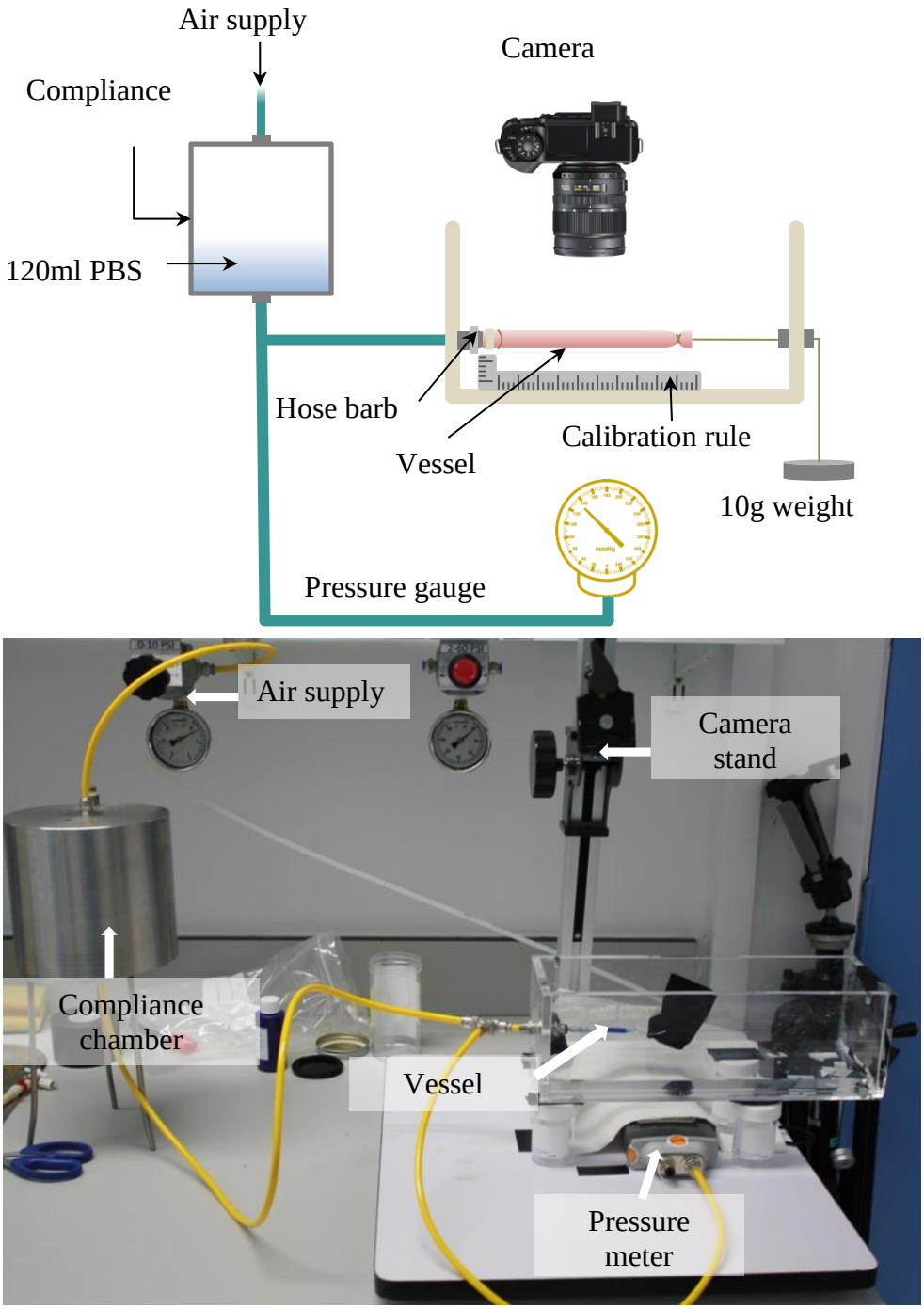

Figure 2.18 Dilation testing. Top: schematic of dilation testing rig. Bottom: photograph of dilation set-up.

2.9.3.1. DATA AND STATISTICAL ANALYSIS

The images were taken such that the digital display of the pressure meter and the calibration rule were in the field of view. Representative images are displayed in Figure 2.19.

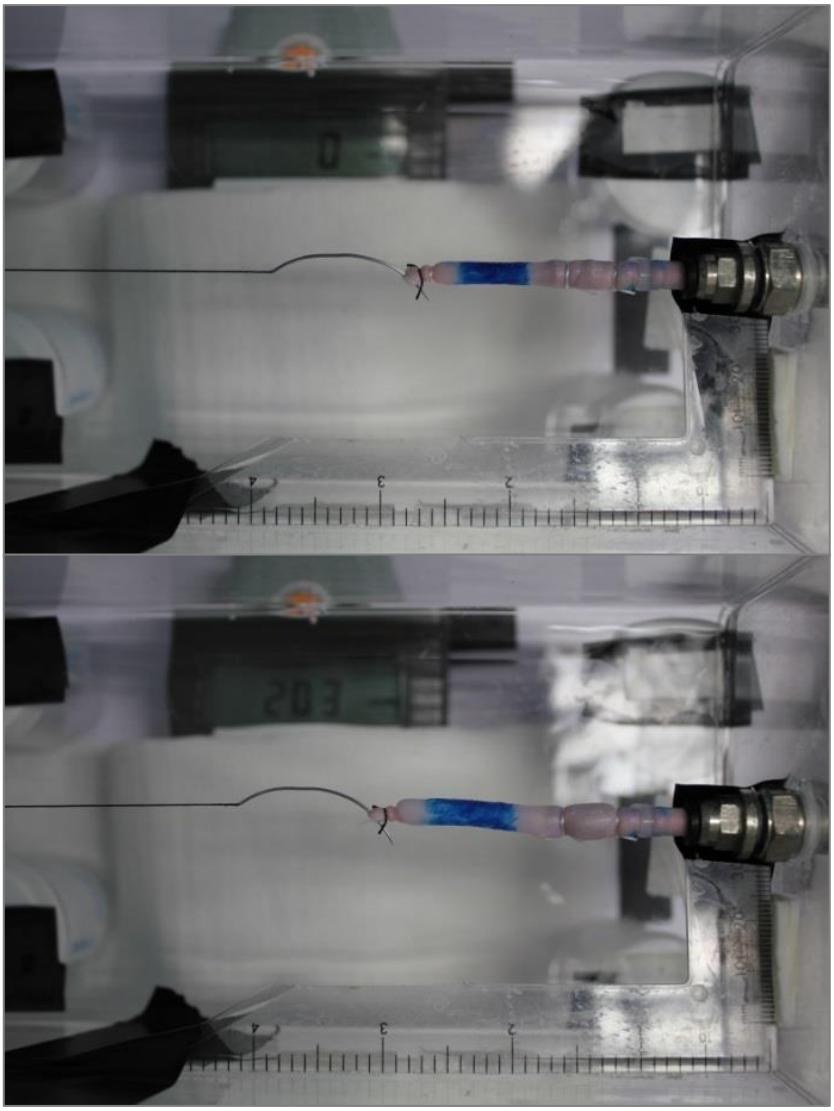

Figure 2.19 Representative images taken during dilation test. Top: at 0 mmHg. Bottom: 203 mmHg.

The images were calibrated within Image-Pro Plus (Media Cybernetics Inc., MD, USA) using the calibration rule to determine the number of pixels per millimetre. The 'Trace' feature in Image-Pro Plus was used to trace along both sides of the arterial wall. The tissue dye enhances the contrast for these images and enables this feature to work. The average distance between the trace lines was then recorded against the pressure seen on the digital display of the pressure gauge in the image. The 'Trace' feature was then used again to determine the average length of the vessel, using the sutures as a reference marker. This value was also recorded alongside the pressure. The image analysis method is shown

in Figure 2.20. This was completed for arteries from six animals for each treatment condition (FRESH/VEH/CCE).

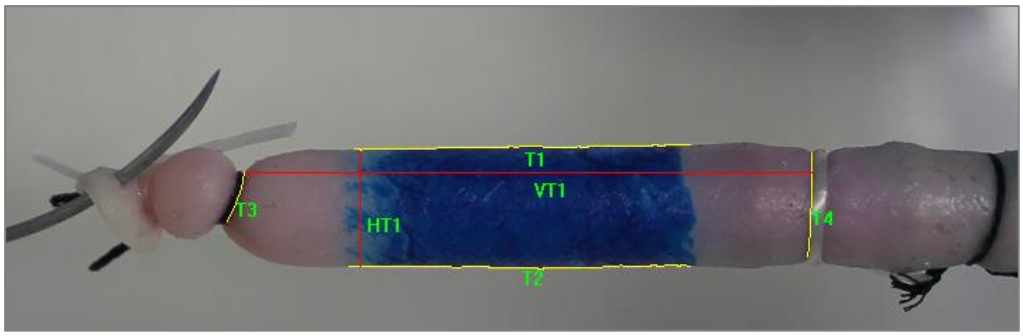

Figure 2.20 Representative image of image analysis method used for determining vessel dimensions. T1-4: tracelines. HT1: average diameter. VT1: average length. Approximate magnification 3x.

The data was then interpolated so that values of average diameter and length could be determined at exact 20 mmHg intervals; from 0 – 180 mmHg. This was performed so that each vessel could be compared to all other vessels and was implemented in MATLAB (MathWorks, Cambridge, UK).

A one-way ANOVA with post-hoc Tukey test was used to determine significance between treatment groups across the pressure range. For matched vessels which were subject to non-destructive dilation testing prior to and following CCE treatment, a two-tailed paired sample t-test was used to test for significance. A p-value of <0.05 denoted statistical significance.

2.9.4. CHARACTERISATION OF *EX VIVO* MODEL BIOMECHANICS

The biomechanical properties of vessels pre-treated either with the CCE gel (BIOCCE) or with a vehicle gel (BIOVEH) and then subsequently cultured in the bioreactor for 12 days (as per the end-stage model) were also characterised.

This was carried out using the same method for uniaxial tensile testing described in Section 2.9.2.

Three animals were used for these experiments, with both carotid arteries from each animal, providing a contralateral control. A total of three arteries were used for each treatment group (BIOVEH/BIOCCE).

CHAPTER 3

EX VIVO MODEL OF AAA

CHAPTER 3 *EX VIVO* MODEL OF AAA

This chapter describes the methodology used to generate an experimental AAA model using porcine carotid arteries in a dynamic flow bioreactor. The first section details the experimental groups throughout this project, including the various controls used for model validation. The vessel pre-treatment used to experimentally induce SMC with an aneurysmal phenotype and the configuration of the bioreactor are also detailed within this chapter.

The bioreactor system used in the present study was used to impart flow-related mechanical forces through the arterial wall *ex vivo* in order to mimic the physiological forces present *in vivo.*

The bioreactor used in this study is existing equipment and was built and designed by Sotirios Korossis of the Institute of Medical and Biological Engineering at the University of Leeds (Riches et al., 2013). The surgical removal of the tissue was carried out by Marc Bailey, Katy Bridge and Kathryn Griffin variously in pairs. Animal sacrifice was carried out under Schedule 1 to the Animals (Scientific Procedures) Act 1986 by Central Biomedical Services technicians and veterinarian.

3.1. INTRODUCTION

Experimental models of disease are essential for elucidating mechanisms of pathogenesis, therapeutics and treatment. Their importance is, perhaps, even more significant in AAA disease because its tendency to only be detected clinically once the aorta has dilated significantly: at end-stage disease. Experimental models are required to investigate the processes involved before the artery reaches a critical size where rupture becomes a problem.

Genetic, physical and chemical animal models have been developed and used for investigations for a number of years (Trollope et al., 2011). Almost three decades ago, peri-adventitial elastase treatment was first used in mice to induce an experimental AAA, and this has since progressed to using a combination of

collagenase or flow disturbance and elastase when translating the methodology to large animals (Anidjar et al., 1990, Goericke et al., 2009, Moláček et al., 2009, Kloster et al., 2015).

Early research concentrated on small animal models due to their relatively low cost, genetic malleability and ease of husbandry. Large animal models are desirable due to a more closely matched geometry and physiology to humans, but these are limited by practical requirements such as housing and handling costs. The advent of bioreactors has, in recent years, enabled large animal tissue to be studied *ex vivo* without the practicalities and logistics of keeping large animals, by mimicking the physiological environment for a small tissue construct (Yazdani and Berry, 2009, Touroo and Williams, 2012).

The aim of this chapter is to describe the methodology used to create a chemically induced *ex vivo* porcine tissue AAA model in a bioreactor. The bioreactor enables media to flow through the lumen of the artery, imparting shear stress and intraluminal pressure on the SMCs and endothelial cells, whilst maintaining tissue viability for up to 12 days.

3.2. MATERIALS AND REAGENTS

3.2.1. REAGENTS

The supplier details for the reagents used to create the *ex vivo* bioreactor model are detailed below, in Appendix A.7.1, Table A.8. Details of media composition AAA are given in Table 2.2.

3.2.2. MATERIALS AND CONSUMABLES

The supplier details of materials and consumables used throughout this chapter are detailed in Appendix A.7.2, Table A.9.

3.2.3. BIOREACTOR COMPONENTS

The components for the main bioreactor chamber and the equipment used in tandem with the bioreactor are pictured in Figure 3.1 and details are given in Table 3.1 and Table 3.2 respectively.

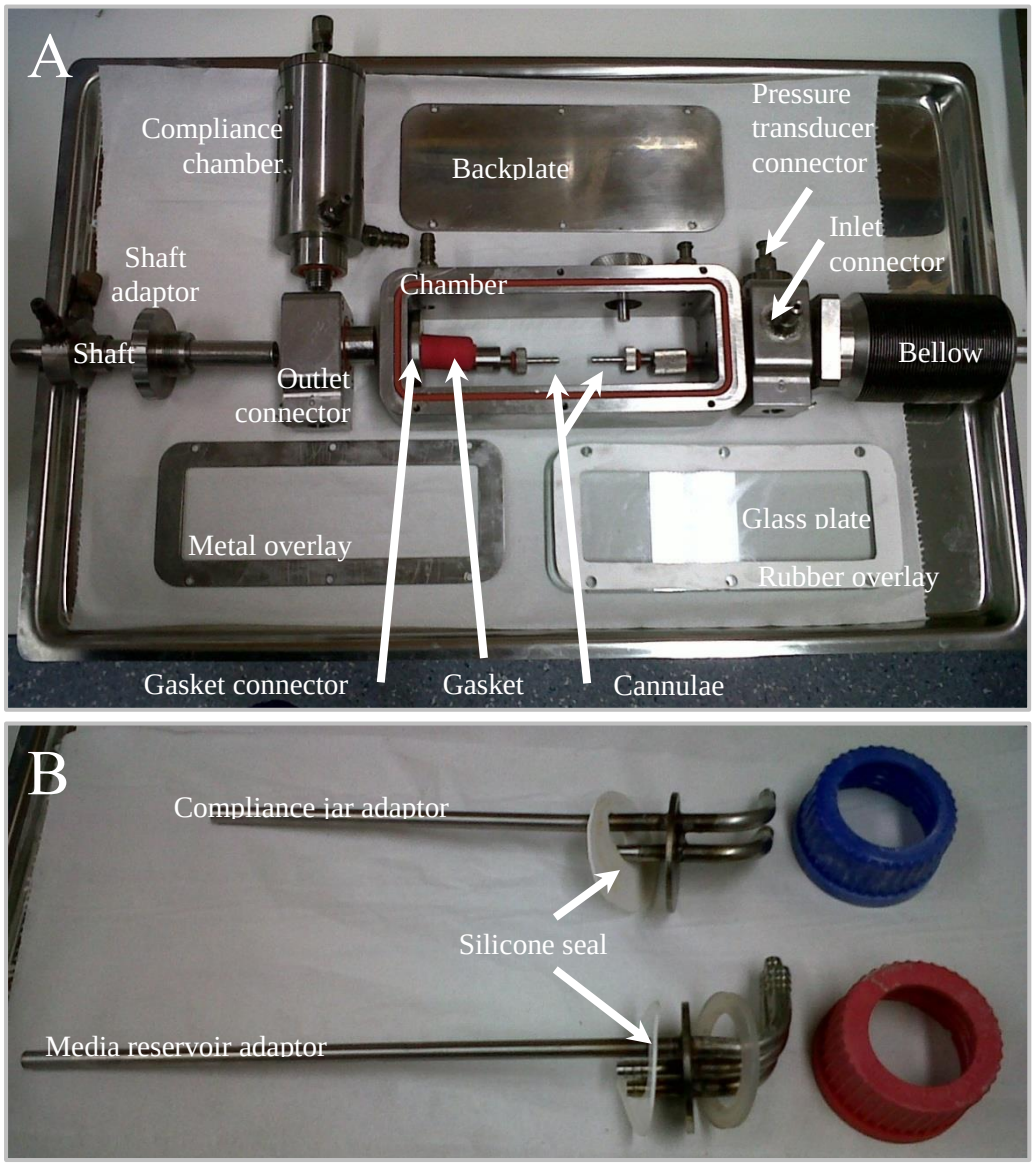

Figure 3.1 Disassembled components of bioreactor. A) Components of main bioreactor chamber. B) media reservoir and compliance jar adaptors. Tissue paper backing included for photo contrast.

Table 3.1 Bioreactor components for single bioreactor system (two are usually run in parallel).

Item	Details	Qty.
Bellows	316- stainless steel	1
Inlet connector	316- stainless steel	1
Chamber	316- stainless steel	1
Outlet connector	316- stainless steel	1
Shaft	316- stainless steel	1
Shaft adaptor	316- stainless steel	1
Gasket connector	316- stainless steel	
Compliance chamber	316- stainless steel	1
Backplate	316- stainless steel	1
Glass plate	Float glass (custom manufactured by Instrument Glasses, Enfield, UK)	1
Metal overlay	316- stainless steel	1
Rubber overlay	Silicone rubber	1
Cannula	316- stainless steel	2
Gasket	Silicone rubber (custom manufactured by Thomson Bros. Ltd, Newcastle, UK)	1
O-rings	Silicone rubber (Thomson Bros. Ltd., Newcastle, UK)	10
Screws	(M3 and M6) 316- stainless steel	24
Media reservoir bottle	1000ml glass bottle (Simax, Czech Republic)	1
Media reservoir adaptor	316- stainless steel	1
Compliance jar	500ml glass bottle (Simax, Czech Republic)	1
Compliance jar adaptor	316- stainless steel	1
Silicone seal	Silicone rubber	2

Table 3.2 Bought-in bioreactor components and equipment.

Item	Supplier
Medical gas cylinder (5% CO_2 v/v O_2)	BOC Medical, Greater Manchester, UK
Temperature controlled water bath	Techne, Bibby Scientific Ltd, Staffs. UK
Variable peristaltic pump (Masterflex Model 77200-50)	Cole-Parmer, London, UK
Masterflex tubing	Phar Med, Saint Gobain, West Midlands, UK
Silicone tubing	Cole-Parmer, London, UK
Electrocardiogram (ECG) machine (ECG Triscope Press 8041)	SW Healthcare, FL, US
Temperature monitor and probe	Eurotherm, West Sussex, UK

3.2.4. MEDIA COMPOSITION

For whole organ culture, in both the bioreactor and in culture plates, a 30% foetal calf serum culture (FCS) medium was used as it has been shown previously to preserve whole vessel viability (Porter et al., 1996). Whole organ culture medium was composed of 30% v/v FCS, 2mM L-Glutamine, 10 units/mL penicillin, 10µg/mL streptomycin; 250ng/mL Fungizone® and 0.05% v/v Gentamicin. For each bioreactor chamber, a volume of 816.5 ml was used (240 ml FCS, 8ml L-Glutamine, 8ml Antibiotic-Antimycotic and 495µl of Gentamicin).

For washing, transport and short term storage of tissue, FGM was used throughout the process.

3.3. TISSUE FOR *EX VIVO* AAA MODEL

Porcine carotid arteries were selected to be used in order to create the experimental AAA as firstly, they provide a relatively long length of artery free

from side branches and secondly, there are two of them within each animal providing a contralateral control and thereby reducing bias due to inter-animal variance. It was necessary for any tissue involved with organ or cell culture to be harvested and maintained in complete sterility. Tissue harvesting occurred in a sterile theatre setting.

3.3.1. ANIMALS

All animal procedures were conducted according to UK Home Office regulations by trained technicians. A project license was not required as no regulated procedures were performed as part of the experiments. Female 65kg pigs were sedated with Stresnil (Elanco Animal Health, Hampshire, UK), anaesthetised with Hypnovel (Hoffman La Roche, Basel, Switzerland) and terminated via Pentoject (Animalcare, Yorkshire, UK) injection according to Schedule 1 under the Animals (Scientific Procedures) Act 1986. Both left and right carotid arteries (PCA) were harvested under aseptic conditions via anterior approach (Figure 3.3). The vessels were then excised of adventitia and superfluous connective tissue in a Class II laminar flow cabinet (Figure 3.2).

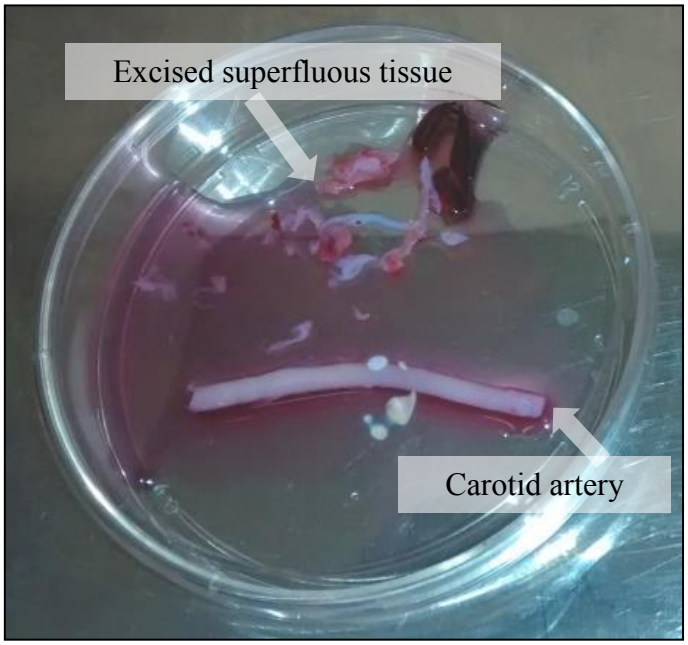

Figure 3.2 Superfluous connective tissue and adventitia were excised from the porcine carotid arteries following harvesting.

3.3.1.1. SURGICAL APPROACH

Surgical extraction of the tissue was performed by a team of two trainee surgeons. In all cases an anterior approach to the carotid artery was made through the neck of the animal. One incision was made through which both left and right common carotid arteries were harvested. The sternohyoideus muscle was located and the approach to each carotid artery was located laterally to the sternohyoideus on both sides, superior to the salivary gland. The common carotid artery lies in close proximity to the vagus nerve and the internal jugular vein. Images of the surgical approach used for all tissue harvesting are shown in Figure 3.3. Although the carotid artery was selected for this project specifically for its relatively long length with lack of side branches, occasionally a side branch would be present which is an anatomical peculiarity of singular animals. If a side branch was present, it was sutured closed in order to retain characterised flow and pressure throughout the carotid artery when installed in the bioreactor.

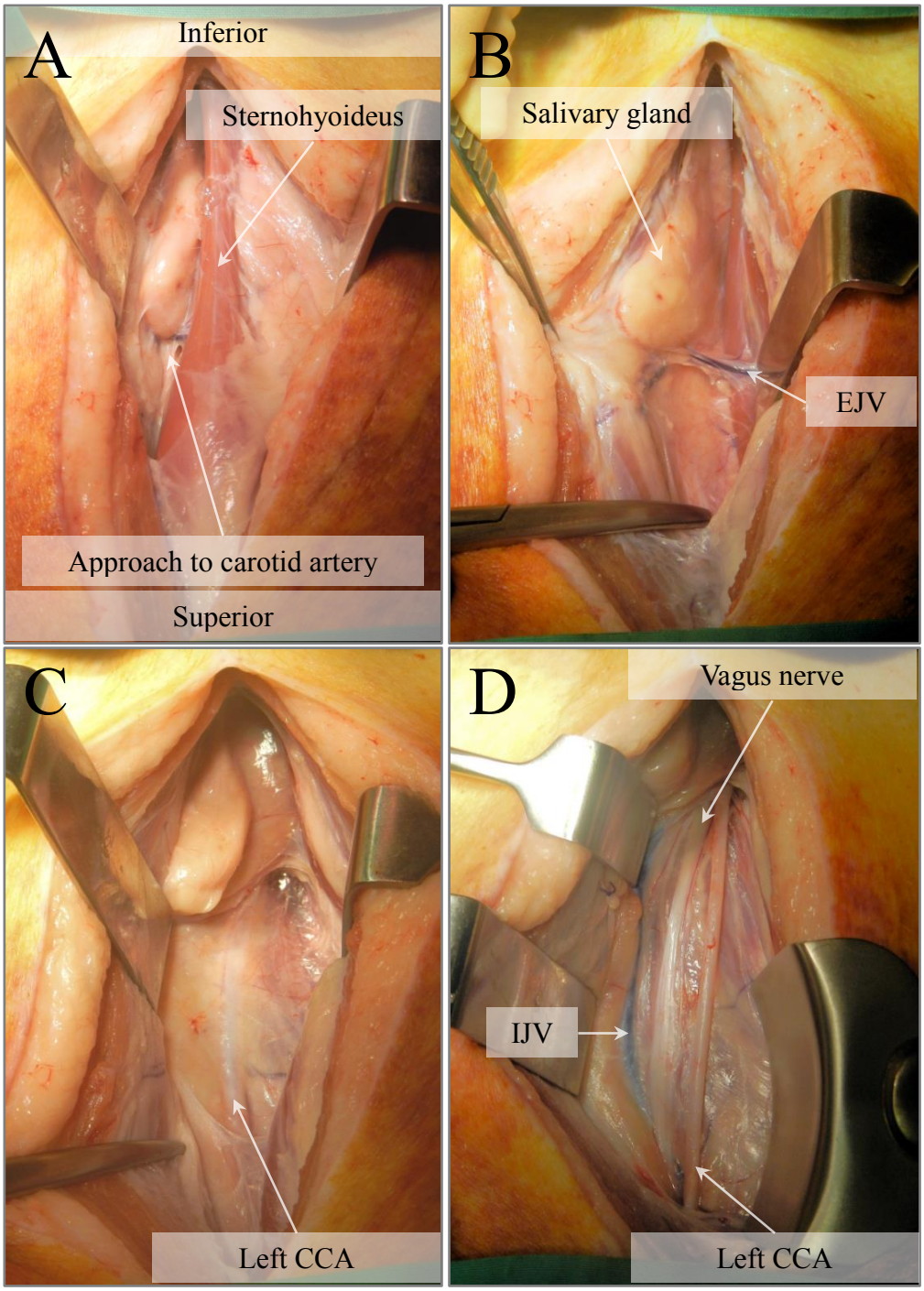

Figure 3.3 Surgical approach to left common carotid artery used for all sterile harvests throughout this study. CCA = common carotid artery, IJV = internal jugular vein. Images are in order from A to D in chronological order

3.3.2. NON-STERILE DISSECTION OF CAROTID ARTERY

Porcine aortic arch and carotid artery sections were obtained from 7 – 8 month old Large White pigs from a local abattoir. The carotid artery was isolated from the segment and all connective tissue and surrounding vasculature was removed by blunt dissection removed within 3 to 4 hours of slaughter. Arteries were then washed for 30 minutes in PBS containing EDTA (2.7mM; 0.1% w/v) in order to remove excess blood.

3.4. BIOREACTOR FOR ORGAN CULTURE

3.4.1. BIOREACTOR CONFIGURATION

The bioreactor system used for experimentally inducing AAA *ex vivo* was designed and constructed in the Institute of Medical and Biological Engineering at the University of Leeds by Dr. Sotirios Korossis (Riches et al., 2013). The system was designed to culture a length of artery under dynamic flow culture (with the capacity to be steady or pulsatile flow) and maintain it for up to twelve days. Briefly, the bioreactor consisted of four main parts: i) media reservoir and gas exchange, ii) variable peristaltic flow pump, iii) compliance chambers and iv) the bioreactor chamber itself.

Media reservoirs of 30% FCS organ culture media were contained within a water bath running at 44°C, allowing for heat loss along the system to maintain the media in the bioreactor chamber at 37°C. Gas (5% v/v CO_2 in O_2) was supplied into the media reservoir through a hydrophobic sterile 0.22µm filter (Millex®, Millipore, Hertfordshire, UK) to maintain sufficient oxygen levels throughout the system.

A variable peristaltic pump (Masterflex Model 77200-50, Cole-Parmer, London) forced media from the media reservoir outlet to the compliance jar inlet via Masterflex tubing. The peristaltic pumping action of the pump introduced a non-characterised pulsatile component into the system flow and so the purpose of the compliance jar was to transform it to steady flow (Figure 3.4). The

compliance jar was then connected to the bioreactor chamber inlet with silicone tubing. At the inlet, the inlet pressure was monitored using a sterile pressure transducer (Argon Medical, TX, USA) and ECG machine. From the inlet, the media passed through two cannulae with an inner diameter of 1mm and an outer diameter of 3mm, onto which the artery was mounted using sutures of sterile catgut. The cannula at the outlet (Figure 3.5) was able to translate back and forth to accommodate any changes in length of the artery which may occur, for example, due to pressurisation. The media was then pumped from the outlet cannula through silicone tubing to a downstream compliance chamber attached to the bioreactor chamber. This downstream compliance chamber simulated the compliance of downstream vasculature which would be present physiologically. From here, the media was pumped into the bioreactor chamber outside of the lumen of the artery, enabling gas exchange and nutrient delivery to the adventitia. The media was then pumped back to the reservoir through silicone tubing.

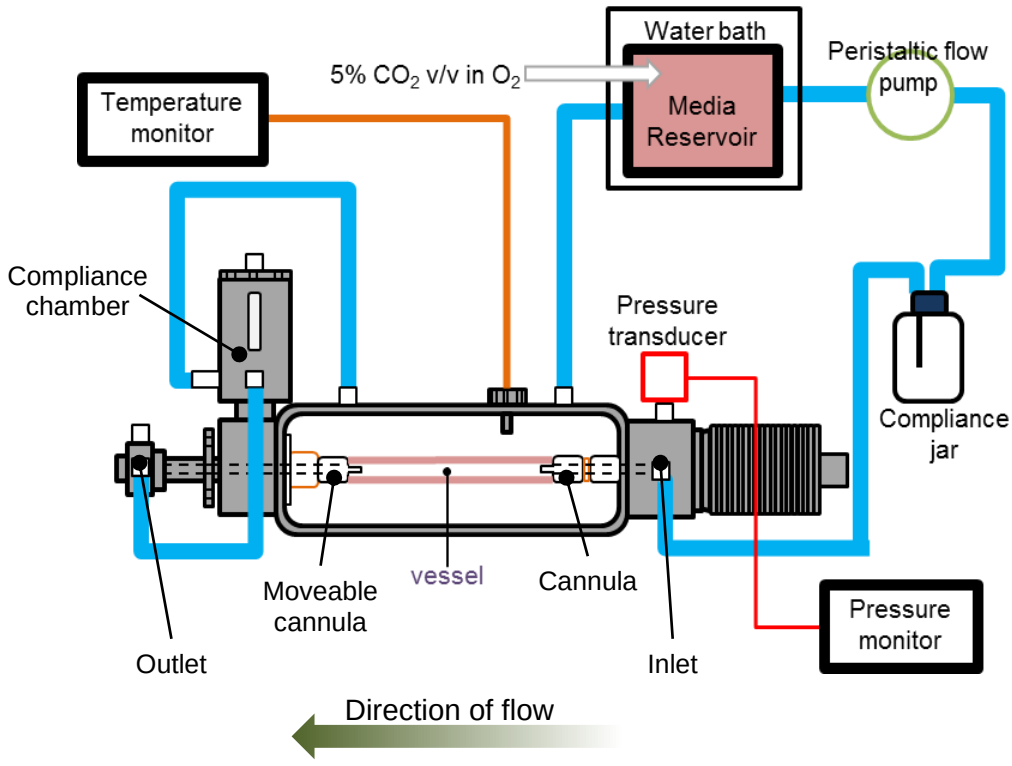

Figure 3.4 Schematic of bioreactor configuration used to generate *ex vivo* AAA experimental model

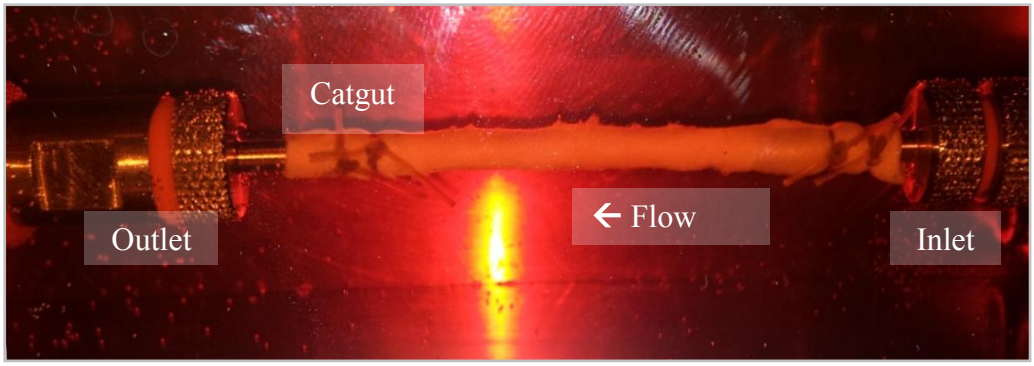

Figure 3.5 Porcine carotid artery installed into the bioreactor chamber with flow direction right to left. Catgut sutures are used to affix the artery onto the cannulae.

The bioreactor enabled flow through the lumen of the artery, imparting shear stress (sensed through shear stress responsive genes in the endothelium) and pressure through the arterial wall in an attempt to mimic the dynamic environment which is present physiologically *in vivo* (Osol, 1995, Miller, 2002, Lu and Kassab, 2011). The shear stress was not monitored or quantified in this study as it requires a computational fluid dynamics simulation model to determine local wall shear stress.

3.4.2. STERILISATION OF BIOREACTOR FOR ORGAN CULTURE

It was of utmost importance that the bioreactor system and its related components were sterilised and able to remain so during the whole procedure. During the experiment, the bioreactor was monitored for signs of contamination and was immediately dismantled if any were observed. Prior to experimentation, all parts of each bioreactor were completely disassembled and the various components laid out on metal trays (Figure 3.1). The trays and all of the separate components were then autoclaved at 121°C and 15 lb.sq.in for 20 minutes. After this, the bioreactor was fully assembled with the exception of the tubing and the front glass plate in a Class II flow hood. The partly-assembled bioreactor was then autoclaved once more prior to the installation of the artery. Tubing, the front glass plates, and the media reservoir and compliance jar reservoir adaptors were autoclaved separately.

3.5. CREATION OF *EX VIVO* PORCINE MODEL

3.5.1. COMBINED COLLAGENASE AND ELASTASE PRE-TREATMENT

The combined collagenase and elastase (CCE) gel enabled focal application of a protease treatment to the artery. The agar gel was produced by making a 1% w/v solution of Ultrapure® Low Melting Point (LMP) agar powder (Invitrogen, Life Technologies, Renfrewshire, UK) in HBSS. This solution was then sterilised via autoclaving prior to the experimental set-up.

On the day of the experiment, the 1% w/v agar in HBSS gel was then heated in a water bath to 70°C until the gel had completely liquefied. The gel was then held at a temperature of 40°C in the water bath to maintain its liquid state. Solutions of elastase (porcine pancreatic, 50 $u.mg^{-1}$, MP Biomedicals, Illkirch, France) and collagenase (Type IIa, Worthington Biochemical, NJ, USA) in HBSS were sterilised via syringe-filtering through 0.22μm Millipore® filters. These solutions were added to an equal volume of melted agar gel solution to produce a gel with final concentrations of 1.5 $mg.ml^{-1}$ elastase and 3 $mg.ml^{-1}$ collagenase, referred to as CCE treatment gel according to previous work on protocols in our laboratory (Riches et al., 2013). The vehicle (VEH) gel was produced by adding an equal volume of sterile HBSS to the melted 1% w/v agar in HBSS solution. The gels were then left at 4°C until set; generally less than five minutes was required. Figure 3.6 shows the solidified treatment gels.

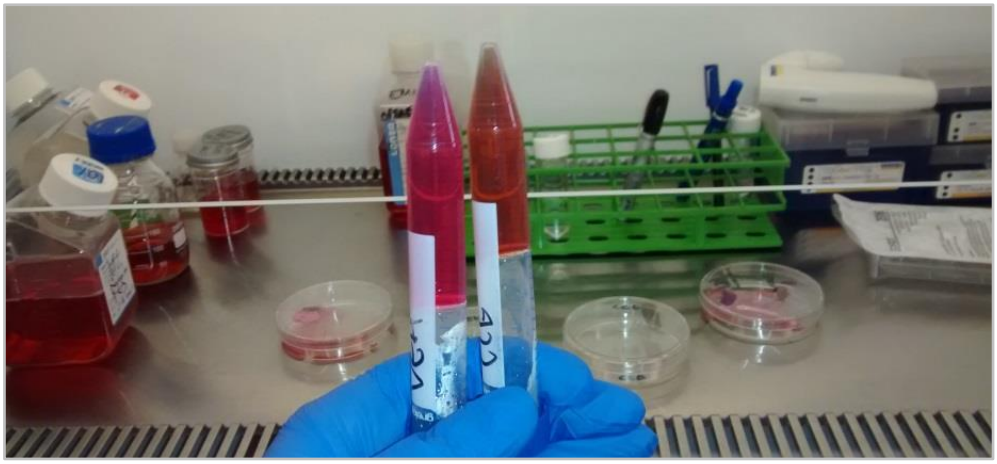

Figure 3.6 Vehicle and CCE gels were held at 4°C until they were sufficiently set for focal application.

Two rings of tissue were then removed from the end of each artery to provide tissue for static culture, histology and FRESH SMC explant culture. The centre portion of each artery and the two corresponding rings of tissue were then treated with either the CCE or vehicle gel using a sterile swab (Figure 3.7). The treated tissue was then incubated for three hours at 37°C in a humidified incubator gassed with 5% CO_2 v/v in air.

Figure 3.7 Focal treatment with either vehicle (left) or CCE gel (right) on porcine carotid artery - treatment incubation set-up.

Following the incubation period, the treatment gel was then gently removed using a sterile swab and the tissue was washed with FGM.

3.5.1.1. STATIC CULTURE

The two tissue rings treated with the gel pre-treatment were then placed into a 6-well plate and supplemented with 4 ml 30% FCS whole organ culture medium changed at 3 day intervals. Throughout the culture period, tissue was maintained at 37°C in a humidified incubator gassed with 5% CO_2 in air.

Figure 3.8 Arterial rings cultured under static conditions in a 6-well plate. Tissue treated with left) vehicle gel and right) CCE gel. Tissue rings were either fixed for histology or used for SMC explant.

3.5.1.2. BIOREACTOR CULTURE

Each whole artery was mounted into the bioreactor using two loops of sterile γ-irradiated catgut at each end. Each bioreactor chamber was supplied with 816.5 ml of 30% FCS whole organ culture medium (Section 3.2.4) in the respective reservoir. Throughout the culture period, the media reservoirs were held at 44°C in a water bath, higher than the required 37°C required for the artery in order to accommodate heat loss between the reservoir and the chamber. Chamber temperature was monitored with a probe installed in the top of the chamber. A low-flow rate supply of 5% CO_2 v/v in O_2 was filtered through a 0.22μm filter

and gassed through the media reservoir continuously throughout the culture time. The pressure at the inlet was recorded using a sterile pressure transducer and an upstream clamp was used to equalise any pressure disparity between the separate chambers. The pressure in each of the bioreactors running in parallel was maintained approximately the same using an upstream clamp of the bioreactor system.

3.6. BIOREACTOR DYNAMIC ENVIRONMENT

In order to characterise the dynamic environment which the bioreactor provided, the flow rate and local pressures at various points around the bioreactor were measured. There were four available points in the bioreactor system at which the pressure was able to be measured using a transducer connected to an ECG machine. These points are shown as red numbers in Figure 3.9: they correspond to 1) the bioreactor inlet, 2) the lumen of the vessel, 3) the shaft of the bioreactor and 4) the chamber outlet. The pressures were measured using both an artificial artery (silicone tubing) and a non-sterile porcine carotid artery.

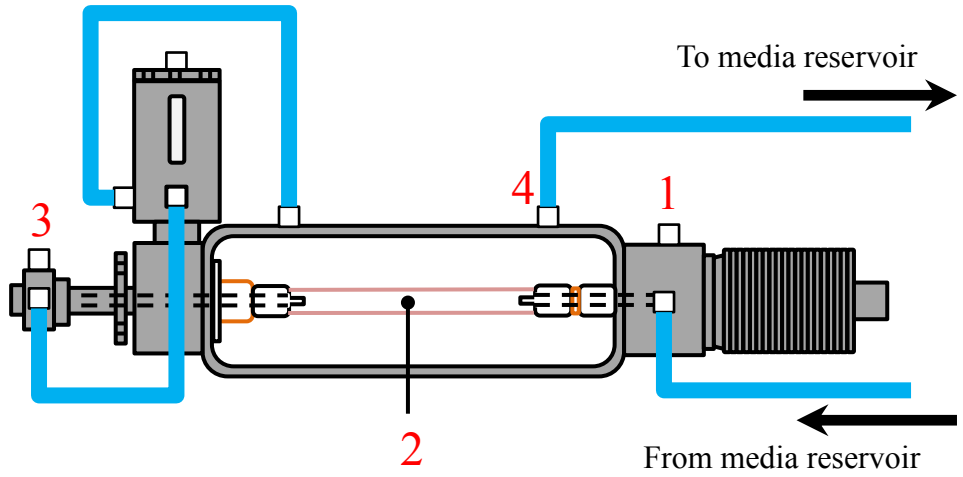

Figure 3.9 Bioreactor schematic showing the four available local pressure measuring points (shown as red numbers).

3.6.1. CALIBRATION OF PRESSURE TRANSDUCERS

The pressure transducers were connected to the ECG machine and were then calibrated using a manual sphygmomanometer (Figure 3.10). During this, the pressure was manually increased in 20mmHg increments up to 140mmHg using the sphygmomanometer. The pressure reading on the ECG machine was recorded at each of the 20mmHg pressure increments. The measured vs. the actual pressure was imported in Microsoft Excel 2013 (Microsoft, WA, USA) and a linear best fit line determined using in-built least squares regression code. The linear equation of the linear best fit line was used as a calibration equation. Pressure readings from the ECG machine via the pressure transducer were converted to actual readings using this equation. The pressure calibration graphs can be found in Appendix E.

During sterile bioreactor experiments, it was not possible to calibrate the pressure transducer prior to initiating the experiment. This would have compromised the sterility of the system. A brand new, unused pressure transducer was used for each bioreactor experiment.

Figure 3.10 Manual sphygmomanometer used for calibration of pressure transducers.

3.6.2. MEASUREMENT OF LUMINAL PRESSURE

The pressure at position 2, in the lumen of the artery, was measured by inserting a modified hypodermic needle connected to a pressure transducer through the arterial wall. The tip of the hypodermic needle was milled down to achieve a flat profile to eliminate the resistance of flow which would be present with a standard graduated tip.

Measurement of the luminal pressure at position 2 was not possible with the front glass plate in place on the front of the bioreactor chamber. This was overcome by measuring pressures at positions 1, 3 and 4 relative to position 1. The glass plate was then removed and the fluid flow diverted so that it returned to the media reservoir before reaching the bioreactor chamber. In this way, pressures at positions 1, 2 and 3 could be measured and expressed as a pressure drop relative to position 1. The two sets of data were then able to be combined in a full data set. Figure 3.11 shows the measurement of the luminal pressure at position 2 with the glass plate removed from the chamber.

Figure 3.11 Measurement of luminal pressure with front glass plate removed from bioreactor chamber.

3.6.3. FLOW RATE CALIBRATION

The pump used throughout the course of this study (Masterflex Model 77200-50) was controlled with a continuous control dial with arbitrary number markings. The actual flow rate was measured by setting up the bioreactor and allowing the system to fill up with fluid so that it was returning to the media reservoir. The silicone tube leading back to the media reservoir was then detached and allowed to empty into a measuring cylinder. The system was left to empty fluid into the measuring cylinder for 1 minute before the silicone tube was removed. The volume of the fluid in the measuring cylinder corresponded to the actual flow rate, given in $ml.min^{-1}$.

A porcine carotid artery was installed into the bioreactor and the flow rate was measured in triplicate at 7 separate flow rates corresponding to the arbitrary numbers on the continuous control knob of the pump: 1, 1.5, 2, 2.5, 3, 3.5 and 4. Hand drawn lines were added on to the control dial to denote the pump reading values at 1.5, 2.5 and 3.5. The results are shown in Figure 3.12.

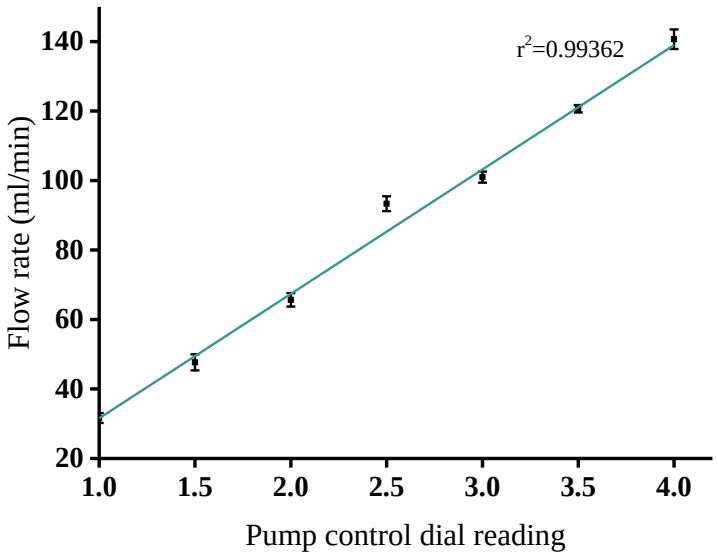

Figure 3.12 Flow rate calibration with porcine carotid artery with linear fit trendline (r^2=0.99). Graph shows mean ± 95% confidence intervals, (n=3).

A linear best fit line was applied to the data using Origin Pro 8.5.1 graphing software with in-built linear regression code (OriginLab Corporation, MA, US), giving an adjusted R^2 value of 0.99 (Figure 3.12). An adjusted R^2 value gives an indication of the degree of variation explained only by the independent variables that actually affect the dependent variable. From this, it was concluded that the pump control dial acted to alter the flow rate in a linear manner, rather than exponential. This relationship could then be used to determine the required flow rate through the bioreactor system.

The normal carotid flow rate in humans is in the range of approximately 360 – 720 $ml.min^{-1}$ (Bogren et al., 1994, Oshinski et al., 2006). However, a much lower flow rate of 120 $ml.min^{-1}$ found throughout the literature was chosen for the bioreactor experiments: the *ex vivo* nature of the experiments demanded that the flow rate must allow optimal oxygen perfusion and nutrient delivery for the tissue (Swartz et al., 2005, Hahn et al., 2006, Aper et al., 2007, Riches et al., 2013). Although a relatively large difference between the chosen and physiological flow rates was present, both the vehicle control and CCE treated arteries were cultured using the same flow rate so the relative differences could be analysed.

3.6.4. CHARACTERISATION OF LOCAL PRESSURES

The local pressures at positions 1, 2, 3 and 4 were measured at three different flow rates using a pressure transducer (Argon Medical, TX, US) and an ECG machine (SW Healthcare, FL, US). The flow rates corresponded to the arbitrary number markings on the control dial on the pump, as a point of reference. The mean local pressures at the specified positions when a porcine carotid artery was installed are shown in Figure 3.13.

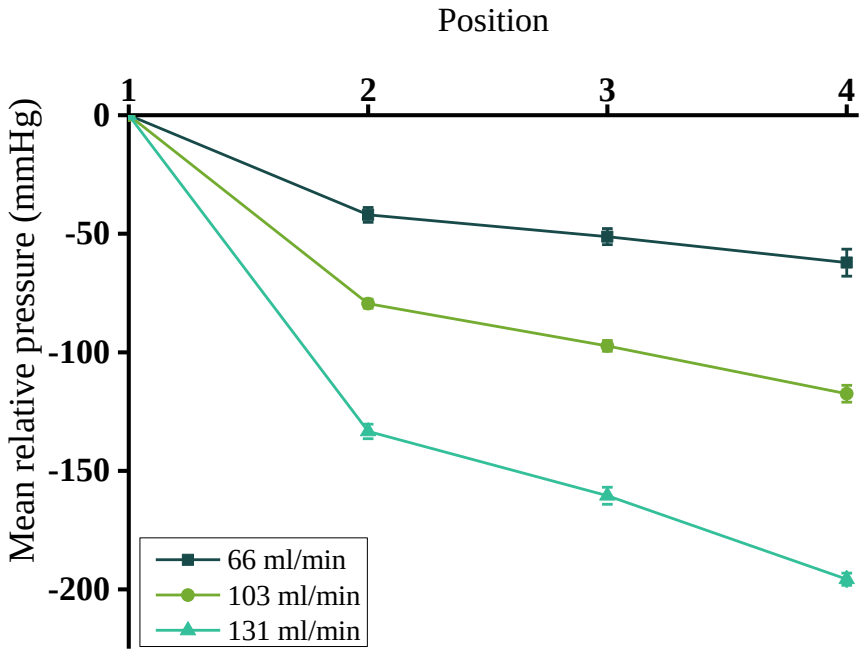

Figure 3.13 Mean relative pressures at specified positions around the bioreactor at three flow rates with non-sterile porcine carotid artery. (n=5), graph shows mean ± 95% confidence intervals.

In all cases, the sharpest pressure drop occurred between position 1 and position 2, the inlet and luminal pressure respectively. The pressure drop increased when the flow rate was increased – from 42.0±3.1 to 133.4±3.1 mmHg at the lowest (66ml.min^{-1}) and highest (131ml.min^{-1}) flow rates respectively in the carotid artery, which was as expected.

The proportion of the pressure drop throughout the bioreactor system at the three specified flow rates are shown in Table 3.3. The greatest proportion of the pressure drop throughout the system occurred between positions 1 and 2, at the bioreactor inlet and in the lumen of the artery respectively. At each flow rate, the proportional pressure drop at each position was similar. Increasing the flow rate up to 131 ml.min^{-1} in steady flow did not affect the pressure profile of the bioreactor system.

Table 3.3 Percentage pressure drop between specified bioreactor positions at flow rates of 66, 103 and 131 ml.min^{-1}.

	Flow rate		
Position	**66 ml.min^{-1} (%)**	**103 ml.min^{-1} (%)**	**131 ml.min^{-1} (%)**
1 - 2	48.0 ± 0.7	46.9 ± 0.7	47.4 ± 4.2
2 - 3	39.8 ± 2.8	42.9 ± 1.6	39.9 ± 2.0
3 - 4	12.3 ± 2.3	10.2 ± 2.1	12.7 ± 2.7

The characterisation of local pressures throughout the bioreactor system is important as the *ex vivo* AAA model required the artery to remain sterile in order to be cultured as a whole organ for up to twelve days and subsequently derive a SMC explant culture for structural and functional assays. In order to maintain sterility in the system, it was not possible in the current configuration to measure the luminal pressure in the artery (at position 2). The characterisation of the pressure drop shown in Table 3.3 enables a calculation of the luminal pressure in the artery installed in the bioreactor from measuring the pressure at the inlet (position 1). The luminal pressure was a mean 47.4% drop relative to the pressure at the bioreactor inlet. The measurement of the pressure at the bioreactor inlet was possible during the creation of the *ex vivo* AAA model without compromising sterility.

3.6.5. *EX VIVO* AAA MODEL PRESSURES

During the course of this study, nine successful bioreactor experiments were completed. The pressure at the bioreactor inlet and the temperature of the media in the bioreactor chamber were recorded once per day during the experiments.

The luminal pressure in the porcine carotid artery was maintained at approximately 65 mmHg via monitoring of the ECG machine, the diastolic pressure of the carotid artery in humans and within the normal range for pigs

(73 – 230 mmHg in systole and 52 – 165 mmHg in diastole) (Hodgkin et al., 1982, Morgan and Hosking, 2007). In order to accomplish this, the silicone tubing returning from the bioreactor chamber to the media reservoir could be clamped to increase the upstream pressure throughout the bioreactor system to the required value.

From the data presented in Section 3.6.4, the pressure at the inlet should be 47.4% greater than 65 mmHg giving the desired inlet pressure at 96 mmHg. The inlet pressures taken over the course of eight bioreactor experiments, three of which ran for three days, are shown in Figure 3.14. The mean inlet pressures between CCE and VEH treated arteries were indistinguishable (94.2±1.6 vs. 96.0±1.8 mmHg respectively, mean ± 95% confidence intervals, p=0.14, normalised 2-sample two-tailed t-test). The two outliers in the data presented are from the same animal – the bioreactor system design is such that it is complex to manually decrease pressure whereas increasing system pressure is simply achieved by clamping upstream.

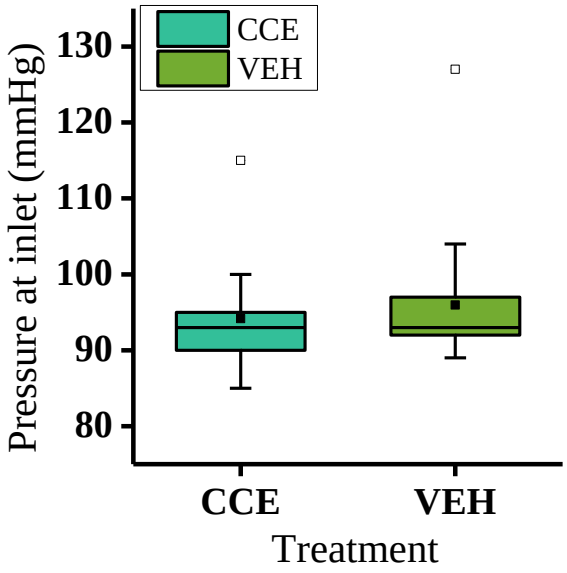

Figure 3.14 Inlet pressures of CCE and VEH treated porcine vessels (n=8). □ = outlier (from same animal in both groups). ■ =mean, shaded area = interquartile range, centre line = median, whiskers = minimum to maximum.

3.7. DISCUSSION

The method described throughout this chapter enabled aseptic parallel culture of viable porcine carotid arteries under steady flow conditions for up to twelve days. When CCE treatment was applied to the artery prior to culture, it is understood that a SMC phenotype is induced which is comparable to human AAA SMCs (Riches et al., 2013). Following CCE pre-treatment, a period of three days of bioreactor culture was chosen to model early-stage AAA disease. Previously in a mouse model, it was shown that although aneurysmal dilatation was observed after 14 days, phenotypic switching of the SMCs was present only seven days after elastase perfusion (Ailawadi et al., 2009). The rationale for choosing a culture period of three days to simulate early AAA was to elucidate any alterations in SMCs prior to switching phenotype. These potential alterations may then serve as molecular targets for therapeutics.

The use of steady flow through the arterial lumen was used in the only other AAA bioreactor model to date. However, the methods differ greatly between the two studies: Touroo and Williams seeded stromal vascular fraction cells onto previously dilated ePTFE scaffolds and then used the bioreactor to differentiate the cells and seed the scaffold (Touroo and Williams, 2012). The model described in this chapter was not intended to induce differentiation from stem cells, but removes the functional organ and cultures it in an *ex vivo* environment. Therefore, the structure of the organ and organisation of the cells are exactly as they would exist *in vivo* as the artery is installed into the bioreactor and does not require tissue conditioning. Bioreactors are more commonly used for imparting forces onto a scaffold seeded with some type of stem cell with an aim of differentiating the cells into the desired phenotypes using mechanotransduction (Niklason et al., 1999, Sivarapatna et al., 2015). Although pulsatile flow is closer to the physiological haemodynamics, it has been shown that steady flow is able to induce an AAA SMC phenotype after 12 days in the bioreactor, as validated by human AAA SMCs previously in this laboratory by human AAA SMCs (Riches et al., 2013).

The luminal pressure was maintained at approximately 65mmHg, measured by calculating the pressure drop from the bioreactor inlet. This value was selected

as it is within the normal range for carotid pressure in pigs and humans (Hodgkin et al., 1982, Morgan and Hosking, 2007). This value was, however, at the low end of these pressure ranges: the artery once subjected to CCE treatment was relatively weak and so a balance was struck between physiological pressure and risk of rupture of the arteries. Once rupture of an artery had occurred in the bioreactor, the cells in the artery were no longer subjected to a known pressure and flow regime, if at all.

The use of a bioreactor in this model of AAA enables a whole organ culture of a porcine carotid artery under simulated physiological conditions. Although very widely used, relatively low cost, and relatively simple to implement, a common criticism of *in vitro* models which investigate the behaviour of cells in a monolayer is the absence of an extracellular matrix. Recently a burgeoning area of research into three-dimensional cell culture has emerged and it is argued that a 3D environment better represents the geometry, signalling environment and cell-cell interactions which exist *in vivo* (Lee et al., 2008). The bioreactor allowed the culture of arterial cells in a relatively natural state: flow through the lumen, pressure imparted transmurally, CO_2 and O_2 control and physiological pressure. In this respect, the *ex vivo* bioreactor has a benefit over *in vitro* disease models. Additionally, both Dadgar *et al.* and Kratzberg *et al.* aimed to induce sufficient passive stretch in arterial tissue such that it may form an experimental aneurysm (Dadgar et al., 1997, Kratzberg et al., 2009). They concluded that the pathological remodelling seen in AAA was an active process and would require arteries to remain functional and viable whilst it was induced with elastase or collagenase. Again, the bioreactor model of AAA maintained viability of the artery and SMCs and enabled this active remodelling after application of the CCE treatment.

The bioreactor AAA model also offers benefits over animal models. The porcine arteries used were significantly larger than mouse or rat arteries and were more comparable in size and anatomy to humans (Trollope et al., 2011). The practicalities and cost of husbandry of large animals is significant: the bioreactor AAA model allows the artery to remain viable as a whole organ under flow for up to 12 days without the need for additional costs required for

husbandry of a large animal. In the first *in vivo* aneurysm model in swine, Goericke *et al.* noted that high time and monetary costs might limit the routine use of this model (Goericke et al., 2009). However, the use of the pig AAA model is becoming more common in recent years and has been used to assess implantation of mesenchymal stem cells as a therapeutic treatment for AAA (Turnbull et al., 2011, Houdek et al., 2013, Lin et al., 2013, Kloster et al., 2015).

Another benefit that the AAA bioreactor model may offer over *in vivo* models is the ability to manipulate and control the haemodynamic environment. Lin *et al.* induced an AAA in pigs using an arterial stenosing cuff, without the use of a chemical agent designed to degrade the ECM (such as elastase) (Lin et al., 2013). The dynamic environment has been linked to AAA progression, amongst other cardiovascular diseases. Turbulent flow contributes to aneurysm development via endothelial injury and accelerated degeneration of the arterial wall by an increase in oxidative stress (Miller, 2002). Regions of low shear stress in the vasculature contribute towards vascular diseases such as AAA and atherosclerosis: increased inflammatory cell infiltration, endothelial dysfunction and release of MMP-9 and MMP-2 are all correlated with low shear stress (Dua and Dalman, 2010, Norman and Powell, 2010, Lu and Kassab, 2011). Interestingly, altered haemodynamics and AAA formation have been associated with vascular complications of lower-limb amputees. Vollmar *et al.* found the prevalence of AAA to be 5 times greater in patients who underwent amputation (Vollmar et al., 1989). A bioreactor AAA model offers the opportunity to more tightly control the flow rate and pressure through the lumen of the artery without the need for using reagents to increase heart rate and blood pressure *in vivo*. A model is able to be used to investigate the relationship of pulse pressure, flow rate and flow turbulence with the development of AAA and SMC dysfunction.

As with every disease model, the limitations of using the bioreactor model to elucidate AAA development and processes should be considered carefully. Firstly, the dynamic environment in which the artery was cultured *ex vivo* was steady flow in this study as opposed to physiological pulsatile flow. It is well documented within the tissue engineering and regenerative medicine field that

cyclic stretch, coupled with shear stress, is required for differentiation of mesenchymal stem cells into vascular cells (Sivarapatna et al., 2015) and reviewed in Riehl et al. (2012). The function of the mature smooth muscle cell has been shown to be affected by cyclic tensile strain. Perpendicular SMC alignment, increased apoptosis and degradation of α-smooth muscle actin (a contractile protein), all associated with increased levels of cyclic strain are all mediated through the p38 MAPK pathway (Chen et al., 2003, Goldman et al., 2003, Wernig et al., 2003). Various biochemical markers secreted by SMCs are also affected by cyclic strains, including ECM molecules and growth factors (Stegemann et al., 2005). A limitation of this model is that the bioreactor experiments were conducted under steady flow which does not impart cyclic stretch to the artery as it would be subjected to physiologically. This flow regime may therefore affect SMC function and so appropriate control groups were included throughout the study in order to understand the effect of the bioreactor flow without any pre-treatment. Using isolated cultured SMCs presents another limitation inherent to *in vitro* cell culture work and to the culture of SMCs in particular. SMCs possess different embryological origins and have the ability to undergo phenotypic modulation. It must therefore be considered that culturing isolated SMCs *in vitro* may have an impact on their phenotype (Xie et al., 2011). Cell expansion and culture *in vitro* also does not reflect the natural 3D cell environment where cells are surrounded by an ECM and other SMCs. Coupled with the intrinsic ability of SMCs to modulate their phenotype, the effect of SMC isolation, expansion and culture *in vitro* may have undocumented effects. Certainly, there have been other studies which do document this SMC heterogeneity in culture (Huber and Badylak, 2012, Proudfoot and Shanahan, 2012). The nature of *in vitro* study is that the observed behaviour of SMCs is comparable to that observed *in vivo*. However, using the selected functional characterisation assays detailed in Chapter 2, this limitation is unavoidable.

It is thought that the inherent structure of the abdominal aorta leads to predisposition of the specific site for AAA formation (Norman and Powell, 2010). One of the structural parameters contributing to AAA formation *in vivo* is the downstream bifurcation of the aorta into the femoral arteries: this causes

turbulent blood flow and concentrated loci of high and low shear stress which have been found to correlate with areas of disease (Ku, 1997). Another study has found that higher bifurcation angle is associated with AAA (Sharp et al., 1982). The lack of bifurcation in the bioreactor to induce these physiological concentrations of stress in the upstream artery may therefore also be considered a limitation of the model. The *ex vivo* bioreactor AAA model is especially suited to studies involving geometry, as it can be controlled precisely which is not typically feasible *in vivo*.

Once the artery has been removed from the pig, the only cells that are present in any significant number in the bioreactor are SMCs and endothelial cells. The majority of fibroblasts are removed via blunt dissection (as shown in Figure 3.2). However, other studies have shown that there are many other types of cells contributing to AAA formation. The inflammatory infiltrate of the AAA is a well characterised feature: mast cells, leukocytes and macrophages are found in greater numbers in AAA compared to occlusive atherosclerotic arteries (Koch et al., 1990). Mast cells are considered to play a major role in AAA formation via MMP activation and secretion, such that a mast cell inhibitor has recently been trialled in AAA patients (Swedenborg et al., 2011, Sillesen et al., 2015). Infiltration of leukocytes into the media of the aorta lead to SMC depletion and generation of reactive oxygen species (Davis et al., 2015). Macrophages secrete inflammatory cytokines and chemokines in AAAs such as monocyte chemotactic protein-1 (MCP-1), interleukin-8 (IL-8) and tumour necrosis factor-α (TNF-α) (Koch et al., 1993, Satoh et al., 2004). Any compounding effects of cells which are not native to the artery but are recruited during AAA development on the function of SMCs are eliminated in the bioreactor model of AAA. This is at once both a limitation and a benefit of the model: it does not exactly simulate the conditions *in vivo* attributed to other cell types which may affect the structure of the arterial tissue and the SMCs, yet the contributions of the SMCs to AAA formation can be studied with clarity if they are isolated from such compounding factors.

The *ex vivo* bioreactor model of AAA allowed culture of a porcine artery for up to 12 days under dynamic flow conditions. When the artery was focally pre-

treated with a combination of collagenase and elastase, the SMCs in the artery after 12 days in bioreactor culture are comparable to human end-stage AAA SMCs (Riches et al., 2013). The local pressures at positions throughout the bioreactor under steady flow have been characterised in order to understand the dynamic culture environment. The flow rate through the bioreactor under steady flow has also been calibrated with regards to the peristaltic pump. The bioreactor AAA model represents a practical and relatively low cost large animal model of AAA which has been used to characterise the structure and function of SMCs over time and their contribution to arterial biomechanics in the subsequent chapters of this thesis. The aim is to uncover therapeutic targets of AAA in SMCs in the early-stages of the disease.

CHAPTER 4

TISSUE STRUCTURE OF *EX VIVO* AAA MODEL

CHAPTER 4 TISSUE STRUCTURE OF *EX VIVO* AAA MODEL

This chapter examines the changes in structure of tissue in terms of histoarchitecture and luminal perimeter due to the bioreactor AAA model methodology described in the previous chapter (Chapter 3). Firstly, the effect of dynamic/static culture, CCE treatment and model stage (EARLY/END) on tissue histoarchitecture will be examined. The last section details the vessel dilation seen in the bioreactor AAA model in terms of luminal perimeter (Section 2.7.2.2).

4.1. INTRODUCTION

A ubiquitous characteristic of AAA is the degradation and fragmentation of the extracellular matrix (ECM), most notably the elastin component. The function of elastin is to provide the recoiling mechanism of the arterial wall in response to blood pressure pulses. The other main component of the ECM is load-bearing collagen fibrils; the fate of collagen in response to AAA formation appears to be less consistent, with various studies finding levels to increase, decrease and remain unchanged. It is, however, the generally accepted view that collagen content tends to increase in AAA. These alterations in the composition of the ECM are coupled with a loss of SMCs throughout the arterial wall (Lopez-Candales et al., 1997, Henderson et al., 1999). When considering suitability of animal models, often the argument for the success of a model centres around the ability to mimic the histological structure of the human disease as opposed to a more crude surgical patch model (Daugherty and Cassis, 2004, Tsui, 2010, Trollope et al., 2011). The gold standard mark of success for experimental AAA models is to be able to induce a progressive dilatation of the artery.

Exploring the structure of the ECM in the *ex vivo* model is useful, not only to compare it to the structure of human AAA, but also to compare it to other *in vivo* models as a comparator. To do this, histological staining of elastin and collagen and immunostaining of α-smooth muscle actin (α-SMA) were

undertaken across various treatment groups with various combinations of treatment and culture conditions at two different time-points. The effects of the CCE treatment and dynamic bioreactor culture alone were investigated, as well as the effect of the combination of both.

Porcine carotid arteries were subjected to either a pre-treatment containing a combination of collagenase and elastase or a vehicle gel treatment. The treatment was washed off after 3 hours and the arteries were cultured in parallel bioreactors. This method is fully described in Chapter 3. The arteries were cultured in the bioreactor for either 3 days or 12 days representing the early and end-stage disease respectively (Riches et al., 2013). Corresponding arterial rings were also cultured statically.

4.2. CHAPTER AIMS AND OBJECTIVES

The aim of the work presented in this chapter was to investigate the histoarchitecture and gross morphology of the tissues produced using the *ex vivo* bioreactor model of AAA protocol as fully described in Chapter 3. The effect of the bioreactor culture and the CCE treatment used alone and in combination was examined. In terms of arterial structure, the *ex vivo* AAA model tissue was then compared to human AAA tissue as reported in the literature as an evaluation of the model. These changes in gross morphology as a result of treatment or culture regime were investigated with respect to time, as determined at two time-points representing the early- and end-stage AAA disease.

4.2.1. OBJECTIVES

Specifically, the objectives of this chapter were:

1 To examine changes in the gross morphology of the whole vessel under various treatment and culture regimes at two time-points, 3 days (EARLY) and 12 days (END).

2 To examine the levels of elastin, collagen and α-smooth muscle actin qualitatively at these points
3 To determine changes in the luminal perimeter of the artery at these points

4.3. TISSUE MORPHOLOGY

Quantitative measurements of the gross morphology of the arteries once installed into the bioreactor was not possible, or precise enough, as maintaining sterility was of utmost importance during the culture period. Therefore, introducing new components into the chamber as a reference for image analysis from photographs was not deemed possible. Representative qualitative images of the arteries installed into the bioreactor and after removal are shown in Figure 4.1. In general, the BIOVEH arteries did not show distension, even when pressurised. In contrast, CCE treated tissue tended to be much more distended when subjected to the same pressure and flow conditions in the bioreactor. Often, the wall of the BIOCCE arteries was observed to be translucent – this can be seen in Figure 4.1A in the centre of the BIOCCE artery. Once the BIOVEH and BIOCCE arteries were removed from the bioreactor, the greater degree of distention in the BIOCCE arteries compared to BIOVEH arteries was still apparent.

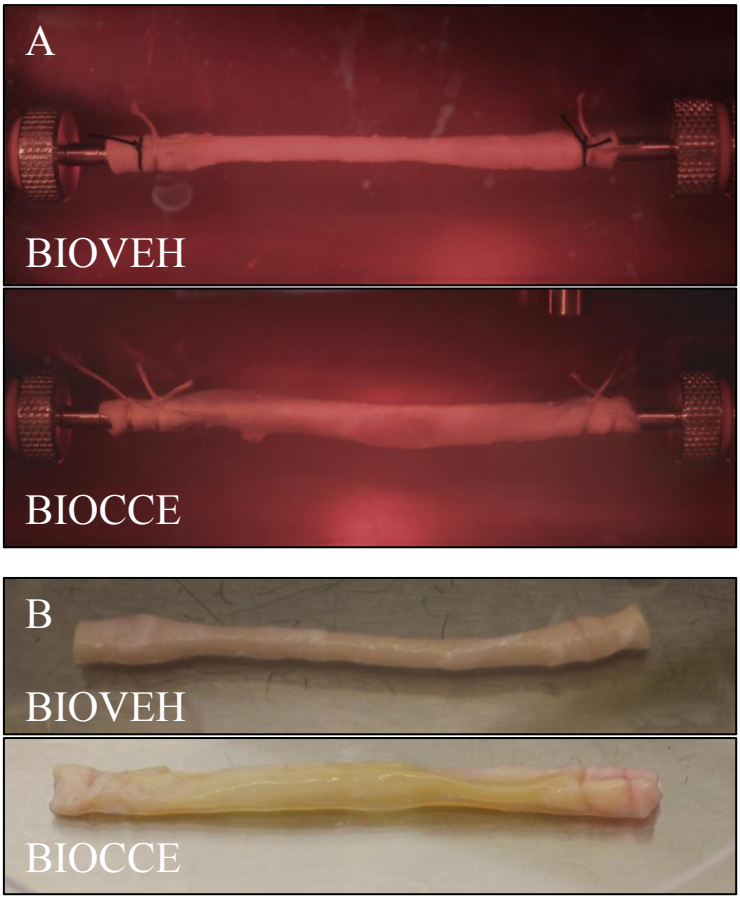

Figure 4.1 Observed differences in tissue morphology after culture in bioreactor. Representative images of BIOVEH and BIOCCE vessels A) during culture in bioreactor and B) after removal from bioreactor chamber after 12 days in culture (END).

4.4. HISTOARCHITECTURE OF CULTURED ARTERIES

Tissue samples from the five experimental groups (details in Table 2.1) were fixed and used for histological and immunohistochemical analysis. Briefly, these five groups were: FRESH, tissue was fixed immediately following harvest; SVEH, tissue was treated with vehicle gel pre-treatment and cultured in a 6-well plate; SCCE, tissue was treated with CCE gel pre-treatment and cultured in a 6-well plate; BIOVEH, tissue was treated with vehicle gel pre-treatment and cultured in the bioreactor; BIOCCE, tissue was treated with CCE gel pre-treatment and cultured in the bioreactor.

Each of these static and bioreactor cultured experimental groups was either cultured for 3 days, with an aim to mimic early-stage AAA disease (EARLY)

or for 12 days, mimicking the end-stage AAA disease (END). Tissue sections were stained either with Sirius Red for collagen staining or with α-smooth muscle actin (α-SMA) and Miller's elastin. The methods used for immunohistochemical and histological analysis are given in detail in Sections 2.7.1 and 2.7.2 respectively.

4.4.1. STATIC CULTURE

Qualitative histological analysis did not reveal any considerable alterations in SVEH tissue compared to FRESH in both EARLY and END models; both had a presence of ordered elastin (stained purple) throughout the media, distinct arterial layers and a collagenous adventitia (Figure 4.2, A, B, D, E; Figure 4.3, A, B, D, E). EARLY-SCCE tissue displayed fragmented and disrupted elastin fibres throughout all three arterial layers, although some elastin fibres were still present in the tissue. There were no gross changes in collagen histoarchitecture in EARLY-SCCE tissue compared to FRESH (Figure 4.2, D and F). In END-SCCE a complete absence of elastin fibres was observed alongside punctate α-SMA staining (Figure 4.3, C). No obvious difference was observed in terms of distribution of collagen in END-SCCE compared to FRESH (Figure 4.3, D and F).

The gross morphology of FRESH, SVEH and SCCE sections were all comparable to each other with no notable changes in medial thickness or lumen size. In both the EARLY model and the END model, SVEH histoarchitecture was comparable to FRESH (Figure 4.2, A, B, D, E; Figure 4.3 A, B, D, E). However in SCCE tissue there was only a partial loss of the elastin network in the EARLY model, yet there was almost a full loss of elastin throughout the arterial wall in the END model (Figure 4.2, C; Figure 4.3, C).

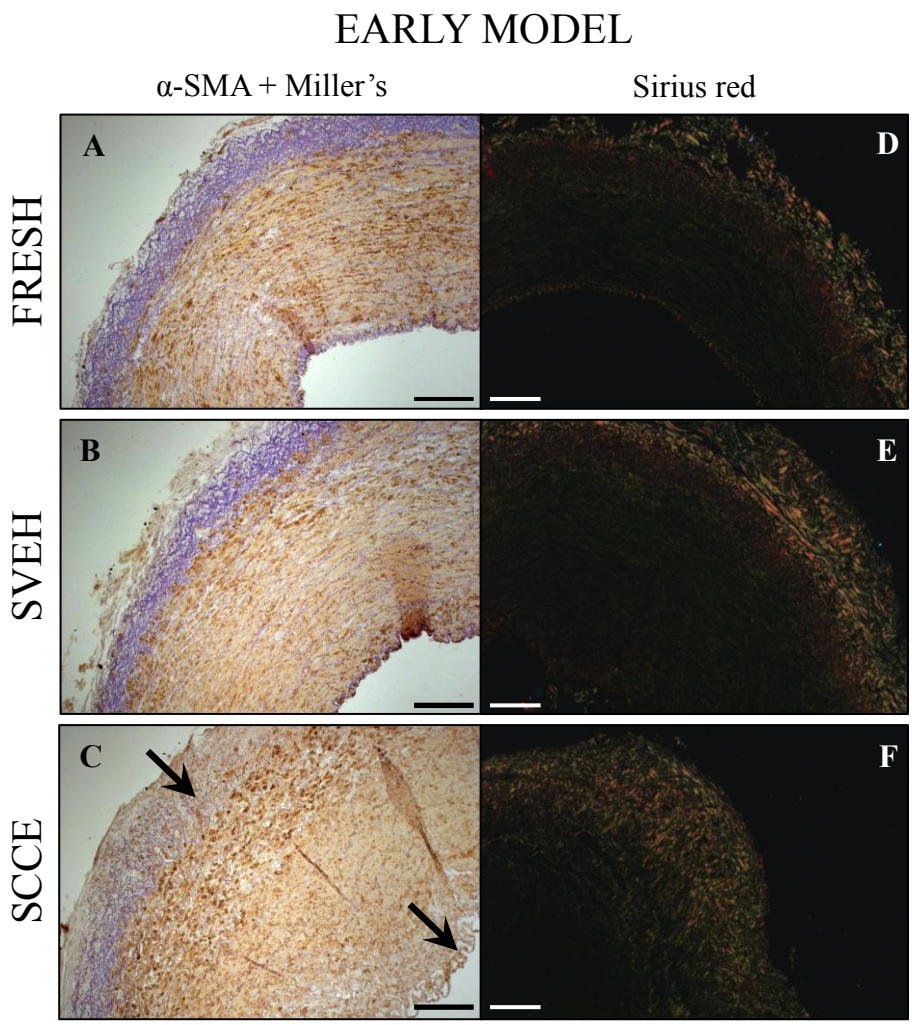

Figure 4.2 Representative images of α-smooth muscle actin with Miller's elastin co-stain (left; A, B, C) and Picrosirius Red stain (right; D, E, F) of EARLY FRESH (A, D), SVEH (B, E) and SCCE (C, F) tissue. Brown = α-SMA, purple = elastin, red/green = collagen. Arrows indicate loss of elastin fibres. Scale bar = 200µm.

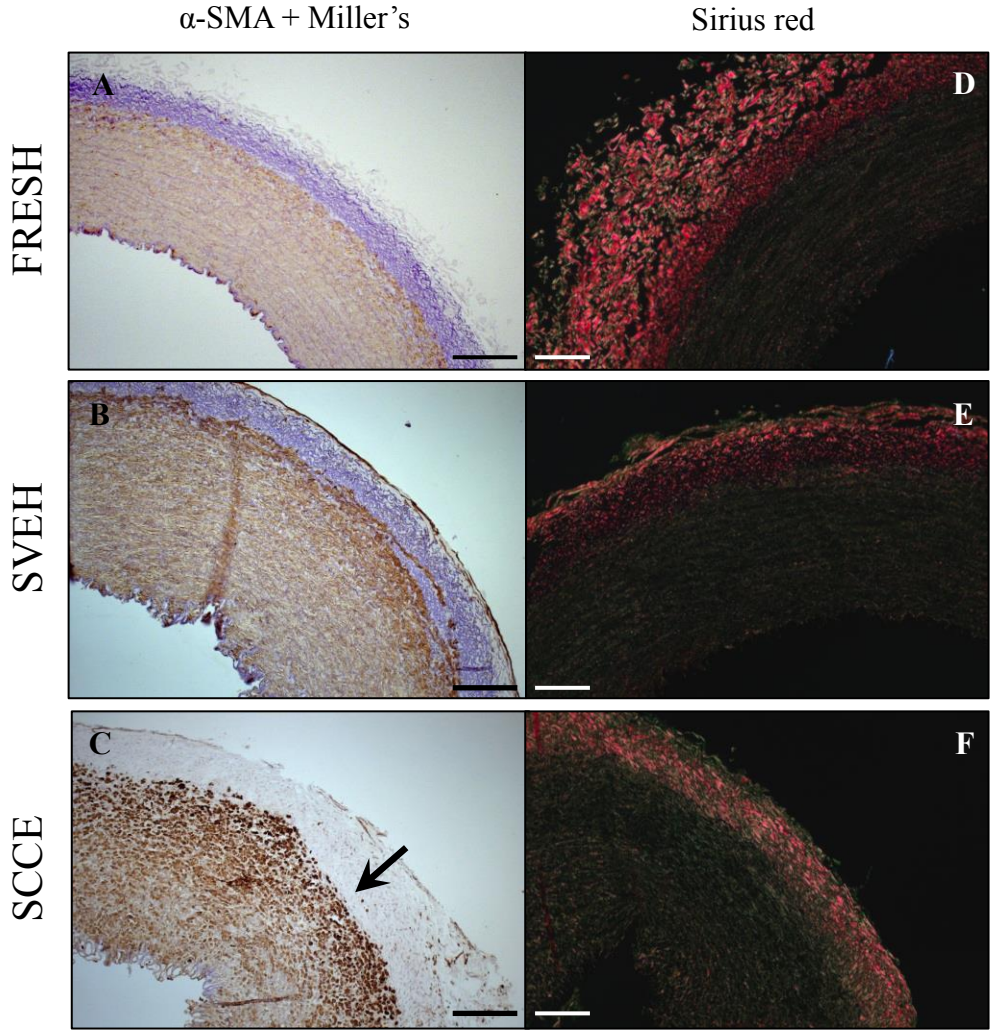

Figure 4.3 Representative images of α-smooth muscle actin with Miller's elastin co-stain (left; A, B, C) and Picrosirius Red stain (right; D, E, F) of EARLY FRESH (A, D), SVEH (B, E) and SCCE (C, F) tissue. Brown = α-SMA, purple = elastin, red/green = collagen. Arrows indicate loss of elastin fibres. Scale bar = 200µm.

4.4.2. BIOREACTOR CULTURE

In the EARLY model, BIOVEH tissue retained distinct arterial layers with abundant α-SMA in the media, an internal elastic lamina next to the lumen and an adventitia rich in elastin and collagen: features also found in FRESH tissue (Figure 4.4, A and C). Gross morphology of BIOVEH tissue in the EARLY model was also comparable to FRESH tissue. The collagen content of BIOVEH

tissue was similar to that of FRESH and statically cultured tissue, with uniform presence throughout the media and to a greater degree in the adventitia.

Even within the time-frame of the EARLY model, BIOCCE tissue had a distended shape, with medial thinning and a large lumen (Luminal diameter is analysed in Section 2.7.2.2). There is a complete loss of elastin throughout the artery and an absence of the internal elastic lamina (Figure 4.4, B and D). Throughout the media there was α-SMA actin staining comparable to BIOVEH tissue, indicating an abundance of SMC. Despite considerable changes in gross morphology and the loss of the elastin network, the arrangement of collagen fibres in EARLY-BIOCCE tissue did not appear different from BIOVEH, FRESH or statically cultured tissue, with uniform presence throughout the media (Figure 4.4, C and D).

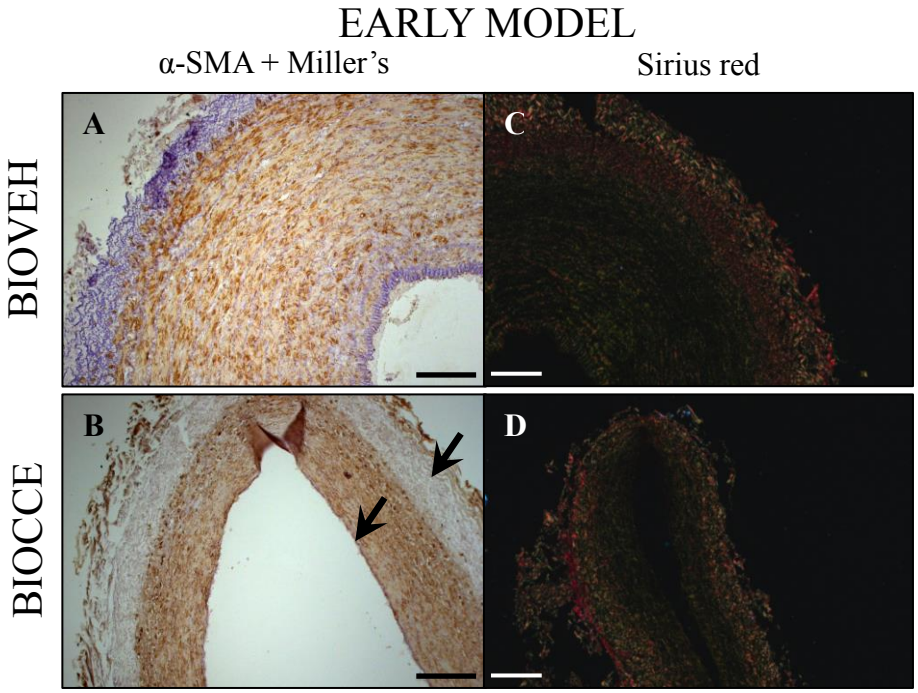

Figure 4.4 Representative images of α-smooth muscle actin with Miller's elastin co-stain (left; A, B) and Picrosirius Red stain (right; C, D) of EARLY-BIOVEH (A, C) and BIOCCE (B, D) tissue. Brown = α-SMA, purple = elastin, red/green = collagen. Arrows indicate loss of medial elastin fibres and internal elastic lamina. Scale bar = 200μm.

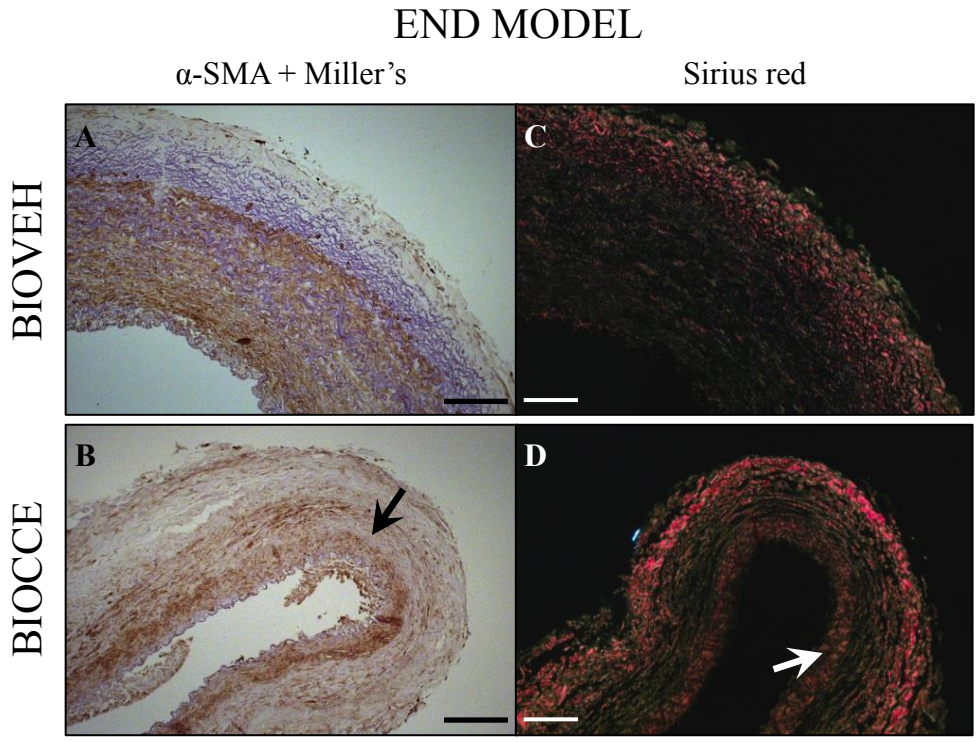

Figure 4.5 Representative images of α-smooth muscle actin with Miller's elastin co-stain (left; A, B) and Picrosirius Red stain (right; C, D) of END BIOVEH (A, C) and BIOCCE (B, D) tissue. Brown = α-SMA, purple = elastin, red/green = collagen. B: Arrow shows loss of α-SMA. D: Arrow shows potential periluminal collagen deposition. Scale bar = 200μm.

After culture in the bioreactor for 12 days, END-BIOVEH tissue retained its elastin network throughout all three arterial layers and the arrangement of collagen fibres mirrored in FRESH tissue (Figure 4.5 A and C). END-BIOVEH tissue had uniform α-SMA staining, once again indicating the abundance of SMC in the media. Much like the EARLY-BIOCCE tissue (Figure 4.4, B and D), END-BIOCCE tissue also showed altered gross morphology with medial thinning and arterial distention (Figure 4.5, B and D). END-BIOCCE tissue appeared to have a complete loss of the elastin network throughout all arterial layers, again mirroring the histoarchitecture of EARLY-BIOCCE tissue. The α-SMA staining was heterogeneous throughout the arterial wall, a phenomenon which was not observed in any other experimental groups in either the END or EARLY model. The configuration of collagen fibres in END-BIOCCE tissue was also unique, with a potential deposition of collagen adjacent to the lumen (Figure 4.5, D). Quantification of collagen content by image analysis of Sirius

red stained sections was not attempted and so this is only subjective and qualitative evidence of this periluminal deposition.

In summary, application of vehicle pre-treatment did not affect the histoarchitecture of the tissue whether it was subjected to either static (SVEH) or bioreactor culture (BIOVEH). After both 3 days (EARLY) and 12 days (END) in culture in the bioreactor, VEH treated arteries (BIOVEH) had a similar architecture to fresh tissue fixed straight after harvest (FRESH). Application of CCE treatment disrupted the elastin network in arteries cultured statically and in the bioreactor. However, the gross morphology of the tissue was only considerably altered when the artery was subjected to both CCE pre-treatment and bioreactor culture (BIOCCE). This alteration in tissue morphology was observable in both the EARLY and END models. It is a possibility that after 12 days in culture in the bioreactor, arteries which received CCE pre-treatment deposit collagen around the lumen of the artery (END-BIOCCE), a feature which was not observed in the EARLY model.

4.5. LUMINAL DIAMETER

The ubiquitous characteristic of the AAA from which its name is derived is arterial dilation; to be termed aneurysmal in clinical terms the diameter must reach 150% of the original (Powell, 1998, Nordon et al., 2011). Bearing this in mind, the luminal perimeter of ten fixed, stained sections from each group was measured using ImageJ and idealised as the diameter of a circle with circumference equal to this measured luminal perimeter (as described in Section 2.7.2.2). The results are presented in Figure 4.6. The luminal diameters of BIOVEH and BIOCCE vessels are presented as a percentage of the luminal diameter of their respective FRESH vessel from the same animal in order to mitigate the effects of inter-animal variance.

The luminal diameter of BIOVEH vessels was not affected by culture time in the bioreactor. BIOCCE vessels typically had a greater luminal diameter than BIOVEH vessels at both model stages, though this difference was more pronounced in the EARLY model compared to the END model. There was a

marked decrease in the BIOCCE treated vessel in the END model compared to the EARLY model; in the EARLY model, BIOCCE vessels reached the 150% aneurysmal threshold.

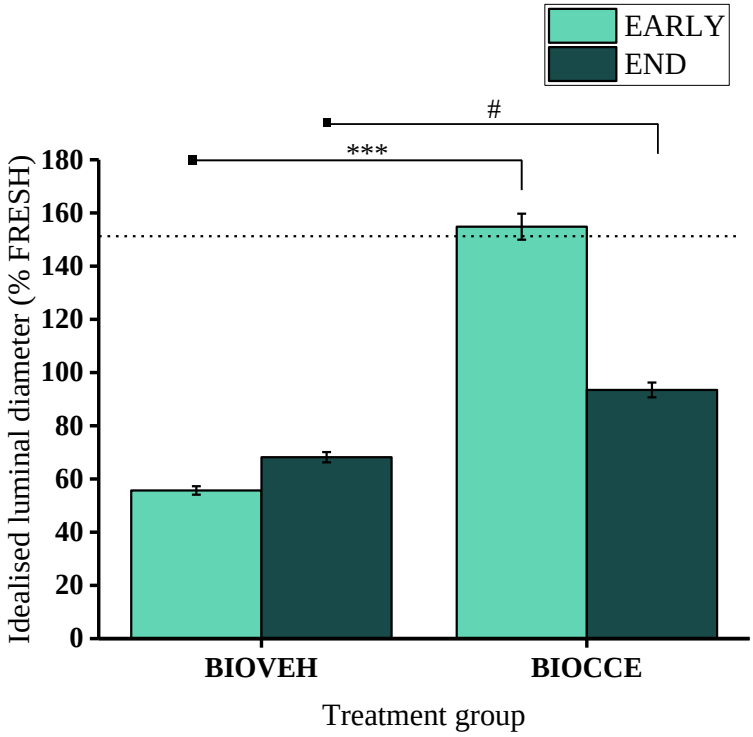

Figure 4.6 Mean luminal perimeter normalised to FRESH tissue per animal. Data shown is mean ± 95% confidence intervals, n=3 animals, 10 measurements per animal, two-sample t-test for post-hoc two-way ANOVA analysis, ***p<0.001, #p=0.06. Dotted line indicates 150% of the FRESH vessel diameter which is the commonly accepted clinical threshold of aneurysm.

For statistical analysis, to test the effect of model stage and treatment group on the luminal diameter of the arteries, a 2x2 independent ANOVA was used. The first factor was model stage (EARLY, END) and the second factor was vessel treatment (BIOVEH, BIOCCE). FRESH vessels were not included as the BIOVEH and BIOCCE vessels were normalised to the measurements of FRESH vessels in order to account for inter-animal variation and therefore the statistical tests were performed on logarithmically transformed data. The ANOVA showed that model stage had a significant effect on luminal diameter, $F(1, 96) = 5.97$, $p<0.05$. Vessel treatment also had a significant effect on luminal diameter, $F(1, 96) = 68.54$, $p<0.001$. The interaction between model stage and

vessel treatment also had a significant effect, $F(1, 96) = 29.51$, $p<0.001$. To explore this interaction, a two-tailed t-test was performed per model stage (EARLY/ END) on logarithmically transformed data comparing BIOVEH and BIOCCE models. In the EARLY model, BIOCCE vessels had a significantly increased idealised luminal circumference compared to BIOVEH vessels (153.9 ± 5.2% vs. 55.5 ±1.6% respectively, $p<0.001$). In the END model, however, the idealised luminal diameters of BIOCCE vessels were not significantly different compared to BIOVEH vessels (68.2 ± 1.94% vs. 88.3 ± 2.8% respectively, $p=0.06$). However, this level of significance may suggest a trend towards a larger diameter in BIOCCE tissue compared to BIOVEH tissue in the END model.

4.6. DISCUSSION

A common characteristic of AAAs is severe degradation of the extracellular matrix and a depletion of SMCs (He and Roach, 1994, Lopez-Candales et al., 1997). In this chapter, histological and immunohistochemical staining of elastin, collagen and an SMC marker (α-smooth muscle actin) were carried out on the *ex vivo* AAA model tissue.

When subjected to static culture in a 6-well plate, VEH treated tissue did not exhibit any notable changes in the histoarchitecture when compared to FRESH tissue, in neither the EARLY model nor the END model. The elastin network remained intact and there was an abundance of SMCs throughout VEH treated tissue.

Application of the CCE gel pre-treatment prior to static culture in a 6-well plate resulted in notable degradation of the elastin network in both the static and bioreactor cultured tissue, whereas there was no observed difference in the collagen network. In FRESH tissue, collagen was present in a uniform arrangement throughout the media and to a greater degree in the adventitia. The distribution was mirrored in VEH and CCE treated tissue which had been cultured under static conditions. In the EARLY model, CCE treated tissue exhibited a fragmented and degraded elastin network, although some elastin

remnants remained after 3 days in static culture. However, in the END model, there was virtually a complete removal of the elastin network throughout the tissue and more punctate α-SMA staining was observed. This punctate staining may indicate a slight loss of SMCs in the media in CCE treated tissue. Vessel sections from tissue which was cultured under static conditions exhibited no obvious changes in gross vessel morphology compared to FRESH tissue (Figure 3.8).

The histoarchitecture of the BIOVEH tissue in both the EARLY and END models was indistinguishable from FRESH tissue; there was a rich layer of SMCs in the media, an intact elastin network, a collagen-rich adventitia, and a uniform distribution of collagen throughout the media. This indicates that the bioreactor conditions were not causing considerable alterations to the composition and configuration of the extracellular matrix.

In contrast to this, BIOCCE tissue showed virtually complete degradation of the elastin network in both the EARLY and END stage models. In the EARLY model, BIOCCE tissue exhibited a media rich with SMCs, whereas in the END model, the tissue exhibited much weaker SMC-specific staining, suggesting a possible loss of SMCs over time. A depletion of SMCs and degradation of the elastin network are ubiquitous hallmarks of the end-stage human AAA, and so the results presented for BIOCCE tissue suggest that the BIOCCE model was able to mimic the human disease (Campa et al., 1987, He and Roach, 1994, Lopez-Candales et al., 1997, Henderson et al., 1999). As histology and immunohistochemistry are typically a qualitative technique and so any conclusions made about an increase or decrease in elastin content should be supported with quantitative biochemical assays. An example of such is measurement of the elastin crosslink peptides desmosine and isodesmosine with enzyme-linked immunosorbent assay (ELISA) or high performance liquid chromatography (HPLC) (Osakabe et al., 1995).

The only tissue in which a difference in the collagen network was observed was BIOCCE tissue: a deposition of collagen around the lumen of the artery which was not present in any other experimental groups. This may be explained by looking towards the end-stage human disease: AAA tissue is typically

characterised as being stiffer yet weaker than normal aortic tissue (Thubrikar et al., 2001, Geest et al., 2006). This increased stiffness is attributed to the increased collagen content found in AAA tissue, as collagen is the component of the extracellular matrix which is responsible for the increased stiffness of arterial tissue at high strains (Rizzo et al., 1989). It is conceivable that his increase in collagen content is an attempt by the SMCs to stabilise the mechanical forces of the arterial wall to prevent aortic rupture once degradation of the elastin network has occurred. Although collagen degradation is present in early AAA, the rate of collagen synthesis is sufficient to balance this (Satta et al., 1997). However, over time, the rate of collagen degradation outstrips the rate of synthesis leading to a greater propensity to rupture (Shimizu et al., 2006). In an ApoE knockout mouse model of AAA, it was shown that an early ECM stabilisation mechanism occurred between 14 and 28 days after angiotensin II infusion (Haskett et al., 2013). The elastase-perfused abdominal aortae of rats have been shown to exhibit per-luminal depositions of collagen in the earlier stages of the disease, which was then not present one week later (Deb and Ramamurthi, 2014).

However, it should be carefully noted that the collagen deposition observed in END-BIOCCE model tissue was analysed qualitatively and subjectively. In order to quantify collagen content using Sirius Red staining, circularly polarized light must be used. If linearly polarized light is used for collagen visualisation (as was in this study), fibres which are aligned parallel to the transmission axis of the polarising filter would appear dark and would not be quantifiable via image analysis methods (Whittaker and Canham, 1991, Whittaker et al., 1994). For image analysis validation purposes, it would be beneficial in future studies to perform quantitative biochemical assays of collagen content alongside histological microscopic techniques as there is less sensitivity in the latter approach (Segnani et al., 2015). Examples of such may be Western blotting for Collagen-1 or a hydroxyproline content assay (Lopez-De Leon and Rojkind, 1985). It is therefore recommended that further study is undertaken to truly quantify changes in collagen content in END-BIOCCE tissue.

The possible peri-luminal deposition of collagen in BIOCCE tissue may be the first steps in the pathological modelling process found in human AAA disease. It suggests that the BIOCCE tissue may behave with increased stiffness compared to BIOVEH tissue. Biomechanical analysis of the experimental groups was carried out in this study and the results are presented and discussed in Chapter 6.

In both the EARLY and the END model, the gross morphology of the BIOCCE tissue was drastically different from that of FRESH or BIOVEH tissue. BIOCCE tissue was distended, with a typically thinner media and a much larger lumen. Image analysis of the stained sections was able to determine the changes in the luminal perimeter of the artery. The clinical definition of AAA is a dilatation of greater than 150% of the normal aortic diameter and so some type of measurement of the arterial dilatation was thought to be an essential metric of the study (Nordon et al., 2011). The justification for converting the measured luminal perimeter into an idealised luminal diameter was that the tissue could be viewed in comparison with clinical and *in vivo* studies. However, it must be stressed that the tissue was fixed in a non-pressurised state and so effect of luminal pressure are not considered using this method. The CCE treatment enzymatically digests components of the ECM (elastin and collagen) and will therefore alter the material properties of the tissue. As such, it is likely that luminal pressure will cause different levels of dilation between VEH and CCE treated tissue. One way of overcoming this problem may be to perfusion fix the tissue; this was considered but was not implemented due to practical concerns. The first concern was the very large amount of tissue fixation agent required to go throughout the bioreactor. The second was that it was of utmost importance that the tissue in the bioreactor remained viable and its complex shape may mean that tissue fixative remains in the system and affects subsequent experiments.

The luminal perimeter of BIOVEH tissue did not change significantly over the course of time, though was decreased compared to FRESH tissue (a range of 55 to 70% of the FRESH luminal perimeter). This indicates that the artery may have undergone some degree of remodelling due to the dynamic conditions in

the bioreactor. Physiologically, narrowing of the lumen can be caused by decreased flow regulated through the endothelium (Brownlee and Langille, 1991). A more physiological dynamic environment, perhaps incorporating a pulsatile flow component may be a welcome addition to this model and would hopefully not induce arterial remodelling through the environment alone. Inwards remodelling is an indicator of active adaptation of the vessel in contrast to passive outwards stretch due to intraluminal pressure.

In the EARLY model, BIOCCE vessels reached the aneurysmal threshold of greater than 150% the luminal perimeter (if the vessel is assumed to be a circle when dilated, the perimeter is the luminal circumference). However, active remodelling of the arteries was observed over time and the luminal perimeter was decreased in the END model compared to the EARLY model. This supports the theory of the peri-luminal deposition of collagen acting as a stabilising component. It is likely that the artery attempted to remodel after the degradation of the elastin attributed to the CCE treatment and so the SMCs secreted collagen and the arterial diameter decreased in order to decrease the wall tension (according to the Law of Laplace, Section 1.7.6). This short-term recovery was also observed in one of the few longitudinal studies in an ApoE knockout mouse model of AAA (Haskett et al., 2013). Microstructural and biomechanical reorganisation which was present at 14 days had recovered by 28 days in that study.

Idealised luminal diameter of BIOVEH and BIOCCE tissue was normalised to the corresponding FRESH tissue within each animal studied. This was done so that the inherent variability in specimens taken from different animals was accounted for. Although the END BIOCCE model did not exhibit a luminal diameter of greater than 150% that of the FRESH vessel, it suggested that the artery was undergoing compensatory remodelling after the initial injury caused by the CCE treatment, whereas the BIOVEH artery remained stable over the course of the experiment. The histological staining showed that this remodelling may have occurred via SMC collagen synthesis and deposition.

In summary, this chapter gave a histological, immunohistochemical and morphological characterisation of arteries either subjected to CCE or VEH pre-

treatment under static and dynamic culture regimes over a period of up to 12 days. Bioreactor culture alone (VEH) did not alter the histoarchitecture of the artery, but did cause a narrowing of the lumen. BIOCCE tissue showed a loss of elastin consistent in both the EARLY and END stage models, whereas there was a decrease in SMC density over time. Peri-luminal deposition of collagen solely observed in BIOCCE tissue may be part of a compensatory stabilisation mechanism, leading the artery to decrease in diameter over time.

The characterisation of cellular and biomechanical aspects of the experimental AAA model was also performed in this study and are found in Chapters 5 and 6 respectively.

CHAPTER 5

STRUCTURE AND FUNCTION OF *EX* VIVO AAA MODEL SMCS

CHAPTER 5 STRUCTURE AND FUNCTION OF *EX VIVO* AAA MODEL SMCS

This chapter describes the structure and function of the SMCs derived from the tissues examined in Chapter 4. The SMCs are derived from tissue which aimed to model AAA disease in an *ex vivo* bioreactor model. Firstly, the cellular and cytoskeletal structure of the SMCs will be examined. The last section will explore the functional capacity of the SMCs in terms of proliferation, migration, senescence and MMP secretion.

5.1. INTRODUCTION

A widely researched property of SMCs is their ability to undergo profound changes in phenotype in order to respond to the changing physiological environment (reviewed in Owens et al. (2004) and given in more detail in Section 1.7.2.1). This change in phenotype brings about changes to the structure and function of the SMCs: contractile, differentiated cells have aligned actin fibres and low turnover and ECM secretion whereas synthetic, de-differentiated cells have a larger, hypertrophic appearance and are able to proliferate, migrate and remodel the ECM more readily (Shi and Chen, 2016).

SMCs in end-stage human AAA disease and a few experimental animal models have been characterised and found to be dysfunctional and attenuated in number compared to SMCs derived from healthy arterial tissue (Lopez-Candales et al., 1997, Ailawadi et al., 2009, Curci, 2009, Riches et al., 2013). SMCs in human AAA disease taken from tissue removed during surgical repair have higher levels of apoptosis (coupled with lower number of SMCs in the tissue), increased replicative senescence, are involved with increased levels of reactive oxygen species (ROS) and have a decreased ECM synthesis rate (Henderson et al., 1999, Liao et al., 2000, Carmo et al., 2002, Miller et al., 2002, Riches et al., 2013). It was shown in a murine elastase model that phenotypic switching of SMCs occurred early on in AAA formation, a study impossible to execute with human tissue (Ailawadi et al., 2009).

Attention has turned to SMCs in the treatment of AAA disease as they are the biological mechanism for stabilising, synthesising and remodelling the ECM (degradation of which is ubiquitous in AAA). The paracrine effect of SMCs has been demonstrated in animal models, where seeding of SMCs was able to stabilise AAA progression (Allaire et al., 2002, Losy et al., 2003). As the SMCs are variously (and potentially uniquely) dysfunctional in end-stage human AAA, they have come to be viewed as a potential target for AAA therapeutic treatment (Riches et al., 2013, Airhart et al., 2014).

The early phenotypic switch of SMCs in AAA, coupled with the dysfunction inherently linked to structure and function has driven one of the main aims of this work, to use an *ex vivo* large animal model to characterise alteration in SMC structure and function with respect to time. By investigating the behaviour of the SMCs in the early disease, early therapeutic targets may be revealed which may have potential to stabilise AAA progression before it has become overtly unstable.

5.2. CHAPTER AIMS AND OBJECTIVES

The aim of this chapter was to characterise the structure and function of the SMCs derived from the bioreactor AAA model and to examine the effects of CCE treatment and dynamic culture in the bioreactor. The SMCs were also characterised at two time-points representing the early- and end-stage of AAA disease, with a view to mapping the phenotypic modulation of the SMCs and gaining insight into the early, pre-dilating AAA.

5.2.1. OBJECTIVES

The specific objectives of this chapter were:

1 To characterise the cellular and cytoskeletal morphology of the SMCs and relate this to the model stage, treatment and culture regime

2 To explore the function of the SMCs in relation to model stage, treatment and culture regime in terms of proliferation, senescence, MMP secretion and migration

5.3. SMOOTH MUSCLE CELL STRUCTURE

SMCs are able to alter their shape depending on phenotype, therefore an analysis of the shape and structure of the SMCs from the various experimental groups was carried out. The morphology of a cell is generally mediated through changes in the cytoskeleton. Alterations in the morphology of a cell would incur a realignment of signalling molecules and thus cause an alteration in cellular function (Worth et al., 2001a). In classical SMC phenotypic characterisation, a synthetic SMC exhibits rhomboid morphology with high proliferation and migration. Conversely, a contractile SMC phenotype exhibits the typical spindle morphology with low rates of proliferation and migration (Section 1.7.2.1) (Shi and Chen, 2016).

5.3.1. SMC CIRCULARITY

The shape of the SMCs was characterised using circularity, a dimensionless geometric descriptor (Helmy and Azim, 2012). The method of determining cellular circularity is detailed in Section 2.8.1. The values lie in between 0 and 1 where 1 is a perfect circle and as the value approaches 0 the shape is an increasingly elongated polygon. The circularity of 50 cells from at least ten microscope fields of view during three sequential cell passages was recorded and the mean circularity recorded, as depicted in Figure 5.1. A sample size of three animals per model stage was used.

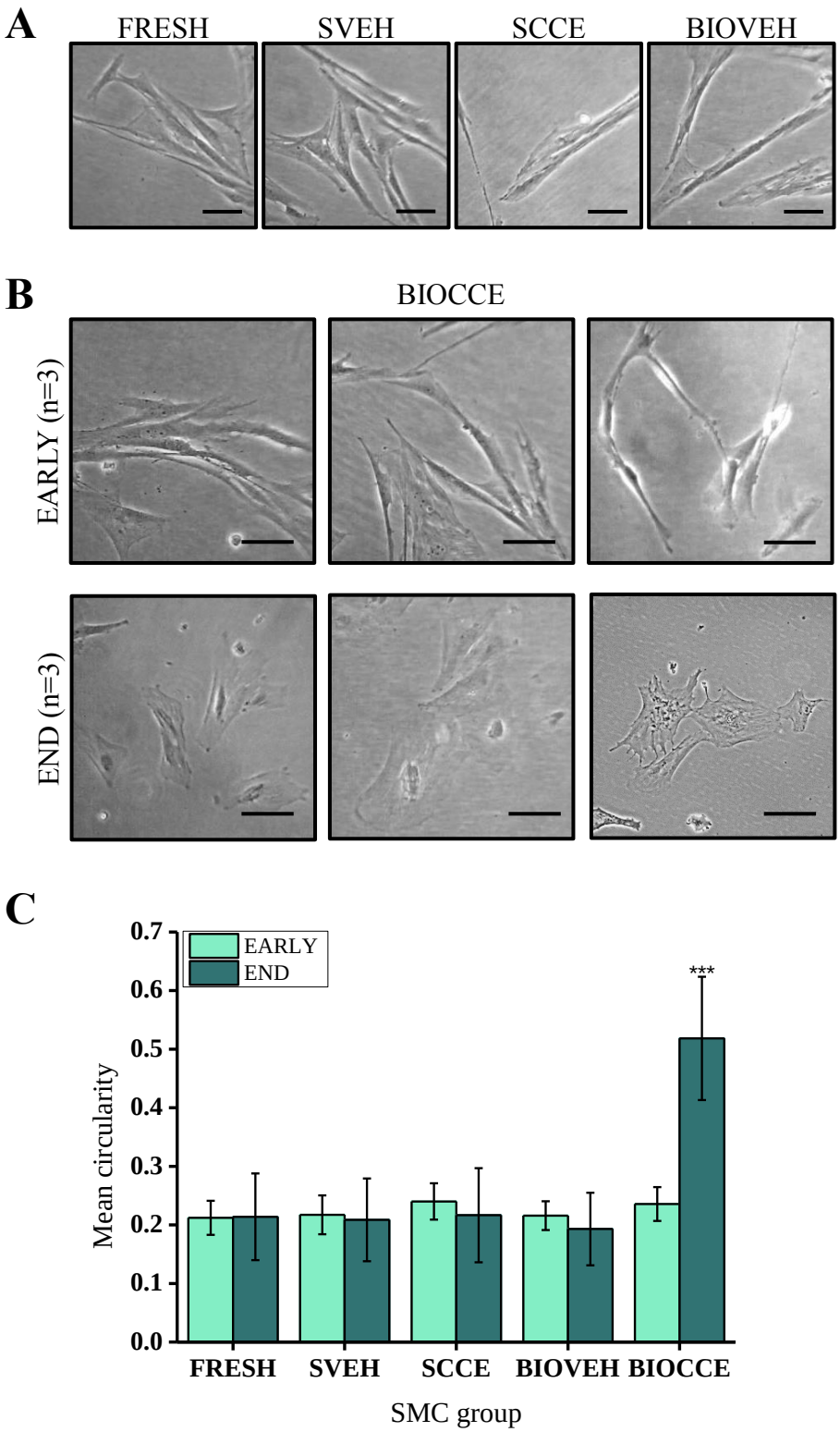

Figure 5.1 SMC morphology. A: Representative images of FRESH, SVEH, SCCE and BIOVEH SMC. B: Representative images of EARLY and END BIOCCE SMC. C: Quantification of SMC circularity, (*p<0.001, two way ANOVA with post-hoc Tukey test). Graph shows mean ± 95% confidence intervals. Scale bar = 100µm, (n=3). Left END BIOCCE image courtesy of Gurprit Mudhar.**

The combination of CCE gel pre-treatment and bioreactor culture for 12 days (END) was required to induce a significant increase in SMC circularity. The change in BIOCCE-SMC phenotype had not yet occurred in the EARLY model. Neither CCE treatment nor bioreactor culture alone induced a change in SMC phenotype in the END model; an increase in circularity only occurred in the END model when CCE treatment and bioreactor culture were used in tandem.

In terms of statistical significance, to test the effect of model stage and treatment group on SMC circularity, measurements were analysed using a 2x5 independent ANOVA. The first factor was model stage (EARLY, END) and the second factor was SMC group (FRESH, SVEH, SCCE, BIOVEH, BIOCCE). The ANOVA showed a significant main effect in model stage, $F(1, 1490)=65.02$, $p<0.001$. Whether the model was EARLY or END stage had a significant impact on SMC circularity. The main effect of SMC group was significant, $F(4, 1490)=132.60$, $p<0.001$. The interaction between model stage and SMC group was also significant, $F(4, 1490)=112.96$, $p<0.001$. In order to explore the nature of the interaction, tests of SMC circularity within each model were performed using a one-way ANOVA. In the EARLY model, there was no significant difference in SMC circularity across all SMC groups ($F(4,745)=2.09$). The effect of SMC circularity within the END model was significant, $F(4, 745)=237.79$, $p<0.001$. A Tukey post-hoc test revealed that BIOCCE SMC had a significantly increased circularity compared to all other SMC groups. The mean circularity for all of the groups is presented in Table 5.1.

Table 5.1 Mean circularity measurements, mean±95% confidence intervals. ***significantly higher circularity in END-BIOCCE SMCs vs. all other groups.

Treatment condition	EARLY	END
FRESH	0.21±0.03	0.21±0.07
SVEH	0.22±0.03	0.21±0.07
SCCE	0.24±0.03	0.23±0.08
BIOVEH	0.22±0.02	0.20±0.07
BIOCCE	0.24±0.03	0.52±0.11***

5.3.2. F-ACTIN CYTOSKELETON

SMCs explanted from END-BIOCCE tissue and the corresponding BIOVEH and FRESH controls were stained with DAPI and rhodamine-phalloidin stain in order to visualise the cell nuclei and actin cytoskeleton using the method given in Section 2.8.2. Representative images are shown in Figure 5.2.

FRESH-SMCs were spindle shaped with aligned actin fibres reaching from pole to pole (Figure 5.2A). BIOVEH-SMCs also exhibited the characteristic spindle SMC shape with aligned actin fibres, much like the FRESH-SMCs (Figure 5.2B and C, arrows). In contrast to this, END-BIOCCE cells exhibited a rhomboid phenotype with a disrupted actin cytoskeleton. Actin fibres were not aligned within the cell and were disordered (Figure 5.2D and E, arrows).

END-BIOCCE SMC had a rhomboid phenotype and a disrupted actin cytoskeleton. This was solely a qualitative assessment from observation of 5 images per treatment condition (FRESH/ BIOVEH/ BIOCCE) per animal (15 images total). Three animals were used per model stage (45 images total).

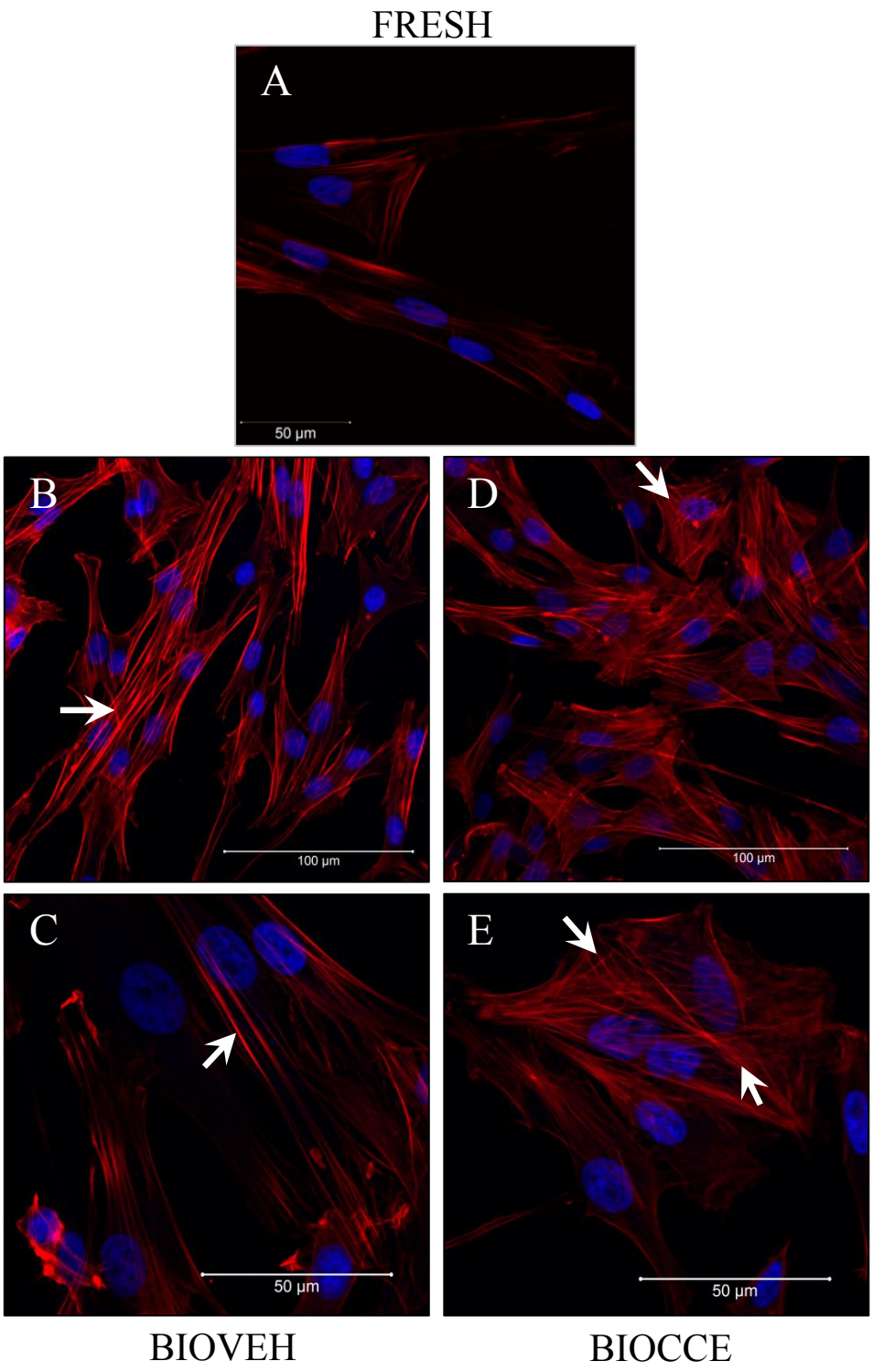

Figure 5.2 Immunofluorescence of cytoskeleton. Representative images showing nuclei (DAPI, blue) and f-actin (rhodamine phalloidin, red) of A) FRESH SMC, B and C) END-BIOVEH SMC, D and E) END-BIOCCE SMC. Arrows show: B and C) aligned actin fibres; D and E) disrupted actin fibres.

5.4. SMOOTH MUSCLE CELL FUNCTION

In humans, SMCs explanted from end-stage AAA tissue exhibit impaired function including increased levels of senescence, impaired proliferation and altered MMP release (Chapter 1). The function of the SMCs from the *ex vivo* AAA model was therefore characterised at two time-points in order to develop a temporal overview of alteration in SMC function with a view to relating this to changes observed in SMC structure (Section 5.3).

5.4.1. PROLIFERATION

The proliferation of the SMCs from each of the treatment groups was also analysed using cell counting. The method is described in full in Section 2.8.3. Each proliferation assay was repeated three times per animal with passage-matched experiments (p3, p4 and p5). The proliferation curves for each model are shown in Figure 5.3 and area under the curve analysis for proliferative capacity is shown in Figure 5.4.

SMC were seeded at a known density, serum-starved to bring them into a quiescent state and then grown in 10% FCS FGM for 7 days. Quadruplicate cell counts were taken at days 0, 2, 4 and 7.

Overall, END-BIOCCE SMCs (possessing rhomboid morphology) exhibited impaired proliferative capacity compared to controls, similar to the characteristics of end-stage human AAA-SMC (Liao et al., 2000, Riches et al., 2013). In contrast, EARLY SMCs subjected to only 3 days in bioreactor culture were observed to be undergoing hyperproliferation. The proliferative capacity of BIOVEH SMCs was indistinguishable from matched FRESH controls.

Statistically, the impact of treatment and culture conditions on SMC proliferation was analysed using a one-way ANOVA per model stage (EARLY, END). In the END model (Figure 5.3A), the results were significant, $F(2, 213)=15.03$, $p<0.001$. A post-hoc Tukey test revealed that there was no significant difference between FRESH and BIOVEH-SMC (1930±209% vs. 2232±98% of cells at day 0 at day 7 respectively, $p=0.35$) but BIOCCE-SMC

proliferation was significantly impaired (1165±56% at day 7) compared to both FRESH ($p<0.001$) and BIOVEH-SMC ($p<0.001$). In the EARLY model (Figure 5.3B), the results were also significant, $F(4, 395)=3.39$, $p<0.01$. A post-hoc Tukey test showed that, again, there was no significant difference in proliferation in BIOVEH-SMC compared to FRESH (1973±57% vs. 1819±48% at day 7, respectively, $p=0.82$) but BIOCCE-SMC was significantly different (2648±71% at day 7) compared to both FRESH ($p<0.05$) and BIOVEH-SMC ($p<0.05$). However, the proliferative capacity of BIOCCE-SMC was increased in the EARLY model, in contrast to an impairment of proliferation observed in the END model compared to both FRESH and BIOVEH SMCs.

The two models were then compared by using area under the curve (AUC) analysis on the proliferation curves seen in Figure 5.3. The AUC analysis is shown in Figure 5.4. There was no difference in the proliferative capacity of FRESH and BIOVEH SMCs between the EARLY and END models: only BIOCCE SMCs showed an alteration in proliferation.

AUC analysis and a two-tailed two-sample t-test of model stage per treatment group showed that there was no significant difference between the EARLY and END models in the FRESH (5799±866 and 6089±1820 for EARLY and END respectively, $p=0.8$) and BIOVEH groups (5609±958 and 7823±3017 for EARLY and END respectively, $p=0.25$). However, there was a significant difference in BIOCCE-SMC proliferation between the EARLY and END models (8252±1034 vs. 3307±760 respectively, $p<0.001$).

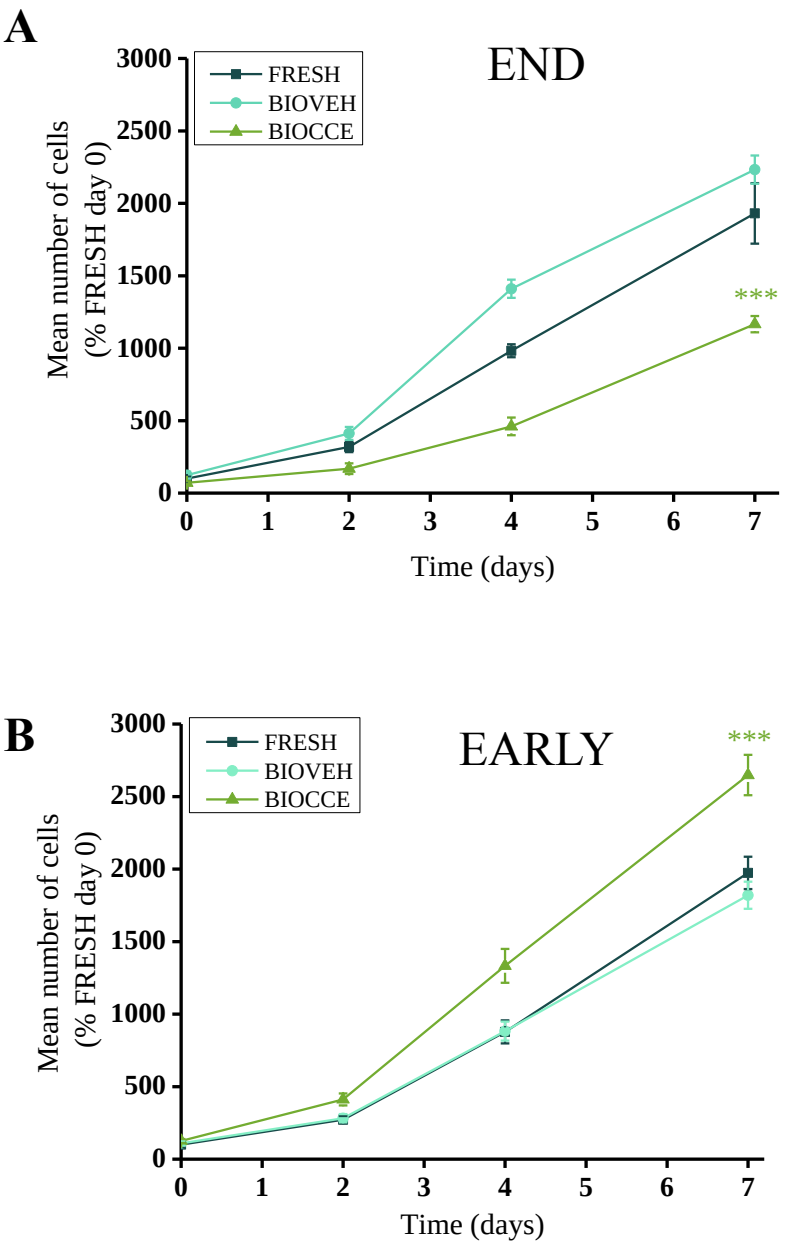

Figure 5.3 Passage-matched mean proliferation curves. A) EARLY model and B) END model. ***p<0.001, *p<0.05. One-way ANOVA with post-hoc Tukey Test. Graph shows mean ± 95% confidence intervals (n=3). END proliferation data for 1 animal courtesy of Gurprit Mudhar.

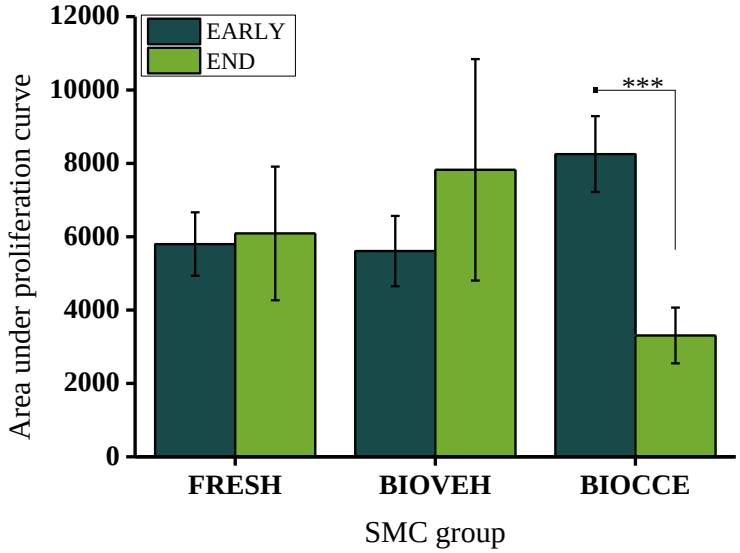

Figure 5.4 Area under curve analysis for proliferation. ***p<0.001, two-sample two-tailed t-test. Graph shows mean ± 95% confidence intervals.

5.4.2. MIGRATION

A scratch wound migration assay was used to determine the migratory capacity of SMCs in the EARLY and END AAA model and the results are presented in Figure 5.5. The method used for assessment of cellular migration is given in Section 2.8.4. The assay was repeated three times per animal with passage-matched cells. The cell counts for BIOVEH and BIOCCE-SMC on each plate were normalised to the FRESH control in order to mitigate effects of inter-animal and passage-related variance during each assay and so the FRESH data was omitted from the graphs.

The spread of the migration data was extremely large and so few conclusions can be made about the effect of model stage, treatment and culture regime on SMC migration (Figure 5.5).

SMC migratory capacity amongst the groups was analysed using a 2x2 two-way ratio ANOVA on data which had been log transformed for normalisation. The first factor was model stage (EARLY, END) and the second factor was treatment group (BIOVEH, BIOCCE). The ANOVA showed no main effect of model stage, $F(1, 26)=0.005$, $p=0.945$. The migratory capacity of SMCs did not

change with respect to the model stage. The main effect of treatment group was also not significant, $F(1, 26)=0.08$, $p=0.78$. Treatment group also did not affect the migratory capacity of SMCs. The interaction between model stage and treatment group was not significant, $F(1, 26)=0.64$, $p=0.43$. The mean number of cells migrated past 200μm per mm of wound width (expressed as a percentage of FRESH-SMC) for BIOVEH-SMC was 159±168% and 157±168% for EARLY and END models respectively (mean±95% confidence intervals). For BIOCCE-SMC the means were 231±247% and 68±38% for EARLY and END models respectively (Figure 5.5).

5.4.2.1. Effect of SMC orientation

As can be seen in the graph in Figure 5.5, the confidence intervals were extremely large, indicating that the values lay within a large data range. It was noticed that the orientation of SMC in relation to the scratch wound may have affected the migration data. As can be seen in the representative images in Figure 5.5, when the SMC aligned in an orientation which was perpendicular to the scratch wound (Panel A) the count of cells that migrated past the 200μm marker was larger than when the cells laid in an orientation which was parallel to the scratch wound (Panel B).

The hypothesis that SMC orientation affected the outcome of the scratch wound migration assay was tested by identifying the scratch wound images within the same treatment group (FRESH, BIOVEH, BIOCCE) on the same plate for each animal which had the greatest disparity in the count of cells migrated past 200μm per mm of wound width (Highest, Lowest, n=15). The angle deviation from normal to the scratch wound (0°) for each of the images in the Highest and Lowest groups was determined using ImageJ (http://imagej.nih.gov/ij/). The results for this are presented in Figure 5.6.

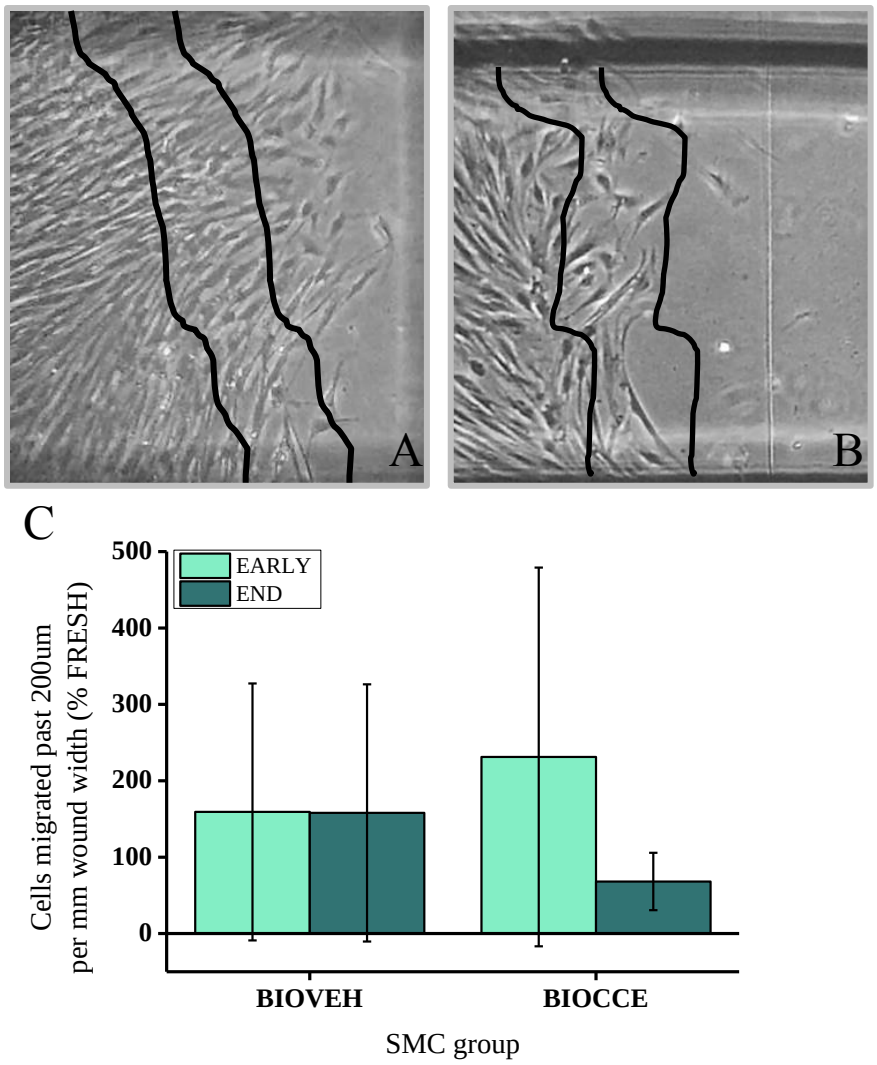

Figure 5.5 Scratch wound migration analysis. Representative images of A) EARLY-BIOCCE SMC and B) END-BIOCCE SMC showing 200µm marker (black lines at 0µm and 200µm). C) Quantification of migrated cells. Graph shows mean migration counts at 24 hours normalised to FRESH-SMC ± 95% confidence intervals (n=3). Two-way ratio ANOVA with post-hoc Tukey test.

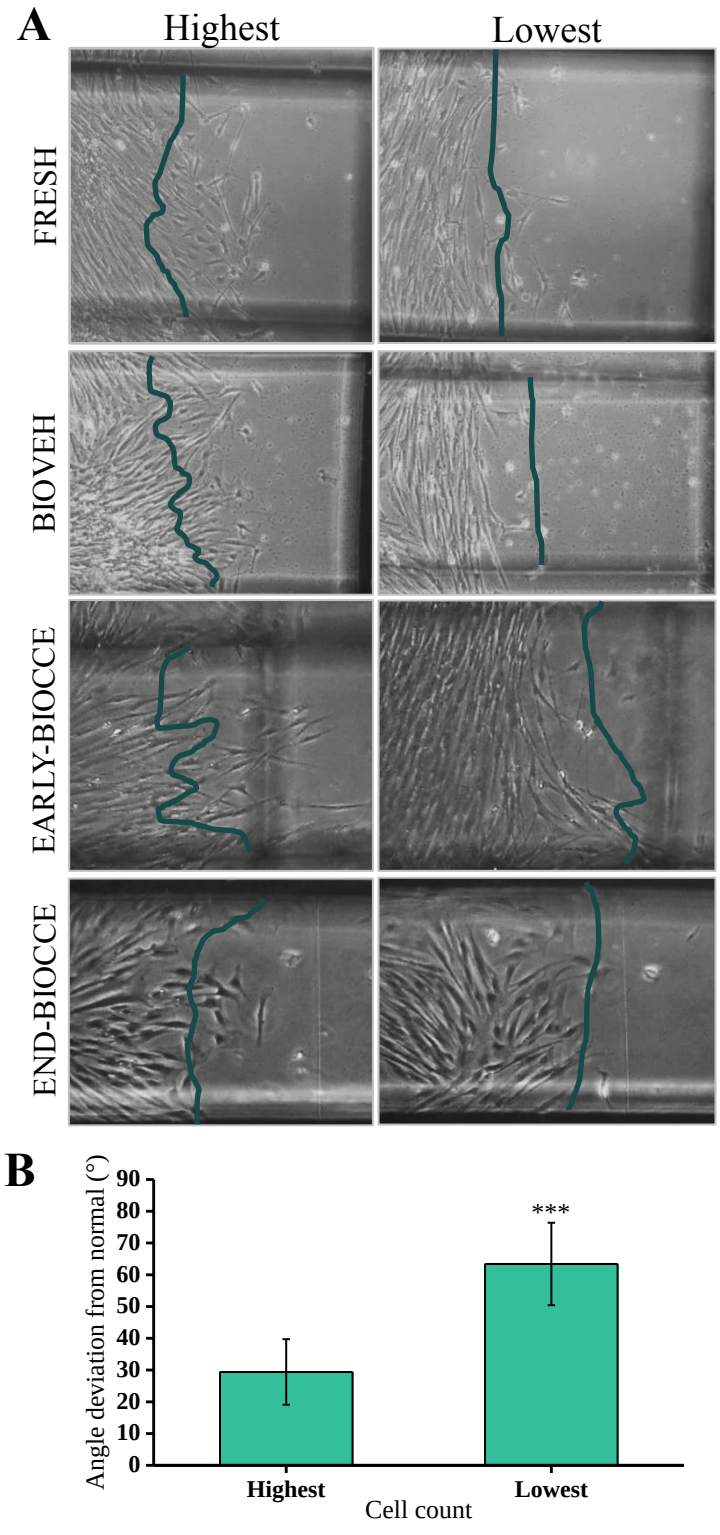

Figure 5.6 Effect of SMC orientation on migration. A) Representative images of greatest cell count disparity within assay with 200µm traceline included. B) Significant increase in angle deviation from normal to scratch wound in the lowest cell counts vs. highest, ***p<0.001, two sample t-test. Graph shows mean ± 95% confidence intervals (n=15).

A one-tailed two sample t-test revealed that the mean angle deviation from normal to the scratch wound, taken as 0°, was greater in the lowest migration cell count compared to that of the highest (63±13° vs. 29±10° respectively, $p<0.001$). There was a mean 53% decrease in deviation angle from the lowest cell count to the highest cell count. This effect of SMC orientation on count of cells migrated past 200μm per mm wound width was found across all treatment groups.

Despite the large spread of data seen in both BIOVEH-SMC groups and the EARLY BIOCCE-SMC groups (Figure 5.5), thought to be attributed to SMC orientation, the BIOCCE-SMC group had a consistently low count of cells migrated past 200μm per mm wound width. A two-sample one-tailed t-test showed that there was a possible trend for the mean migration cell count of END-BIOCCE SMC to be generally lower compared to FRESH SMC (28.4±14.6 vs. 12.7±5.9 cells migrated past 200μm per mm wound width respectively, $p=0.08$). The results for this are shown in Figure 5.7.

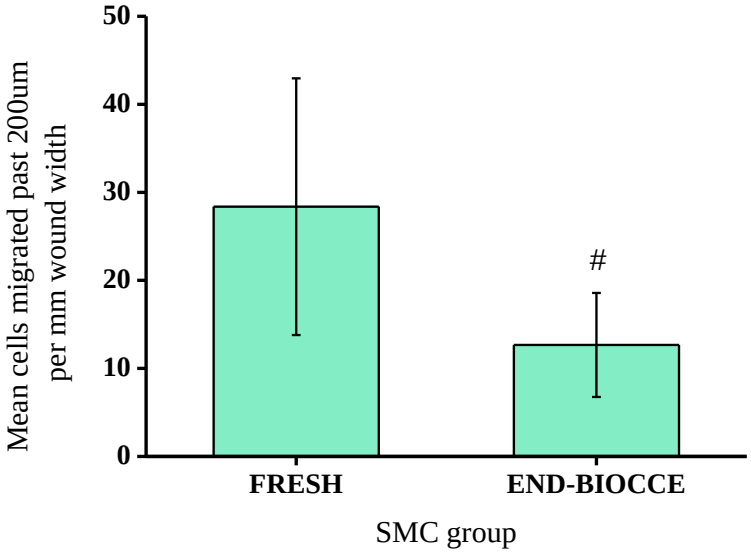

Figure 5.7 Mean scratch wound migration cell counts for FRESH and END-BIOCCE SMC. Graph shows mean ± 95% confidence intervals. Two-sample t-test, #p=0.08, non-significant trend (n=3 animals).

5.4.3. SENESCENCE

Cell senescence was determined via β-galactosidase staining at pH 6, a marker of cell senescence not found in pre-senescent, quiescent or immortal cells. Senescence staining was performed using the method given in Section 2.8.5. The assay was repeated three times per animal with passage-matched results. Ten microscopic fields of view were taken at 40x magnification and the senescence index was represented by calculating the mean percentage of β-galactosidase stained positive cells within each microscopic image. Representative images and the graphed results are shown in Figure 5.8.

Given the nature of the experiment, it was unsurprising that there was some level of increase in senescence in the control model. In the EARLY model, BIOCCE SMC senescence was 25.1% greater than in BIOVEH SMC, rising to 50.9% greater in the END model. There was a significant increase in levels of senescence due to the application of CCE gel compared to vehicle control; the disparity in senescence levels between BIOVEH-SMC and BIOCCE-SMC doubled in the period between the EARLY and END model.

In order to statistically test the effect of model stage (EARLY, END) and SMC group (FRESH, BIOVEH, BIOCCE) on SMC senescence, a 2x3 independent ANOVA was used. The results are displayed in Figure 5.8.

. The ANOVA revealed that there was no effect of model stage, $F(1, 352)=0.00464$, $p=0.95$, but there was a significant effect of SMC group, $F(2, 352)=42.8$, $p<0.001$. The interaction between model stage and SMC group was significant, $F(2, 352)=12.0$, $p<0.001$. To explore the nature of the interaction, additional tests (one-way ANOVA per model stage) were performed. The effect of SMC group within the EARLY model was significant, $F(2, 266)=9.5$, $p<0.001$. A post-hoc Tukey test showed that levels of senescence between FRESH and BIOVEH SMC were indistinguishable ($p=0.4$), whilst there was a statistically significant increase in senescence in BIOCCE compared to BIOVEH (140±26% vs. 112±20% respectively, $p<0.01$). SMC group exerted a significant effect within the END model, $F(2, 86)=33.5$, $p<0.001$. A post-hoc Tukey test showed that there was an increase in senescence between both

BIOVEH compared to FRESH (218±35% vs. 100±16% respectively, p<0.001) and BIOCCE compared to BIOVEH (330±42% vs. 218±35% respectively, p<0.01).

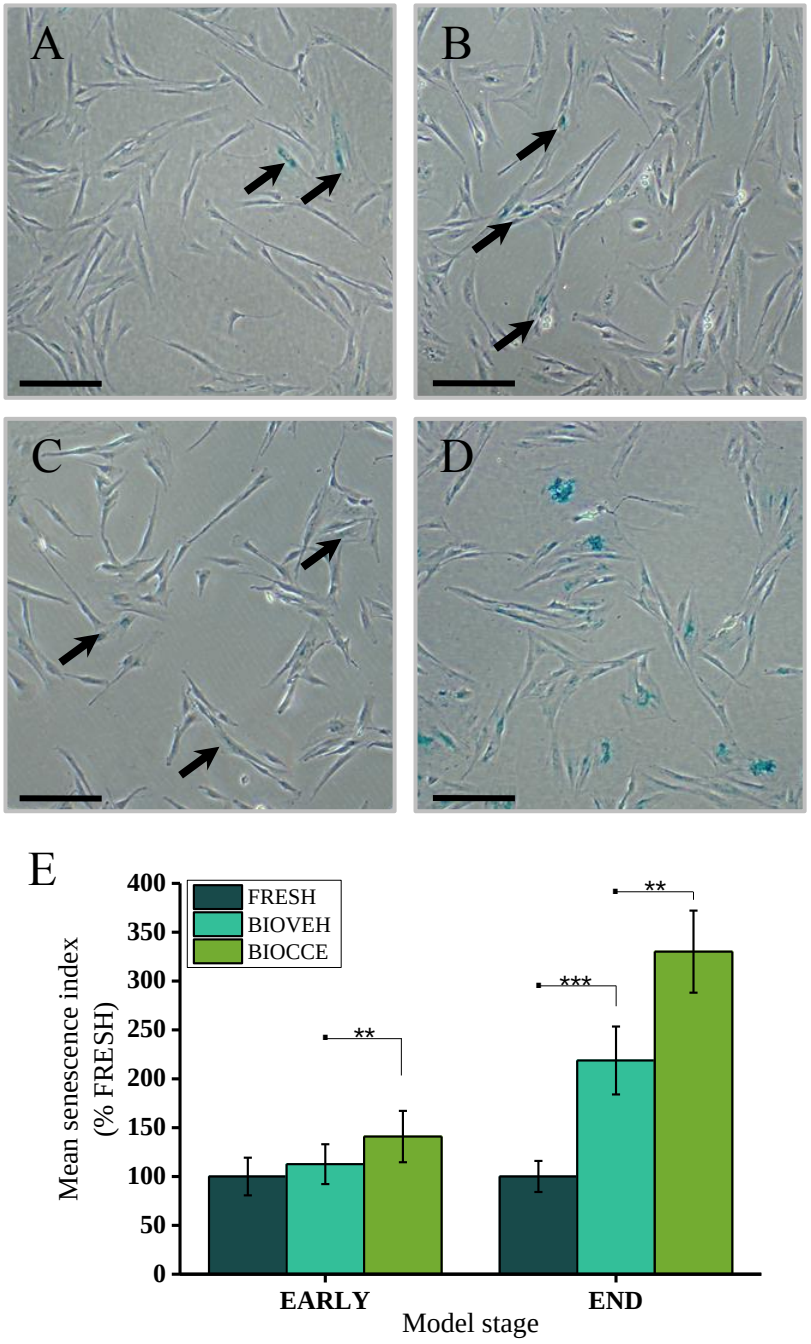

Figure 5.8 Senescence analysis with β-galactosidase staining. Representative images of A) FRESH, B) BIOVEH, C) EARLY-BIOCCE and D) END-BIOCCE SMC. Arrows indicate subtle blue stain. Scale bar = 200µm. E) Quantification of β-galactosidase positive cells. One-way ANOVA per model stage, **p<0.01, ***p<0.001. Graph shows mean ± 95% confidence intervals (n=3).

5.4.4. SECRETION OF MMP-2 AND MMP-9

AAA is a pathological remodelling disease and so indications of alterations in remodelling capability in the *ex vivo* model were analysed (Galis and Khatri, 2002). Secretion of MMP-2 and MMP-9 (gelatinases) is an indication of SMC protease remodelling activity and they are secreted at higher levels in human AAA tissue compared to healthy tissue (Goodall et al., 2002b, Wilson et al., 2008). Levels of MMP-2 and MMP-9 were measured using gelatin zymography of conditioned media obtained from non-stimulated and stimulated SMC from three treatment groups (FRESH, BIOVEH, BIOCCE) at two model stages (EARLY, END). Samples were incorporated within a gelatin substrate and were subjected to sodium dodecyl sulphate-polyacrylamide gel electrophoresis (SDS-PAGE). They were then analysed using densitometry of clear bands of lysis against blue stained gelatin background. Full detail of the method is given in Section 2.8.6.

5.4.4.1. SAMPLE LOADING VOLUME CALIBRATION

A calibration was performed to determine the sample loading volume; optimally this would be the greatest volume before saturation of the substrate occurs and with any increase in sample loading volume there is no such increase in relative densitometry of the bands of gelatin digestion (Figure 5.9). Samples in volumes from 5µl to 30µl from two experimental groups (FRESH-SMC from an animal in the EARLY group and FRESH-SMC from an animal in the END group) were loaded onto a zymogram. It can be seen in Figure 5.9 that the point of saturation starts at 20µl of sample volume and so this was chosen as the sample loading volume for all further experiments.

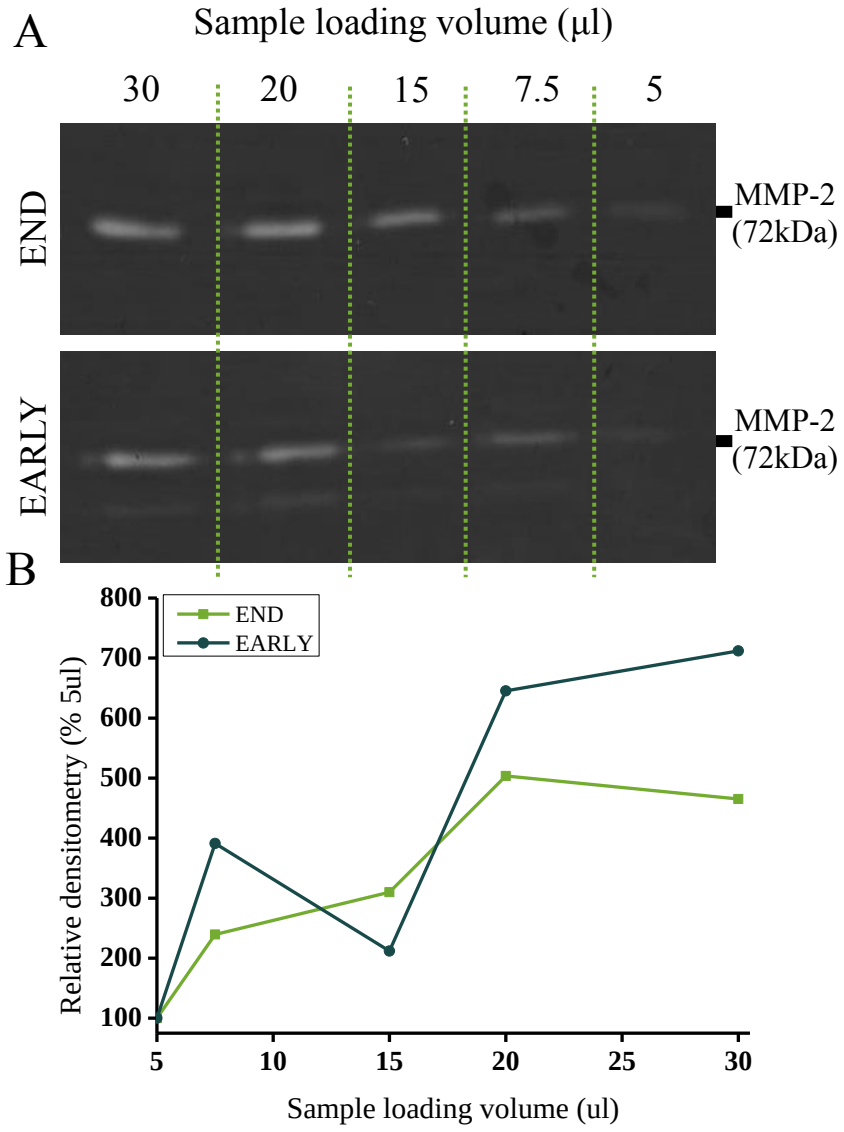

Figure 5.9 Sample loading volume calibration. A) Volumes of sample (5-30µl) were loaded onto zymograms which were incubated for 26 hours. B) Densitometry of the clear bands was plotted and from this 20µl was considered optimal.

5.4.4.1. RELATIVE MMP-2 AND MMP-9 LEVELS

Out of six arteries tested (n=3 for EARLY and END), only one END artery secreted any detectable levels of MMP-9. Secretion of MMP-9 was below the

limits of detection in all other arteries, where MMP-2 only was released by the SMCs. Representative images of zymograms are shown in Figure 5.10. The relative densitometry measurements normalised to a FRESH SMC control treated with PBS for each animal are shown in Figure 5.11.

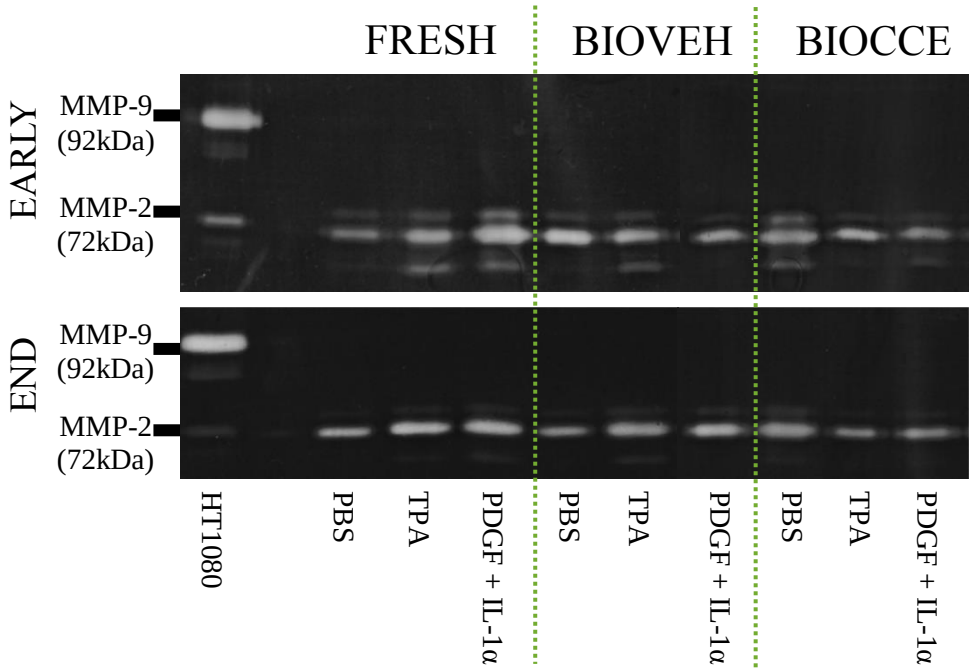

Figure 5.10 Representative zymogram images. Top: EARLY model. Bottom: END model. Relative densitometry to FRESH SMC treated with no stimulus (PBS) was taken.

Total MMP secretion tended to be lower in the END model compared to the EARLY model, although this was not statistically significant. MMP secretion in FRESH and BIOVEH SMCs was indistinguishable, whereas BIOCCE SMCs secreted lower levels of MMPs. Both TPA and PDGF+IL-1α (detailed in Section 2.8.6) stimulated MMP secretion to a similar degree.

In terms of statistics, to investigate the influence of model stage (END, EARLY), SMC group (FRESH, BIOVEH, BIOCCE) and stimulation (PBS, TPA, PDGF+IL-1α) on relative total MMP levels, a 2x3x3 three-way ANOVA on logarithmic transformed values was used. The ANOVA showed that there

was not a significant effect of model stage, $F(1, 36) = 3.76$, $p=0.06$. However, a p-value of 0.06 indicates a possible trend towards a decrease in MMP levels in the END model compared to the EARLY model. The effect of SMC group on relative MMP levels was significant, $F(2, 36) = 8.40$, $p<0.001$. A Tukey post-hoc test showed that there was no difference in relative MMP levels between FRESH and BIOVEH SMCs ($p=0.907$). There was a decrease in relative MMP levels in BIOCCE SMCs compared to both FRESH ($p<0.01$) and BIOVEH SMCs ($p<0.01$). The effect of the type of stimulant applied to the SMCs on the relative MMP levels was also significant, $F(2, 36) = 8.89$, $p<0.001$. The Tukey test showed that there was an increase in relative MMP levels between PBS control and TPA ($p<0.001$). There was also an increase in relative MMP levels in PDGF+IL-1α treated SMCs compared to SMCs treated with PBS ($p<0.01$). The degree of stimulation from TPA and PDGF+IL-1α was not different; there was no difference between relative MMP levels in stimulated groups ($p=0.923$). The interaction between model stage, SMC group and stimulation was found to be not statistically significant, $F(4, 36) = 0.22$, $p=0.928$.

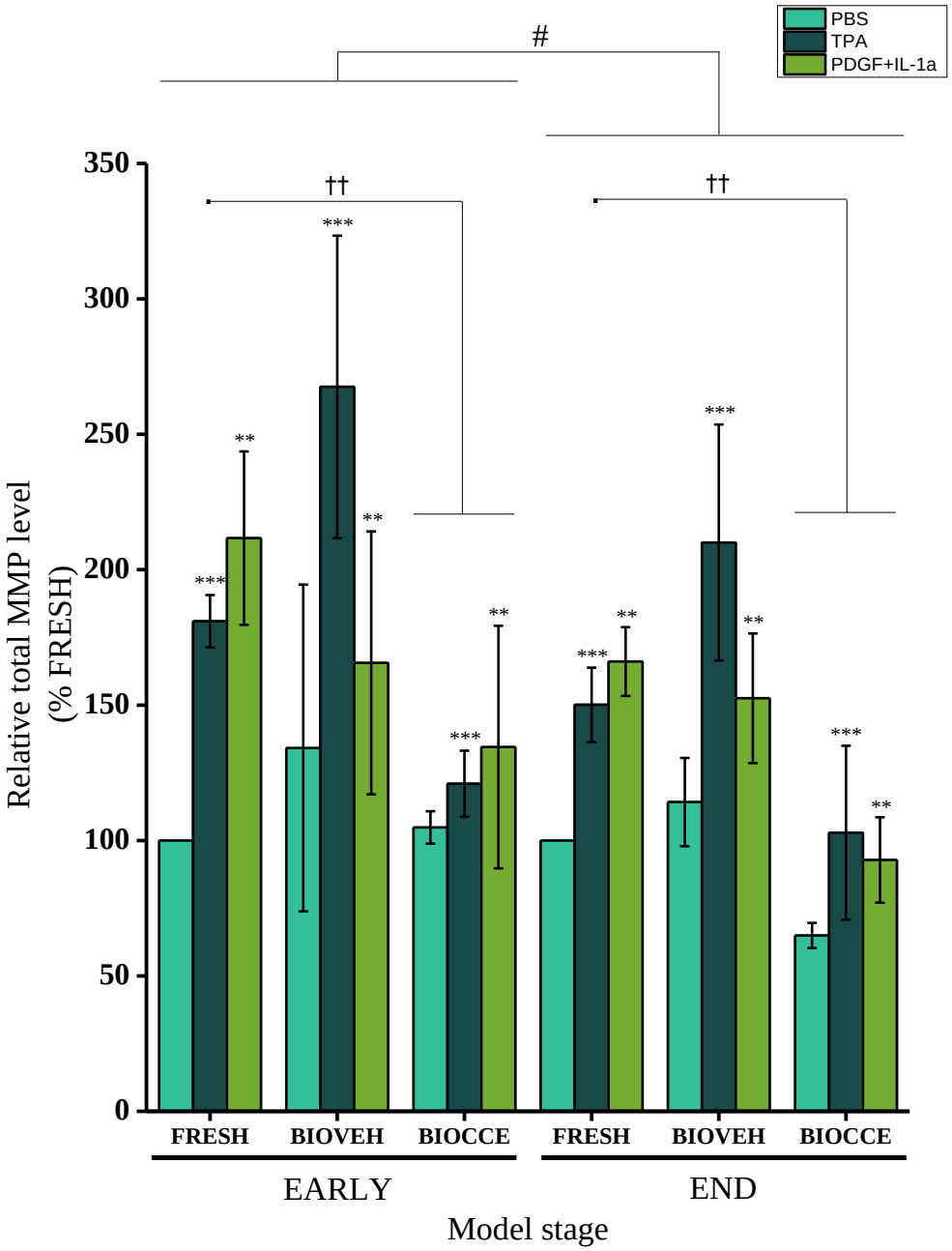

Figure 5.11 Quantification of relative MMP levels each normalised to FRESH SMC control treated with PBS. Three-way ANOVA with post-hoc Tukey test; ††p<0.01 FRESH vs. BIOCCE, ***p<0.001 TPA vs. PBS, **p<0.01 PDGF+IL-1 vs. PBS, #p=0.06 EARLY vs. END. Graph shows mean ± 95% confidence intervals (n=3).

5.5. DISCUSSION

SMCs are not terminally differentiated and are able to switch their phenotype, most commonly from a spindle-shape contractile phenotype to a rhomboid secretory phenotype (Owens et al., 2004, Porter and Riches, 2013). It has been shown that human AAA cells have a rhomboid shape with significantly increased cell area compared to human saphenous vein SMC (Riches et al., 2013). It was also shown in the aforementioned study that by treating a porcine carotid artery with CCE treatment and then culturing this in the bioreactor for 12 days, the explanted SMCs exhibit a similar increase in cell area to that observed in human AAA SMCs.

In this study, the cell circularity was measured from two time-points in the model (EARLY and END) and within that five different treatment groups depending on the type of pre-treatment and culture conditions (FRESH, SVEH, SCCE, BIOVEH, BIOCCE). When the artery was treated with VEH pre-treatment, no significant increase in cell circularity was observed in either the EARLY or END models, whether it was cultured statically (SVEH) or in the bioreactor (BIOVEH). Arteries treated with the CCE pre-treatment and cultured statically in a 6-well plate (SCCE) also did not exhibit any significant alterations in SMC circularity at either EARLY or END stage. It was shown that, mirroring the results seen in the previous study in 2013, BIOCCE-SMC showed a significantly increased cell circularity (over 2-fold) compared to FRESH and BIOVEH-SMC, but solely in the END model (Riches et al., 2013). In the EARLY model, BIOCCE-SMC showed no change in cell morphology compared to the other groups. END-BIOCCE SMC not only showed a significant alteration in SMC morphology, but also generally exhibited a disrupted actin cytoskeleton whereas FRESH and BIOVEH-SMC had apparently normal, aligned actin fibres (Figure 5.2). Disorganisation of the cytoskeleton may lead to realignment of signalling molecules (Worth et al., 2001a). This may then alter SMC function in which is associated with phenotypic modulation.

There are two main conclusions that can be made from these findings. Firstly, the change in SMC phenotype is only induced when the artery they are

explanted from is subject to both CCE pre-treatment and dynamic flow culture. The combination of these factors must be present in order to induce phenotypic switching. Secondly, the phenotypic switch observed in BIOCCE-SMC after 12 days culture in the bioreactor had not occurred after 3 days.

Human AAA-SMC have been observed to exhibit a hypertrophic, rhomboid appearance compared to SMCs from non-aneurysmal aorta (Liao et al., 2000, Riches et al., 2013). AAA tissue for those studies was harvested during elective or emergency repair; once the aneurysm had progressed to a state of real risk of rupture or actual rupture. The nature of the disease inhibits the study of human AAA-SMC in the early stages of the disease prior to clinical presentation and dilatation hence the essential use of disease models for AAA. It has been demonstrated in a mouse model that a phenotypic switch in SMC occurs early on in the development of AAA (Ailawadi et al., 2009). The data presented in this chapter supports the concept of a phenotypic switch in early AAA disease, prior to vessel dilatation. In the END model, SMCs exhibited a rhomboid appearance with increased circularity whereas SMCs in the EARLY model were indistinguishable from FRESH SMCs with a spindle appearance. It is well known that SMCs are able to reversibly differentiate as a reaction to the extracellular environmental cues and that this process plays a role in various cardiovascular diseases (Owens et al., 2004). The *ex vivo* model supports a change in SMC phenotype over the course of the experiments (from the EARLY to the END model) as demonstrated by the changes in circularity and the disordered f-actin cytoskeleton.

A change in SMC function in relation to this change in structure with respect to time was also observed. In the END model, the SMCs had adopted a rhomboid appearance and showed consistently impaired proliferation throughout three sequential passages (50% decrease vs. FRESH). Unexpectedly, as no change in circularity had occurred at that point, the EARLY model SMCs had a consistently higher proliferation rate compared to both matched FRESH (40% increase) and BIOVEH controls and END model BIOCCE SMCs. Contrary to the typically characterised SMC phenotypes described in Chapter 1, EARLY

SMCs exhibited spindle morphology at the same time as having increased proliferative capacity.

The reversible differentiation of SMCs in response to environmental cues is typically characterised as switching between a spindle-shaped cell with low proliferation and reduced ECM turnover and a large, hypertrophic rhomboid shaped cell with increased proliferatory and migratory capabilities (Shi and Chen, 2016). In this *ex vivo* bioreactor model of AAA, a change in phenotype was observed between the EARLY and END models though not in the same way as classical SMC differentiation. In the END model, SMCs were rhomboid with increased circularity yet had significantly impaired proliferation compared to the spindle-shaped matched controls. This mirrors the findings of Riches *et al.* and Liao *et al.* who found that human AAA-SMCs taken from end-stage AAA tissue (i.e. during repair) were larger, rounder and had significantly impaired proliferation compared to non-AAA SMC (Liao et al., 2000, Riches et al., 2013). However, studies on proliferation of AAA-SMCs have been inconsistent and others have observed that AAA-SMCs exhibit enhanced proliferation (Patel et al., 1996, Gacchina et al., 2011).

The findings presented in this chapter using an *ex vivo* bioreactor model of AAA may be able to contribute towards a narrative: it has shown that SMC proliferation may indeed be both impaired and enhanced during AAA progression depending on time. The role of SMC proliferation in AAA progression has been linked with the so far unexplained protective effect that diabetes mellitus has on AAA. Increased levels of advanced glycation end products (AGEs) in patients that are characteristic of diabetes have been shown to increase SMC proliferation, hence enabling increased matrix synthesis and therefore possibly AAA stability (Sakata et al., 2000, Pafili et al., 2015). Intriguingly, the SMCs found in patients with diabetes mellitus also exhibit a rhomboid, anti-proliferatory phenotype *in vitro* (Riches et al., 2014). This study demonstrated that this switch in phenotype was able to be controlled by two microRNAs; transfection of premiR143/145 into non-diabetic SMCs induced the pathological phenotype, whereas transfection of antimiR143/145 into diabetic SMCs restored the normal phenotype. The role of microRNAs,

including miR143 and miR145 amongst many others, in AAA development has inspired a wealth of studies within recent years and as such SMC microRNAs are seen as a therapeutic target for AAA (reviewed in (Boon and Dimmeler, 2011, Albinsson and Sward, 2013)).

In this study, it was difficult to make conclusions of the migratory capacity of the *ex vivo* AAA model due to the large degree of error in the experiments thought to be attributed to orientation of the SMCs with respect to the wound. As a note, it is maybe preferable that the migratory capacity of porcine SMCs derived from the *ex vivo* model be analysed using a Boyden chamber technique in order to eliminate this complication; as the cells start in a suspension and migrate downwards through the membrane, the initial conditions of the cells are equal. However, there was a trend in the END model towards impaired migration in BIOCCE-SMCs compared to FRESH SMCs which is contrary to the mechanism of perceived normal SMC differentiation (Owens et al., 2004, Shi and Chen, 2016).

This chapter also shows that BIOCCE-SMCs had a sharp rise in senescence levels between the EARLY and END models, more so than BIOVEH controls. This mirrors the human disease: it has been shown that AAA-SMC are typically more senescent than SMCs derived from non-aneurysmal aorta (Liao et al., 2000, Riches et al., 2013). These aforementioned studies directly measured markers of senescence in AAA-SMC but it was shown by Cafueri *et al.* that SMCs derived from aneurysmal tissue showed clear signs of telomere attrition (Cafueri et al., 2012). Telomeres are structures which are located at the ends of chromosomes and are inextricably linked with the mechanisms of proliferation and senescence. Each replicative cell cycle (i.e. during proliferation) results in a shortening of the length of the telomere until it reaches a critical length, in which case the cell becomes senescent (Calado and Young, 2009). Increased telomere shortening in AAA tissue may very well be an indicator of a period of hyper-proliferation when the tissue remained within the patient, prior to extraction for the study. The data presented in this chapter supports this, as the SMCs underwent a period of hyper-proliferation in the EARLY model, before

reverting to rhomboid senescent SMCs with impaired proliferation in the END model.

MMPs (and their inhibitors) are heavily implicated in the progression of AAAs. These proteases are secreted as part of the normal tissue remodelling process, but in the case of AAA matrix degradation and synthesis is unbalanced (reviewed in Keeling et al. (2005) and Galis and Khatri (2002)). In this study, levels of MMP-2 and MMP-9 were examined specifically. Out of the six samples analysed, only SMCs from one animal secreted any detectable levels of MMP-9. All samples secreted higher levels of MMP-2, including proMMP-2 and intermediate MMP-2. BIOCCE-SMCs typically secreted lower levels of MMPs compared to the matched controls, and secretions of MMPs tended to be higher in the EARLY model compared to the END model. It was demonstrated that END SMCs have an aberrant phenotype, with impaired proliferation and markedly increased levels of senescence. Therefore, it was not unexpected that they secreted lower levels of MMPs.

Due to the increased proliferation in the EARLY BIOCCE SMCs it was expected that a similar increase in MMP secretion would have been observed. However, there were similar basal MMP levels compared to the matched EARLY FRESH and BIOVEH control SMCs. An explanation for this may be that SMCs at the same density were left to adhere for less than 24 hours before being transferred to serum free media to induce the SMCs into a quiescent state. When in such a state, cells will arrest in the G_0 phase of the cell cycle where they are neither dividing nor preparing to divide. Any contribution of proliferation to MMP levels should therefore be minimised as a typical cell cycle length for porcine SMCs is 32 hours (Breton et al., 1986). In addition, stimuli treatments were carried out in minimal growth media (containing only 0.4% FCS) and so the SMCs will be minimally proliferating. Therefore, it is assumed that MMP levels would have been investigated on a very similar SMC density across all groups. It is conceivable that further investigation would reveal increased MMP secretion in the EARLY model tissue due to the increased SMC number as a result of the observed hyperproliferation.

MMP-2 and MMP-9 are found in abundance in human AAA tissue, to the extent that attempts have been made to assess their suitability as an AAA biomarker (Longo et al., 2002, Eugster et al., 2005, Wilson et al., 2008). MMP-2 is typically found to be associated with smaller aneurysms, earlier on in their progression, whereas MMP-9 becomes dominant once the aortic diameter had increased (Freestone et al., 1995). MMP-2 expression was increased in SMCs derived from end-stage human AAA tissue cultured *in vitro* (Crowther et al., 2000). AAAs are characterised by considerable overexpression of various MMPs. The levels of overexpression in the model may be considered modest in comparison however an intra-luminal thrombus (ILT) is not present in the model. ILT is commonly found in human AAAs and is a rich source of MMPs and pro-inflammatory cytokines (Fontaine et al., 2002). The lack of an ILT in this model may therefore be considered a limitation of the model as it plays a major role in exacerbation of the pathological remodelling associated with AAA. In animal models, ILT are typically only present in angiotensin II infusion in ApoE knockout mice and the elastase perfusion method in rats only (Wilson et al., 2013).

In contrast to human AAA tissue, the END model SMCs secreted reduced levels of MMPs compared to matched controls. This may be explained by the fact that the nature of the model requires arterial cells alone (adventitial fibroblasts, SMCs and endothelial cells) are isolated from the animal for culture in the bioreactor and so removes the effect of the rest of the entity, most notably the immune system. MMPs are secreted not just by SMCs, but also by macrophages, B lymphocytes, mesenchymal stromal cells and the intraluminal thrombus (Fontaine et al., 2002, Tsuruda et al., 2008, Ciavarella et al., 2015, Zhang and Wang, 2015). The origin of MMP-2 in AAAs is SMCs and fibroblasts whereas MMP-9 is highly expressed by macrophages, which were not present in the *ex vivo* model (Ailawadi et al., 2003). The removal of these compounding factors may explain why increased MMP production is not observed in the EARLY and END model SMCs.

Although their rhomboid morphology is similar, contrary to de-differentiated rhomboid secretory SMCs, AAA-SMCs have impaired proliferation and

migration and possess increased levels of senescence which are sustained through *in vitro* culture passages. This persistent phenotype may point to the role of epigenetic mechanisms and microRNAs in SMC phenotypic modulation in AAA disease (Boon and Dimmeler, 2011, Davis et al., 2015). It was shown in both previous and current studies in our laboratory that the *ex vivo* END model is able to mimic these criteria in END-BIOCCE SMCs (Riches et al., 2013). Conversely, the data presented in this chapter have shown that differentiated SMCs with spindle morphology exhibit increased proliferation which contradicts the classical characterisation of SMC phenotype (Shi and Chen, 2016). Hyperproliferation in SMCs has been documented as a cellular response to arterial insult (Owens et al., 2004). It is hypothesised that as the SMCs hyperproliferate, they become senescent more quickly as the proliferation-associated telomeres are shortened more rapidly resulting in a dysfunctional, aberrant and senescent SMC phenotype in the later stages of the disease, as described in the END model. Indeed, as mentioned previously, shortened telomeres appear to be a feature of human AAA-SMCs (Cafueri et al., 2012). The SMCs are unable to proliferate sufficiently to balance their descent into senescence and apoptosis, resulting in the observed loss of SMCs in AAA tissue (Lopez-Candales et al., 1997). Due to the nature of AAA disease, any validation of the EARLY model with human tissue, prior to clinical presentation, is virtually impossible.

Considering the results presented in this chapter, it would be inappropriate to include EARLY and END BIOCCE SMCs as part of the classical SMC phenotype. As discussed in Chapter 1, SMCs are typically characterised as having two distinct phenotypes: a spindle shape contractile phenotype with low proliferative and migratory capacity or a hypertrophic rhomboid shape synthetic phenotype which is highly proliferative and migratory (Rzucidlo et al., 2007, Shi and Chen, 2016). The data indicated that BIOCCE SMCs exhibited a distinct phenotype incorporating both classical differentiated and de-differentiated characteristics. BIOCCE SMCs also entered a state of early senescence compared to the experimental control groups and exhibited high numbers of senescence-associated β-galactosidase positive cells. In the last two decades, a specific senescent cell phenotype has been identified in humans and

this was recently characterised in human SMCs and implicated in vascular calcification (Coppé et al., 2008, Burton et al., 2010, Liu et al., 2013). This senescence associated secretory phenotype (SASP) leads SMCs to display a commonly altered secretome similar to a wound healing response, including increased levels of TGFβ1, IL-1, IL-6 and IL-8 (Adams, 2009). This state of cellular senescence is a protective mechanism triggered by DNA damage in two distinct pathways. Telomeres are structures which prevent the ends of the chromosome being recognised as a double strand DNA break. Telomeres become shorter when cells divide, as mentioned previously, and when they reach a critical length they are no longer able to protect against the DNA damage response and senescence is triggered. This first mechanism is replicative senescence (Burton and Krizhanovsky, 2014). The second mechanism is mediated via factors independent of telomere length which involve DNA damage, such as ROS or various oncogenes (Nelson et al., 2014). Further investigation in our laboratory has revealed that both END BIOCCE SMCs and human AAA SMCs have higher numbers of aberrant nuclei and increased levels of γ-H2AX, both indicators of DNA damage (unpublished). This is compelling evidence showing that the documented structure and dysfunction of human AAA SMCs and END BIOCCE SMCs are possibly part of accelerated senescence due to DNA damage and so have adopted SASP.

Previous investigation in this laboratory also found a similar contradiction to the classical SMC phenotype in SMCs from patients with Type 2 diabetes mellitus. This distinct phenotype was able to be reversibly driven by miR-143 and 145: transfection of antimiR-143 and 145 into diabetic SMCs restored normal morphology and function (Riches et al., 2014). This was characterised as a distinct diabetic SMC phenotype, however it may also be found in AAA SMCs. It is extremely interesting to note that diabetes is typically considered to have a protective effect from AAA disease and so further investigation into this link is heavily encouraged.

In summary, this chapter has characterised the structure and function of SMCs explanted from an *ex vivo* bioreactor model of AAA. CCE treatment and flow culture used in combination induce a persistent SMC phenotype similar to that

seen in human end-stage AAA tissue. The END model produced SMCs which were rhomboid with a disordered cytoskeleton, had an impaired proliferative capacity, and had high levels of senescence with low MMP secretion. The EARLY model has revealed a period of hyper-proliferation, potentially accelerating the onset of general SMC senescence. This may have revealed a potential molecular target of early hyperproliferative markers for stabilisation of SMC numbers in AAA as a therapeutic treatment.

CHAPTER 6

EX VIVO MODEL BIOMECHANICS

CHAPTER 6 *EX VIVO* MODEL BIOMECHANICS

This chapter describes the development of methodology for biomechanical testing of the *ex vivo* model arterial tissues as examined in Chapter 4. The tissue was subjected to various treatment and culture regimes, details of which are given in Chapter 3. The effects of CCE treatment and bioreactor culture on tissue biomechanics were explored in order to validate the END *ex vivo* bioreactor model with human AAA biomechanical data reported in the literature. The first section of this chapter gives the results of the whole artery dilation testing. Following this, the results for uniaxial tensile testing of the END AAA model are given.

6.1. INTRODUCTION

Once an AAA has developed, the aorta will continue to expand at a rate proportional to its diameter until rupture of the AAA will inevitably occur unless elective repair is undertaken (Brady et al., 2004, Kent, 2014). Rupture of the arterial wall is a mechanical failure whereby the haemodynamic stresses exceed the failure strength of the aorta and so biomechanical properties of the aneurysmal wall have been widely studied over the years (Sumner et al., 1970, Vorp et al., 2003, Kontopodis et al., 2015, Schriefl et al., 2015). Although rupture is the catastrophic end-point of AAA, aneurysmal biomechanics are relevant throughout the AAA initiation and development process. Alterations in the matrix stemming from dysfunction of SMCs – responsible for ECM secretion – and high expression of MMPs throughout AAA tissue directly affect biomechanics and therefore the function of the aorta (Shah, 1997, Galis and Khatri, 2002, Curci, 2009). The typical mechanical behaviour of arterial tissue follows a biphasic linear pattern where elastin governs the biomechanical behaviour at low strains and during increasing strain collagen fibres are gradually recruited through a transition phase. Increasing strain further, the biomechanics enter a collagen phase with greater strength and stiffness. This typical biphasic curve can be seen in Figure 1.7.

Myriad modelling and experimental techniques have been employed to investigate the biomechanical properties of AAA. Peak wall stress has been modelled variously, from using idealized AAA models with two-dimensional analysis right up to patient-specific finite element and fluid structure interaction models (Stringfellow et al., 1987, Scotti et al., 2008, Nestola et al., 2016). In order to determine bulk material properties of AAA (necessary for computational model inputs), experimental work has been used. The simplest and most implementable method for determining bulk material properties is the uniaxial test. Many studies into biphasic arterial behaviour and the effect of aneurysm used uniaxial tensile tests to compare the composition of the matrix and its alterations in AAA and their subsequent effect on AAA biomechanics (Sumner et al., 1970, Sakalihasan et al., 1993, He and Roach, 1994, Thubrikar et al., 2001, Tavares Monteiro et al., 2014, Schriefl et al., 2015) . *Ex vivo* mechanical testing has shown AAA tissue to have a greatly reduced strength whilst being stiffer, especially in the circumferential orientation (Vorp et al., 1996, Thubrikar et al., 2001, Geest et al., 2006). The AAA wall was assumed to be linearly elastic and isotropic in earlier studies, though this has since been deemed unsuitable for purpose as aneurysmal tissue is materially non-linear and undergoes large strains prior to failure (Raghavan and Vorp, 2000, Vande Geest et al., 2008). Uniaxial tensile testing is considered to be the least complex and simplest test of mechanical properties. For most biological tissues, uniaxial tensile testing is usually conducted in two tissue orientations for consideration of the anisotropy. However, the simplicity of the uniaxial tensile testing method is reflected in the results, as it does not conclusively allow the mechanical properties of the whole organ to be determined.

Uniaxial/biaxial tensile testing techniques require the removal of tissue from the patient and so are suited for tissue removed during repair surgery. However, in order to investigate the mechanical properties of aneurysms at earlier stages of the disease to appreciate temporal changes, development of non-invasive methods was necessary. Systemic pressurisation of the AAA *in vivo* results in changes in the AAA diameter during systole and diastole which are able to be measured by ultrasound, magnetic resonance imaging (MRI) and computerised tomography scan (CT scan). Concordant with *ex vivo* uniaxial testing, AAAs

measured *in vivo* have been found to have increased stiffness and reduced distensibility compared to healthy aorta (Lanne et al., 1992, Ganten et al., 2008, Hoegh and Lindholt, 2009, Molacek et al., 2011). These *in vivo* imaging techniques rely on measuring the diameter of the artery in relation to characterised pressurisation via imagine techniques. This method can also be performed *ex vivo* as it is a more functional test. Maintaining the artery as a whole organ as opposed to manipulating tissue into flat strips would provide more informed analysis of the artery functioning as a physiological organ. The anisotropic response of AAA tissue is not able to be conclusively assessed using the simpler method of uniaxial tensile testing (Vorp and Geest, 2005, Zeinali-Davarani et al., 2013). Whole artery pressure-dilation techniques for determining biomechanical properties of animal AAA models are able to be directly compared to *in situ* human AAAs and so a clinical comparison can be made (Tierney et al., 2010). In addition, it may not be practical to segment tissue with very low yield such as small animal aortae into strips suitable for uniaxial tensile testing (Collins et al., 2011, Haskett et al., 2013).

Biomechanical validation of experimental AAAs in animal models appears to be more commonly used only in recent years. In small animal models, uniaxial/biaxial tensile testing and both *in vivo* and *ex vivo* whole artery pressure-dilation testing have been used to assess arterial biomechanics (Collins et al., 2011, Haskett et al., 2013, Phillips et al., 2015, Trachet et al., 2015, Zidi and Allaire, 2015). For large animals, there is a smaller body of work which has used uniaxial/biaxial tensile testing and *ex vivo* whole artery pressure-dilation testing (Kratzberg et al., 2009, Tierney et al., 2010, Zeinali-Davarani et al., 2013).

Investigating the biomechanical behaviour of the *ex vivo* bioreactor model of AAA enables biomechanical validation compared to human disease. It also enables the relationship between the dysfunction in the SMCs – responsible for secreting and degrading ECM – and the function of the artery as a whole organ to be elucidated.

6.2. CHAPTER AIMS AND OBJECTIVES

The aim of this chapter was to characterise the effects of the CCE treatment and bioreactor culture, as detailed in Chapter 3, in terms of the arterial biomechanics. Two methods were used to achieve this, with the aim of selecting the most appropriate method of biomechanical testing for the END AAA model tissue. The methods used were whole artery dilation testing and uniaxial tensile testing.

6.2.1. OBJECTIVES

The specific objectives of this chapter were

1 To characterise the effects of CCE treatment using whole artery dilation testing
2 To characterise the effects of CCE treatment using uniaxial tensile testing
3 To determine the optimum testing method for testing END model tissue
4 To characterise the END model tissue in terms of biomechanics

6.3. WHOLE ARTERY PRESSURE-DILATION TESTING

The purpose of the CCE treatment gel was to disrupt the extracellular matrix of the artery by degrading both elastin and collagen. The effects of the CCE gel on arterial tissue were therefore characterised so that the biomechanics of the vessels at a 'zero-state' (the point when arteries are installed into the bioreactor following gel pre-treatment) and the effects of bioreactor culture on CCE treated and vehicle treated tissue could be analysed. The methods for producing the CCE gel are given in Section 3.5.1.

It was found that there was no significant difference in arterial compliance between FRESH, VEH or CCE tissue when the diameter of each vessel was normalised to the diameter at 0 mmHg of each respective artery (Figure 6.1A).

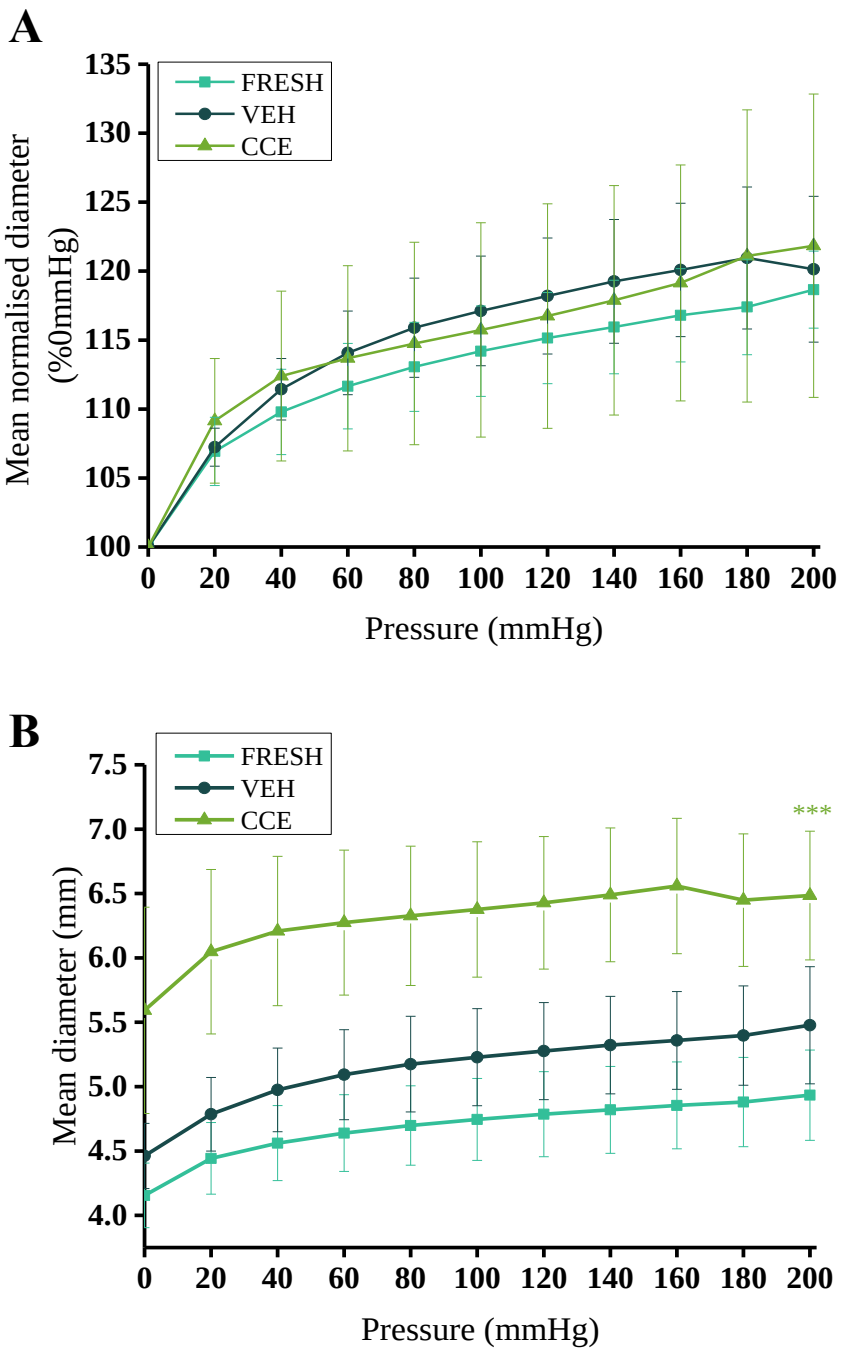

Figure 6.1 Arterial compliance of FRESH, VEH and CCE pre-treatment. A) pressure-diameter curve with normalised mean. B) mean raw diameter of vessels. (*p<0.001, n=6). Graph shows mean±95% confidence intervals. Statistical analysis used was a one-way ANOVA with post-hoc Tukey test for means comparison.**

However, when the data was not normalised and the raw mean data was plotted there was a significant increase in the mean diameter in CCE arteries compared

to FRESH arteries (5.6±0.8 mm vs. 4.2±0.3 mm, p<0.001) (Figure 6.1B). There was no difference in mean diameter in VEH arteries compared to FRESH (4.5±0.3 mm vs. 4.2±0.3 mm) in terms of raw mean diameter.

6.3.1.1. MATCHED VESSEL DILATION TESTING

In order to confirm that this increase in mean diameter in CCE treated vessels was not an artefact of tissue sample selection; the experiment was repeated by measuring the diameters of a further six arteries which had not been subjected to any pre-treatment over a physiological range of pressures (0 to 100 mmHg). This was done so that the extracellular matrix would not be irreparably damaged during testing which |would affect results. Subsequently, all of the arteries were then treated with CCE gel and then dilation tested once more in a matched repeated experiment.

In this matched experiment, the arteries had a significantly increased mean diameter once they had received CCE treatment compared to before (6.4±0.4mm vs. 5.3±0.3 mm, p<0.001, n=6) (Figure 6.2).

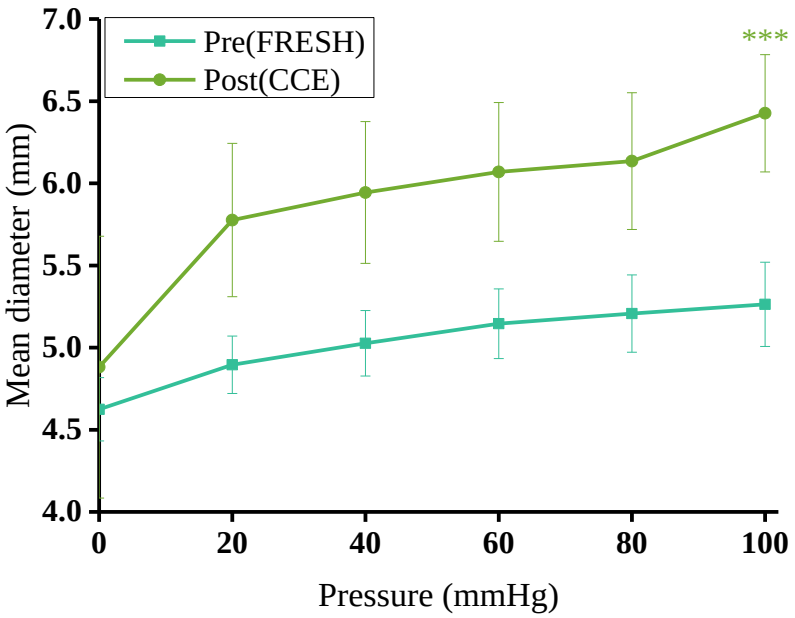

Figure 6.2 Matched dilation experiments before and after CCE treatment. ***p<0.001, (n=6). Graph shows mean ± 95% confidence intervals. Statistical analysis used was a two-tailed paired t-test.

6.3.2. BURST PRESSURE

The systemic pressure of the dilation rig was not allowed to exceed 5000 mmHg for safety reasons. If the artery did not burst within this range, the burst pressure was recorded as 5000 mmHg.

FRESH and VEH tissue had burst pressures which were indistinguishable (3902±463 mmHg vs. 3736±496 mmHg respectively, p=0.85). However there was a steep decrease of about 90% in burst pressure of CCE tissue compared to FRESH tissue (351±135 mmHg vs. 3902±463 mmHg, p<0.001) (Figure 6.3).

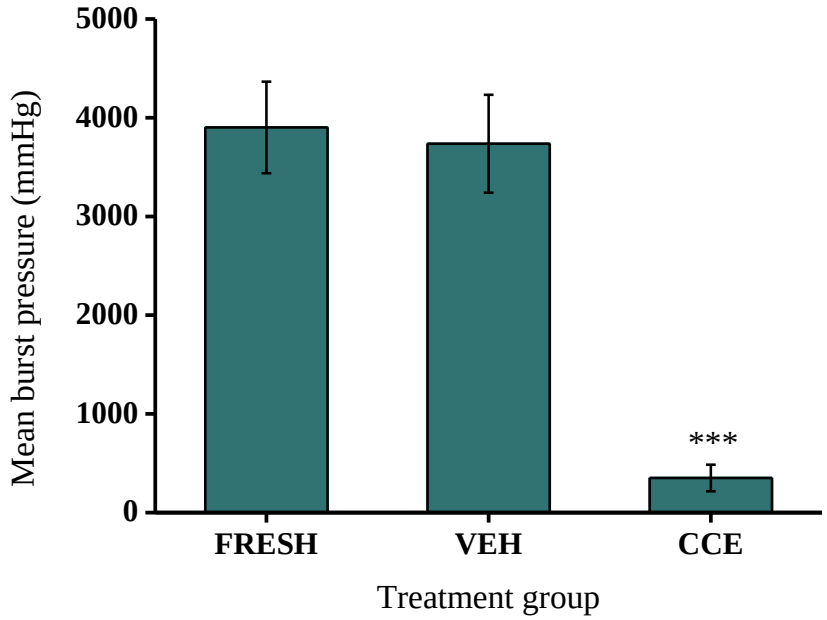

Figure 6.3 Burst pressure of non-sterile FRESH, VEH and CCE treated arteries. ***p<0.001, graph shows mean ± 95% confidence intervals (n=6). Statistical analysis used was a one-way ANOVA with post-hoc Tukey test for means comparison.

6.4. UNIAXIAL TENSILE TESTING

The effects of the pre-treatment gel were characterised using uniaxial tensile testing methods and, in addition, the biomechanics of the END AAA model were also tested. These tissues were obtained from a local abattoir and stored for short periods of time before testing could commence hence there was no guarantee on the viability of the tissue.

Three sets of carotid arteries underwent END AAA model protocol (as per Section 3.5) and were then subjected to uniaxial tensile testing. Explantation of viable SMCs was possible for all arteries once the bioreactor was dismantled and so all of the END model arteries tested were viable when tensile testing commenced. Each carotid artery in the set was either subjected to vehicle (BIOVEH) or CCE (BIOCCE) gel pre-treatment. Each artery was cut into six strips; three of circumferential orientation and three of longitudinal orientation (Figure 2.10).

Data was only considered from tissue strips which had failed in the centre of the strip and not at the grips for the tensile testing equipment. This was done so that only the true failure of the tissue was taken into account and it was not skewed by early failure by physical damage from the grips. Using these criteria, in the circumferential orientation three VEH arteries and one BIOVEH artery had only two tissue strips truly fail, and one BIOVEH artery only had one tissue strip truly fail. In the longitudinal orientation, two FRESH arteries and one artery each from VEH, CCE, BIOVEH and BIOCCE experimental groups had only two tissue strips truly fail. Low tissue yield, and the circumference of the arteries were factors in this. Matched experiments between dilation testing and uniaxial tensile testing reduced tissue yield in FRESH, VEH and CCE groups and tissue harvesting limitations led to low tissue yield in BIOVEH and BIOCCE groups. Arterial circumference was a limiting factor – especially in the circumferential orientation – due to the requirement for 6 mm gauge length with additional tissue needed for obtaining an effective grip. The results are presented as engineering stress and engineering strain as any change in tissue cross-sectional area during testing was not recorded and quantified.

The tissue strips were not subjected to any preload or preconditioning regime. Preload can mask the inherent properties in the tissue in the elastin phase by starting the data collection at an arbitrary value rather than the true relaxed state of the tissue. It was tested with a crosshead displacement rate of $10mm.min^{-1}$, corresponding to a steady strain rate of $0.028s^{-1}$ in 1X PBS maintained at 37°C in order to mimic physiological conditions.

6.4.1. TISSUE BEHAVIOUR

Images were taken during the uniaxial tensile testing of BIOCCE and BIOVEH tissue. It was observed that BIOVEH tissue tended to fail at one point in the strip at the ultimate tensile strength (Figure 6.4). However, BIOCCE tissue did not have as much of a defined failure point in the tissue as BIOVEH tissue. BIOVEH tissue generally failed at one point and then propagated across the tissue in a defined route.

Tissue thickness was also heterogeneous in BIOCCE tissue which may have led to predisposed failure points in the tissue strips (Figure 6.5).

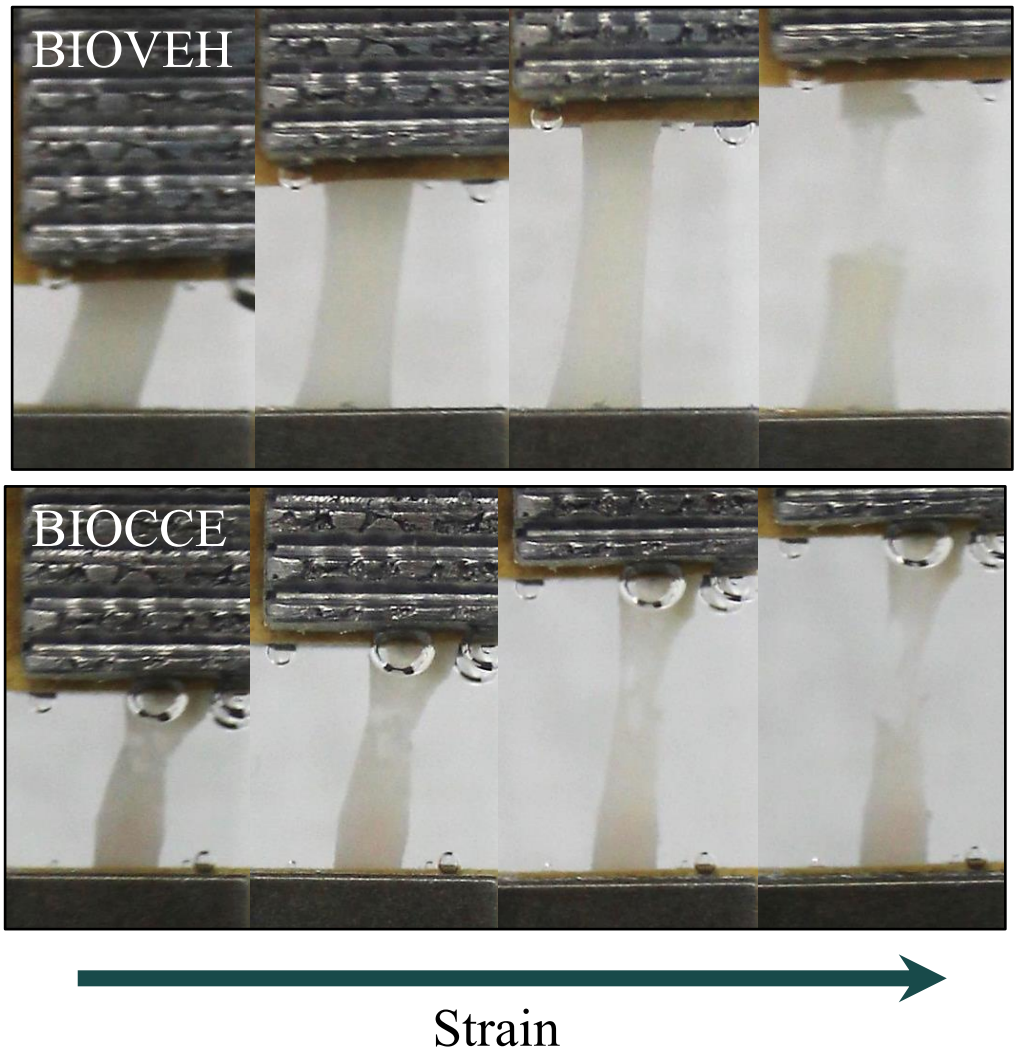

Figure 6.4 Representative images of tissue strips undergoing uniaxial tensile testing.

6.4.2. ARTERIAL THICKNESS

The mean thickness of each tissue strip was calculated from three separate thickness measurements using a digital micrometer. END-BIOCCE tissue was non-uniform and areas of translucent tissue where the thickness was especially low were visible (Figure 6.5).

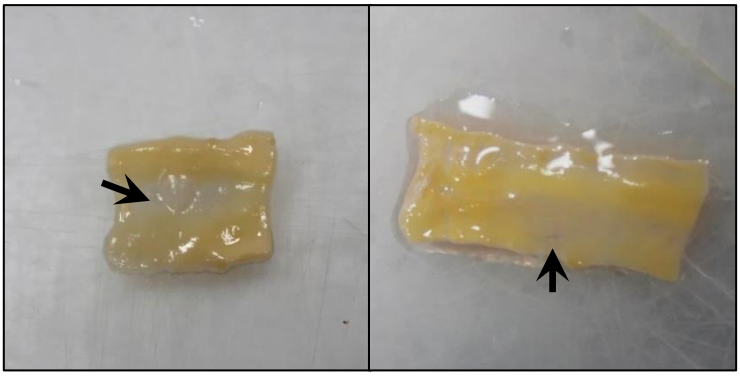

Figure 6.5 Non-uniformity of arterial thickness in END-BIOCCE tissue. Arrows indicate translucent areas in excessively thinned tissue.

The application of CCE treatment induced a significant reduction in arterial thickness. In addition, bioreactor culture on either VEH or CCE treated arteries induced a marked reduction in arterial thickness.

A one-way ANOVA showed that there was a significant difference in mean arterial thickness between experimental groups, $F(4, 136)=18.1$, $p<0.001$. The results for this are displayed in

Figure 6.6. A post-hoc Tukey test revealed that the thickness of FRESH and VEH arteries did not differ. There was a decrease in thickness in CCE tissue compared to FRESH tissue (0.65±0.04mm vs. 0.85±0.06mm respectively, $p<0.001$). The effect of bioreactor culture in both VEH and CCE treated tissue was to reduce thickness by a similar degree (0.81±0.09mm vs. 0.66±0.05mm, VEH and BIOVEH respectively, $p<0.05$, 19% reduction; 0.65±0.04mm vs. 0.52±0.12mm, CCE and BIOCCE respectively, $p<0.05$, 21% reduction).

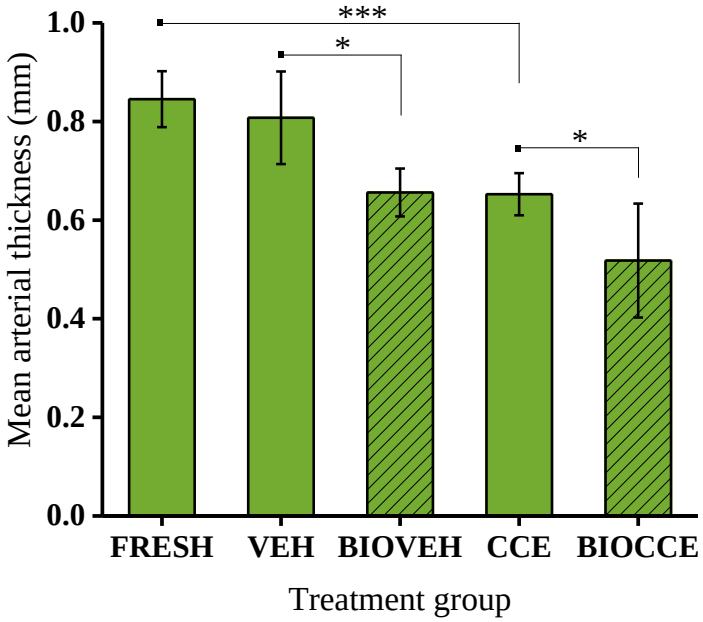

Figure 6.6 Mean arterial thickness. Shaded columns represent viable tissue. Graph shows mean ± 95% confidence intervals. ***p<0.001, *p<0.05 FRESH/VEH/CCE (n=6), BIOVEH/BIOCCE (n=3). Statistical analysis used was one-way ANOVA with post-hoc Tukey test.

6.4.3. TISSUE BEHAVIOUR

Representative stress-strain graphs for each of the tissue treatment groups in both the longitudinal and circumferential orientations are shown in Figure 6.7. The stress-strain data for the rest of the strips are found in Appendix F.

The FRESH tissue exhibited characteristic anisotropic biphasic behaviour as observed in arterial tissue tests. It was generally stiffer circumferentially in both the elastin and collagen regions. This behaviour was mirrored in the VEH tissue with similar stiffness in both the elastin and collagen regions, transition strains and failure strengths. Tissue subjected to CCE treatment was generally much weaker compared to FRESH or VEH tissue, and the longitudinally orientated tissue tended to be much weaker than circumferential tissue. It was also more compliant in both the elastin and collagen regions in both orientations and generally acted more ductile with a higher failure strain. There was usually a higher degree of anisotropy in CCE tissue where the longitudinally orientated tissue was weaker compared to circumferential tissue typically to a greater

degree than in FRESH or VEH tissue. However, CCE tissue did mirror the characteristic arterial biphasic behaviour seen in FRESH and VEH tissue. BIOVEH tissue again was much weaker and more compliant compared to FRESH or VEH tissue. Similar to FRESH and VEH tissue, BIOVEH tissue exhibited biphasic elastin-collagen behaviour and strain at failure meaning that it possessed a similar degree of ductility. BIOCCE tissue was typically the group which had the lowest failure stress and stiffness measurements in both the elastin and collagen regions. In the longitudinal orientation in particular, BIOCCE tissue was markedly weak and ductile. BIOCCE tissue also tended not to have a distinct failure point whereas all of the other groups did. This behaviour can be seen qualitatively in Figure 6.4.

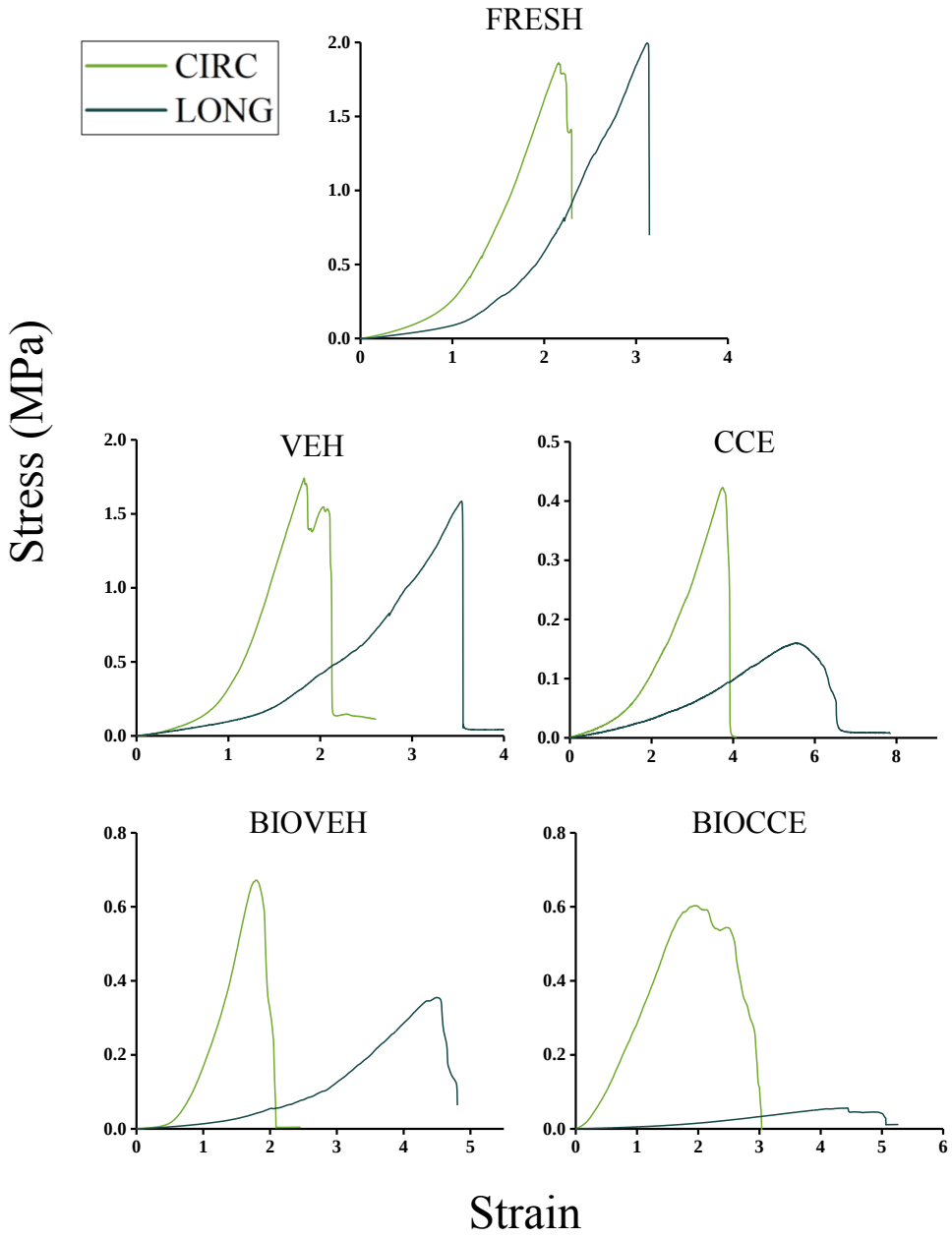

Figure 6.7 Representative engineering stress-strain graphs for each of the treatment groups in both circumferential and longitudinal orientation.

Additionally, in four out of seventeen BIOCCE test strips (almost a quarter of total BIOCCE strips) the stress-strain behaviour was not clearly biphasic as arterial tissue is commonly characterised. There was no presence of a distinct elastin region before the collagen fibres were recruited in the collagen region, finally leading to failure of the tissue once the strain increased beyond that. Three of the four test strips were circumferentially orientated and one was

longitudinally orientated. Three test strips were from the same artery (two circumferential and one longitudinal).

The raw data stress-strain curves for each of the four strips are shown in Figure 6.8. The values for elastin region stiffness and transition strain for these strips were taken to be zero.

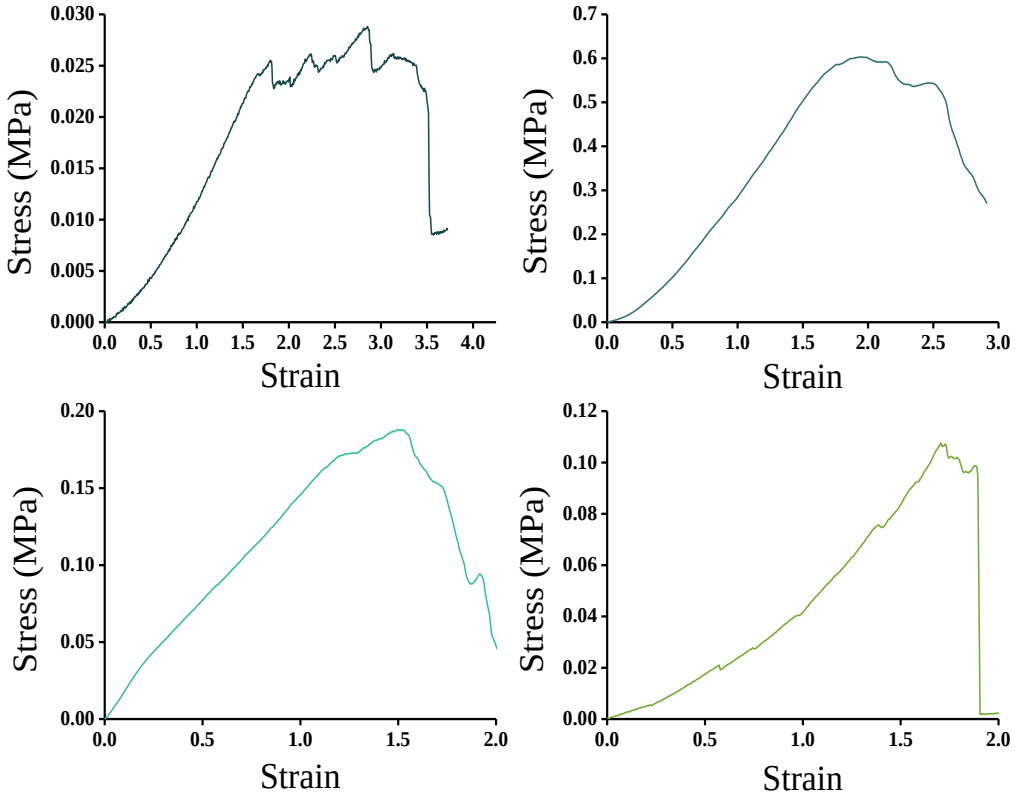

Figure 6.8 Raw stress-strain curves for BIOCCE tissue which did not exhibit distinct biphasic behaviour with absence of elastin region.

6.4.4. EFFECT OF TREATMENT ON ELASTIN REGION STIFFNESS

The stiffness of the elastin region is the resistance of the artery in the low strain region, as described in Section 1.5.2. The ability of the artery to expand and contract to drive to create a pressure pulse which drives blood through them relies on the biomechanical properties of elastin. The mean elastin region stiffness for the arteries in circumferential and longitudinal orientations is displayed in

Figure 6.9. The circumferential and longitudinal orientations are presented separately due to the well-documented anisotropy found in arterial tissue (Vorp and Geest, 2005, Gasser et al., 2006).

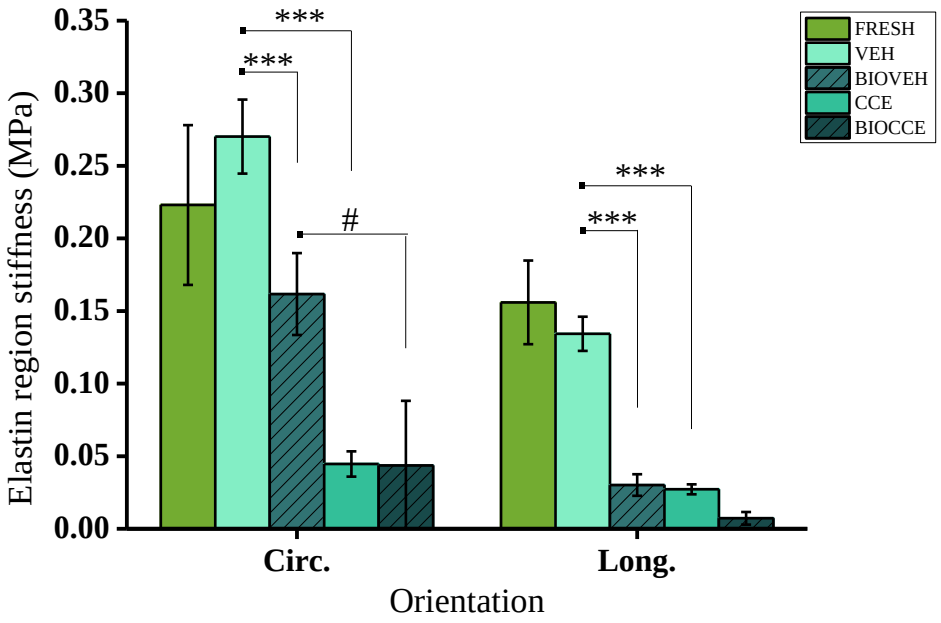

Figure 6.9 Elastin region stiffness. FRESH, VEH, CCE (n=6); BIOVEH, BIOCCE (n=3); ***p<0.001, #p=0.06. Shaded columns represent viable tissue. Graphs show mean ± 95% confidence intervals. Statistical analysis used was a one-way ANOVA per orientation with post-hoc Tukey test for means comparison.

Overall, VEH treatment alone did not affect elastin region stiffness in either orientation. CCE treatment alone significantly reduced elastin region stiffness in both orientations compared to VEH. Bioreactor culture reduced elastin region stiffness in vehicle treated arteries in both orientations. Bioreactor culture on CCE treated arteries did not have any significant effect in either orientation. BIOCCE arteries tended to have a lower elastin region stiffness compared to BIOVEH arteries, but this was non-significant.

To test statistical significance, a one-way ANOVA per tissue orientation was used to test for significant effects of treatment on elastin region stiffness and a post-hoc Tukey test was used for means comparison. Firstly, the results from the circumferential direction will be described. The results were significant, $F(4, 60) = 34.6$, $p<0.001$. There was no significant difference in elastin region

stiffness between FRESH and VEH arteries (0.22±0.06 vs. 0.27±0.03 MPa respectively). Application of CCE treatment without culture induced significantly decreased elastin region stiffness compared to VEH (0.04±0.01 vs. 0.27±0.03 MPa respectively, $p<0.001$). The effect of bioreactor culture in VEH arteries was to decrease the elastin region stiffness (0.27±0.03 vs. 0.16±0.03 MPa, VEH and BIOVEH respectively, $p<0.01$). In CCE treated arteries there was no difference between CCE and BIOCCE treated arteries (0.04±0.01 vs. 0.06±0.05 respectively). There was a non-significant trend towards a decreased elastin region stiffness in BIOCCE arteries compared to BIOVEH arteries. BIOCCE and BIOVEH arteries (0.06±0.05 vs. 0.16±0.03 MPa respectively, $p=0.06$).

In the longitudinal orientation, the results were also significantly different, $F(4, 61) = 79.4$, $p<0.001$. The Tukey test showed that elastin region stiffness in FRESH and VEH arteries were similar (0.16±0.03 vs. 0.13±0.01 MPa respectively). The effect of CCE treatment alone reduced the stiffness in the elastin region compared to VEH (0.03±0.003 vs. 0.13±0.01, $p<0.001$). In both VEH treated arteries, the effect of bioreactor culture was to reduce elastin region stiffness (0.03±0.01 vs. 0.13±0.01, BIOVEH and VEH respectively, $p<0.001$). There was no effect of bioreactor culture on CCE treated arteries (0.01±0.004 vs. 0.03±0.003 MPa, BIOCCE and CCE respectively).

6.4.5. Effect of treatment on collagen region stiffness

Collagen is the less elastic component of the arterial extracellular matrix and it provides strength to the tissue at higher strains. It is formed into fibres which are gradually recruited into a load-bearing role as strain is increased (Thubrikar et al., 2001). The collagenase contained within the CCE gel treatment would have degraded a proportion of the collagen in the artery and so the stiffness in the collagen region amongst the treatment groups was analysed. SMCs are also able to secret collagen as part of a remodelling process, so the biomechanics in the collagen region gave an insight into the function of the SMCs. The mean

collagen region stiffness for each of the experimental groups is shown in Figure 6.10.

The results for measurements of collagen region stiffness appeared to follow the same trend as for elastin region stiffness. VEH treatment did not affect collagen region stiffness in either orientation. CCE treatment significantly reduced collagen region stiffness in both orientations compared to VEH control. Bioreactor culture significantly reduced collagen region stiffness in both orientations in VEH arteries, but had no effect in CCE arteries.

A one-way ANOVA was performed per tissue strip orientation. In the circumferential direction, there was a significant effect of arterial treatment on collagen region stiffness, $F(4, 60) = 27.8$, $p<0.001$. The Tukey test showed that there was no difference in collagen region stiffness between FRESH and VEH arteries (1.46±0.38 vs. 1.54±0.11 MPa respectively). The application of CCE treatment significantly reduced collagen region stiffness compared to VEH control (0.36±0.07 vs. 1.54±0.11 MPa respectively, $p<0.001$). The effect of bioreactor culture on VEH treated arteries was to significantly decrease collagen region stiffness (0.89±0.10 vs. 1.54±0.11 MPa, BIOVEH and VEH respectively, $p<0.001$). In contrast to this, in CCE treated arteries there was no effect of bioreactor culture (0.24±0.09 vs. 0.36±0.07 MPa, BIOCCE and CCE respectively).

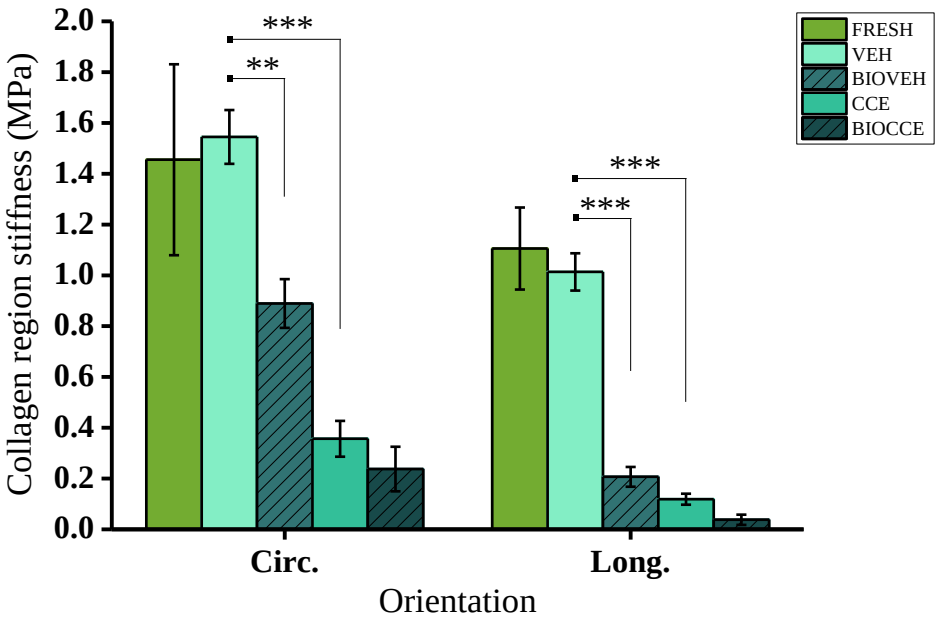

Figure 6.10 Collagen region stiffness. FRESH, VEH, CCE (n=6); BIOVEH, BIOCCE (n=3); **p<0.01, ***p<0.001. Shaded columns represent viable tissue. Graphs show mean ± 95% confidence intervals. Statistical analysis used was a one-way ANOVA per orientation with post-hoc Tukey test for means comparison.

The results in the longitudinal direction mirrored the effects in the circumferential direction. The ANOVA revealed that there was a significant effect of arterial treatment on collagen region stiffness in the longitudinal orientation, $F(4, 61) = 35.5$, $p<0.001$. A post-hoc Tukey test was then used for means comparison. There was no significant difference in collagen region stiffness between FRESH and VEH arteries (1.11±0.16 vs. 1.01±0.07 MPa respectively). CCE treatment alone induced a significant reduction in collagen region stiffness compared to VEH control (0.12±0.02 vs. 1.01±0.07 respectively, $p<0.001$). Bioreactor culture significantly reduced collagen region stiffness in VEH treated arteries (0.21±0.04 vs. 1.01±0.07 MPa, BIOVEH and VEH respectively, $p<0.001$). There was no significant effect of bioreactor culture on CCE treated arteries (0.04±0.02 vs. 0.12±0.02 MPa, BIOCCE and CCE respectively).

6.4.6. EFFECT OF TREATMENT ON TRANSITION STRAIN

Transition strain is the point where the collagen fibres are recruited as such to bear a majority of the load applied to the tissue. A shift in transition strain amongst any of the experimental groups is evidence for tissue remodelling, as the configuration of the collagen fibres will have changed as opposed to being passively removed (details of the collagen and elastin configuration are included in Section 1.5.2). Analysing changes in the transition strain allows analysis of the behaviour of the extracellular matrix (and therefore SMC function). The transition strain results are shown in Figure 6.11.

In summary, there was no change in transition strain in either orientation in any of the treatment groups which did not undergo bioreactor culture. Bioreactor culture induced a decrease in transition strain in CCE arteries alone in the circumferential orientation. In the longitudinal orientation, the fact that there was no observed differences between FRESH/VEH and VEH/BIOVEH, yet there was a significant difference between FRESH/BIOVEH suggests a potential trend towards an increased transition strain in VEH arteries undergoing bioreactor culture. The transition strains of arteries which underwent bioreactor culture seemed to diverge; there was a marked difference in transition strain between BIOVEH and BIOCCE arteries in the longitudinal orientation.

A one-way ANOVA was performed per orientation. In the circumferential direction, the effect of arterial treatment on transition strain was significant, $F(4, 60) = 2.91$, $p<0.05$. The Tukey test showed that there was no significant difference in the transition strains between FRESH and VEH arteries (0.96±0.17 vs. 0.92±0.08 respectively). Application of CCE gel alone also did not have any observable effect on transition strain compared to VEH control (1.04±0.14 vs. 0.92±0.08 respectively). Bioreactor culture exerted no effect on VEH treated arteries (0.78±0.18 vs. 0.92±0.08, BIOVEH and VEH respectively). In CCE treated arteries, bioreactor culture led to a significant decrease in transition strain (0.54±0.29 vs. 1.03±0.14, BIOCCE and CCE respectively, $p<0.05$).

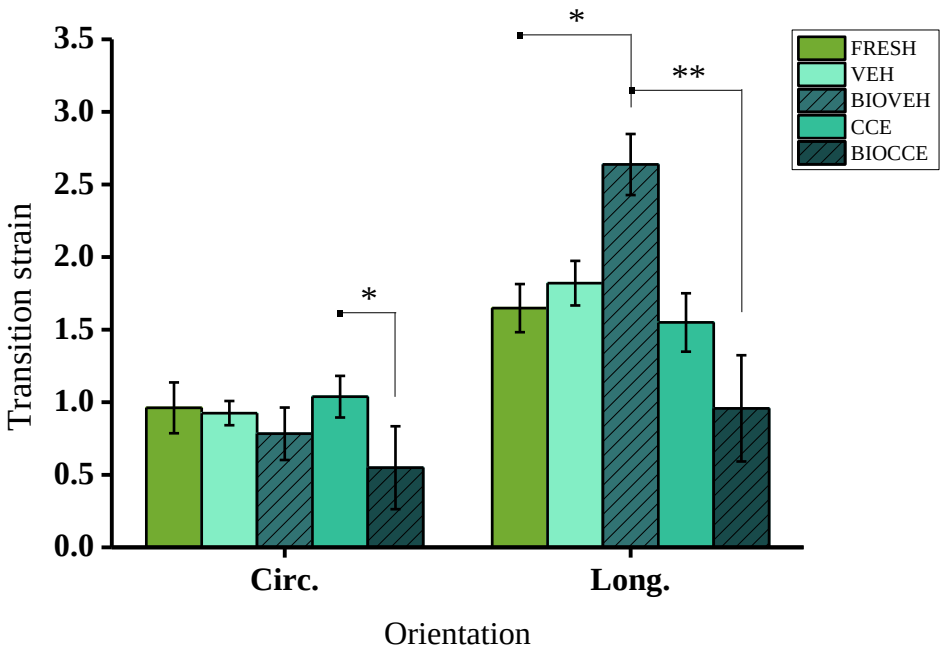

Figure 6.11 Transition strain. FRESH, VEH, CCE (n=6); BIOVEH, BIOCCE (n=3); *p<0.05, **p<0.01. Shaded columns represent viable tissue. Graphs show mean ± 95% confidence intervals. Statistical analysis used was a one-way ANOVA per orientation with post-hoc Tukey test for means comparison.

In the longitudinal orientation, the ANOVA showed that there was a significant effect of arterial treatment on transition strain, $F(4, 60) = 4.12$, $p<0.01$. Post-hoc analysis with a Tukey test showed that there was no significant difference between FRESH and VEH arteries (1.64±0.17 vs. 1.82±0.15 respectively). There was no effect of application of CCE treatment compared to VEH control on transition strain (1.54±0.2 vs. 1.82±0.15 respectively). BIOVEH arteries had an increased transition strain compared to FRESH arteries (2.63±0.2 vs. 1.64±0.17 respectively, $p<0.05$). However, compared directly to its counterpart which did not undergo bioreactor culture, BIOVEH and VEH arteries were indistinguishable (2.63±0.2 vs. 1.82±0.15 respectively, $p=0.13$). There was a marked reduction in transition strain in BIOCCE arteries compared to BIOVEH arteries (0.95±0.37 vs. 2.63±0.21 respectively, $p<0.01$).

6.4.7. EFFECT OF TREATMENT ON ULTIMATE TENSILE STRENGTH

The rupture of an AAA physiologically is due to the failure of the tissue at its weakest point. The ultimate tensile strength (UTS) is the maximum stress reached during the test and would correlate to rupture pressure in the human disease; for this reason the UTS was measured for each treatment group. The UTS results are shown in Figure 6.12.

Overall, CCE treatment alone, in the absence of any culturing of the artery, significantly reduced the UTS in both orientations. In VEH arteries, bioreactor culture led to significantly decreased UTS in both orientations. In the circumferential orientation, BIOVEH arteries tended to be stronger than BIOCCE arteries, although this trend was non-significant.

A one-way ANOVA was performed per orientation. In the circumferential orientation, the ANOVA showed that there was a significant effect of arterial treatment on UTS, $F(4, 60) = 36.4$, $p<0.001$. A Tukey test showed that there was no change in UTS between FRESH and VEH arteries (1.44±0.34 vs. 1.70±0.16 MPa respectively). Application of CCE treatment alone induced a decrease in UTS compared to VEH control (0.41±0.09 vs. 1.7±0.16 MPa respectively, $p<0.001$). Bioreactor culture induced a significant decrease in UTS in VEH treated arteries (0.88±0.11 vs. 1.70±0.16 MPa respectively, $p<0.001$). However, this effect of bioreactor culture was not seen in CCE treated arteries (0.30±0.14 vs. 0.41±0.09, BIOCCE and CCE respectively). There was a trend towards decreased UTS in BIOCCE arteries compared to BIOVEH, although was not statistically significant (0.30±0.14 vs. 0.88±0.11 MPa respectively, $p=0.06$).

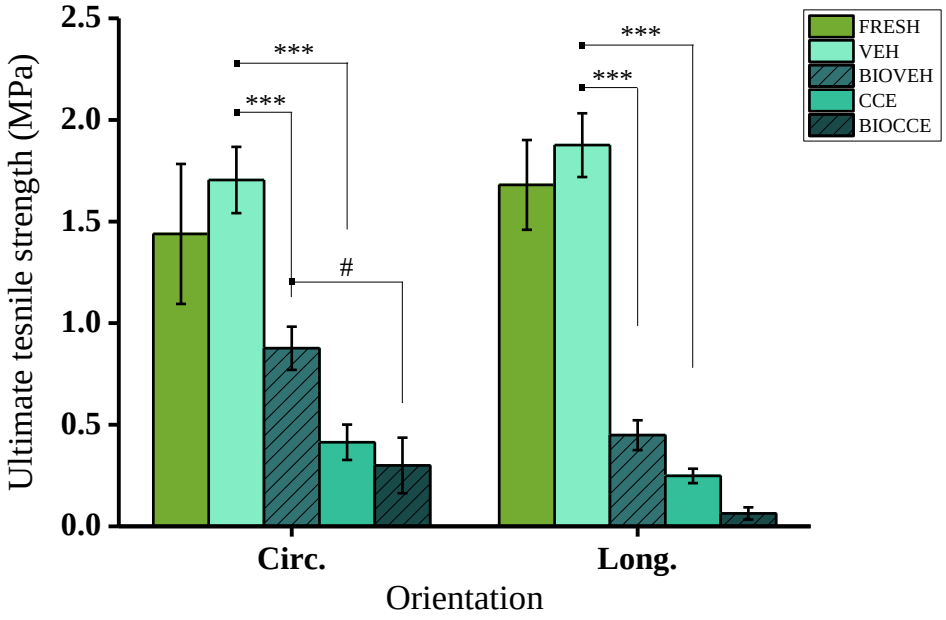

Figure 6.12 Ultimate tensile strength. FRESH, VEH, CCE (n=6); BIOVEH, BIOCCE (n=3); ***p<0.001, #p=0.06. Shaded columns represent viable tissue. Graphs show mean ± 95% confidence intervals. Statistical analysis used was a one-way ANOVA per orientation with post-hoc Tukey test for means comparison.

In the longitudinal orientation, the results reflected the behaviour in the circumferential orientation. The ANOVA showed a significant effect of arterial treatment on UTS, $F(4, 61) = 48.3$, $p<0.001$. The Tukey test showed that the UTS of FRESH and VEH arteries were alike (1.68±0.22 vs. 1.88±0.16 MPa respectively). CCE treated arteries had a decreased UTS compared to VEH control (0.25±0.04 vs. 1.88±0.16 MPa respectively, $p<0.001$). The effect of bioreactor culture in VEH treated arteries was a significant reduction in UTS (0.45±0.07 vs. 1.88±0.16 MPa respectively, $p<0.001$). This effect of bioreactor culture was not observed in CCE treated arteries, where there was no difference in UTS (0.06±0.03 vs. 0.24±0.04 MPa, BIOCCE and CCE respectively).

6.5. COMPARISON OF UNIAXIAL AND DILATION TESTING

As both the whole vessel dilation tests and the uniaxial tensile tests for FRESH, VEH and CCE tissue were performed on matched tissue from the same animals,

a direct comparison can be drawn. The UTS and the burst pressure (two of the most easily comparable parameters) of the arteries were compared. The mean UTS of all of the tissue strips tested, both circumferential and longitudinal, was calculated and compared with the burst pressure. The data was imported into Microsoft Excel (Microsoft, WA, USA) and a linear best fit line was determined using in-built least squares regression code. The R^2 value gives an indication of the correlation between the two parameters and in this case $R^2 = 0.7686$ (Figure 6.13). This indicates that there is a correlation of failure stress between the two methods but it is not strong. The data from all treatment conditions are pooled to give a sufficiently large dataset for regression analysis.

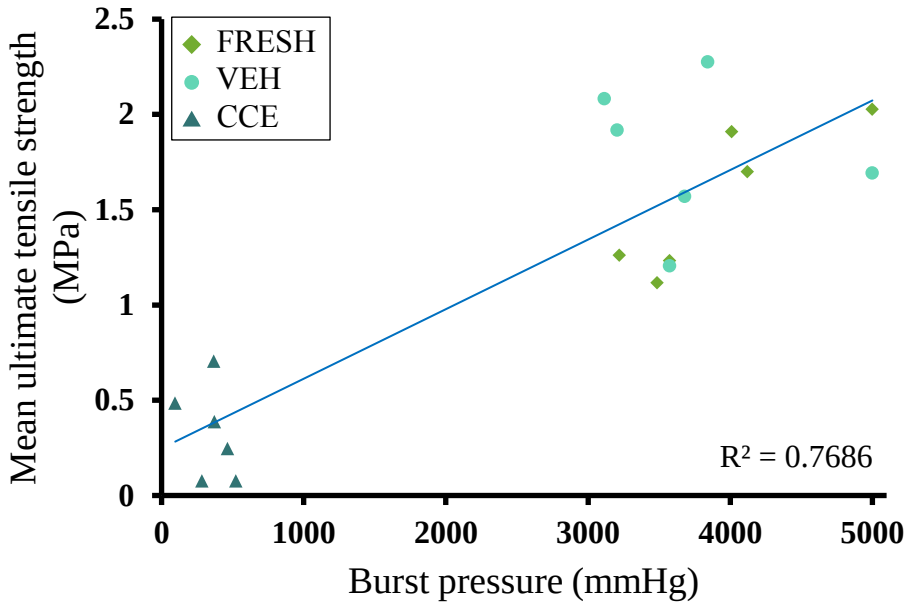

Figure 6.13 Comparison of whole vessel burst pressure and uniaxial tensile testing parameters (burst pressure vs. mean ultimate tensile strength). $R^2 = 0.7686$ using a linear line of best fit.

6.6. DISCUSSION

This chapter presented a biomechanical analysis of the effect of the CCE treatment and END AAA model tissue behaviour using two different testing methodologies. The END AAA model was experimentally produced using the methodology outlined in Chapter 3. Briefly, a gel containing a combination of collagenase and elastase (CCE) was focally applied peri-adventitially to a

porcine artery and left for 3 hours. The treatment was then removed and the artery was installed into a bioreactor able to impart luminal pressure and flow through the artery for 12 days. The characterisation of the CCE treatment was only carried out using non-sterile arteries due to high cost and ease of implementation: the tissue did not undergo culture for any length of time and so sterility was not necessary.

Whole artery pressure-dilation testing showed that the burst pressure was drastically decreased in CCE tissue compared to FRESH or VEH tissue. It also revealed that the tissue compliance between untreated tissue and that which underwent VEH or CCE treatment was indistinguishable. Compliance is the relationship between a change in pressure and a change in diameter. A proportion of the same tissue which underwent CCE characterisation in whole artery pressure-dilation testing was used in matched uniaxial tensile testing experiments. A disparity between the marked change in CCE tissue biomechanics compared to FRESH or VEH controls observed in the uniaxial tests compared to no alterations in the tissue in the pressure-dilation tests emerged. The mean change in diameter was then examined rather than the normalised change in diameter and it was found that the CCE treated tissue has an increased mean diameter compared to both FRESH and VEH tissue.

It was then hypothesised that the CCE treatment induces an increase in mean diameter in the range of pressures measured. As a bias of experimental groupings of arteries could not be ruled out, a further set of repeated experiments was carried out where the tissue was non-destructively tested prior to and after CCE treatment. In this second set of experiments it was confirmed that CCE treatment significantly increased mean arterial diameter despite having no effect on compliance.

The reason for this may lie within the configuration of elastin and collagen in the arterial tissue. Elastin is the component of the ECM which is responsible for arterial compliance and is degraded via elastase during application of the CCE treatment. In Chapter 4, histological analysis revealed that CCE treated tissue exhibited clear elastin loss and so the potential elastic energy residing in the tissue would have decreased. Other studies have shown that elastin degradation

in arteries leads to an increase in arterial diameter. In selective elastolytic and collagenolytic *in vitro* pressure-dilation arterial studies, Dobrin *et al.* showed that elastase degraded arteries had increased diameter and were stiffer at lower pressures whilst collagenase treated arteries were more compliant and weaker overall (Dobrin et al., 1984). Subsequent studies concurred that elastin degradation leads to an increased arterial diameter with increased stiffness at lower pressures and equated this with pre-stresses within elastin present even at zero-load (Fonck et al., 2007).

The significant increase in mean arterial diameter even at zero-load as a direct effect of the CCE treatment was shown in repeated experiments on the same arterial tissue. The CCE treatment did induce a significant increase in mean diameter, but did not induce a change in stiffness at any level of pressure. It is thought that this is attributed to the inclusion of collagenase in addition to elastase within the CCE treatment. Collagenase degrades collagen which is the component of the arterial wall associated with stiffness at higher loads and wall strength. Therefore the lack of increased stiffness at lower pressures associated with elastinolytic studies when characterising the effects of CCE treatment may be attributed to the decreased stiffness associated with collagenase activity. Decreased arterial strength and stiffness has also been associated with degradation of collagenase (Dadgar et al., 1997). As the burst pressure of the CCE treated tissue was severely decreased compared to controls, collagen degradation had a significant effect on the mechanical properties of the artery. However, the matched uniaxial tensile testing experiments revealed a significant decrease in both the elastin and collagen regions which was not mirrored in the pressure-dilation experiments. It is thought that this was an experimental artefact in the methodology for the CCE tissue: when the PBS was allowed to flow into the artery lumen, prior to zeroing the pressure meter, it caused a deformation in the weakened tissue. This deformation was not then observed during the experiment as it occurred outside the pressure range.

Whole artery pressure-dilation testing and uniaxial tensile testing were both used for CCE treatment characterisation whereas the END AAA model biomechanics were characterised using uniaxial tensile testing only. Although

whole artery pressure-dilation testing enables multidirectional mechanics of the whole artery, which is a limitation of uniaxial tensile testing, there was a small amount of tissue once the artery had been removed from the bioreactor. If the artery was punctured in some way during the experimental set-up then it would not be feasible to conduct pressure-dilation testing. Up to three strips per artery were tested using uniaxial tensile testing, generating a larger dataset than pressure-dilation testing. In addition, the experimental artefact due to the arbitrary position of zero-state pressure was thought to be a limitation in the whole artery pressure-dilation testing method.

CCE treatment induced a decrease in arterial thickness. As shown by the pressure-dilation experiments, the mean diameter of the arteries increased and so it is expected that the thickness would decreased via a Poisson's ratio mechanism. Regardless of tissue treatment, bioreactor culture induced a decrease in arterial thickness by a similar amount (19% and 21% decrease for VEH vs. BIOVEH and CCE vs. BIOCCE respectively). This may be attributed to the bioreactor environment inducing a decrease in thickness but may also be as a result of experimental practicalities. This decrease in thickness may be partly due to changes in the bioreactor environment compared to the physiological environment as the tissue adapts to the bioreactor environment. The pressure pulse which arterial tissue is subject to in the body was not present in the bioreactor flow profile, as the arteries were cultured under steady flow. Incorporation of a physiological pulsatile component which exerts cyclic stretch and a dynamic pressure gradient on the arterial wall may mitigate this unwanted remodelling. The installation of the tissue into the bioreactor and potential stretching of the tissue over time (as the shaft of the bioreactor translates outwards to accommodate the increase in tissue length once pressurised) may also cause longer term visco-plastic relaxation changes in tissue dimension. The viscoelastic behaviour of arterial and AAA tissue was not investigated in this study but has been relatively widely studied (Holzapfel et al., 2002, Čanić et al., 2006, Zhang et al., 2008). The manipulation of the tissue once removed from the bioreactor should also be considered as a factor in the decreased thickness of the tissue. As the elastin has been virtually totally degraded during the course of the experiments (as a result of CCE treatment, bioreactor culture or a

combination of both), the remaining collagen may therefore become uncrimped prior to testing. Ideally, the tissue would not be handled at all prior to testing, however this is unavoidable for the chosen method. Therefore, geometric alterations in the tissue may not be caused solely by bioreactor remodelling. Lastly, an inherent bias may have also existed as generally the largest part of the artery was selected for uniaxial tensile testing to ensure sufficient tissue for the machine grips.

The uniaxial tensile testing revealed that CCE treated tissue had overall decreased stiffness and strength. This is expected as the components of the ECM which contribute to strength and stiffness were degraded by application of the CCE treatment. The FRESH arteries had a mean UTS of 1.44±0.34 MPa and 1.68±0.22 MPa in the circumferential and longitudinal orientations respectively. This is comparable to the failure strength of fresh and frozen porcine arteries (Stemper et al., 2007b) (1.15 ± 0.39 MPa and 1.32 ± 0.31 MPa respectively). The stiffness in both the elastin and collagen regions, the transition strain and the ultimate tensile strength of VEH tissue was indistinguishable from FRESH tissue. The gel application method alone, without the addition of collagenase or elastase, did not alter the mechanical properties of the tissue.

The Young's moduli of porcine carotid arteries, as tested by Silver *et al.*, were 0.15 MPa and 1.61 MPa for the elastin and collagen region respectively in the circumferential orientation and 0.22 MPa and 1.47 MPa for the elastin and collagen region respectively in the longitudinal orientation (Silver et al., 2003). The values obtained for the Young's moduli of FRESH tissue was comparable to the study by Silver *et al.* (0.22±0.06 MPa elastin region, 1.46±0.38 MPa collagen region in the circumferential orientation and 0.16±0.03 MPa elastin region, 1.11±0.16 MPa collagen region in the longitudinal orientation).

Generally, CCE treated tissue had a much greater degree of anisotropy in terms of arterial strength (Figure 6.7). Longitudinally orientated tissue strips were drastically weaker than circumferentially orientated tissue strips. This level of anisotropy was greater in BIOCCE tissue compared to CCE tissue. AAA tissue

has been associated with a higher degree of anisotropy compared to healthy abdominal aortic tissue (Geest et al., 2006).

The UTS of BIOCCE tissue was 0.30±0.14 MPa and the stiffness of the elastin and collagen regions were 0.06±0.05 MPa and 0.24±0.09 MPa respectively in the circumferential orientation; the UTS of BIOCCE tissue was 0.06±0.03 MPa and the elastin and collagen region stiffness was 0.01±0.004 MPa and 0.04±0.02 MPa respectively in the longitudinal orientation. Raghavan *et al.* reported UTS values in end-stage human AAA tissue of 0.70±0.12 MPa and 0.65±0.10 MPa in the circumferential and longitudinal orientations respectively (Raghavan et al., 1996). The stiffness of the elastin and collagen regions were 0.56±0.11 MPa and 5.39±0.88 MPa respectively in the circumferential orientation and 0.42±0.06 MPa and 4.08±0.68 MPa respectively in the longitudinal orientation. They reported a modest decrease in stiffness in AAA tissue compared to normal aorta, but a drastic decrease in arterial strength. The BIOCCE tissue is significantly weaker than FRESH tissue, mirroring the results of Raghavan *et al.*, but also has markedly decreased overall stiffness which contradict this study. This may be attributed to the time-scale of the *ex vivo* AAA model: the END model has undergone remodelling in the bioreactor for 12 days whereas human AAA tissue at elective repair may have been undergoing pathological remodelling for a period of many years. The SMCs responsible for ECM secretion in the END model have been shown to be dysfunctional and senescent in Chapter 5 and so there may be limited opportunity for remodelling to occur in the short period where the SMCs are functionally active.

There was a significant decrease in arterial strength and stiffness in both elastin and collagen regions in BIOVEH tissue compared to VEH tissue. In contrast, there was no change in arterial strength and stiffness in the BIOCCE tissue compared to CCE tissue. Bioreactor culture for 12 days only altered the material properties in VEH treated tissue and had no effect on CCE treated tissue. This may be linked with the functional properties of the SMCs in the tissue which are responsible for ECM secretion: END-BIOCCE SMCs have been shown to be dysfunctional whereas END-BIOVEH SMCs are functionally similar to FRESH SMCs (Chapter 5). Therefore, the SMCs in VEH treated tissue may still

have the ability to remodel the artery whereas the SMCs in CCE treated tissue have lost this and become dysfunctional.

Although there was a decrease in overall stiffness and strength in BIOCCE and BIOVEH tissue, there was evidence of active remodelling of the ECM as opposed to simple passive degradation of the tissue once in the bioreactor: the transition strain of BIOCCE tissue was significantly decreased in both orientations. BIOVEH tissue had an increased transition strain in the longitudinal orientation which was 2-fold higher than BIOCCE tissue. In addition, as detailed in Chapter 4, BIOVEH arteries tended to remodel inwards and exhibited a smaller luminal diameter. This evidence of inward remodelling may point to active remodelling rather than passive degradation, which would result in outwards remodelling as the tissue becomes weaker. Passive degradation of the tissue (such as that seen in CCE tissue compared to FRESH/VEH) would not alter the point at which the collagen fibres are recruited into a load bearing role (as described by the model in Figure 1.8).

As seen in Chapter 4, collagen staining the arterial sections revealed a possible deposition of collagen around the lumen in the END model. The decrease in transition strain may also provide evidence of collagen deposition as collagen is recruited at lower strains in END-BIOCCE tissue and collagen is deposited not in parallel with the native collagen, but so it is able to be recruited in the low strain typically elastin governed region. In addition, approximately one quarter of the END-BIOCCE tissue strips tested did not have a distinct elastin region which again suggests that collagen has been deposited for load bearing in the low strain region (Figure 6.8). These data suggest that the process of arterial stiffening and weakening seen in AAA tissue compared to healthy aortic tissue may have begun in the END-BIOCCE model. Further study on ECM secretion and collagen quantification, alongside longer periods of bioreactor culture is therefore recommended to investigate this possibility.

Unexpectedly, due to the gross appearance of the tissue, there was no significant differences in strength or overall stiffness between BIOVEH or BIOCCE tissue. There was, however, a persistent trend towards decreased elastin region stiffness, collagen region stiffness and ultimate tensile strength in BIOCCE

tissue compared to BIOVEH tissue. This highlights a limitation of the study in which there were relatively low sample sizes in BIOVEH and BIOCCE arteries due to the number of experiments carried out and the low tissue yield per experiment. Due to the limited amount of tissue, there was typically not an opportunity to test additional tissue strips if one did not truly fail and was damaged by the tissue grips. In future, the characterisation of the biomechanics of the END-BIOCCE tissue would benefit from additional experiments to increase the sample size.

The END-BIOCCE tissue exhibited clear non-uniformity in arterial thickness (Figure 6.5). The mean thickness of three measurements was used in this method to calculate the engineering stress (Section 2.9.2.2, Equation 2). It is suggested that using force per unit width to calculate the engineering stress in future experiments would be advisable, in order to accommodate non-uniform tissue thickness.

Two methods of biomechanical analysis were critically analysed and uniaxial tensile testing was selected as the most suitable method for this particular tissue. Despite the highlighted differences between the biomechanical properties of the END-BIOCCE model tissue and human AAA tissue, the END-BIOCCE model showed evidence of ECM remodelling in terms of collagen deposition and a decrease in arterial strength which are properties found in AAA tissue. The effect of the CCE treatment on the function of the artery has been characterised in order to better understand the environment the SMCs reside in during bioreactor culture. The function of the SMCs has been linked with the function of the artery as a whole organ via such biomechanical analysis.

CHAPTER 7

DISCUSSION, CONCLUSIONS AND FUTURE WORK

CHAPTER 7 DISCUSSION, CONCLUSIONS AND FUTURE WORK

Abdominal aortic aneurysm (AAA) is a progressive dilatation of the abdominal aorta which without intervention results in rupture (Golledge et al., 2006, Nordon et al., 2011). With an estimated prevalence of 5% in men over 65 and thought to account for 1.5% of the total mortality in males over 55, it is not an uncommon disease (Choke et al., 2005, Michel et al., 2011, Nordon et al., 2011).

Currently, the only treatment available is surgical repair once AAA diameter has exceeded 5.5cm: this is considered to be the point where the risk of rupture outweighs the surgical risk (Kent, 2014). Endovascular aneurysm repair (EVAR) is a minimally invasive procedure, but is not appropriate for every patient (Golledge et al., 2006). Open surgical repair (OSR) is a major surgical procedure with a mean 30-day mortality rate of over 5% (Nordon et al., 2011).

AAA progression is typically asymptomatic (Sakalihasan et al., 2005). The silent nature of AAA has often led to incidental diagnosis when addressing other medical complaints. As such, The National Abdominal Aortic Aneurysm Screening Programme (NAAASP) was implemented in the UK in 2010, offering AAA screening to all men over 65 years of age(Benson et al., 2016). A screening programme offers the unique opportunity to diagnose AAA at an earlier stage in its development and gain insight into the progression of the disease over time. However, current surgical treatments are still only offered once the AAA is determined to have a considerable rupture risk. By understanding the early stages of AAA progression, new targets for therapeutics may be revealed.

A hurdle to the study of early AAA disease is the paucity of early-stage human AAA tissue which is available. Animal models are therefore widely used in AAA research in order to understand the underlying mechanisms and a wide range of techniques are used (Trollope et al., 2011).

Smooth muscle cells (SMCs) are the principal cellular component of the arterial wall but are depleted and dysfunctional in AAAs (Keen et al., 1994, Lopez-Candales et al., 1997, Liao et al., 2000, Riches et al., 2013). They exhibit a distinct phenotype and this phenotypic switch occurs early on in AAA formation (Ailawadi et al., 2009). SMC seeding has shown therapeutic potential for AAA in a rat model (Losy et al., 2003, Allaire et al., 2004). Given their inherently plastic nature and their seemingly protective role in AAA disease, they are an appealing target of study.

The overall aim of this study was to explore the early stages of AAA disease using an *ex vivo* porcine bioreactor model and to further evaluate the established model. The adopted approach was to pre-treat porcine carotid arteries with a protease treatment containing a combination of collagenase and elastase (CCE) before culture for a specified length of time in a bioreactor under steady flow. Following CCE treatment, bioreactor culture for twelve days resulted in SMCs which were phenotypically comparable to human end-stage AAA SMCs (END model) (Riches et al., 2013). For this thesis, a culture period of three days was selected to attempt to simulate early AAA development (EARLY model). In a mouse model, although an aneurysmal arterial dilation was observed 14 days after treatment, there was evidence that SMCs had undergone phenotypic switching only seven days after treatment. Therefore, in the EARLY model, arteries were culture for three days in order to investigate the SMC behaviour prior to phenotypic switching (Ailawadi et al., 2009).

Following this, the tissue was either used for histology, immunohistochemistry and SMC explant cultures or for biomechanical analysis. The long term strategy was envisaged to create a reproducible and logistically simple large animal model of AAA which would be able to inform research to develop SMC therapeutic targets in early AAA disease.

During the course of this study, the structure and function of SMCs from the early and end-stage AAA model were characterised. The tissue from the end-stage model was characterised biomechanically in order to understand the relationship between the observed SMC dysfunction and the function of the

artery as a whole organ. Both early and end-stage models were qualitatively characterised using histology and immunohistochemistry. The local dynamics in the bioreactor were also characterised using porcine carotid arteries: previously, this had only been done using artificial silicone arteries.

This study directly followed a previous investigation in our laboratory which used protease pre-treatment followed by culture under steady flow in a bioreactor for twelve days to produce SMCs which were found to be comparable to human end-stage AAA SMCs (Riches et al., 2013). In that study, it was found that only a combination of collagenase and elastase (neither protease alone) prior to bioreactor culture was able to induce this AAA SMC phenotype. It was, however, unclear as to the contributions of the bioreactor and the treatment alone. The characterisation of the ECM was also limited in that study. In this thesis, by including static culture controls, the contributions of the culture environment and the protease treatment were able to be separated and explored. In addition, biomechanical and histological analysis allowed a greater insight into the status of the ECM. An early AAA model was also developed, in an attempt to temporally map the SMC behaviour, prior to the phenotypic switch. This switch is regarded as an early event in AAA formation (Ailawadi et al., 2009). In the current study, there were several principal findings.

1. Both CCE treatment and dynamic culture are required to induce SMC phenotypic switch

The previous study investigating the *ex vivo* bioreactor AAA model showed that by treating the artery with a combination of collagenase and elastase, after twelve days culture in the bioreactor the SMCs were phenotypically comparable to human AAA SMCs (Riches et al., 2013). However, the roles of protease treatment and bioreactor culture in SMC phenotype separately were not determined in that study. In this study, appropriate vehicle treatment and static culture controls were selected and investigated. In cellular terms, it was found that the combination of CCE pre-treatment and bioreactor culture was required for the SMCs to undergo this switch in phenotype. Neither CCE treatment nor

bioreactor culture alone was able to induce this change. The morphology and behaviour of SMCs derived from control arteries which were applied with a vehicle gel and then cultured in the bioreactor were comparable to fresh SMCs. This study was able to reproduce the reduced proliferation, rhomboid, end-stage AAA SMC phenotype which was comparable to human AAA SMC.

2. Early and end-stage model SMCs exhibit two distinct phenotypes

Another finding was revealed when the SMCs from the EARLY model were characterised in terms of structure and function. The structure of these EARLY SMCs were indistinguishable from control cells and exhibited a typical spindle morphology with aligned actin cytoskeleton. According to the classical SMC phenotype, this morphology would suggest a contractile SMC with low proliferation. However, the EARLY SMCs consistently exhibited hyperproliferation; in the END model SMC proliferation was significantly impaired. This behaviour, coupled with the finding that senescence levels of BIOCCE SMCs was significantly increased in the END model may point to accelerated aging with ensuing senescence in the SMCs. Indeed, it has already been shown that SMCs and endothelial cells from human AAA tissue exhibit shortened telomeres, indicative of early hyperproliferation in the human disease (Cafueri et al., 2012). Further unpublished data from our laboratory has also shown that human AAA SMCs have increased levels of nuclear aberrancy and DNA damage (Riches *et al.*, unpublished). These indications of DNA damage are also found in the end-stage BIOCCE SMCs. These observations are not without precedent, as SMCs from patients with diabetes mellitus have also been shown to exhibit a phenotype which is neither classically differentiated or de-differentiated (Riches et al., 2014). SMCs may therefore exist within a phenotypic spectrum rather than existing between binary differentiated and de-differentiated phenotypes.

The *ex vivo* model was able to produce SMCs which were phenotypically similar to human AAA SMCs indicative of prematurely aged cells.

3. BIOCCE SMCs may be attempting to stabilise the ECM

The EARLY and END model tissue, alongside the experimental control groups, were characterised using histology and immunohistochemistry specific to SMCs and the components of the ECM, elastin and collagen. The application of the CCE treatment resulted in a loss of elastin, but no notable loss of collagen. The END BIOCCE tissue also appeared to exhibit a peri-luminal deposition of collagen, as shown by increased intensity of Sirius red stain viewed with linearly polarized light. Although this deposition was subjective and not quantitative, this would be an interesting direction for future study especially as collagen content is typically increased in AAAs (Rizzo et al., 1989). It has been reported that initial collagen degradation is mitigated by an increase in collagen synthesis (Shimizu et al., 2006). This process gradually becomes more unbalanced over time and so during later stages of AAA development, the rate of collagen synthesis is overcome by the rate of degradation (Satta et al., 1997). This increase in collagen is thought to be a mechanism of ECM stabilisation. An attempt at ECM stabilisation in an early-stage mouse AAA model has been previously reported (Haskett et al., 2013). The EARLY model arteries had a diameter which was encompassed within the clinical definition for AAA: 1.5-fold the healthy diameter of the aorta (Nordon et al., 2011). However, in the END stage model, arteries had remodelled inwards and presented a diameter which was once again comparable to control arteries. In conjunction with the indication of collagen deposition, this may again indicate some sort of ECM compensatory stabilising mechanism orchestrated by the isolated SMCs in the early stages of the disease.

4. SMCs from the end-stage model exhibit disordered cytoskeleton

Fluorescence microscopy of the actin cytoskeleton revealed that in addition to rhomboid morphology, the end-stage BIOCCE SMCs had a disordered f-actin cytoskeleton. It is thought that this reorganisation of the cytoskeleton may mediate changes in SMC behaviour associated with phenotypic modulation due to the reorganisation of signalling molecules (Worth et al., 2001a).

5. The bioreactor caused arterial remodelling, regardless of pre-treatment

Biomechanical analysis revealed that during bioreactor culture, BIOCCE arteries showed a decreased transition strain in both orientations. This also supports the previous finding that collagen content may have increased and that the arteries were actively remodelling to adapt to the insult to the ECM from the CCE treatment. Control arteries which were treated with a vehicle gel only prior to culture in the bioreactor also appeared to undergo active remodelling. The arterial diameter tended to be decreased compared to control arteries and there was a significant increase in transition strain in one orientation. Neither of these behaviours are suggestive of passive degradation as changes in transition strain are driven by collagen remodelling (Bank et al., 1996). Inwards remodelling of the artery is indicative of active remodelling as the luminal pressure was greater than the outer pressure – the artery was resisting the pressure gradient. In terms of arterial tissue and biomechanics, the control arteries were affected by the dynamic environment in the bioreactor. Ideally, a bioreactor would completely mirror the *in vivo* situation and so the addition of a pulsatile component to the flow would be a natural development of the model. In this way, the tissue would be subjected to cyclic stress and possibly oscillatory shear stress as it would physiologically (Osol, 1995). A more complex simulation of physiological flow in the bioreactor may lead to the biomechanical behaviour of the tissue to behave in a more similar way to fresh tissue.

6. End-stage SMCs showed a loss of remodelling capabilities

The strength and stiffness of CCE treated arteries was not affected by bioreactor culture, unlike vehicle control treated arteries. In addition, there was a trend towards decreased levels of MMP secretion which is necessary for arterial remodelling. Although there was evidence that at some point during the twelve days in culture the SMCs in the CCE treated arteries attempted to stabilise the ECM, this was not sufficient to alter the biomechanical function of the artery in the end-stage model. The dysfunctional, senescent SMCs indicated a potential loss of remodelling capabilities in the end-stage model. Further biomechanical

analysis of the early-stage model may elucidate the temporal changes in biomechanics; it is conceivable that collagen was secreted when the SMCs are still relatively active before the tissue is degraded due to impaired SMC function. Although MMPs are greatly implicated in the formation and development of AAA, it may be that in the *ex vivo* model, the cells primarily responsible were not present. Adventitial mast cells and macrophages have been shown to produce copious amounts of MMPs in AAA tissue (Thompson et al., 1995, Tsuruda et al., 2008). The intra-luminal thrombus and polymorphonuclear neutrophils have also been shown to secrete high levels of MMPs (Fontaine et al., 2002). In isolation, once SMCs switch to the end-stage AAA phenotype, they are not active and are possibly limited in their ability to secrete MMPs.

Overall, it appears that, from the literature and the data included in this study, AAA SMCs do not fit into the classical SMC phenotype, exhibiting characteristics from both differentiated and de-differentiated SMCs (Figure 7.1). A previously identified distinct senescent cell phenotype, senescence associated secretory phenotype (SASP), is characterised by an altered secretome. An intriguing path of future study would be to characterise the secretome of the early and end-stage BIOCCE SMCs in order to investigate if they have, or are likely to adopt this distinct phenotype.

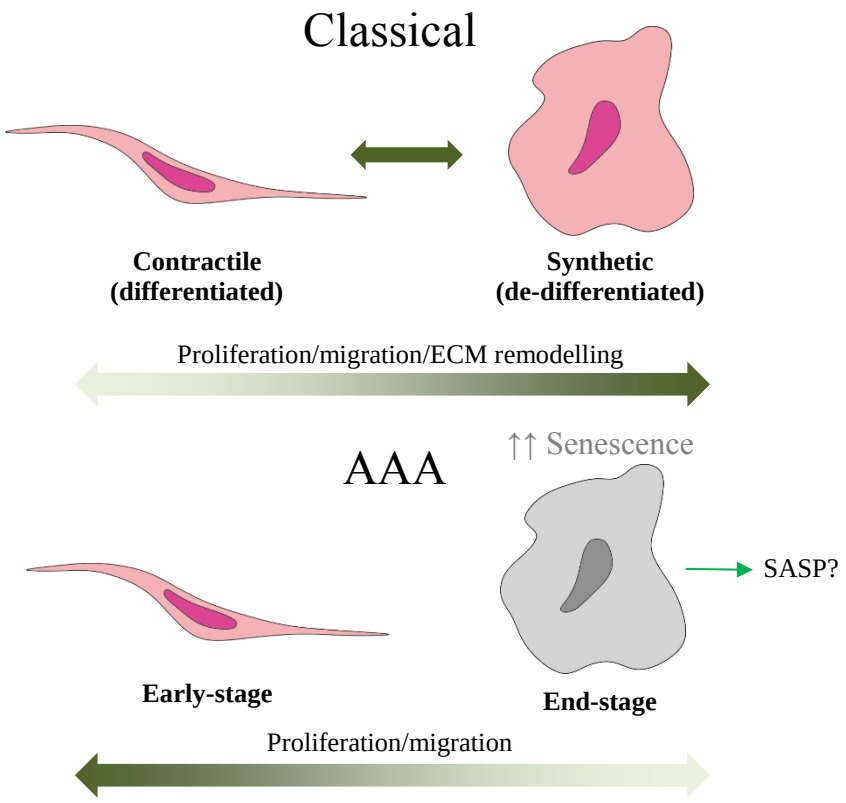

Figure 7.1 Distinct AAA phenotype outside of classical SMC phenotype characterisation. SASP = senescence-associated secretory phenotype

For the first time, this study has characterised SMC structure and function in an *ex vivo* large animal model specifically in the early stages of the disease. It has shown that SMCs may undergo a period of hyperproliferation and may attempt to remodel and stabilise the ECM. It is conceivable that this hyperproliferation in the early-stages of the disease may later lead to widespread cellular senescence and DNA damage in AAA disease. Molecular targets for proliferation, senescence or DNA damage markers may provide an insight to AAA therapeutics. Additionally, this particular *ex vivo* model has been characterised in terms of biomechanics. Biomechanical analysis is an important descriptor of arterial function; rupture in AAA is a mechanical failure of the arterial wall. Biomechanics analysis characterise the function of the arterial wall and changes to the ECM mediated through SMCs via MMP secretion.

7.1. STRENGTHS AND LIMITATIONS

The *ex vivo* nature of the model presents as a double-edged sword, with unique strengths and weaknesses. Firstly, the SMCs are able to be virtually isolated from confounding factors allowing sole exploration of the role of SMCs in AAA development. Such confounding factors may be differences in the dynamic culture environment that may exist between individual animals or patients or the presence of immune cells (such as mast cells, macrophages, neutrophils) which likely contribute to AAA formation (Satta et al., 1998, Sun et al., 2007, Tsuruda et al., 2008, Lai et al., 2016). Therefore, although the SMCs are removed from the physiological environment when cultured *ex vivo*, it enables their exact role to be established. In addition, an *ex vivo* model is logistically more practical compared to *in vivo* models. Although not within the scope of this current project, the *ex vivo* nature also allows more direct control of the dynamic culture environment. This would enable some investigation into the role of haemodynamics in AAA development even outside of safe physiological parameters for living subjects.

The non-physiological steady flow may have had an effect on the behaviour of the SMCs (Osol, 1995, Hoshina et al., 2003, Lehoux et al., 2006, Hahn and Schwartz, 2009). Although the SMC phenotype in the end-stage model has been previously validated with human AAA SMCs, it was not feasible to also validate the early-stage model due to scarcity of human AAA tissue in the earliest stages of development. Further to this, the arteries in the end-stage model displayed no significant dilatation, as they did in the early-stage model (Chapter 4). This was thought to be some sort of ECM stabilisation mechanism. However, the clinical definition of AAA is a focal dilatation of the arterial wall; the end-stage AAA model does not technically meet this criterion (Nordon et al., 2011). An intriguing future study would be to maintain the arteries in the bioreactor for longer than twelve days. Another limitation is that little is known about the nature of the flow through the vessel in the bioreactor. Turbulent and low-shear flow is known to exacerbate (or potentially even cause) vascular dysfunction, and so this may provide an insightful view into AAA pathogenesis with the *ex*

vivo model (Davies, 1995, Miller et al., 2002, Lin et al., 2013). Ideally, the same technique used clinically for flow analysis, magnetic resonance angiography (MRA), would be used to visualise the flow through the bioreactor. However, the bioreactor was constructed primarily of stainless steel and so MRA analysis is not possible. A combination of ultrasound with computational fluid dynamics (CFD) modelling may, however, enable better understanding of the bioreactor flow in various conditions (Scotti et al., 2008, Vande Geest et al., 2008). Peak wall shear stress (WSS) has been shown to be a promising indicator of AAA growth and rupture; building knowledge of the flow would enable WSS analysis (Vorp and Geest, 2005, Scotti et al., 2008, Xiong et al., 2008, Kontopodis et al., 2015).

7.2. RECOMMENDATIONS FOR FUTURE WORK

1. Investigation into control of dynamic culture environment and its effect on arterial and cellular behaviour

One of the advantages to using a bioreactor *ex vivo* model over an *in vivo* model is that the dynamic culture environment can be more tightly controlled in terms of flow type, flow rate, pressure and various pulsatile waveforms. The scope of this study was to identify the point at which the SMCs underwent a switch in phenotype and so a temporal analysis was undertaken. However, in terms of paths for future study, the bioreactor *ex vivo* model is perfectly suited to the effect of the dynamic environment on AAA progression. For example, comparing arterial tissue and SMC phenotype in arteries cultured under physiological and high pressure may provide an insight into the role of hypertension in AAA, already thought to play a role (Nordon et al., 2011). Higher flow rates or an addition of downstream resistance may be able to model increased stiffness in the vasculature due to the effect of aging or smoking, and also be able to look at AAA progression in more 'aged' arteries. Age and smoking are major risk-factors for development of AAA (Lederle et al., 2003, Sakalihasan et al., 2005).

2. Biomechanical analysis of the early-stage model

Time and resource limitations meant that it was not feasible to undertake biomechanical analysis of the early-stage model. For future study, the uniaxial tensile testing method employed in this thesis to characterise biomechanics of the end-stage model arteries could be used for the early-stage model. This would be a natural progression of the model and also may illuminate further the possible ECM stabilisation by peri-luminal collagen deposition seen in this study and its effects on the arterial function.

3. Analysis of secretome in early and end-stage model

Senescence-associated secretory phenotype cells (SASPs) are characterised through an altered secretome. Analysis of the secretome of the SMCs from the early and end-stage models would enable more conclusions to be made about the true phenotypic nature of the SMCs in this model. If a combination of dynamic culture and protease degradation induces a classical SASP SMC, then this may be able to inform future therapies for early AAA development involving slowing of vascular aging and stabilisation or replenishment of functional SMCs.

4. Investigation into role of DNA damage in SMC senescence

Some further work to this thesis has already commenced (Riches et al., unpublished). Nuclear aberrancy and γ-H2AX, a marker of double-stranded DNA damage, are both significantly increased in human AAA SMCs and end-stage SMCs in the *ex vivo* model. The role of DNA damage on SMC structure and function using the *ex vivo* model and possible methods of mitigating this damage would be a very exciting path of future research.

5. Inhibition of proliferation and localisation of proliferation markers

This study identified an early period of hyperproliferation which may explain the onset of increased SMC dysfunction and senescence. Therefore, a natural progression of the project would be to investigate the role of inhibition of SMC proliferation on AAA development. Proliferative markers, such as Ki67 could be localised using immunohistochemistry in order to visualise this behaviour over time using the *ex vivo* model.

6. Characterisation of flow through bioreactor and computational modelling of peak wall shear stress

The nature of the flow through the artery in the bioreactor is currently not known. A study involving computational simulation of the bioreactor and construction of a computational fluid dynamics (CFD) model would enable more insight into the dynamic environment in which the artery is cultured. A computational model would potentially also allow the rupture locations and pressures to be investigated using peak wall shear stress (WSS) measurements. This would then be validated using the *ex vivo* model.

7. Increased culture period for the *ex vivo* AAA model and the effects on arterial and SMC function

The *ex vivo* model was shown to exhibit a clinically aneurysmal dilatation of 1.5-fold normal arterial diameter in the early model, but then fall back below this value in the end-stage model, thought to be an attempt at stabilisation. Therefore the extension of length of culture time would provide more information as to the effects of SMC dysfunction further on the arterial structure. Tissue viability over a longer period of time may be the major hurdle to this proposed future work, therefore this would have to be further evaluated in terms of establishing conditions to retain viability.

8. Characterisation of microRNA expression in *ex vivo* model SMCs and reversibility potential

MicroRNAs (miRs) are non-coding RNAs which are able to regulate gene expression. They are heavily implicated in AAA formation and progression, reviewed in (Raffort et al., 2016). The identification and expression levels of miRs in the early and end-stage *ex vivo* model could be carried out using a microarray. The rhomboid, anti-proliferative and senescent phenotype found in the end-stage model was similar to the diabetic SMC phenotype also characterised previously within this laboratory (Riches et al., 2014). It was found that elevated expression levels of miR-143/145 were responsible for driving this diabetic phenotype and overexpression or inhibition of these miRs were able to reversibly control the SMC phenotype. Future work on the *ex vivo* model may enable identification of differentially regulated miRs, and then progress onto miR-driven restoration of a healthy phenotype to dysfunctional AAA SMCs and therefore may inform research into therapeutics.

7.3. THESIS SUMMARY AND CONCLUSION

In this study, an *ex vivo* bioreactor model of early-stage AAA was developed and the structure and function of arterial tissue and SMCs were characterised. The biomechanics of the end-stage model tissue were also characterised. A summary of the findings of this thesis and some suggested directions for future work are shown in Figure 7.2.

In this *ex vivo* model, the behaviour of the SMCs is not aligned with classical characterisation of SMC phenotype and so AAA SMC may exhibit a distinct 'aneurysmal' phenotype outside of this. Manipulation of this phenotype in the early stages of AAA prior to manifestation of SMC dysfunction may therefore provide a novel prospect for therapeutics. The advent of AAA screening has provided a window of opportunity for early-stage therapeutics.

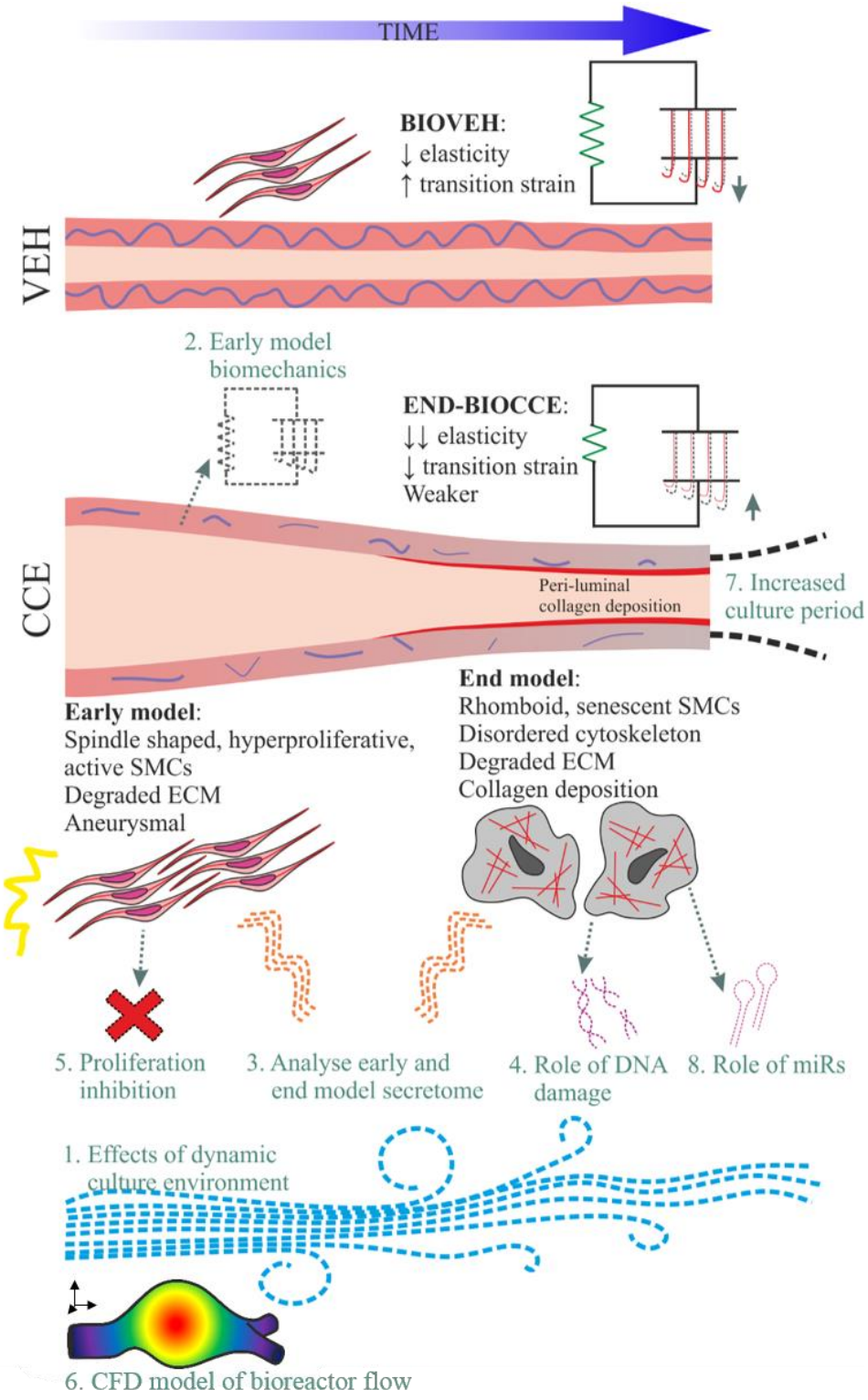

Figure 7.2 Summary of principal thesis findings and directions for future work. Cross section of top: VEH artery and bottom: CCE artery. Principal findings = solid lines, black text. Future work = dotted lines, teal text. CFD = computational fluid dynamics. miR=microRNA. Elastin = purple, collagen = red.

REFERENCES

LIST OF REFERENCES

ABILDGAARD, C. F., HARRISON, J. & JOHNSON, C. A. 1971. Comparative study of blood coagulation in nonhuman primates. *J Appl Physiol,* 30**,** 400-5.

ADAMS, P. D. 2009. Healing and Hurting: Molecular Mechanisms, Functions, and Pathologies of Cellular Senescence. *Molecular Cell,* 36**,** 2-14.

AILAWADI, G., ELIASON, J. L. & UPCHURCH, G. R. 2003. Current concepts in the pathogenesis of abdominal aortic aneurysm. *Journal of Vascular Surgery,* 38**,** 584 - 588.

AILAWADI, G., MOEHLE, C. W., PEI, H., WALTON, S. P., YANG, Z., KRON, I. L., LAU, C. L. & OWENS, G. K. 2009. Smooth muscle phenotypic modulation is an early event in aortic aneurysms. *The Journal of Thoracic and Cardiovascular Surgery,* 138**,** 1392-1399.

AIRHART, N., BROWNSTEIN, B. H., COBB, J. P., SCHIERDING, W., ARIF, B., ENNIS, T. L., THOMPSON, R. W. & CURCI, J. A. 2014. Smooth muscle cells from abdominal aortic aneurysms are unique and can independently and synergistically degrade insoluble elastin. *Journal of Vascular Surgery,* 60**,** 1033-1042.e5.

ALBINSSON, S. & SWARD, K. 2013. Targeting smooth muscle microRNAs for therapeutic benefit in vascular disease. *Pharmacological Research,* 75**,** 28-36.

ALEXANDER, M. R. & OWENS, G. K. 2012. Epigenetic control of smooth muscle cell differentiation and phenotypic switching in vascular development and disease. *Annu Rev Physiol,* 74**,** 13-40.

ALLAIRE, E., HASENSTAB, D., KENAGY, R. D., STARCHER, B., CLOWES, M. M. & CLOWES, A. W. 1998. Prevention of aneurysm development and rupture by local overexpression of plasminogen activator inhibitor-1. *Circulation,* 98**,** 249 - 255.

ALLAIRE, E., MUSCATELLI-GROUX, B., GUINAULT, A.-M., PAGES, C., GOUSSARD, A., MANDET, C., BRUNEVAL, P., MÉLLIÈRE, D. & BECQUEMIN, J.-P. 2004. Vascular Smooth Muscle Cell Endovascular Therapy Stabilizes Already Developed Aneurysms in a Model of Aortic Injury Elicited by Inflammation and Proteolysis. *Annals of Surgery,* 239**,** 417 - 427.

ALLAIRE, E., MUSCATELLI-GROUX, B., MANDET, C., GUINAULT, A.-M., BRUNEVAL, P., DESGRANGES, P., CLOWES, A., MÉLLIÈRE, D. & BECQUEMIN, J.-P. 2002. Paracrine effect of vascular smooth muscle cells in the prevention of aortic aneurysm formation. *Journal of Vascular Surgery,* 36**,** 1018 - 1026.

AMMIRATI, M., CIRIC, I. & RABIN, E. 1988. Induction of experimental aneurysms on the rat common carotid artery using a microsurgical CO2 laser. *Microsurgery,* 9**,** 78-81.

ANDREWS, E., WHITE, W. & BULLOCK, L. 1975. Spontaneous aortic aneurysms in blotchy mice. *American Journal of Pathology,* 78**,** 199-210.

ANIDJAR, S. & KIEFFER, E. 1992. Pathogenesis of Acquired Aneurysms of the Abdominal Aorta. *Annals of Vascular Surgery,* 6**,** 298 - 305.

ANIDJAR, S., SALZMANN, J. L., GENTRIC, D., LAGNEAU, P., CAMILLERI, J. P. & MICHEL, J. B. 1990. Elastase-induced experimental aneurysms in rats. *Circulation,* 82**,** 973 - 81.

APER, T., SCHMIDT, A., DUCHROW, M. & BRUCH, H. P. 2007. Autologous Blood Vessels Engineered from Peripheral Blood Sample. *European Journal of Vascular and Endovascular Surgery,* 33**,** 33-39.

ARGENTA, R. & PEREIRA, A. H. 2009. Modelos animais de aneurisma de aorta. *Jornal Vascular Brasileiro,* 8**,** 148-153.

BAJARDI, G., PECORARO, F. & MIRABELLA, D. 2009. Efficacy of TachoSil® patches in controlling Dacron suture-hole bleeding after abdominal aortic aneurysm open repair. *Journal of Cardiothoracic Surgery,* 4**,** 1-5.

BANK, A. J., WANG, H., HOLTE, J. E., MULLEN, K., SHAMMAS, R. & KUBO, S. H. 1996. Contribution of Collagen, Elastin, and Smooth Muscle to In Vivo Human Brachial Artery Wall Stress and Elastic Modulus. *Circulation,* 94**,** 3263-3270.

BASU, R., MORTON, J., KANDALAM, V., WANG, X., DAVIDGE, S. T., OUDIT, G. Y. & KASSIRI, Z. 2011. Loss of TIMP3 leads to adverse remodelling of the vascular wall structure and development of abdominal aortic aneurysm following angiotensin II treatment. *Circulation,* 124**,** S115 - S116.

BATH, M. F., GOKANI, V. J., SIDLOFF, D. A., JONES, L. R., CHOKE, E., SAYERS, R. D. & BOWN, M. J. 2015. Systematic review of cardiovascular disease and cardiovascular death in patients with a small abdominal aortic aneurysm. *British Journal of Surgery,* 102**,** 866-872.

BENSON, R. A., POOLE, R., MURRAY, S., MOXEY, P. & LOFTUS, I. M. 2016. Screening results from a large United Kingdom abdominal aortic aneurysm screening center in the context of optimizing United Kingdom National Abdominal Aortic Aneurysm Screening Programme protocols. *Journal of Vascular Surgery,* 63**,** 301-304.

BERGOEING, M. P., ARIF, B., HACKMANN, A. E., ENNIS, T. L., THOMPSON, R. W. & CURCI, J. A. 2007. Cigarette smoking increases aortic dilatation without affecting matrix metalloproteinase-9 and -12 expression in a modified mouse model of aneurysm formation. *Journal*

of vascular surgery : official publication, the Society for Vascular Surgery [and] International Society for Cardiovascular Surgery, North American Chapter, 45**,** 1217-1227.e2.

BEST, V. A., PRICE, J. F. & FOWKES, F. G. 2003. Persistent increase in the incidence of abdominal aortic aneurysm in Scotland, 1981 - 2000. *British Journal of Surgery,* 90**,** 1510 - 1515.

BHF. 2008. *British Heart Foundation Factfile: Abdominal Aortic Aneurysms* [Online]. Available: http://www.bhf.org.uk/idoc.ashx?docid=f6657a6e-d1c7-485d-aaae-77e5868c6309&version=-1 [Accessed 6th January 2012].

BLUTH, E. I., MURPHEY, S. M., HOLLIER, L. H. & SULLIVAN, M. A. 1990. Color flow Doppler in the evaluation of aortic aneurysms. *International Angiology,* 9**,** 8 - 10.

BOGREN, H. G., BUONOCORE, M. H. & GU, W.-Z. 1994. Carotid and vertebral artery blood flow in left- and right-handed healthy subjects measured with MR velocity mapping. *Journal of Magnetic Resonance Imaging,* 4**,** 37-42.

BOON, R. A. & DIMMELER, S. 2011. MicroRNAs and Aneurysm Formation. *Trends in Cardiovascular Medicine,* 21**,** 172-177.

BOUDGHENE, F., ANIDJAR, S., ALLAIRE, E., OSBORNE-PELLEGRIN, M., BIGOT, J. M. & MICHEL, J. B. 1993. Endovascular grafting in elastase-induced experimental aortic aneurysms in dogs: feasibility and preliminary results. *J Vasc Interv Radiol,* 4**,** 497-504.

BRADY, A. R., THOMPSON, S. G., FOWKES, F. G. R., GREENHALGH, R. M. & POWELL, J. T. 2004. Abdominal aortic aneurysm expansion risk factors and time intervals for surveillance. *Circulation,* 110**,** 16-21.

BRETON, M., BERROU, E., BRAHIMI-HORN, M. C., DEUDON, E. & PICARD, J. 1986. Synthesis of sulfated proteoglycans throughout the cell cycle in smooth muscle cells from pig aorta. *Exp Cell Res,* 166**,** 416-26.

BROPHY, C. M., MARKS, W. H., REILLY, J. M. & TILSON, M. D. 1991. Decreased Tissue Inhibitor of Metalloproteinases (TIMP) in Abdominal Aortic Aneurysm Tissue: A Preliminary Report. *Journal of Surgical Research,* 50**,** 653 - 657.

BROPHY, C. M., TILSON, J. E., BRAVERMAN, I. M. & TILSON, M. D. 1988. Age of onset, pattern of distribution, and histology of aneurysm development in a genetically predisposed mouse model. *Journal of Vascular Surgery,* 8**,** 45-8.

BROWNLEE, R. D. & LANGILLE, B. L. 1991. Arterial adaptations to altered blood flow. *Can J Physiol Pharmacol,* 69**,** 978-83.

BURTON, D. G. A. & KRIZHANOVSKY, V. 2014. Physiological and pathological consequences of cellular senescence. *Cellular and Molecular Life Sciences,* 71**,** 4373-4386.

BURTON, D. G. A., MATSUBARA, H. & IKEDA, K. 2010. Pathophysiology of vascular calcification Pivotal role of cellular senescence in vascular smooth muscle cells. *Experimental Gerontology,* 45**,** 819-824.

CAFUERI, G., PARODI, F., PISTORIO, A., BERTOLOTTO, M., VENTURA, F., GAMBINI, C., BIANCO, P., DALLEGRI, F., PISTOIA, V., PEZZOLO, A. & PALOMBO, D. 2012. Endothelial and Smooth Muscle Cells from Abdominal Aortic Aneurysm Have Increased Oxidative Stress and Telomere Attrition. *PLoS ONE,* 7**,** e35312.

CALADO, R. T. & YOUNG, N. S. 2009. Telomere Diseases. *New England Journal of Medicine,* 361**,** 2353-2365.

CAMPA, J. S., GREENHALGH, R. M. & POWELL, J. T. 1987. Elastin degradation in abdominal aortic aneurysms. *Atherosclerosis,* 65**,** 13-21.

ČANIĆ, S., TAMBAČA, J., GUIDOBONI, G., MIKELIĆ, A., HARTLEY, C. & ROSENSTRAUCH, D. 2006. Modeling Viscoelastic Behavior of Arterial Walls and Their Interaction with Pulsatile Blood Flow. *SIAM Journal on Applied Mathematics,* 67**,** 164-193.

CARMELIET, P., MOONS, L., LIJNEN, R., BAES, M., LEMAITRE, V., TIPPING, P., DREW, A., EECKHOUT, Y., SHAPIRO, S., LUPU, F. & COLLEN, D. 1997. Urokinase-generated plasmin activates matrix metalloproteinases during aneurysm formation. *Nature Genetics,* 17**,** 439 - 444.

CARMO, M., COLOMBO, L., BRUNO, A., CORSI, F. R. M., RONCORONI, L., CUTTIN, M. S., RADICE, F., MUSSINI, E. & SETTEMBRINI, P. G. 2002. Alteration of elastin, collagen and their cross-links in abdominal aortic aneurysms. *European Journal of Vascular and Endovascular Surgery,* 23**,** 543-549.

CARRELL, T. W., SMITH, A. & BURNAND, K. G. 1999. Experimental techniques and models in the study of the development and treatment of abdominal aortic aneurysm. *Br J Surg,* 86**,** 305-12.

CHEN, Q., LI, W., QUAN, Z. & SUMPIO, B. E. 2003. Modulation of vascular smooth muscle cell alignment by cyclic strain is dependent on reactive oxygen species and P38 mitogen-activated protein kinase. *Journal of Vascular Surgery,* 37**,** 660-668.

CHO, B. S., WOODRUM, D. T., ROELOFS, K. J., STANLEY, J. C., HENKE, P. K. & UPCHURCH, G. R., JR. 2009. Differential regulation of aortic growth in male and female rodents is associated with AAA development. *J Surg Res,* 155**,** 330-8.

CHOKE, E., COCKERILL, G., WILSON, W. R. W., SAYED, S., DAWSON, J., LOFTUS, I. & THOMPSON, M. M. 2005. A review of biological

factors implicated in abdominal aortic aneurysm rupture. *European Journal of Vascular and Endovascular Surgery,* 30**,** 227 - 244.

CHUTER, T. A. M., VISCOMI, S., SLATER, J. L., NOWYGROD, R. & RISBERG, B. 1997. Canine model of abdominal aortic aneurysm treated by endovascular graft implantation. *Cardiovascular Surgery,* 5**,** 490-496.

CIAVARELLA, C., ALVIANO, F., GALLITTO, E., RICCI, F., BUZZI, M., VELATI, C., STELLA, A., FREYRIE, A. & PASQUINELLI, G. 2015. Human Vascular Wall Mesenchymal Stromal Cells Contribute to Abdominal Aortic Aneurysm Pathogenesis Through an Impaired Immunomodulatory Activity and Increased Levels of Matrix Metalloproteinase-9. *Circulation Journal,* 79**,** 1460-U277.

COLLINS, M. J., BERSI, M., WILSON, E. & HUMPHREY, J. D. 2011. Mechanical properties of suprarenal and infrarenal abdominal aorta: Implications for mouse models of aneurysms. *Medical Engineering & Physics,* 33**,** 1262-1269.

COPPÉ, J.-P., PATIL, C. K., RODIER, F., SUN, Y., MUÑOZ, D. P., GOLDSTEIN, J., NELSON, P. S., DESPREZ, P.-Y. & CAMPISI, J. 2008. Senescence-Associated Secretory Phenotypes Reveal Cell-Nonautonomous Functions of Oncogenic RAS and the p53 Tumor Suppressor. *PLoS Biol,* 6**,** e301.

CORDES, K. R., SHEEHY, N. T., WHITE, M. P., BERRY, E. C., MORTON, S. U., MUTH, A. N., LEE, T.-H., MIANO, J. M., IVEY, K. N. & SRIVASTAVA, D. 2009. miR-145 and miR-143 regulate smooth muscle cell fate and plasticity. *Nature,* 460**,** 705-710.

COX, E. P. 1927. A Method of Assigning Numerical and Percentage Values to the Degree of Roundness of Sand Grains. *Journal of Paleontology,* 1**,** 179-183.

CROWTHER, M., GOODALL, S., JONES, J. L., BELL, P. R. F. & THOMPSON, M. M. 2000. Increased matrix metalloproteinase 2 expression in vascular smooth muscle cells cultured from abdominal aortic aneurysms. *Journal of Vascular Surgery,* 32**,** 575-583.

CURCI, J. A. 2009. Digging in the "Soil" of the Aorta to Understand the Growth of Abdominal Aortic Aneurysms. *Vascular,* 17**,** S21- S29.

D'SOUZA, D. 2009. *Radiopedia.org* [Online]. Available: http://radiopaedia.org/articles/histology-of-blood-vessels [Accessed 6th January 2012].

DADGAR, L., MAROIS, Y., DENG, X. & GUIDOIN, R. 1997. Arterial wall mechanical characteristics after treatment in collagenase: an in vitro aneurysm model. *Clin Invest Med,* 20**,** 25-34.

DAI, D., DING, Y., LEWIS, D. & KALLMES, D. 2006. A proposed ordinal scale for grading histology in elastase-induced, saccular aneurysms. *American Journal of Neuroradiology,* 27**,** 132-138.

DAUGHERTY, A. & CASSIS, L. A. 2004. Mouse Models of Abdominal Aortic Aneurysms. *Arteriosclerosis, Thrombosis, and Vascular Biology,* 24**,** 429-434.

DAVIES, P. F. 1995. Flow-mediated endothelial mechanotransduction. *Physiological Reviews,* 75**,** 519-560.

DAVIS, F. M., RATERI, D. L. & DAUGHERTY, A. 2014. Mechanisms of aortic aneurysm formation: translating preclinical studies into clinical therapies. *Heart,* 100**,** 1498-1505.

DAVIS, F. M., RATERI, D. L. & DAUGHERTY, A. 2015. Abdominal aortic aneurysm: novel mechanisms and therapies. *Current Opinion in Cardiology,* 30**,** 566-573.

DEB, P. P. & RAMAMURTHI, A. 2014. Spatiotemporal mapping of matrix remodelling and evidence of in situ elastogenesis in experimental abdominal aortic aneurysms. *J Tissue Eng Regen Med*.

DEL MORAL, L. R., LARGO, C., RAMIREZ, J. R., CLEMENTE, L. V., HEREDERO, A. F., DE CUBAS, L. R., GARCIA-OLMO, D. & GARCIA-ARRANZ, M. 2015. Potential of mesenchymal stem cell in stabilization of abdominal aortic aneurysm sac. *Journal of Surgical Research,* 195**,** 325-333.

DENAYER, T., STÖHR, T. & VAN ROY, M. 2014. Animal models in translational medicine: Validation and prediction. *New Horizons in Translational Medicine,* 2**,** 5-11.

DI MARTINO, E. S., BOHRA, A., VANDE GEEST, J. P., GUPTA, N., MAKAROUN, M. S. & VORP, D. A. 2006. Biomechanical properties of ruptured versus electively repaired abdominal aortic aneurysm wall tissue. *Journal of Vascular Surgery,* 43**,** 570-576.

DOBRIN, P. B. 1999. Animal models of aneurysms. *Ann Vasc Surg,* 13**,** 641-8.

DOBRIN, P. B., BAKER, W. H. & GLEY, W. C. 1984. Elastolytic and collagenolytic studies of arteries. Implications for the mechanical properties of aneurysms. *Arch Surg,* 119**,** 405-9.

DOBRIN, P. B. & MRKVICKA, R. 1994. Failure of elastin or collagen as possible critical connective tissue alterations underlying aneurysmal dilatation. *Cardiovascular Surgery,* 2**,** 484 - 488.

DUA, M. M. & DALMAN, R. L. 2010. Hemodynamic influences on abdominal aortic aneurysm disease: Application of biomechanics to aneurysm pathophysiology. *Vascular Pharmacology,* 53**,** 11 - 21.

DUBICK, M. A., HUNTER, G. C., PEREZ-LIZANO, E., MAR, G. & GEOKAS, M. C. 1988. Assessment of the role of pancreatic proteases

in human abdominal aortic aneurysms and occlusive disease. *Clinica Chimica Acta,* 177**,** 1-10.

DUPREY, A., KHANAFER, K., SCHLICHT, M., AVRIL, S., WILLIAMS, D. & BERGUER, R. 2010. In Vitro Characterisation of Physiological and Maximum Elastic Modulus of Ascending Thoracic Aortic Aneurysms Using Uniaxial Tensile Testing. *European Journal of Vascular and Endovascular Surgery,* 39**,** 700-707.

ETON, D., WARNER, D., OWENS, C., MCCLENIC, B., CAVA, R., OFEK, B., BORHANI, M., BARANIEWSKI, H. & SCHULER, J. J. 1996. Results of endoluminal grafting in an experimental aortic aneurysm model. *Journal of Vascular Surgery,* 23**,** 819-831.

EUGSTER, T., HUBER, A., OBEID, T., SCHWEGLER, I., GURKE, L. & STIERLI, P. 2005. Aminoterminal propeptide of Type III procollagen and matix metalloproteinases-2 and -9 failed to serve as serum markers for abdominal aortic aneurysm. *European Journal of Vascular and Endovascular Surgery,* 29**,** 378 - 382.

FERGUSON, C. D., CLANCY, P., BOURKE, B., WALKER, P. J., DEAR, A., BUCKENHAM, T., NORMAN, P. & GOLLEDGE, J. 2010. Association of statin prescription with small abdominal aortic aneurysm progression. *American Heart Journal,* 159**,** 307 - 313.

FONCK, E., PROD'HOM, G., ROY, S., AUGSBURGER, L., RÜFENACHT, D. A. & STERGIOPULOS, N. 2007. Effect of elastin degradation on carotid wall mechanics as assessed by a constituent-based biomechanical model. *American Journal of Physiology - Heart and Circulatory Physiology,* 292**,** H2754-H2763.

FONTAINE, V., JACOB, M. P., HOUARD, X., ROSSIGNOL, P., PLISSONNIER, D., ANGLES-CANO, E. & MICHEL, J. B. 2002. Involvement of the mural thrombus as a site of protease release and activation in human aortic aneurysms. *American Journal of Pathology,* 161**,** 1701-1710.

FREESTONE, T., TURNER, R. J., COADY, A., HIGMAN, D. J., GREENHALGH, R. M. & POWELL, J. T. 1995. Inflammation and matrix metalloproteinases in the enlarging abdominal aortic aneurysm. *Arteriosclerosis, Thrombosis, and Vascular Biology,* 15**,** 1145 - 1151.

GACCHINA, C., BROTHERS, T. & RAMAMURTHI, A. 2011. Evaluating smooth muscle cells from CaCl2-induced rat aortal expansions as a surrogate culture model for study of elastogenic induction of human aneurysmal cells. *Tissue Eng Part A,* 17**,** 1945-58.

GADOWSKI, G. R., RICCI, M. A., HENDLEY, E. D. & PILCHER, D. B. 1993. Hypertension accelerates the growth of experimental aortic aneurysms. *J Surg Res,* 54**,** 431-6.

GALIS, Z. S. & KHATRI, J. J. 2002. Matrix metalloproteinases in vascular remodeling and atherogenesis - The good, the bad, and the ugly. *Circulation Research,* 90**,** 251-262.

GANDHI, R. H., IRIZARRY, E., CANTOR, J. O., KELLER, S., NACKMAN, G. B., HALPERN, V. J., NEWMAN, K. M. & TILSON, M. D. 1994. ANALYSIS OF ELASTIN CROSS-LINKING AND THE CONNECTIVE-TISSUE MATRIX OF ABDOMINAL AORTIC-ANEURYSMS. *Surgery,* 115**,** 617-620.

GANTEN, M. K., KRAUTTER, U., VON TENGG-KOBLIGK, H., BOCKLER, D., SCHUMACHER, H., STILLER, W., DELORME, S., KAUCZOR, H. U., KAUFFMANN, G. W. & BOCK, M. 2008. Quantification of aortic distensibility in abdominal aortic aneurysm using ECG-gated multi-detector computed tomography. *Eur Radiol,* 18**,** 966-73.

GASSER, T. C., OGDEN, R. W. & HOLZAPFEL, G. A. 2006. *Hyperelastic modelling of arterial layers with distributed collagen fibre orientations*.

GEEST, J. P. V., SACKS, M. S. & VORP, D. A. 2006. The effects of aneurysm on the biaxial mechanical behaviour of human abdominal aorta. *Journal of Biomechanics,* 39**,** 1324 - 1334.

GERTZ, S. D., KURGAN, A. & EISENBERG, D. 1988. Aneurysm of the rabbit common carotid artery induced by periarterial application of calcium chloride in vivo. *J Clin Invest,* 81**,** 649-56.

GHOSHAL, S. & LOFTIN, C. D. 2012. Cyclooxygenase-2 Inhibition Attenuates Abdominal Aortic Aneurysm Progression in Hyperlipidemic Mice. *PLoS ONE,* 7**,** e44369.

GIAMBERNARDI, T. A., GRANT, G. M., TAYLOR, G. P., HAY, R. J., MAHER, V. M., MCCORMICK, J. J. & KLEBE, R. J. 1998. Overview of matrix metalloproteinase expression in cultured human cells. *Matrix Biology,* 16**,** 483-496.

GITLIN, J. M., TRIVEDI, D. B., LANGENBACH, R. & LOFTIN, C. D. 2007. Genetic deficiency of cyclooxygenase-2 attenuates abdominal aortic aneurysm formation in mice. *Cardiovascular Research,* 73**,** 227-236.

GOERICKE, S. L., PAROHL, N., ALBERT, J., DUDDA, M. & FORSTING, M. 2009. Elastase-induced aneurysm in Swine: proof of feasibility in a first case. A technical note. *Interventional Neuroradiology,* 15**,** 413 - 416.

GOLDMAN, J., ZHONG, L. & LIU, S. Q. 2003. Degradation of α-actin filaments in venous smooth muscle cells in response to mechanical stretch. *American Journal of Physiology - Heart and Circulatory Physiology,* 284**,** H1839-H1847.

GOLLEDGE, J., MULLER, J., DAUGHERTY, A. & NORMAN, P. 2006. Abdominal aortic aneurysm: Pathogenesis and implications for

management. *Arteriosclerosis, Thrombosis, and Vascular Biology*, 26**,** pp 2605 - 2613.

GOLLEDGE, J. & NORMAN, P. E. 2010. Atherosclerosis and Abdominal Aortic Aneurysm : Cause, Response, or Common Risk Factors? *Arteriosclerosis, Thrombosis, and Vascular Biology,* 30**,** 1075 - 1077.

GOODALL, S., CROWTHER, M., BELL, P. R. & THOMPSON, M. M. 2002a. The association between venous structural alterations and biomechanical weakness in patients with abdominal aortic aneurysms. *Journal of Vascular Surgery,* 35**,** 937-942.

GOODALL, S., PORTER, K. E., BELL, P. R. & THOMPSON, M. M. 2002b. Enhanced Invasive Properties Exhibited by Smooth Muscle Cells are Associated with Elevated Production of MMP-2 in Patients with Aortic Aneurysms. *European Journal of Vascular and Endovascular Surgery,* 24**,** 72-80.

GORIN, D. R., ARBID, E. J., D'AGOSTINO, R., KENT YUCEL, E., SOLOVAY, K. S., LA MORTE, W. W., QUIST, W. C., MULLIGAN, N. & MENZOIAN, J. O. 1997. A new generation endovascular graft for repair of abdominal aortic aneurysms. *The American Journal of Surgery,* 173**,** 159-164.

GOSGNACH, W., MESSIKA-ZEITOUN, D., GONZALEZ, D., PHILIPE, M. & MICHEL, J. B. 2000. Shear stress induces iNOS expression in cultured smooth muscle cells: role of oxidative stress. *American Journal of Physiology: Cell Physiology,* 279**,** C1880 - C1888.

GREAT BRITAIN 1986. Animals (Scientific Procedures) Act 1986. *c. 14.* London.

GRESHAM, G. A. & HOWARD, A. N. 1961. Aortic rupture in the Turkey. *Journal of Atherosclerosis Research,* 1**,** 75-80.

GROTE, K., FLACH, I., LUCHTEFELD, M., AKIN, E., HOLLAND, S. M., DREXLER, H. & SCHIEFFER, B. 2003. Mechanical stretch enhances mRNA expression and proenzyme release of matrix metalloproteinase-2 (MMP-2) via NAD(P)H oxidase-derived reactive oxygen species. *Circ Res,* 92**,** e80-6.

HAHN, C. & SCHWARTZ, M. 2009. Mechanotransduction in vascular physiology and atherogenesis. *Nature Reviews Molecular Cell Biology,* 10**,** 53 - 62.

HAHN, M. S., MCHALE, M. K., WANG, E., SCHMEDLEN, R. H. & WEST, J. L. 2006. Physiologic Pulsatile Flow Bioreactor Conditioning of Poly(ethylene glycol)-based Tissue Engineered Vascular Grafts. *Annals of Biomedical Engineering,* 35**,** 190-200.

HAN, M., DONG, L. H., ZHENG, B., SHI, J. H., WEN, J. K. & CHENG, Y. 2009. Smooth muscle 22 alpha maintains the differentiated phenotype

of vascular smooth muscle cells by inducing filamentous actin bundling. *Life Sci,* 84**,** 394-401.

HANSSON, G. K., GENG, Y. J., HOLM, J., HÅRDHAMMAR, P., WENNMALM, A. & JENNSICHE, E. 1994. Arterial smooth muscle cells express nitric oxide synthase in response to endothelial injury. *Journal of Experimental Medicine,* 180**,** 733 - 738.

HARDMAN, D., EASSON, W. J., HOSKINS, P. R., DÖSSEL, O. & SCHLEGEL, W. C. 2010. Computation of the Distribution of Monocyte Deposition in Abdominal Aortic Aneurysm Disease. *International Federation for Medical and Biological Engineering Proceedings,* 25**,** 1961-1964.

HARRIS, P. L., VALLABHANENI, S. R., DESGRANGES, P., BECQUEMIN, J.-P., VAN MARREWIJK, C. & LAHEIJ, R. J. F. 2000. Incidence and risk factors of late rupture, conversion, and death after endovascular repair of infrarenal aortic aneurysms: The EUROSTAR experience. *Journal of Vascular Surgery,* 32**,** 739-749.

HASKETT, D., AZHAR, M., UTZINGER, U. & VANDE GEEST, J. P. 2013. Progressive alterations in microstructural organization and biomechanical response in the ApoE mouse model of aneurysm. *Biomatter,* 3.

HASKETT, D., AZHAR, M. & VANDE GEEST, J. 2011. *Biomechanical Considerations of Animal Models of Aortic Aneurysms,* London, Springer.

HE, C. M. & ROACH, M. R. 1994. The composition and mechanical properties of abdominal aortic aneuryms. *Journal of Vascular Surgery,* 20**,** 6-13.

HELLENTHAL, F. A. M. V. I., BUURMAN, W. A., WODZIG, W. K. W. H. & SCHURINK, G. W. H. 2009a. Biomarkers of AAA progression. Part 1: extracellular matrix degeneration. *Nature Reviews Cardiology,* 6**,** 464-474.

HELLENTHAL, F. A. M. V. I., BUURMAN, W. A., WODZIG, W. K. W. H. & SCHURINK, G. W. H. 2009b. Biomarkers of abdominal aortic aneurysm progression. Part 2: inflammation. *Nature Reviews Cardiology,* 6**,** 543 - 552.

HELLENTHAL, F. A. M. V. I., GEENEN, I. L. A., TEIJINK, J. A. W., HEENEMAN, S. & SCHURINK, G. W. H. 2009c. Histological features of human abdominal aortic aneurysm are not related to clinical characteristics. *Cardiovascular Pathology,* 18**,** 286-293.

HELLER, J. A., WEINBERG, A., ARONS, R., KRISHNASASTRY, K. V., LYON, R. T., DEITCH, J. S., SCHULICK, A. H., BUSH, H. L. & KENT, K. C. 2000. Two decades of abdominal aortic aneurysm repair: Have we made any progress? *Journal of Vascular Surgery,* 32**,** 1091 - 1100.

HELMY, I. M. & AZIM, A. M. A. 2012. Efficacy of ImageJ in the assessment of apoptosis. *Diagnostic Pathology,* 7**,** 6.

HENDERSON, E. L., GENG, Y. J., SUKHOVA, G. K., WHITTEMORE, A. D., KNOX, J. & LIBBY, P. 1999. Death of smooth muscle cells and expression of mediators of apoptosis by T lymphocytes in human abdominal aortic aneurysms. *Circulation,* 99**,** 96 - 104.

HODGKIN, B. C., BURKETT, D. E. & SMITH, E. B. 1982. Noninvasive measurement of systolic and diastolic blood pressure in swine. *American Journal of Physiology - Heart and Circulatory Physiology,* 242**,** H127-H130.

HOEGH, A. & LINDHOLT, J. S. 2009. Basic science review. Vascular distensibility as a predictive tool in the management of small asymptomatic abdominal aortic aneurysms. *Vasc Endovascular Surg,* 43**,** 333-8.

HOLZAPFEL, G. A. 2001. Biomechanics of soft tissue. *The handbook of materials behavior models,* 3**,** 1049-1063.

HOLZAPFEL, G. A., GASSER, T. C. & STADLER, M. 2002. A structural model for the viscoelastic behavior of arterial walls: Continuum formulation and finite element analysis. *European Journal of Mechanics - A/Solids,* 21**,** 441-463.

HOSHINA, K., SHO, E., SHO, M., NAKAHASHI, T. K. & DALMAN, R. L. 2003. Wall shear stress and strain modulate experimental aneurysm cellularity. *J Vasc Surg,* 37**,** 1067-74.

HOUDEK, K., MOLACEK, J., TRESKA, V., KRIZKOVA, V., EBERLOVA, L., BOUDOVA, L., NEDOROST, L., TOLINGER, P., KOCOVA, J., KOBR, J., BAXA, J., LISKA, V., WITTER, K. & TONAR, Z. 2013. Focal histopathological progression of porcine experimental abdominal aortic aneurysm is mitigated by atorvastatin. *International Angiology,* 32**,** 291-306.

HOVSEPIAN, D. M., ZIPORIN, S. J., SAKURAI, M. K., LEE, J. K., CURCI, J. A. & THOMPSON, R. W. 2000. Elevated plasma levels of matrix metalloproteinase-9 in patients with abdominal aortic aneurysms: a circulating marker of degenerative aneurysm disease. *Journal of Vascular and Interventional Radiology,* 11**,** 1345 - 1352.

HUBER, A. & BADYLAK, S. F. 2012. Phenotypic changes in cultured smooth muscle cells: limitation or opportunity to tissue engineering of hollow organs? *Journal of Tissue Engineering and Regenerative Medicine,* 6**,** 505-511.

HULTGREN, R., GRANATH, F. & SWEDENBORG, J. 2007. Different Disease Profiles for Women and Men with Abdominal Aortic Aneurysms. *European Journal of Vascular and Endovascular Surgery,* 33**,** 556-560.

HUNGERFORD, J. E., OWENS, G. K., ARGRAVES, W. S. & LITTLE, C. D. 1996. Development of the aortic vessel wall as defined by vascular smooth muscle and extracellular matrix markers. *Dev Biol,* 178**,** 375-92.

HYNECEK, R. L., DERUBERTIS, B. G., TROCCIOLA, S. M., ZHANG, H., PRINCE, M. R., ENNIS, T. L., KENT, K. C. & FARIES, P. L. 2007. The creation of an infrarenal aneurysm within the native abdominal aorta of swine. *Surgery,* 142**,** 143-149.

JAGADESHAM, V. P., SCOTT, D. J. A. & CARDING, S. R. 2008. Abdominal aortic aneurysms: an autoimmune disease? *Trends in Molecular Medicine,* 14**,** 522-529.

JOHNSEN, S. H., FORSDAHL, S. H., SINGH, K. & JACOBSEN, B. K. 2010. Atherosclerosis in Abdominal Aortic Aneurysms: A Causal Event or a Process Running in Parallel? The Tromsø Study. *Arteriosclerosis, Thrombosis, and Vascular Biology,* 30**,** 1263 - 1268.

KARAPOLAT, S., UNLU, Y., ERKUT, B., KOCAK, H. & ERDOGAN, F. 2006. Influence of indomethacin in the rat aneurysm model. *Ann Vasc Surg,* 20**,** 369-75.

KARLSSON, L., BERGQVIST, D., LINDBÄCK, J. & PÄRSSON, H. 2009. Expansion of small diameter abdominal aortic aneurysms is not reflected by the release of inflammatory mediators IL-6, MMP-9 and CRP in plasma. *European Journal of Vascular and Endovascular Surgery,* 37**,** 420 - 424.

KARTHIKESALINGAM, A., NICOLI, T. K., HOLT, P. J., HINCHLIFFE, R. J., PASHA, N., LOFTUS, I. M. & THOMPSON, M. M. 2011. The Fate of Patients Referred to a Specialist Vascular Unit with Large Infra-renal Abdominal Aortic Aneurysms over a Two-year Period. *European Journal of Vascular and Endovascular Surgery,* 42**,** 295-301.

KEELING, W. B., ARMSTRONG, P. A., STONE, P. A., BANDYK, D. F. & SHAMES, M. L. 2005. An Overview of Matrix Metalloproteinases in the Pathogenesis and Treatment of Abdominal Aortic Aneurysms. *Vascular and Endovascular Surgery,* 39**,** 457-464.

KEEN, R. R., NOLAN, K. D., CIPOLLONE, M., SCOTT, E., SHIVELY, V. P., YAO, J. S. T. & PEARCE, W. H. 1994. Interleukin-1 beta induces differential gene expression in aortic smooth muscle cells. *Journal of Vascular Surgery,* 20**,** 774-786.

KENT, K. C. 2014. Abdominal Aortic Aneurysms. *New England Journal of Medicine,* 371**,** 2101-2108.

KIN, K., MIYAGAWA, S., FUKUSHIMA, S., SHIRAKAWA, Y., TORIKAI, K., SHIMAMURA, K., DAIMON, T., KAWAHARA, Y., KURATANI, T. & SAWA, Y. 2012. Tissue- and Plasma-Specific MicroRNA Signatures for Atherosclerotic Abdominal Aortic Aneurysm. *Journal of*

the American Heart Association: Cardiovascular and Cerebrovascular Disease, 1**,** e000745.

KLOSTER, B. O., LUND, L. & LINDHOLT, J. S. 2015. Induction of continuous expanding infrarenal aortic aneurysms in a large porcine animal model. *Annals of Medicine and Surgery,* 4**,** 30-35.

KOBIELARZ, M. & JANKOWSKI, L. J. 2013. Experimental characterization of the mechanical properties of the abdominal aortic aneurysm wall under uniaxial tension. *Journal of Theoretical and Applied Mechanics,* 51**,** 949--958.

KOCH, A. E., HAINES, G. K., RIZZO, R. J., RADOSEVICH, J. A., POPE, R. M., ROBINSON, P. G. & PEARCE, W. H. 1990. Human abdominal aortic aneurysms. Immunophenotypic analysis suggesting an immune-mediated response. *American Journal of Pathology,* 137**,** 1199 - 1213.

KOCH, A. E., KUNKEL, S. L., PEARCE, W. H., SHAH, M. R., PARIKH, D., EVANOFF, H. L., HAINES, G. K., BURDICK, M. D. & STRIETER, R. M. 1993. Enhanced production of the chemotactic cytokines interleukin-8 and monocyte chemoattractant protein-1 in human abdominal aortic aneurysms. *Am J Pathol,* 142**,** 1423-31.

KONTOPODIS, N., METAXA, E., PAPAHARILAOU, Y., TAVLAS, E., TSETIS, D. & IOANNOU, C. 2015. Advancements in identifying biomechanical determinants for abdominal aortic aneurysm rupture. *Vascular,* 23**,** 65-77.

KONTOPODIS, N., PANTIDIS, D., DEDES, A., DASKALAKIS, N. & IOANNOU, C. V. 2016. The - Not So - Solid 5.5cm Threshold for Abdominal Aortic Aneurysm Repair: Facts, Misinterpretations, and Future Directions. *Frontiers in surgery,* 3**,** 1.

KÓNYA, A., WRIGHT, K., GOUNIS, M. & KANDARPA, K. 2008. Animal Models for Atherosclerosis, Restenosis, and Endovascular Aneurysm Repair. *In:* CONN, P. M. (ed.) *Sourcebook of Models for Biomedical Research.* Totowa, NJ: Humana Press Inc.

KRATZBERG, J. A., WALKER, P. J., RIKKERS, E. & RAGHAVAN, M. L. 2009. The effect of proteolytic treatment on plastic deformation of porcine aortic tissue. *Journal of the Mechanical Behavior of Biomedical Materials,* 2**,** 65-72.

KU, D. N. 1997. Blood flow in arteries. *Annual Review of Fluid Mechanics,* 29**,** 399-434.

LABORDE, J. C., PARODI, J. C., CLEM, M. F., TIO, F. O., BARONE, H. D., RIVERA, F. J., ENCARNACION, C. E. & PALMAZ, J. C. 1992. Intraluminal bypass of abdominal aortic aneurysm: feasibility study. *Radiology,* 184**,** 185-190.

LAI, C. H., WANG, K. C., LEE, F. T., TSAI, H. W., MA, C. Y., CHENG, T. L., CHANG, B. I., YANG, Y. J., SHI, G. Y. & WU, H. L. 2016. Toll-

Like Receptor 4 Is Essential in the Development of Abdominal Aortic Aneurysm. *Plos One,* 11**,** 17.

LANNE, T., SONESSON, B., BERGQVIST, D., BENGTSSON, H. & GUSTAFSSON, D. 1992. Diameter and compliance in the male human abdominal aorta: influence of age and aortic aneurysm. *Eur J Vasc Surg,* 6**,** 178-84.

LASHERAS, J. C. 2007. The Biomechanics of Arterial Aneurysms. *Annual Review of Fluid Mechanics,* 39**,** 293-319.

LEDERLE, F. A. 2012. The Strange Relationship between Diabetes and Abdominal Aortic Aneurysm. *European Journal of Vascular and Endovascular Surgery,* 43**,** 254-256.

LEDERLE, F. A., JOHNSON, G. R., WILSON, S. E., CHUTE, E. P., LITTOOY, F. N., BANDYK, D., KRUPSKI, W. C., BARONE, G. W., ACHER, C. W. & BALLARD, D. J. 1997. Prevalence and Associations of Abdominal Aortic Aneurysm Detected through Screening. *Annals of Internal Medicine,* 126**,** 441 - 449.

LEDERLE, F. A., NELSON, D. B. & JOSEPH, A. M. 2003. Smoker's relative risk for aortic aneurysm compared with other smoking-related diseases: a systematic review. *Journal of Vascular Surgery,* 38**,** 329-334.

LEDERMAN, A., SALITURE NETO, F. T., FERREIRA, R., DE FIGUEIREDO, L. F. P., OTOCH, J. P., AUN, R. & DA SILVA, E. S. 2014. Endovascular model of abdominal aortic aneurysm induction in swine. *Vascular Medicine,* 19**,** 167-174.

LEE, J., CUDDIHY, M. J. & KOTOV, N. A. 2008. Three-dimensional cell culture matrices: State of the art. *Tissue Engineering Part B-Reviews,* 14**,** 61-86.

LEHOUX, S., CASTIER, Y. & TEDGUI, A. 2006. Molecular mechanisms of the vascular responses to haemodynamic forces. *J Intern Med,* 259**,** 381-92.

LEROUGE, S., RAYMOND, J., SALAZKIN, I., QIN, Z., GABOURY, L., CLOUTIER, G., OLIVA, V. L. & SOULEZ, G. 2004. Endovascular aortic aneurysm repair with stent-grafts: experimental models can reproduce endoleaks. *J Vasc Interv Radiol,* 15**,** 971-9.

LIAO, S., CURCI, J. A., KELLEY, B. J., SICARD, G. A. & THOMPSON, R. W. 2000. Accelerated Replicative Senescence of Medial Smooth Muscle Cells Derived from Abdominal Aortic Aneurysms Compared to the Adjacent Inferior Mesenteric Artery. *Journal of Surgical Research,* 92**,** 85-95.

LIAO, S., MIRALLES, M., KELLEY, B. J., CURCI, J. A., BORHANI, M. & THOMPSON, R. W. 2001. Suppression of experimental abdominal aortic aneurysms in the rat by treatment with angiotensin-converting enzyme inhibitors. *J Vasc Surg,* 33**,** 1057-64.

LIJNEN, H. R. 2001. Plasmin and matrix metalloproteinases in vascular remodelling. *Journal of Thrombosis and Haemostasis,* 86**,** 324 - 333.

LIM, J., WOLFF, J., RODD, C. D., COOPER, D. G. & EARNSHAW, J. J. 2015. Outcome in Men with a Screen-detected Abdominal Aortic Aneurysm Who are not Fit for Intervention. *European Journal of Vascular and Endovascular Surgery,* 50**,** 732-736.

LIN, P. Y., WU, Y. T., LIN, G. C., SHIH, Y. H., SAMPILVANJIL, A., CHEN, L. R., YANG, Y. J., WU, H. L. & JIANG, M. J. 2013. Coarctation-induced degenerative abdominal aortic aneurysm in a porcine model. *Journal of Vascular Surgery,* 57**,** 806-+.

LINDHOLT, J. S., VAMMEN, S., FASTING, H., HENNEBERG, E. W. & HEICKENDORFF, L. 2000. The plasma level of matrix metalloproteinase-9 may predict the natural history of small abdominal aortic aneurysms. A preliminary study. *European Journal of Vascular and Endovascular Surgery,* 20**,** 281 - 285.

LIPPINCOTT, WILLIAMS & WILKINS 2009. *Professional Guide to Diseases,* China, Wolters Kluwer Health.

LIU, Y. W., DROZDOV, I., SHROFF, R., BELTRAN, L. E. & SHANAHAN, C. M. 2013. Prelamin A Accelerates Vascular Calcification Via Activation of the DNA Damage Response and Senescence-Associated Secretory Phenotype in Vascular Smooth Muscle Cells. *Circulation Research,* 112**,** E99-+.

LO, R. C. & SCHERMERHORN, M. L. 2016. Abdominal aortic aneurysms in women. *Journal of Vascular Surgery,* 63**,** 839-844.

LONGO, G. M., XIONG, W. F., GREINER, T. C., ZHAO, Y., FIOTTI, N. & BAXTER, B. T. 2002. Matrix metalloproteinases 2 and 9 work in concert to produce aortic aneurysms. *Journal of Clinical Investigation,* 110**,** 625-632.

LOPEZ-CANDALES, A., HOLMES, D., LIAO, S., SCOTT, M. J. & W, S. A. 1997. Decreased vascular smooth muscle cell density in medial degeneration of human abdominal aortic aneurysms. *American Journal of Pathology,* 150**,** 993 - 1007.

LOPEZ-DE LEON, A. & ROJKIND, M. 1985. A simple micromethod for collagen and total protein determination in formalin-fixed paraffin-embedded sections. *J Histochem Cytochem,* 33**,** 737-43.

LOSY, F., DAI, J., PAGES, C., GINAT, M., MUSCATELLI-GROUX, B. A., GUINAULT, A.-M., ROUSSELLE, E., SMEDILE, G., LOISANCE, D., BECQUEMIN, J.-P. & ALLAIRE, E. 2003. Paracrine secretion of transforming growth factor-Î²1 in aneurysm healing and stabilization with endovascular smooth muscle cell therapy. *Journal of Vascular Surgery,* 37**,** 1301-1309.

LU, D. & KASSAB, G. S. 2011. Role of shear stress and stretch in vascular mechanobiology. *Journal of the Royal Society Interface,* 8**,** 1379 - 1385.

MAJESKY, M. W. 2007. Developmental Basis of Vascular Smooth Muscle Diversity. *Arteriosclerosis, Thrombosis, and Vascular Biology,* 27**,** 1248-1258.

MANNING, M. W., CASSI, L. A., HUANG, J., SZILVASSY, S. J. & DAUGHERTY, A. 2002. Abdominal aortic aneurysms: fresh insights from a novel animal model of the disease. *Vasc Med,* 7**,** 45-54.

MARINOV, G. R., MAROIS, Y., PARIS, E., ROBY, P., FORMICHI, M., DOUVILLE, Y. & GUIDOIN, R. 1997. Can the infusion of elastase in the abdominal aorta of the Yucatan miniature swine consistently produce experimental aneurysms? *J Invest Surg,* 10**,** 129-50.

MAYNAR, M., QIAN, Z., HERNANDEZ, J., SUN, F., DEMIGUEL, C., CRISOSTOMO, V., USON, J., PINEDA, L. F., ESPINOZA, C. G. & CASTANEDA, W. R. 2003. An animal model of abdominal aortic aneurysm created with peritoneal patch: Technique and initial results. *Cardiovascular and Interventional Radiology,* 26**,** 168-176.

MCCORMICK, M. L., GAVRILA, D. & WEINTRAUB, N. L. 2007. Role of Oxidative Stress in the Pathogenesis of Abdominal Aortic Aneurysms. *Arteriosclerosis, Thrombosis, and Vascular Biology,* 27**,** 461 - 469.

MCMILLAN, W. D., TAMARINA, N. A., CIPOLLONE, M., JOHNSON, D. A., PARKER, M. A. & PEARCE, W. H. 1997. Size matters: the relationship between MMP-9 expression and aortic diameter. *Circulation,* 96**,** 2228 - 2232.

MICHEL, J. B., MARTIN-VENTURA, J. L., EGIDO, J., SAKALIHASAN, N., TRESKA, V., LINDHOLT, J., ALLAIRE, E., THORSTEINSDOTTIR, U., COCKERILL, G. & SWEDENBORG, J. 2011. Novel aspects of the pathogenesis of aneurysms of the abdominal aorta in humans. *Cardiovascular Research,* 90**,** 18-27.

MILLER, F. J. 2002. Aortic Aneurysms: It's All About the Stress. *Arteriosclerosis, Thrombosis, and Vascular Biology,* 22**,** 1948 - 1949.

MILLER, F. J., SHARP, W. J., FANG, X., OBERLEY, L. W., OBERLEY, T. D. & WEINTRAUB, N. L. 2002. Oxidative stress in human abdominal aortic aneurysms: a potential mediator of aneurysmal remodelling. *Arteriosclerosis, Thrombosis, and Vascular Biology,* 22**,** 560 - 565.

MIROSLAV, Z., JIRI, B. & MICHAL, D. 2009. Biaxial Tension Tests with Soft Tissues of Arterial Wall. *Engineering Mechanics,* 16**,** 3 - 11.

MOHAN, D. & MELVIN, J. W. 1982. Failure properties of passive human aortic tissue. I--uniaxial tension tests. *J Biomech,* 15**,** 887-902.

MOLACEK, J., BAXA, J., HOUDEK, K., TRESKA, V. & FERDA, J. 2011. Assessment of abdominal aortic aneurysm wall distensibility with

electrocardiography-gated computed tomography. *Ann Vasc Surg,* 25**,** 1036-42.

MOLÁČEK, J., TŘEŠKA, V., KOBR, J., ČERTÍK, B., SKALICKÝ, T., KUNTSCHER, V. & KŘÍŽKOVÁ, V. 2009. Optimization of the model of abdominal aortic aneurysm--experiment in an animal model. *J Vasc Res,* 46**,** 1-5.

MONSON, K. L., GOLDSMITH, W., BARBARO, N. M. & MANLEY, G. T. 2003. Axial Mechanical Properties of Fresh Human Cerebral Blood Vessels. *Journal of Biomechanical Engineering,* 125**,** 288-294.

MORGAN, A. J. & HOSKING, S. L. 2007. Non-invasive vascular impedance measures demonstrate ocular vasoconstriction during isometric exercise. *British Journal of Ophthalmology,* 91**,** 385-390.

MURPHY, E. H., JOHNSON, E. D. & ARKO, F. R. 2007. Device-specific resistance to in vivo displacement of stent-grafts implanted with maximum iliac fixation. *J Endovasc Ther,* 14**,** 585-92.

NAKAHASHI, T. K., HOSHINA, K., TSAO, P. S., SHO, E., SHO, M., KARWOWSKI, J. K., YEH, C., YANG, R.-B., TOPPER, J. N. & DALMAN, R. L. 2002. Flow loading induces macrophage antioxidative gene expression in experimental aneurysms. *Arteriosclerosis, Thrombosis, and Vascular Biology,* 22**,** 2017 - 2022.

NELSON, D. M., MCBRYAN, T., JEYAPALAN, J. C., SEDIVY, J. M. & ADAMS, P. D. 2014. A comparison of oncogene-induced senescence and replicative senescence: implications for tumor suppression and aging. *Age (Dordr),* 36**,** 9637.

NEREM, R. M. & SELIKTAR, D. 2001. Vascular tissue engineering. *Annual Review of Biomedical Engineering,* 3**,** 225-243.

NESTOLA, M. G. C., GIZZI, A., CHERUBINI, C. & FILIPPI, S. 2016. Three-band decomposition analysis in multiscale FSI models of abdominal aortic aneurysms. *International Journal of Modern Physics C,* 27**,** 19.

NEUMANN, F. & UNGAR, H. 1973. Spontaneous aortic rupture in turkeys and the vascularization of the aortic wall. *Canadian Veterinary Journal,* 14**,** 136-138.

NIKLASON, L. E., GAO, J., ABBOTT, W. M., HIRSCHI, K. K., HOUSER, S., MARINI, R. & LANGER, R. 1999. Functional Arteries Grown in Vitro. *Science,* 284**,** 489-493.

NORDON, I. M., HINCHCLIFFE, R. J., HOLT, P. J., LOFTUS, I. M. & THOMPSON, M. M. 2009. Review of Current Theories for Abdominal Aortic Aneurysm Pathogenesis. *Vascular,* 17**,** 253 - 263.

NORDON, I. M., HINCHLIFFE, R. J., LOFTUS, I. M. & THOMPSON, M. M. 2011. Pathophysiology and epidemiology of abdominal aortic aneurysms. *Nature Reviews Cardiology,* 8**,** 92-102.

NORMAN, P. E. & POWELL, J. T. 2010. Site Specificity of Aneurysmal Disease. *Circulation,* 121**,** 560 - 568.

OSAKABE, T., SEYAMA, Y. & YAMASHITA, S. 1995. Comparison of ELISA and HPLC for the determination of desmosine or isodesmosine in aortic tissue elastin. *J Clin Lab Anal,* 9**,** 293-6.

OSHINSKI, J. N., CURTIN, J. L. & LOTH, F. 2006. Mean-average wall shear stress measurements in the common carotid artery. *Journal of cardiovascular magnetic resonance : official journal of the Society for Cardiovascular Magnetic Resonance,* 8**,** 717-722.

OSOL, G. 1995. Mechanotransduction by Vascular Smooth Muscle. *Journal of Vascular Research,* 32**,** 275 - 292.

OWENS, G. K., KUMAR, M. S. & WAMHOFF, B. R. 2004. Molecular regulation of vascular smooth muscle cell differentiation in development and disease. *Physiol Rev,* 84**,** 767-801.

PAFILI, K., GOUNI-BERTHOLD, I., PAPANAS, N. & MIKHAILIDIS, D. P. 2015. Abdominal aortic aneurysms and diabetes mellitus. *Journal of Diabetes and its Complications,* 29**,** 1330-1336.

PALMAZ, J. C., TIO, F. O., LABORDE, J. C., CLEM, M., RIVERA, F. J., MURPHY, K. D. & ENCARNACION, C. E. 1995. Use of Stents Covered with Polytetrafluoroethylene in Experimental Abdominal Aortic Aneurysm. *Journal of Vascular and Interventional Radiology,* 6**,** 879-885.

PARODI, J. C., PALMAZ, J. C. & BARONE, H. D. 1991. Transfemoral Intraluminal Graft Implantation for Abdominal Aortic Aneurysms. *Annals of Vascular Surgery,* 5**,** 491-499.

PATEL, M. I., GHOSH, P., MELROSE, J. & APPLEBERG, M. 1996. Smooth muscle cell migration and proliferation is enhanced in abdominal aortic aneurysms. *Australian and New Zealand Journal of Surgery,* 66**,** 305-308.

PERLSTEIN, T. S. & LEE, R. T. 2006. Smoking, Metalloproteinases, and Vascular Disease. *Arteriosclerosis, Thrombosis, and Vascular Biology,* 26**,** 250 - 256.

PETERSEN, E., WÅGBERG, F. & ÄNGQUIST, K.-A. 2002. Proteolysis of the Abdominal Aortic Aneurysm Wall and the Association with Rupture. *European Journal of Vascular and Endovascular Surgery,* 23**,** 153 - 157.

PETRINEC, D., LIAO, S., HOLMES, D. R., REILLY, J. M., PARKS, W. C. & THOMPSON, R. W. 1996. Doxycycline inhibition of aneurysmal degeneration in an elastase-induced rat model of abdominal aortic aneurysm: preservation of aortic elastin associated with suppressed production of 92 kD gelatinase. *J Vasc Surg,* 23**,** 336-46.

PHILLIPS, E. H., YRINEO, A. A., SCHROEDER, H. D., WILSON, K. E., CHENG, J.-X. & GOERGEN, C. J. 2015. Morphological and Biomechanical Differences in the Elastase and AngII apoE-/- Rodent Models of Abdominal Aortic Aneurysms. *BioMed Research International,* 2015**,** 12.

PORTER, KAREN E. & RICHES, K. 2013. The vascular smooth muscle cell: a therapeutic target in Type 2 diabetes? *Clinical Science,* 125**,** 167-182.

PORTER, K. E., VARTY, K., JONES, L., BELL, P. R. & LONDON, N. J. 1996. Human saphenous vein organ culture: a useful model of intimal hyperplasia? *Eur J Vasc Endovasc Surg,* 11**,** 48-58.

POWELL, J. T. 1998. Mortality results for randomised controlled trial of early elective surgery or ultrasonographic surveillance for small abdominal aortic aneurysms. *The Lancet,* 352**,** 1649-1655.

PROUDFOOT, D. & SHANAHAN, C. 2012. Human vascular smooth muscle cell culture. *Methods Mol Biol,* 806**,** 251-63.

PYO, R., LEE, J. K., SHIPLEY, J. M., CURCI, J. A., MAO, D., ZIPORIN, S. J., ENNIS, T. L., SHAPIRO, S. D., SENIOR, R. M. & THOMPSON, R. W. 2000. Targeted gene disruption of matrix metalloproteinase-9 (gelatinase B) suppresses development of experimental abdominal aortic aneurysms. *Journal of Clinical Investigation,* 105**,** 1641 - 1649.

QIU, J., ZHENG, Y., HU, J., LIAO, D., GREGERSEN, H., DENG, X., FAN, Y. & WANG, G. 2014. Biomechanical regulation of vascular smooth muscle cell functions: from in vitro to in vivo understanding. *Journal of the Royal Society Interface,* 11**,** 20130852.

RAAZ, U., TOH, R., MAEGDEFESSEL, L., ADAM, M., NAKAGAMI, F., EMRICH, F. C., SPIN, J. M. & TSAO, P. S. 2014. Hemodynamic regulation of reactive oxygen species: implications for vascular diseases. *Antioxid Redox Signal,* 20**,** 914-28.

RAFFORT, J., LAREYRE, F., CLEMENT, M. & MALLAT, Z. 2016. Micro-RNAs in abdominal aortic aneurysms: insights from animal models and relevance to human disease. *Cardiovascular Research,* 110**,** 165-177.

RAGHAVAN, M. L., KRATZBERG, J., CASTRO DE TOLOSA, E. M., HANAOKA, M. M., WALKER, P. & DA SILVA, E. S. 2006. Regional distribution of wall thickness and failure properties of human abdominal aortic aneurysm. *Journal of Biomechanics,* 39**,** 3010-3016.

RAGHAVAN, M. L. & VORP, D. A. 2000. Toward a biomechanical tool to evaluate rupture potential of abdominal aortic aneurysm: identification of a finite strain constitutive model and evaluation of its applicability. *Journal of Biomechanics,* 33**,** 475-482.

RAGHAVAN, M. L., WEBSTER, M. W. & VORP, D. A. 1996. Ex vivo biomechanical behaviour of abdominal aortic aneurysm: assessment

using a new mathematical model. *Annals of Biomedical Engineering,* 24**,** 573 - 582.

REILLY, J. M., SAVAGE, E. B., BROPHY, C. M. & TILSON, M. D. 1990. Hydrocortisone rapidly induces aortic rupture in a genetically susceptible mouse. *Archives of surgery (Chicago, Ill. : 1960),* 125**,** 707-709.

RENSEN, S. S. M., DOEVENDANS, P. & VAN EYS, G. 2007. Regulation and characteristics of vascular smooth muscle cell phenotypic diversity. *Netherlands Heart Journal,* 15**,** 100-108.

RICHES, K., ALSHANWANI, A. R., WARBURTON, P., O'REGAN, D. J., BALL, S. G., WOOD, I. C., TURNER, N. A. & PORTER, K. E. 2014. Elevated expression levels of miR-143/5 in saphenous vein smooth muscle cells from patients with Type 2 diabetes drive persistent changes in phenotype and function. *J Mol Cell Cardiol,* 74**,** 240-50.

RICHES, K., ANGELINI, T. G., MUDHAR, G. S., KAYE, J., CLARK, E., BAILEY, M. A., SOHRABI, S., KOROSSIS, S., WALKER, P. G., SCOTT, D. J. & PORTER, K. E. 2013. Exploring smooth muscle phenotype and function in a bioreactor model of abdominal aortic aneurysm. *J Transl Med,* 11**,** 208.

RICHES, K., MORLEY, M. E., TURNER, N. A., O'REGAN, D. J., BALL, S. G., PEERS, C. & PORTER, K. E. 2009. Chronic hypoxia inhibits MMP-2 activation and cellular invasion in human cardiac myofibroblasts. *Journal of Molecular and Cellular Cardiology,* 47**,** 391-399.

RIEHL, B. D., PARK, J. H., KWON, I. K. & LIM, J. Y. 2012. Mechanical Stretching for Tissue Engineering: Two-Dimensional and Three-Dimensional Constructs. *Tissue Engineering Part B-Reviews,* 18**,** 288-300.

RIZZO, R. J., MCCARTHY, W. J., DIXIT, S. N., LILLY, M. P., SHIVELY, V. P., FLINN, W. R. & YAO, J. S. T. 1989. Collagen types and matrix protein content in human abdominal aortic aneurysms. *Journal of Vascular Surgery,* 10**,** 365-373.

ROACH, M. R. & BURTON, A. C. 1957. THE REASON FOR THE SHAPE OF THE DISTENSIBILITY CURVES OF ARTERIES. *Canadian Journal of Biochemistry and Physiology,* 35**,** 681-690.

RUCKER, R. B. & TINKER, D. 1977. Structure and metabolism of arterial elastin. *Int Rev Exp Pathol,* 17**,** 1-47.

RUEL, J. & LACHANCE, G. 2009. A new bioreactor for the development of tissue-engineered heart valves. *Annals of Biomedical Engineering,* 37**,** 674 - 681.

RZUCIDLO, E. M., MARTIN, K. A. & POWELL, R. J. 2007. Regulation of vascular smooth muscle cell differentiation. *Journal of Vascular Surgery,* 45**,** A25-A32.

SAKALIHASAN, N., HEYERES, A., NUSGENS, B. V., LIMET, R. & LAPIERE, C. M. 1993. Modifications of the extracellular matrix of aneurysmal abdominal aortas as a function of their size. *Eur J Vasc Surg,* 7**,** 633-7.

SAKALIHASAN, N., LIMET, R. & DEFAWE, O. D. 2005. Abdominal aortic aneurysm. *The Lancet,* 365**,** 1577-1589.

SAKATA, N., MENG, J. & TAKEBAYASHI, S. 2000. Effects of advanced glycation end products on the proliferation and fibronectin production of smooth muscle cells. *J Atheroscler Thromb,* 7**,** 169-76.

SANO, M., SASAKI, T., HIRAKAWA, S., SAKABE, J., OGAWA, M., BABA, S., ZAIMA, N., TANAKA, H., INUZUKA, K., YAMAMOTO, N., SETOU, M., SATO, K., KONNO, H. & UNNO, N. 2014. Lymphangiogenesis and Angiogenesis in Abdominal Aortic Aneurysm. *PLoS ONE,* 9**,** e89830.

SATOH, H., NAKAMURA, M., SATOH, M., NAKAJIMA, T., IZUMOTO, H., MAESAWA, C., KAWAZOE, K., MASUDA, T. & HIRAMORI, K. 2004. Expression and localization of tumour necrosis factor-alpha and its converting enzyme in human abdominal aortic aneurysm. *Clin Sci (Lond),* 106**,** 301-6.

SATOH, K., BERK, B. C. & SHIMOKAWA, H. 2011. Vascular-derived reactive oxygen species for homeostasis and diseases. *Nitric Oxide-Biology and Chemistry,* 25**,** 211-215.

SATTA, J., HAUKIPURO, K., KAIRALUOMA, M. I. & JUVONEN, T. 1997. Aminoterminal propeptide of type III procollagen in the follow-up of patients with abdominal aortic aneurysms. *J Vasc Surg,* 25**,** 909-15.

SATTA, J., LAURILA, A., PAAKKO, P., HAUKIPURO, K., SORMUNEN, R., PARKKILA, S. & JUVONEN, T. 1998. Chronic inflammation and elastin degradation in abdominal aortic aneurysm disease: an immunohistochemical and electron microscopic study. *European Journal of Vascular and Endovascular Surgery,* 15**,** 313-319.

SCHANZER, A. & MESSINA, L. 2012. Two Decades of Endovascular Abdominal Aortic Aneurysm Repair: Enormous Progress With Serious Lessons Learned. *Journal of the American Heart Association,* 1.

SCHMOKER, J. D., LEE, C. H., TAYLOR, R. G., CHUNG, A., TROMBLEY, L., HARDIN, N., RUSSELL, S. R. & HOWARD, A. 2008. A novel model of blunt thoracic aortic injury: a mechanism confirmed? *J Trauma,* 64**,** 923-31.

SCHRIEFL, A. J., SCHMIDT, T., BALZANI, D., SOMMER, G. & HOLZAPFEL, G. A. 2015. Selective enzymatic removal of elastin and collagen from human abdominal aortas: Uniaxial mechanical response and constitutive modeling. *Acta Biomaterialia,* 17**,** 125-136.

SCOTTI, C. M., JIMENEZ, J., MULUK, S. C. & FINOL, E. A. 2008. Wall stress and flow dynamics in abdominal aortic aneurysms: finite element analysis vs. fluid-structure interaction. *Comput Methods Biomech Biomed Engin,* 11**,** 301-22.

SEGNANI, C., IPPOLITO, C., ANTONIOLI, L., PELLEGRINI, C., BLANDIZZI, C., DOLFI, A. & BERNARDINI, N. 2015. Histochemical Detection of Collagen Fibers by Sirius Red/Fast Green Is More Sensitive than van Gieson or Sirius Red Alone in Normal and Inflamed Rat Colon. *PLoS ONE,* 10**,** e0144630.

SHAH, P. K. 1997. Inflammation, Metalloproteinases and Increased Proteolysis. An Emerging Pathophysiological Paradigm in Aortic Aneurysm. *Circulation,* 96**,** 2115 - 2117.

SHANTIKUMAR, S., AJJAN, R., PORTER, K. E. & SCOTT, D. J. A. 2010. Diabetes and the Abdominal Aortic Aneurysm. *European Journal of Vascular and Endovascular Surgery,* 39**,** 200-207.

SHARP, W. V., DONOVAN, D. L., TEAGUE, P. C. & MOSTELLER, R. D. 1982. ARTERIAL OCCLUSIVE DISEASE - A FUNCTION OF VESSEL BIFURCATION ANGLE. *Surgery,* 91**,** 680-685.

SHI, N. & CHEN, S.-Y. 2016. Smooth Muscle Cell Differentiation: Model Systems, Regulatory Mechanisms, and Vascular Diseases. *Journal of Cellular Physiology,* 231**,** 777-787.

SHIMIZU, K., MITCHELL, R. N. & LIBBY, P. 2006. Inflammation and Cellular Immune Responses in Abdominal Aortic Aneurysms. *Arteriosclerosis, Thrombosis, and Vascular Biology,* 26**,** 987 - 994.

SHO, E., SHO, M., HOSHINA, K., KIMURA, H., NAKAHASHI, T. K. & DALMAN, R. L. 2004. Hemodynamic forces regulate mural macrophage infiltration in experimental aortic aneurysms. *Exp Mol Pathol,* 76**,** 108-16.

SILENCE, J., COLLEN, D. & LIJNEN, H. R. 2002. Reduced Atherosclerotic Plaque but Enhanced Aneurysm Formation in Mice With Inactivation of the Tissue Inhibitor of Metalloproteinase-1 (TIMP-1) Gene. *Circulation Research,* 90**,** 897-903.

SILLESEN, H., ELDRUP, N., HULTGREN, R., LINDEMAN, J., BREDAHL, K., THOMPSON, M., WANHAINEN, A., WINGREN, U. & SWEDENBORG, J. 2015. Randomized clinical trial of mast cell inhibition in patients with a medium-sized abdominal aortic aneurysm. *Br J Surg,* 102**,** 894-901.

SILVER, F. H., SNOWHILL, P. B. & FORAN, D. J. 2003. Mechanical behavior of vessel wall: a comparative study of aorta, vena cava, and carotid artery. *Ann Biomed Eng,* 31**,** 793-803.

SINGH, V. 2008. General Anatomy. Chennai: Elsevier.

SIVARAPATNA, A., GHAEDI, M., LE, A. V., MENDEZ, J. J., QYANG, Y. B. & NIKLASON, L. E. 2015. Arterial specification of endothelial cells derived from human induced pluripotent stem cells in a biomimetic flow bioreactor. *Biomaterials,* 53**,** 621-633.

SMITH, J. D., DAVIES, N., WILLIS, A. I., SUMPIO, B. E. & ZILLA, P. 2001. Cyclic Stretch Induces the Expression of Vascular Endothelial Growth Factor in Vascular Smooth Muscle Cells. *Endothelium,* 8**,** 41-48.

STEGEMANN, J. P., HONG, H. & NEREM, R. M. 2005. Mechanical, biochemical, and extracellular matrix effects on vascular smooth muscle cell phenotype. *Journal of Applied Physiology,* 98**,** 2321-2327.

STEMPER, B. D., YOGANANDAN, N. & PINTAR, F. A. 2007a. Mechanics of arterial subfailure with increasing loading rate. *Journal of Biomechanics,* 40**,** 1806-1812.

STEMPER, B. D., YOGANANDAN, N., STINEMAN, M. R., GENNARELLI, T. A., BAISDEN, J. L. & PINTAR, F. A. 2007b. Mechanics of Fresh, Refrigerated, and Frozen Arterial Tissue. *Journal of Surgical Research,* 139**,** 236-242.

STRINDBERG, G., NICHOLS, P., RICCI, M. A., MARINOV, G., MAROIS, Y., ROBY, P. & GUIDOIN, R. 1998. Experimental modifications to a canine infrarenal aortic aneurysm model for the validation of endovascular stent-grafts: an exploratory study. *J Invest Surg,* 11**,** 185-97.

STRINGFELLOW, M. M., LAWRENCE, P. F. & STRINGFELLOW, R. G. 1987. The influence of aorta-aneurysm geometry upon stress in the aneurysm wall. *J Surg Res,* 42**,** 425-33.

SUMNER, D. S., HOKANSON, D. E. & STRANDNESS, D. E., JR. 1970. Stress-strain characteristics and collagen-elastin content of abdominal aortic aneurysms. *Surg Gynecol Obstet,* 130**,** 459-66.

SUN, J., SUKHOVA, G. K., YANG, M., WOLTERS, P. J., MACFARLANE, L. A., LIBBY, P., SUN, C., ZHANG, Y., LIU, J., ENNIS, T. L., KNISPEL, R., XIONG, W., THOMPSON, R. W., BAXTER, B. T. & SHI, G. P. 2007. Mast cells modulate the pathogenesis of elastase-induced abdominal aortic aneurysms in mice. *J Clin Invest,* 117**,** 3359-68.

SVENSJO, S., BJORCK, M. & WANHAINEN, A. 2013. Current prevalence of abdominal aortic aneurysm in 70-year-old women. *Br J Surg,* 100**,** 367-72.

SWARTZ, D. D., RUSSELL, J. A. & ANDREADIS, S. T. 2005. Engineering of fibrin-based functional and implantable small-diameter blood vessels. *American Journal of Physiology - Heart and Circulatory Physiology,* 288**,** H1451-H1460.

SWEDENBORG, J., MÄYRÄNPÄÄ, M. I. & KOVANEN, P. T. 2011. Mast Cells: Important Players in the Orchestrated Pathogenesis of Abdominal Aortic Aneurysms. *Arteriosclerosis, Thrombosis, and Vascular Biology,* 31**,** 734-740.

TANGIRALA, R. K., RUBIN, E. M. & PALINSKI, W. 1995. Quantitation of atherosclerosis in murine models: correlation between lesions in the aortic origin and in the entire aorta, and differences in the extent of lesions between sexes in LDL receptor-deficient and apolipoprotein E-deficient mice. *Journal of Lipid Research,* 36**,** 2320-8.

TAVARES MONTEIRO, J. A., DA SILVA, E. S., RAGHAVAN, M. L., PUECH-LEAO, P., DE LOURDES HIGUCHI, M. & OTOCH, J. P. 2014. Histologic, histochemical, and biomechanical properties of fragments isolated from the anterior wall of abdominal aortic aneurysms. *J Vasc Surg,* 59**,** 1393-401 e1-2.

THOMPSON, R. W., GERAGHTY, P. J. & LEE, J. K. 2002. Abdominal aortic aneurysms: basic mechanisms and clinical implications. *Current Problems in Surgery,* 39**,** 110-230.

THOMPSON, R. W., HOLMES, D. R., MERTENS, R. A., LIAO, S., BOTNEY, M. D., MECHAM, R. P., WELGUS, H. G. & PARKS, W. C. 1995. Production and localization of 92-Kilodalton gelatinase in abdominal aortic aneurysms. *Journal of Clinical Investigation,* 96**,** 318 - 326.

THOMPSON, S. G., ASHTON, H. A., GAO, L. & SCOTT, R. A. P. 2009. Screening men for abdominal aortic aneurysm: 10 year mortality and cost effectiveness results from the randomised Multicentre Aneurysm Screening Study. *BMJ,* 338.

THUBRIKAR, M. J., LABROSSE, M., ROBICSEK, F., AL-SOUDI, J. & FOWLER, B. 2001. Mechanical properties of abdominal aortic aneurysm wall. *Journal of Medical Engineering & Technology,* 25**,** 133 - 142.

TIERNEY, A. P., DUMONT, D. M., CALLANAN, A., TRAHEY, G. E. & MCGLOUGHLIN, T. M. 2010. ACOUSTIC RADIATION FORCE IMPULSE IMAGING ON EX VIVO ABDOMINAL AORTIC ANEURYSM MODEL. *Ultrasound in Medicine and Biology,* 36**,** 821-832.

TOUROO, J. S. & WILLIAMS, S. K. 2012. A tissue-engineered aneurysm model for evaluation of endovascular devices. *Journal of biomedical materials research. Part A,* 100**,** 3189-3196.

TRACHET, B., BOLS, J., DEGROOTE, J., VERHEGGHE, B., STERGIOPULOS, N., VIERENDEELS, J. & SEGERS, P. 2015. An animal-specific FSI model of the abdominal aorta in anesthetized mice. *Ann Biomed Eng,* 43**,** 1298-309.

TROLLOPE, A., MOXON, J. V., MORAN, C. S. & GOLLEDGE, J. 2011. Animal models of abdominal aortic aneurysm and their role in furthering management of human disease. *Cardiovascular Pathology,* 20**,** 114 - 123.

TSUI, J. C. 2010. Experimental models of abdominal aortic aneurysms. *The Open Cardiovascular Medicine Journal,* 4**,** 221-230.

TSURUDA, T., KATO, J., HATAKEYAMA, K., KOJIMA, K., YANO, M., YANO, Y., NAKAMURA, K., NAKAMURA-UCHIYAMA, F., MATSUSHIMA, Y., IMAMURA, T., ONITSUKA, T., ASADA, Y., NAWA, Y., ETO, T. & KITAMURA, K. 2008. Adventitial mast cells contribute to pathogenesis in the progression of abdominal aortic aneurysm. *Circulation Research,* 102**,** 1368 - 1377.

TURNBULL, I. C., HADRI, L., RAPTI, K., SADEK, M., LIANG, L. F., SHIN, H. J., COSTA, K. D., MARIN, M. L., HAJJAR, R. J. & FARIES, P. L. 2011. Aortic Implantation of Mesenchymal Stem Cells after Aneurysm Injury in a Porcine Model. *Journal of Surgical Research,* 170**,** E179-E188.

TWIGGER, S., PRUITT, K., FERNÁNDEZ-SUÁREZ, X., KAROLCHIK, D., WORLEY, K., MAGLOTT, D., BROWN, G., WEINSTOCK, G., GIBBS, R., KENT, J., BIRNEY, E. & JACOB, H. 2008. What everybody should know about the rat genome and its online resources. *Nature Genetics,* 40**,** 523-527.

VAISHNAV, R. N., YOUNG, J. T., JANICKI, J. S. & PATEL, D. J. 1972. Nonlinear Anisotropic Elastic Properties of the Canine Aorta. *Biophysical Journal,* 12**,** 1008-1027.

VANDE GEEST, J. P., SCHMIDT, D. E., SACKS, M. S. & VORP, D. A. 2008. The effects of anisotropy on the stress analyses of patient-specific abdominal aortic aneurysms. *Ann Biomed Eng,* 36**,** 921-32.

VERBIN, C., DONAYRE, C., KOPCHOK, G., SCOCCIANTI, M. & WHITE, R. A. 1995. ANTERIOR PATCH AORTIC-ANEURYSM MODEL FOR THE STUDY OF ENDOLUMINAL GRAFTS. *Journal of Investigative Surgery,* 8**,** 381-388.

VOGEL, V. & SHEETZ, M. 2006. Local force and geometry sensing regulate cell functions. *Nature Reviews Molecular Cell Biology,* 7**,** 265-275.

VOLLMAR, J. F., PAUSCHINGER, P., PAES, E., HENZE, E. & FRIESCH, A. 1989. AORTIC ANEURYSMS AS LATE SEQUELAE OF ABOVE-KNEE AMPUTATION. *The Lancet,* 334**,** 834-835.

VORP, D. A. 2007. BIOMECHANICS OF ABDOMINAL AORTIC ANEURYSM. *Journal of biomechanics,* 40**,** 1887-1902.

VORP, D. A. & GEEST, J. P. V. 2005. Biomechanical Determinants of Abdominal Aortic Aneurysm Rupture. *Arteriosclerosis, Thrombosis, and Vascular Biology,* 25**,** 1558-1566.

VORP, D. A., RAGHAVAN, M. L., MULUK, S. C., MAKAROUN, M. S., STEED, D. L., SHAPIRO, R. & WEBSTER, M. W. 1996. Wall strength and stiffness of aneurysmal and nonaneurysmal abdominal aorta. *Ann N Y Acad Sci,* 800**,** 274-6.

VORP, D. A., SCHIRO, B. J., EHRLICH, M. P., JUVONEN, T. S., ERGIN, M. A. & GRIFFITH, B. P. 2003. Effect of aneurysm on the tensile strength and biomechanical behavior of the ascending thoracic aorta. *The Annals of Thoracic Surgery,* 75**,** 1210-1214.

WAHLGREN, C. M., LARSSON, E., MAGNUSSON, P. K. E., HULTGREN, R. & SWEDENBORG, J. 2010. Genetic and environmental contributions to abdominal aortic aneurysm development in a twin population. *Journal of Vascular Surgery,* 51**,** 3-7.

WANHAINEN, A., MANI, K. & GOLLEDGE, J. 2016. Surrogate Markers of Abdominal Aortic Aneurysm Progression. *Arteriosclerosis Thrombosis and Vascular Biology,* 36**,** 236-244.

WEBB, R. C. 2003. SMOOTH MUSCLE CONTRACTION AND RELAXATION. *Advances in Physiology Education,* 27**,** 201-206.

WERNIG, F., MAYR, M. & XU, Q. 2003. Mechanical Stretch-Induced Apoptosis in Smooth Muscle Cells Is Mediated by β1-Integrin Signaling Pathways. *Hypertension,* 41**,** 903-911.

WHITBREAD, T., BIRCH, P., ROGERS, S., MAJEED, A., ROCHESTER, J., BEARD, J. D. & GAINES, P. 1996. A new animal model for abdominal aortic aneurysms: Initial results using a multiple-wire stent. *European Journal of Vascular and Endovascular Surgery,* 11**,** 90-97.

WHITTAKER, P. & CANHAM, P. B. 1991. Demonstration of quantitative fabric analysis of tendon collagen using two-dimensional polarized light microscopy. *Matrix,* 11**,** 56-62.

WHITTAKER, P., KLONER, R. A., BOUGHNER, D. R. & PICKERING, J. G. 1994. Quantitative assessment of myocardial collagen with picrosirius red staining and circularly polarized light. *Basic Res Cardiol,* 89**,** 397-410.

WILSON, J. S., VIRAG, L., DI ACHILLE, P., KARŠAJ, I. & HUMPHREY, J. D. 2013. Biochemomechanics of Intraluminal Thrombus in Abdominal Aortic Aneurysms. *Journal of Biomechanical Engineering,* 135**,** 0210111-02101114.

WILSON, W. R. W., ANDERTON, M., CHOKE, E. C., DAWSON, J., LOFTUS, I. M. & THOMPSON, M. M. 2008. Elevated plasma MMP1 and MMP9 are associated with abdominal aortic aneurysm rupture. *European Journal of Vascular and Endovascular Surgery,* 35**,** 580 - 584.

WORTH, N. F., ROLFE, B. E., SONG, J. & CAMPBELL, G. R. 2001a. Vascular smooth muscle cell phenotypic modulation in culture is

associated with reorganisation of contractile and cytoskeletal proteins. *Cell Motil Cytoskeleton,* 49**,** 130-45.

WORTH, N. F., ROLFE, B. E., SONG, J. & CAMPBELL, G. R. 2001b. Vascular smooth muscle cell phenotypic modulation in culture is associated with reorganisation of contractile and cytoskeletal proteins. *Cell Motility and the Cytoskeleton,* 49**,** 130-145.

XIE, C.-Q., RITCHIE, R. P., HUANG, H., ZHANG, J. & CHEN, Y. E. 2011. Smooth muscle cell differentiation in vitro: Models and underlying molecular mechanisms. *Arteriosclerosis, thrombosis, and vascular biology,* 31**,** 1485-1494.

XIONG, J., WANG, S. M., ZHOU, W. & WU, J. G. 2008. Measurement and analysis of ultimate mechanical properties, stress-strain curve fit, and elastic modulus formula of human abdominal aortic aneurysm and nonaneurysmal abdominal aorta. *Journal of Vascular Surgery,* 48**,** 189-195.

YAZDANI, S. K. & BERRY, J. L. 2009. Development of an In Vitro System to Assess Stent-induced Smooth Muscle Cell Proliferation: A Feasibility Study. *Journal of Vascular and Interventional Radiology,* 20**,** 101-106.

ZARAGOZA, C., GOMEZ-GUERRERO, C., MARTIN-VENTURA, J. L., BLANCO-COLIO, L., LAVIN, B., MALLAVIA, B., TARIN, C., MAS, S., ORTIZ, A. & EGIDO, J. 2011. Animal models of cardiovascular diseases. *Journal of Biomedicine and Biotechnology,* 2011.

ZATINA, M. A., ZARINS, C. K., GEWERTZ, B. L. & GLAGOV, S. 1984. Role of medial lamellar architecture in the pathogenesis of aortic aneurysms. *Journal of Vascular Surgery,* 1**,** 442-448.

ZEINALI-DAVARANI, S., CHOW, M.-J., TURCOTTE, R. & ZHANG, Y. 2013. Characterization of Biaxial Mechanical Behavior of Porcine Aorta under Gradual Elastin Degradation. *Annals of Biomedical Engineering,* 41**,** 1528-1538.

ZHANG, L. L. & WANG, Y. 2015. B lymphocytes in abdominal aortic aneurysms. *Atherosclerosis,* 242**,** 311-317.

ZHANG, M.-J., ZHOU, Y., CHEN, L., WANG, Y.-Q., WANG, X., PI, Y., GAO, C.-Y., LI, J.-C. & ZHANG, L.-L. 2015. An overview of potential molecular mechanisms involved in VSMC phenotypic modulation. *Histochemistry and Cell Biology,* 145**,** 119-130.

ZHANG, W., GUO, X. & KASSAB, G. S. 2008. A Generalized Maxwell Model for Creep Behavior of Artery Opening Angle. *Journal of biomechanical engineering,* 130**,** 054502-054502.

ZIDI, M. & ALLAIRE, E. 2015. Mechanical behavior of abdominal aorta aneurysm in rat model treated by cell therapy using mesenchymal stem cells. *Biomech Model Mechanobiol,* 14**,** 185-94.